Multi Scale Micro and Nano Metrology for Advanced Precision Moulding Technologies

Quagliotti, Danilo

Publication date:
2017

Document Version
Publisher's PDF, also known as Version of record

Multi Scale Micro and Nano Metrology for Advanced Precision Moulding Technologies

Danilo Quagliotti

PhD Thesis

Kongens Lyngby, February 2017

Technical University of Denmark
Department of Mechanical Engineering –
Manufacturing Engineering
Produktionstorvet, building 427S,
2800 Kongens Lyngby, Denmark
www.mek.dtu.dk
Phone: (+45) 4525 4763
Fax: (+45) 4593 0190
E-mail: info@mek.dtu.dk

Published in Denmark by
Technical University of Denmark

ISBN: 978-87-7475-480-0

Ecce et naves, cum tam magnae sint
et a ventis validis minentur,
circumferentur a minimo gubernaculo,
ubi impetus dirigentis voluerit.

Epistula Jacobi 3,4.

Preface

This thesis was prepared as one of the requirements of the Ph.D. course of study at the Technical University of Denmark (DTU), Department of Mechanical Engineering. The work was carried out from February 2014 to October 2016 and from January to February 2017 at the Department of Mechanical Engineering, at the Technical University of Denmark (DTU), under the supervision of Associate Prof. Guido Tosello and Prof. Hans Nørgaard Hansen.
From October to December 2016, nine weeks were spent at The University of Nottingham (UK), Faculty of Engineering, under the supervision of Prof. Richard Leach.

I would like to thank all my supervisors for their inspirational contribution to my work. In particular, I would like to express my gratitude to Associate Prof. Guido Tosello for his constant support and motivation, his highly valuable contribution to my work and the endless opportunity I was given during the three years of his great supervision.
My gratitude also goes to Prof. Hans Nørgaard Hansen for his inspiration and his wise and constant guidance.
I would like to thank Prof. Richard Leach for the great hospitality at The University of Nottingham and for giving me the opportunity to collaborate with the Manufacturing Metrology Team.

The work was funded by the Technical University of Denmark. Financial support received by the "Hi-Micro" European project, 7th Framework Programme (FP7-2012-NMP-ICT-FoF: 314055—www.hi-micro.eu), by the Danish foundation Fabriksejer, Civilingeniør Louis Dreyer Myhrwold og hustru Janne Myhrwolds Fond, by the Danish foundation Otto Mønsteds Fond and by the Danish foundation Idella Fond is gratefully acknowledged.

Kgs. Lyngby, February 2017

Danilo Quagliotti

Abstract

The technological revolution that has deeply influenced the manufacturing industry over the past two decades opened up new possibilities for the realisation of advanced micro and nano systems but, at the same time, traditional techniques for quality assurance became not adequate any longer, as the technology progressed.
The gap between the needs of the manufacturing industry and the well-organized structure of the dimensional and geometrical metrology appeared, above all, related to the methodologies and, also, to the instrumentation used to deal with the incessant scaling down of the critical dimensions of the novel micro and nano production.
Nowadays, design methodologies and concurrent tolerance guidelines are not yet available for advanced micro manufacture. Moreover, there are no shared methodologies that deals with the uncertainty evaluation of feature of size in the sub-millimetre scale.
On the other hand, a large choice of measurement equipment is now available but limitations in their use and of the instruments themselves are, in many cases, not completely understood, yet.
In this context, the ambition of the PhD project was to develop and implement a complete metrological framework for advanced precision micro moulded products with micro/nano structured surfaces and micro/nano geometries, across several length scales.
Uncertainty evaluation and traceability, specification intervals formulation, assessment of the moulded parts replication and a deep investigation on the optical instruments currently available for micro/nano dimensional and geometrical measurements were all subjects of the research conducted during the three years of the PhD course of study and that were collected in this final work.
Traceability and uncertainty evaluation were dealt with the development of a comprehensive statistical methodology based on the well-known frequentist approach. It was successfully applied to dimensional and geometrical measurements in the micro/nano length scale.
A novel method was developed on purpose for the formulation of specification intervals. Based on the evaluation of the shrinkage uncertainty, it allows to discriminate between the shrinkage of 1D and 2D features and cope with the influence of length scale. The method was applied and validated in the specific case of a micro-powder injection moulding production. Nevertheless, it is of general validity for any moulding process in which the material undergoes a change in dimensions from the mould cavity, due to a phase transformation. In parallel to the formulation of specification intervals, an investigation of two instruments with two different working principle proved a mutual dependence between the quality of the measurement process and the quality of the production. The measurement process influenced the quality assurance, but the lack of quality of the parts influenced the measurement process.
The surface texture replication was investigated about the amplitude (*Sa*, *Sq*) and the slope (*Sdq*) and assessed by the replication fidelity, i.e., comparing the produced parts with the tool used to replicate the geometry and evaluating the measurement uncertainty. The evaluation included the repeatability and reproducibility of the production process, the amplitude and slope replication of the features on the surface, the evaluation of the uncertainty of the replication fidelity.
The investigation of optical instruments started with the processing of the data of an international comparison of surface texture measurements, in the sub-micrometre scale, by optical instruments, organised under the umbrella of the Scientific Technical Committee on 'Surfaces' (STC-S) of The International Academy for Production Engineering (CIRP). The comparison unveiled the state-of-the-art performance, in the sub-micrometre scale, of the three main microscopes working principle currently used in areal topography measurement (confocal microscopy, coherent scanning interferometry and focus variation microscopy). Results showed that agreement between

optical instruments and reference measurements (by atomic force microscopy) could be reached to some extent, largely depending on the technology of the instruments used.
The limitations of the performance of the optical instruments were, also, inspected in specific cases that can arise during practical operation and that are becoming more and more common in modern micro and nano manufacturing. Several environmental sources were identified (thermal drifts, air conditioning system, stray light), which can introduce substantial environmental noise into the measurements, but, also, internal noise related to a prolonged use of an instrument.

Acknowledgements

During the course of my Ph.D. studies several experts were involved in various ways in my research. I wish to express them my gratitude for their commitment to the project.
I would like to thank

- Dr. Tech. Prof. Leonardo De Chiffre at Department of Mechanical Engineering of the Technical University of Denmark for encouraging and introducing me into this field.
- Mr. René Sobiecki and Mr. Jakob Rasmussen at Department of Mechanical Engineering of the Technical University of Denmark for their unique support and involvement in many of my activities.
- Prof. Giulio Barbato and Dr. Gianfranco Genta at Politecnico di Torino for fruitful discussions and for sharing with me their knowledge in statistical analysis and uncertainty evaluation.
- Dr.-Ing. Henning Zeidler and Dipl.-Ing. André Martin at the Technical University of Chemnitz for their collaboration in relation to a large number of time-consuming measurements.
- Dr.-Ing. Oltmann Riemer and Dr. Carla Flosky at the University of Bremen for their collaboration in relation to a large number of time-consuming measurements.
- Dr. Jun Qian and Dr. Marius Nabuurs at the University of Leuven in relation to a large number of time-consuming measurements.
- Dr. Stefania Gasparin at The LEGO Group for fruitful discussions and collaboration in many activities.
- Dr. Jørgen Garnæs and Dr. Poul Erik Hansen at the Danish Metrology Institute DFM for their valuable collaboration with atomic force microscopy and confocal microscopy.
- Dr. Wahyudin P Syam and Dr. Xiaobing Feng, Manufacturing Metrology Team at The University of Nottigham, for the great time spent together and fruitful discussions.
- Dr. François Blateyron at Digital Surf for his valuable and unique support with MountainsMap® software.
- Dr. Jan Friis Jorgensen and Dr. Anders Kühle at Image Metrology for their valuable and unique support with SPIP™ and topoStitch™ software.

Last, but not the least, I wish to thank the M.Sc. and B.Sc. project students I supervised during my Ph.D. for their commitment to the project, their results and their friendship:
Mr. Federico Baruffi, Mr. Jacek Salaga, Mr. Michael Gani, Mr. Martin Kain and Mr. Dario Loaldi. Their thesis works represented an important contribution to the project:

- Baruffi F 2016 Optical metrology and precision milled metal surfaces for process validation and product quality assurance, M.Sc. Thesis, DTU.
- Salaga J 2016 Dimensional and surface micro/nano metrology for precision moulding technology, M.Sc. Thesis, DTU.
- Gani M and Kain M 2016 Design and Optimization of High Precision Positioning Fixture, B.Sc. Thesis, DTU.
- Loaldi D 2017 Technological signature in precision injection compression moulding of polymer Fresnel lenses, M.Sc. Thesis, DTU.

Table of content

TABLE OF CONTENTS

Table of figures

Chapter 1

Introduction

1.1 Background

Metrology was certainly a need for our ancestors to learn about the world around them but also to establish connections and exchanges with peers, attempting to relate the unknown with what was recognisable and predictable. In some units of measure, still widespread and used, we can recognise the heritage from early days metrology (inch, foot, etc.) and imagine difficulties and limitations faced.
Nowadays, we use metrology daily and we benefit from technological advances, capturing essential information from the nearby environment. Nonetheless, in order for everyone to benefit from the measured information without having to cope with the difficulties that metrology inherently has, guidelines are to be defined and observed by metrologists.
Focusing the attention from everyday life to technology, the issues to consider are more complex and the need to have clear and shared rules becomes absolutely crucial.

In precision manufacturing of conventionally sized products, dimensional metrology is an integral part of all quality assurance systems. Metrological tools in terms of instrumentation, calibration artefacts, standards and well established procedures are available to support the increasing demands for production in global networks of highly complex components and products.

In the context of micro manufacturing, advanced product concepts are based on integrated processes and process chains, include different materials and span across different dimensional scales. These characteristics require detailed knowledge of not only absolute dimensions and geometrical quantities, but also about the uncertainty of measurement, because this is a decisive parameter when dealing with quality control of micro manufactured components.
A metrology structure for micro manufacturing is at an early stage yet. Thus, in many cases, the manufacturing paradigms taken primarily from the macroscopic world are adapted to micro scaled components and functional micro/nano features [1].

1.1.1 Precision and micro injection moulding process technologies

Product miniaturisation and micro-systems have been strong drivers of a technological change, with a significant impact on the manufacturing industry. The continuous miniaturisation of moulded parts and features leads to new challenges in injection moulding processes and specially developed solutions are necessary in all production steps [2].

Precision micro-parts are the key enablers to product functionality and performance in a broad range of applications in life-sciences, medical, consumables and telecommunication devices. Precision moulding and micro injection moulding (μIM) are the strategic technologies for polymer micro-parts (see **Figure 1.1-1**) and parts with micro/nano surfaces manufacture (see **Figure 1.1-2**).

Because of the replication nature of moulding processes, the accuracy needed for micro moulded components manufacture must be ensured by means of a metrological approach to surface replication and dimensional control of both tools and replicated parts ([3]-[7]).

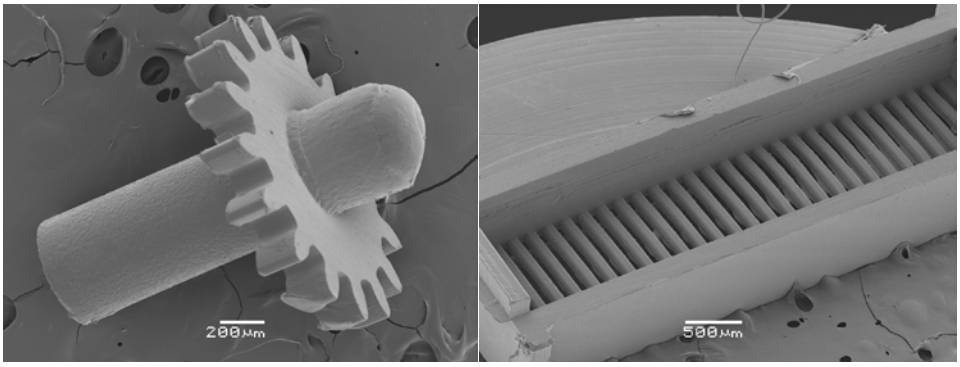

Figure 1.1-1. Three dimensional micro moulded parts: a micro gear (left) and a micro filter (right).

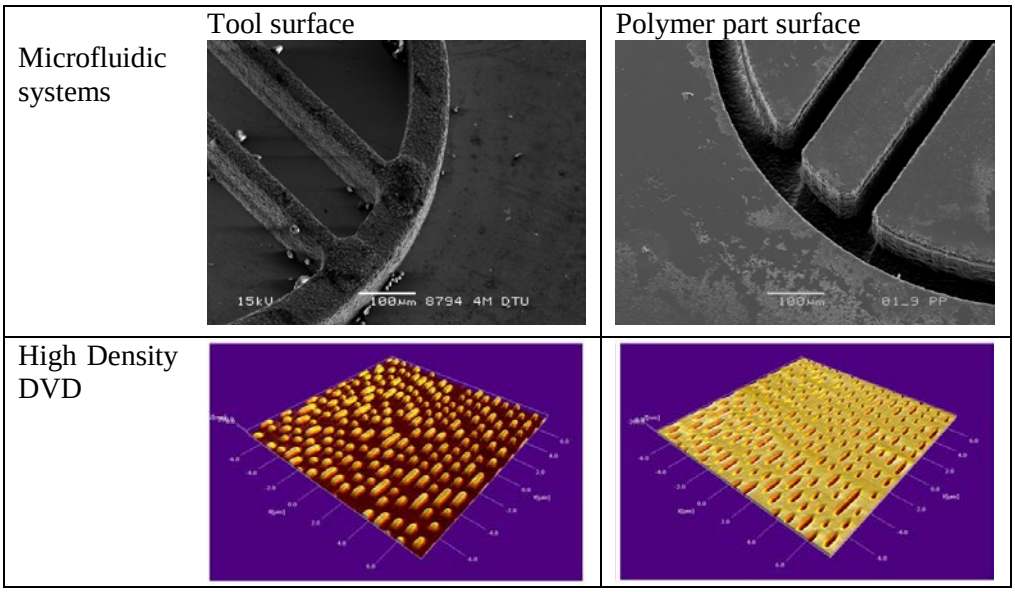

Figure 1.1-2. Precision moulded parts with micro structured surfaces (microfluidic systems, top [3]) and nano structured surfaces (high density DVD, bottom [5]).

1.2 Motivation

Design methodology and concurrent tolerance guidelines are not yet available for advanced micro manufacture. Moreover, at present there are no common procedures that deals with the uncertainty evaluation of feature of size in the sub-millimetre scale. Hence, the development of design and tolerance guidelines is to be supported by metrology methods for the assessment of the measurement uncertainty.

The ambition of the PhD project was to develop and implement a complete metrological framework for advanced precision micro moulded products with micro/nano structured surfaces. Furthermore, it was also objective of this PhD project to develop methods for the dimensional and geometrical metrology of surfaces and micro/nano geometries across several length scales. In fact, when critical dimensions are scaled down and geometrical complexity of objects is increased, the use of a single measurement technology is not sufficient and, as a consequence, design rules for advanced micro manufacture must take into account both process capabilities as well as the capabilities of the measurement equipment used to ensure the production consistency.

1.2.1 Problem identification

The objectives of the PhD project were achieved by applying a systematic approach based on dimensional and geometrical metrology, advanced measurement process analysis and optimisation, statistical analysis, measurement uncertainty modelling, assessment and application to tolerance specification at the micro/nano dimensional scale.
Focus was given to quality assurance of precision moulding and the associated tooling processes.
The tasks comprised:

1. Development of traceable metrology procedures for the characterisation of ultra-smooth and micro/nano structured surfaces.
2. Development of traceable methods allowing for metrology across several length scales on the same components.
3. Development of traceable indirect methods for metrology of above mentioned features.
4. The developed metrology methods were applied as tool for both product (i.e. compliance with specifications) and measurement capability.

1.2.2 Project objectives and scientific methods

The project comprised the following subjects.

Metrology for micro injection moulded components

The precision moulding process was investigated for both micro moulded components and micro/nano structured surfaces, defining the metrological requirements for accurate surface and dimensional replication as well as the measurement process capability. The metrology of injection moulded parts (including dimensions, topography, and tolerances), the link with functionality of µIM components and micro tool accuracy was proven on miniaturized components with sub-millimetre dimensioning and tolerances in the (1-10) µm range.
Research focused on three-dimensional micro components, tolerance allocation and micro structured surface characterisation, developing metrological tools and methods from the millimetre- down to the single-digit micrometre-scale. The metrological capability and the process/product requirements study were supported by a thorough investigation on tolerancing rules for micro and micro/nano structure.
The developed metrology methods were applied to selected study cases of industrial relevance.

Metrology for moulded components with surface finishing at the nanoscale

High precision injection moulded components with micrometre accuracy and surface finishing at the nanometre scale allowed to develop methods for the metrology of the injection moulded parts and surface characterisation at the nanometre scale (including dimensions, topography, and tolerances). Research focused on three-dimensional components and surface characterisation, developing metrological tools and methods from the millimetre- down to the 10 nanometre-scale. Furthermore, the quality of the produced items, especially the accuracy with which the tool surface is copied was investigated for workpieces with micro- and nanostructures on the surface, to ensure that functionalities associated with the design were transferred to the final component as well as the surface roughness.
The developed metrology methods were applied to selected study cases of industrial relevance.

Calibration, traceability at the micro- and nanoscale

A successful verification of a tolerance (also at micro and nanoscale) requires establishment of traceability of the method including the estimation of measurement uncertainty [6]. Calibration procedures and reference artefacts (used in the calibration procedure) were employed in order to decrease (as much as possible) the measurement uncertainty.

1.2.3 Collaborations

The collaboration with Danish and European companies provided the basis for verifying the metrology methods applied to µIM components and for surfaces characterisation at nanoscale. Several study cases of industrial relevance were selected on which the overall investigation was

carried out. The statistical analysis finalised to the uncertainty calculation was a leading task in such activities. Specifically, two collaborations are worth to be mentioned. The European Hi-Micro project and the CIRP international comparison of optical surfaces.
Hereafter these activities are described in detail.

Hi-Micro

The project "Hi-Micro, High Precision Micro Production Technologies" (www.hi-micro.eu) was a Collaborative Research Project supported by the European Commission in the 7th Framework Programme (FP7-2012-NMP-ICT-FoF: 314055).
Aim of the EU project "Hi-Micro" was to realise an innovative approach for the design, manufacturing and quality control of micro components (nominal size less than 1 mm) in order to achieve mass production of precision 3D micro-parts. Manufacturing technologies (additive manufacturing, µ-EDM, and µ-ECM), micro-milling, metrology and quality control were essentials subjects.

CIRP international comparison of optical surface measurements

The comparison was conceived and realized within the context of the well-known International Academy for Production Engineering (CIRP).
The aim of the comparison was to identify the state-of-the-art measurement capability of optical areal surface topography measurement instruments for polymer surfaces roughness, in laboratory conditions, with knowledgeable operators.
Four physical measurement standards were selected and, successively, replicated in an injection moulded process using a commercially available thermoplastic resin. The polymer surface roughness was compared by means of the replicas. The analysis of the comparison results considered the calculation of *Sa*, *Sq*, *Sdq* surface texture parameters (using the same software), the related uncertainties and the *En*-value.

1.3 Structure of the work

The thesis consists of nine chapters. Besides this introduction, conclusions, state of the art of dimensional and geometrical micro nano metrology and state of the art of moulding processes, the research work carried out is collected in five chapters. They are shortly introduced in the following.

- *Uncertainty assessment for micro nano dimensional and topographic measurements* (Chapter 4).
  A complete procedure for post-processing of optical measurements, consequent statistical analysis and uncertainty evaluation is described in the chapter. Specifically, the uncertainty evaluation was developed according to the well-known frequentist approach, implemented and verified, for the first time, for micro/nano dimensional and topographic measurements.
- *Shrinkage calibration method for formulation of multiscale dimensional tolerance specifications* (Chapter 5).
  A novel method for the formulation of specification intervals (tolerances), developed by the author, is presented in this chapter. The method is based on the quantification of the shrinkage. It was applied and validated in the case of a micro powder injection moulding production, nonetheless, it is of general validity for any process in which the material undergoes a change in dimensions due to a phase transformation.
- *Replication assessment of polymer surfaces at sub-micrometre scale* (Chapter 6).
  The chapter investigates the replication fidelity of different moulded specimens, introducing several metrological techniques for analysing a replication process and evaluating the replication fidelity uncertainty.
- *International comparison on surface texture of polymer artefacts using optical instruments* (Chapter 7).

The already mentioned CIRP international comparison is summarised in this chapter, analysing the performance of the three most common optical instruments working principles, i.e., imaging confocal, focus-variation and coherent scanning interferometry.

- *Performance verification of optical instruments for surface topography measurements* (Chapter 8).
  This chapter, instead, shows some limits in the performance of a laser scanning confocal microscope, a focus-variation microscope and a point autofocus instrument, in specific circumstances.

References

[1] Hansen HN, Carneiro K, Haitjema H, De Chiffre L 2006 Dimensional Micro and Nano Metrology *CIRP Annals – Manufacturing Technology* **55-2** 721-743

[2] Heckele M, Schomburg W K 2004 Review on micro molding of thermoplastic polymers *J. of Micromechanics and Microengineering* **14-3** R1-R14

[3] Tosello G, Marinello F, Hansen H N 2012 Characterisation and analysis of microchannels and submicrometre surface roughness of injection moulded microfluidic systems using optical metrology *Plastics, Rubber and Composites: Macromolecular Engineering* **41-1** 29-39

[4] Hansen H N, Hocken R, Tosello G 2011 Replication of micro/nano surface geometries *CIRP Annals – Manufacturing Technology* **60-2** 695-714

[5] Tosello G, Hansen HN, Marinello F, Gasparin S 2010 Replication and dimensional quality control of industrial nanoscale surfaces using calibrated AFM measurements and SEM image processing *CIRP Annals – Manufacturing Technology* **59-1** 63-568

[6] Tosello G, Hansen H N, Calaon M, Gasparin S 2014 Challenges in high accuracy surface replication for micro optics and micro fluidics manufacture *Int. J. Precision Technology* **4** 122-144

[7] Theilade U A, Hansen H N 2007 Surface microstructure replication in injection molding *Int J Adv Manuf Tech* **33** 157-166

Chapter 2

Metrology for advanced precision moulding technologies

2.1 Introduction

As already pointed out in Chapter 1, the manufacture of micro moulded components requires accurate metrology for surface replication and dimensional control of both tools and replicated parts. Design rules for advanced micro/nano manufacture that deals with increased dimensional and geometrical complexity of produced parts must take into account the capabilities of the measurement equipment and the evaluation of the uncertainty.
In the following, instruments and methods currently available for the metrology of micro and nano manufactured parts are provided. Specifically:

- Measurement instruments.
- Calibration, traceability and uncertainty evaluation.
- Tolerance intervals specification.
- Definition of the surface texture parameters used in the thesis.

2.2 Instrumentation for micro and nano metrology

The equipment for micro/nano dimensional and geometrical measurements is described according to the following classification [1]-[3]:

- Micro-topography measurement instruments, which include
  - Contact instruments.
  - Scanning probe and particle beam microscopy.
  - Optical scanning instruments.
  - Areal optical instruments.
- Coordinate metrology.
- Interferometry.
- Computer tomography.

The capabilities of the major working principles are summarised in **Figure 2.2-1**; the measurement range of each working principle is given as a box, in which the lateral range is function of vertical one.

2.2.1 Contact instruments

These instruments have a probe (stylus) that is physically in contact with the surface under measurement. The vertical movement of the stylus is converted into an electrical signal by a transducer. The probe is usually a diamond tip with a cone angle of 60° or 90° and a radius in the range (1-10) μm [1], [4]. The main drawback of contact instruments is that, due to their size, some probes do not completely penetrate into the valleys of the surface texture. In addition, the force applied by the probe can produce plastic deformation (scratches) in soft or polished surfaces [5]. Moreover, areal acquisitions may require extensive measuring time [2].

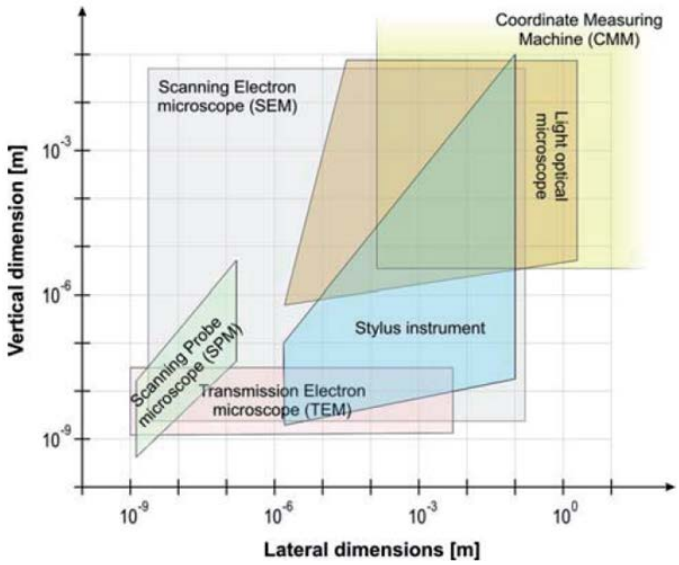

Figure 2.2-1. Measurement range—lateral range vs. vertical range—of the instruments main working principles for dimensional and geometrical micro/nano metrology [1].

2.2.2 Scanning probe and particle beam microscopy

In this class two main sub-categories can be identified for measurements in the nanoscale: Scanning Probe Microscopy (SPM), electron microscopy (SEM, TEM).

Scanning probe microscopy

A probe, with a radius of a few nanometres and connected to a piezoelectric scanner, is used to scan in close proximity of a surface but without a direct contact. Hence, it is considered a non-destructive technique. It is suitable for measurements of several materials like metals, semiconductors or biological specimens.

Based on the type of interaction between the probe and the surface under measurement, the following systems can be recognised:

- Scanning Tunneling Microscopes (STM) (quantum-mechanical tunnelling effect).
- Atomic Force Microscope (AFM) (intermolecular forces).
- Near-field Scanning Optical Microscope (NSOM) (near-field laser beam).

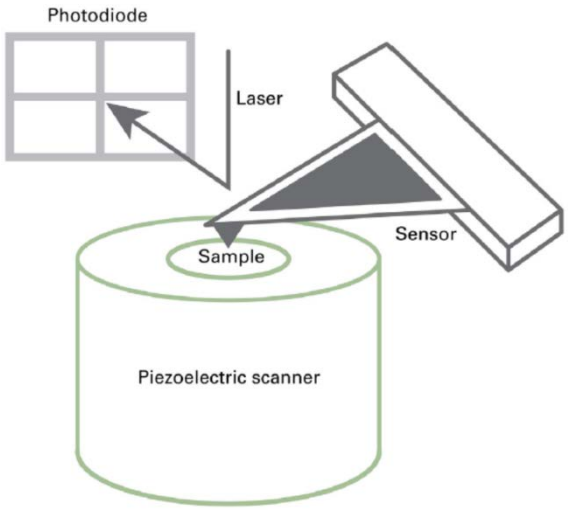

Figure 2.2-2. Schematic image of an Atomic Force Microscope (AFM) [2].

Atomic Force Microscopy (AFM) is the most common among SPM technologies (see **Figure 2.2-2**). The probe, a tip some microns long and with a radius often less than 10 nm, is located at one end of a cantilever that has a length normally between 100 μm and 400 μm.
During a measurement, the tip is subjected to an equilibrium of forces (elastic force of the cantilever and repulsive forces of electric (intermolecular) nature), with resultant force sensitivity in the range (10^{-7}-10^{-12}) N that allows for vertical deflections of the probe while scanning, which are detected by means of an optical system. The measurement scanning area is typically 100 μm × 100 μm, or less, and the vertical range less than 10 μm. The vertical resolution is about 0.1 nm, while the lateral resolution for most AFMs is usually from 2 nm to 10 nm [1].
It is worth to mention a new AFM, Metrological Large Range Atomic Force Microscope (Met. LR-AFM), developed at the German National Metrology Institute (Physikalisch-Technische Bundesanstalt, PTB) [6], which is capable of direct scanning of large areas within a measurement volume of 25 mm × 25 mm × 5 mm. Interesting scanning functions have been implemented, allowing different measurement settings, e.g. step height, lateral pitch, nano-roughness and other nano features.
Furthermore in [7], by a non-raster measurement approach, a SPM was realised as a coordinate metrology system. The probe scans points along free paths on the surface under measurement, achieving similar accuracy of common systems with scan time reduction. Moreover, probes with advanced geometries were developed for characterisation of structures normally not accessible by standard probes (see **Figure 2.2-3**).

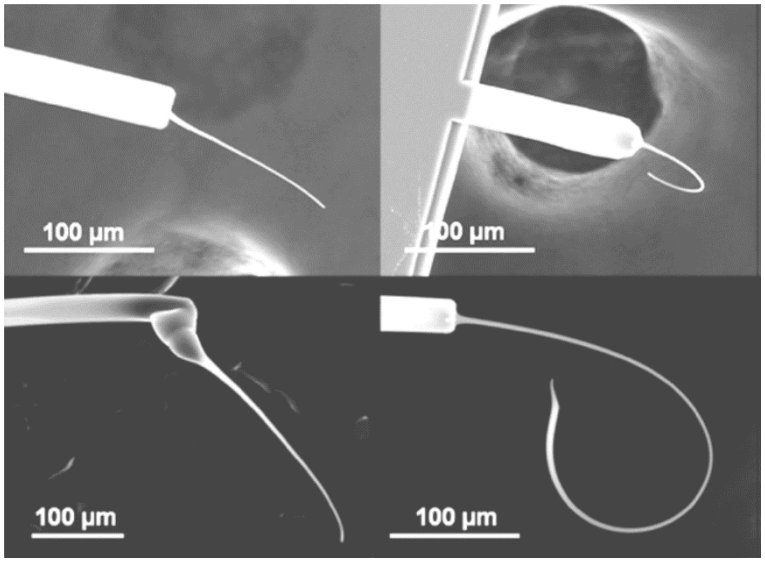

Figure 2.2-3. Four different probes realized with different tip geometries [7].

Scanning Electron Microscope (SEM):

The surface of the specimen under measurement is scanned by an electron beam. When electrons hit the specimen, a characteristic x-ray radiation is emitted which, collected by an x-ray detector, allows for the measurements of physical and chemical properties of the specimen (see **Figure 2.2-4**).
Typical image magnifications that can be achieved are in the range 100×-100000×, with a resolution down to 2 nm, large field of field, long working distance, elemental analysis capability and minimum diffraction effects [8]. SEM can also be used for qualitative image analysis due to its significant visualisation of the specimen under measurement [1]. It provides high resolution imaging with high depth of focus for characterisation of cross-sectional specimens, particle and defect analysis. However, the dataset extracted is inherently 2D and no height information is achievable (unless reconstruction from stereo pairs or triplets of SEM images). Other disadvantages are the need for measurement in high vacuum condition, a relatively low

throughput and a potential consequent to the specimen charging, which cause and image degradation [9].

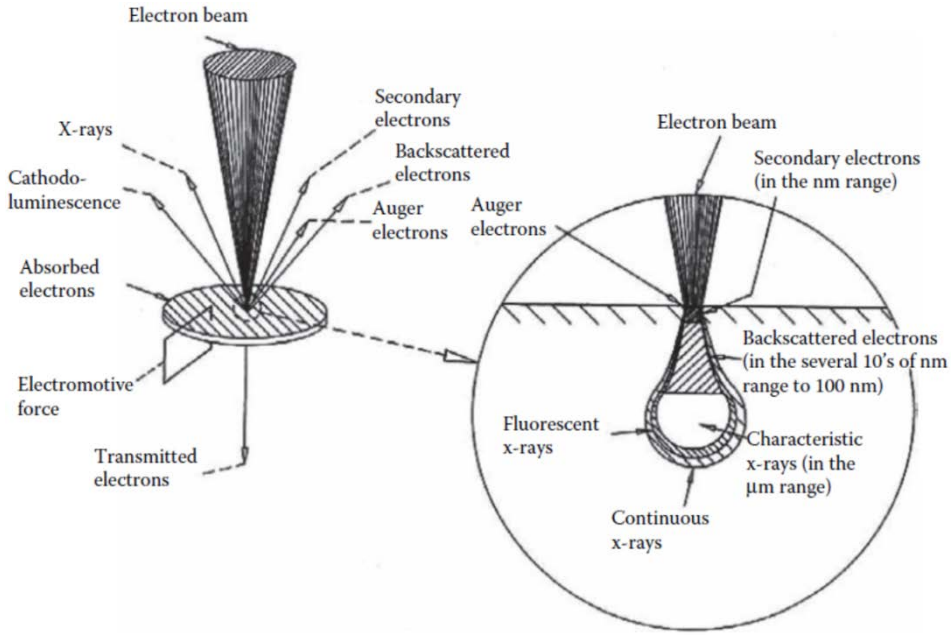

Figure 2.2-4. Close up of the contact point of the electron beam [5].

Transmission Electron Microscope (TEM):

An electron beam is operated according to the same basic principle of an optical microscope. This allow TEM to spread the electron beam over the whole specimen (differently from SEM in which the focus is on only one spot at a time). The electron beam is directed through a series of lenses to the specimen and, after passing through the specimen, it is finally collected at the end of its optical axis. For this reason, a thickness in the range of (50-500) nm is required to limit the chromatic aberration due to energy loss. The resolution is about 0.05 nm with aberration-corrected instruments [2]-[5].

2.2.3 Interferometry

Interferometry is based on the analysis of the interference pattern created by the combination of two or more waves. Different interferometric configurations exist. Many of them are variants of a basic setup, which is the Michelson interferometer shown on the left of **Figure 2.2-5**.
S is a point source, *A* a beam splitter, *B* the detector of the interference fringes, *C* a compensator and M_1, M_2 are retro-reflectors.
The Twyman-Green principle is a modification of the Michelson interferometer: the point source is positioned in the focus of a well-corrected concave lens (on the right of **Figure 2.2-5**). This configuration has almost the same optical path for both beams, making it suitable for white light interference. However, this pattern is sensitive to turbulence and vibration.
In both cases, the measurement of the displacement is carried out by counting the number of fringes according to the movement of the specimen under measurement. Photodetectors and digital electronics are used to count the fringes [2].
The most common interferometers are homodynes, which use a single laser beam f_1 (on the left of **Figure 2.2-6**) and heterodynes which use a dual-frequency laser source containing two orthogonal polarizations, one with a frequency f_1 and the other with a frequency f_2, (on the right of **Figure 2.2-6**). In the homodyne systems, the reference and the measurement beams are split at the interferometer and not inside the laser, therefore, the light can be delivered to the interferometer via a standard fibre optical cable [2].

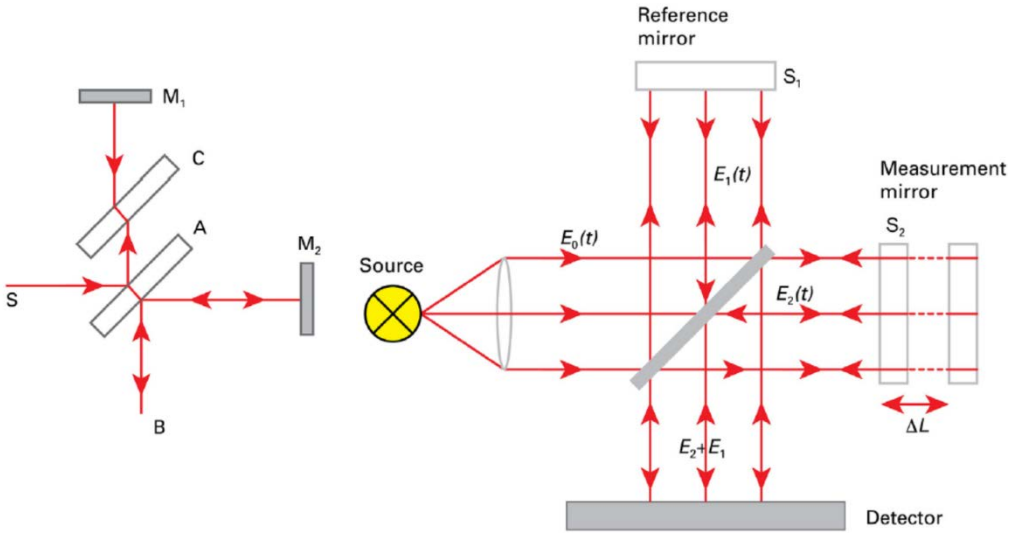

Figure 2.2-5. Left: schema of the original Michelson interferometer. Right: schema of a Twyman-Green interferometer [2].

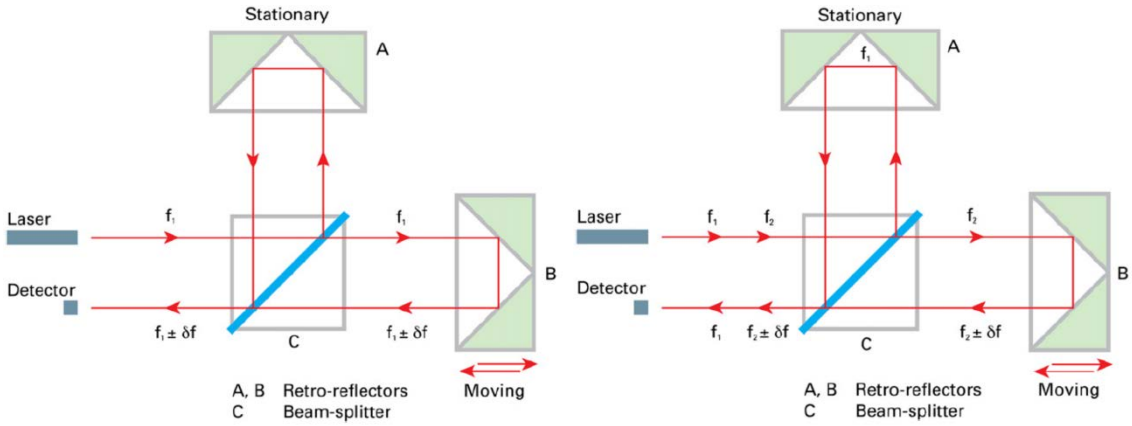

Figure 2.2-6. Left: homodyne interferometer configuration. Right: heterodyne interferometer configuration [2].

The resolution is in the range of (0.1-10) nm, obtained in the direction of the beam propagation, i.e., interferometers are 1-D instruments. The measurements range depends on the coherence length of the source (300 nm for white light, centimetres for spectral lamps and (1-10) m for commercially available laser interferometers) [1].
The error sources which are proportional to the displacement being measured are called cumulative errors; non-cumulative errors if they are independent from the length being measured. Typical errors are [2]:

- Thermal expansion of the metrology frame, proportional to the displacement.
- Refractive index of air, when it is not measured and a theoretical value is used.
- Dead-path length: distance in air between the reference, the measurement reflectors and the beam-splitter.
- Cosine error: despite how perfectly aligned the system appears to be, there will be always a small, residual error that will cause a shorter measurement.
- Non-linearity in the relationship between the measured phase difference and the displacement.

Other error sources, such as acoustic vibration, air turbulence and electronic noise, are described in [2].
Interferometers are used for calibration of 1-D scales, in chip production for wafer-steppers and scanners, as direct traceability when detecting the displacement of the axes in micro and nano coordinate metrology and as link to the primary standards for laser interferometer systems [1].

2.2.4 Optical instruments

The optical instruments in this sub-section are divided in scanning optical instruments and areal optical instruments [2], [3] and [10]. The first class includes triangulation instruments, confocal instruments and point autofocus instruments. The other class groups instead focus-variation instruments, digital holographic microscopy, phase-shifting interferometry and coherence scanning interferometry [11].
Optical instruments perform non-contact measurements, hence, they have the advantage of not damaging the surface of the specimen under investigation. Furthermore, they have relatively high resolution in the vertical direction and can acquire relatively large areas in a reasonable time [12]. On the other hand, dimensional measurements can be limited by the optical diffraction of lights. Furthermore, when an objective lens is used, the optical resolution is restricted by the wavelength of light used but also by the numerical aperture A_N of the optical system, which determines the theoretical maximum slope on the surface that can be measured (Equation (2.2-1)).
In a medium with refractive index n, the maximum accepted angle into the objective is the angle α, given by

$$A_N = n \cdot \sin a \tag{2.2-1}$$

Hence the optical resolution of the objective, i.e., the minimum distance between two lateral features on a surface that can be measured, is given by

$$r = \xi \frac{\lambda}{A_N} \tag{2.2-2}$$

where λ is the wavelength of the incident radiation and ξ is a constant depending on the criterion used for the evaluation of the resolution. The most common ones are the Rayleigh criterion (for non-coherent systems) and the Sparrow criterion (for coherent systems) [2], [13].

2.2.4.1 Optical scanning instruments

Triangulation instruments

Triangulation instruments measure the relative distance to an object or surface as it is shown in **Figure 2.2-7**.
The typical height resolution is 100 nm over several mm of vertical range. For this reason, they are suitable for measuring surfaces with relatively large structure such as paper fabric [14] and road surfaces [15]. When measuring small features, limitations are due to the laser beam which varies throughout the vertical range acting as averaging filter.

Confocal microscopes

A monochromatic light source is normally used in this configuration. Unlike other microscopes, confocal instruments has two special filters (see **Figure 2.2-8** and **Figure 2.2-9**), namely two pinholes, along the optical path: one after the light source and one before the detector [82]. The pinholes discards the light which is not in focus, increasing the lateral optical resolution. The optical resolution can further be increased with the pinholes by limiting the field of view to an area smaller than the limit of Equation (2.2-2). Vertical measurements range is therefore limited by the working distance of the objective and so by the A_N. Increased working distance, governed by the microscope objectives, decreased the A_N resulting in reduced lateral and axial resolution.
The instruments scan vertically within a certain range. Hence, the height is determined by fitting the data corresponding to a maximum intensity [2], [10].

Advantages of this method are the possibility of using objectives with high A_N, high lateral resolution and low influence of the surface colour. Conversely, drawbacks of this system are longer measuring time, with respect to non-scanning instruments, due to light beam scanning and short working distance of the objective that raise the risk of collision on the surface.

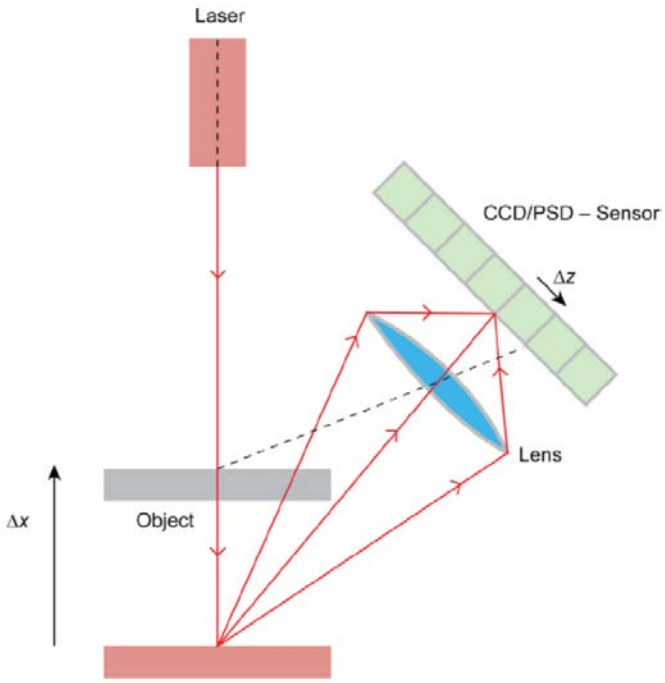

Figure 2.2-7. Principle of a laser triangulation sensor [2].

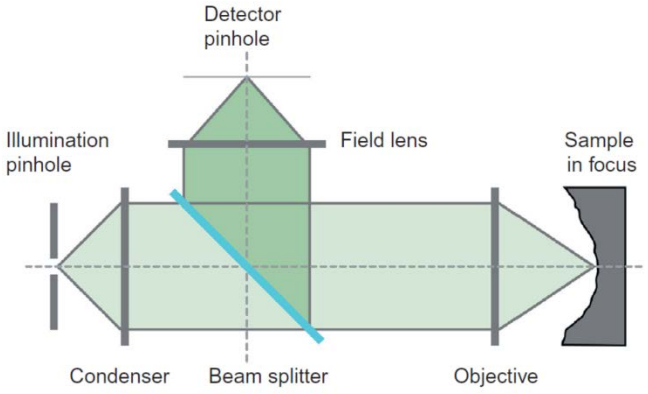

Figure 2.2-8. Confocal set up with object in focus [2].

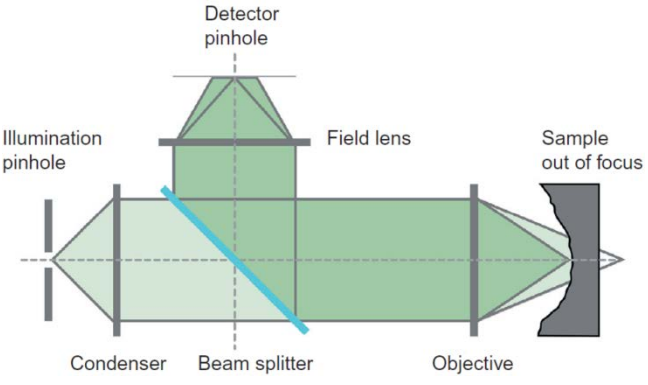

Figure 2.2-9. Confocal set up with object in focus [2].

Chromatic Confocal Microscopes

A non-scanning version of the confocal microscopes adopts non-monochromatic light and consequently chromatic objective lens, with a reduced numerical aperture but also an increased working distance. A different focus distance is due to different wavelengths. The advantage is that there is no vertical scanning. The vertical range is limited by the difference between the focal distance of the shortest optical wavelength and the longest one, resulting in a faster acquisition with respect to the scanning version. However, it has lower vertical resolution and can be influenced by the colour of the surface [10].

Point autofocus instruments

The point autofocus working principle can be implemented by several methods. The one described here is known as *beam offset* method (see **Figure 2.2-10**). It consists of a laser beam source illuminating the specimen under measurement. Both input and reflected beams pass through the optics but at two different sides of the objective, shifted symmetrically (*offset*) with respect to its optical axis. The *offset* axis positive direction is from the input beam towards the reflected beam and it can be oriented in an angle between 0º and 90º with respect to the *x* and *y* axis of the instrument reference system. When the objective nose is rotated to 0º the *offset* axis is oriented as the *-x* axis. Conversely, when the objective nose is rotated to 90º the *offset* axis is oriented as the *y* axis[1].

The working principle is implemented by the so-called *autofocus* sensor which checks the reflected beam for unbalancing. The beam not in focus, in fact, produces a displacement on the *autofocus* sensor that is counter-fed to adjust the relative vertical position of the objective lens, inherently measuring the height (see **Figure 2.2-11**).

Such system is independent of surface colour and transparency. Limitations are limited lateral resolution constrained by the objective optical resolution and long measuring time for areal acquisitions [10].

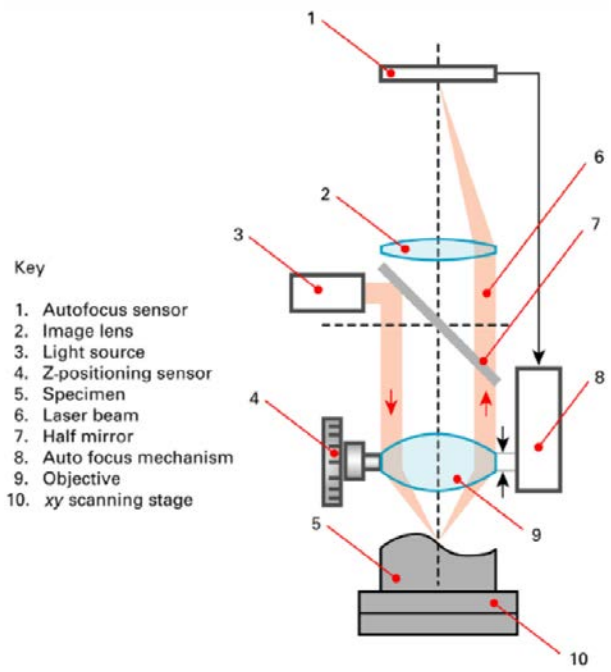

Figure 2.2-10. Point autofocus instrument [2].

[1] The previous considerations implicitly assume that the optical axis of the objective is in a vertical position. Nonetheless, it is also allowed to be set it in horizontal position, i.e., parallel to the *x* axis.

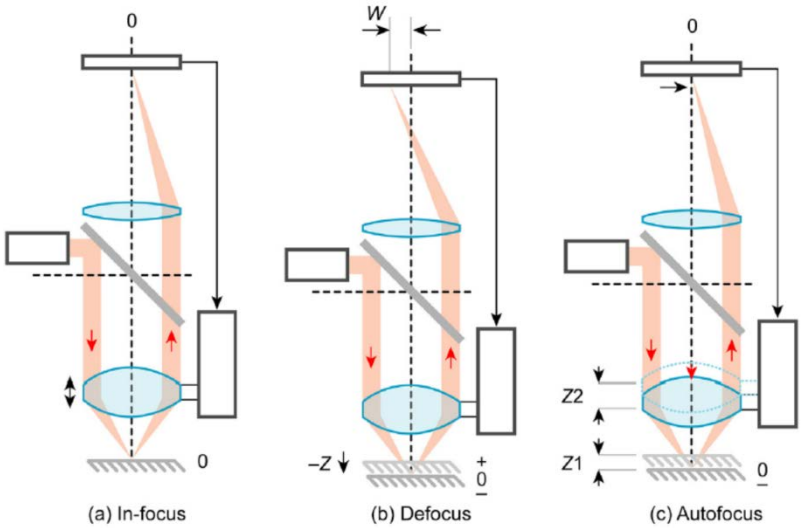

Figure 2.2-11. Principle of point autofocus operation [2].

2.2.4.2 Areal optical instruments

Focus variation instruments

The focus-variation working principle (see **Figure 2.2-12**) combines a small depth of focus with a vertical scanning by the objective lens, sweeping the focus along the vertical features of a surface and continuously capturing data. In this way, topographical and colour information are provided. In addition, the maximum detectable slope is not dependent on the numerical aperture of the objective. Different illumination sources and the focus-variation system allow for measurements of slope angle exceeding 80°. The vertical resolution depends on the chosen objective but not upon the scan height and it can reach 10 nm. The focus-variation working principle requires that the focus varies sufficiently during the vertical scanning in order for surfaces and structures to be detected and reconstructed. Hence, transparent specimens or components with low local roughness cannot be measured [16].

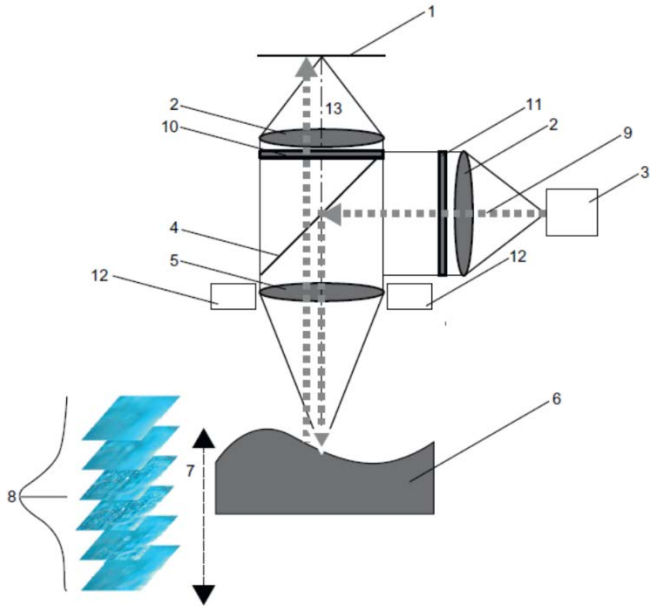

Figure 2.2-12. Schema of a focus variation instrument. 1, sensor; 2, optical components; 3, white light source; 4, beam-splitting mirror; 5, objective; 6, specimen; 7, vertical scanning; 8, focus information curve with maximum position; 9, light beam; 10, analyser; 11, polariser; 12, ring light; 13, optical axis [2].

Digital Holography Microscopes

Digital Holography Microscopy (DHM) is an areal measurement method in which a hologram is the results of the interference of a reflected light beam (from the surface under measurement) with the reference one. The interference pattern is reconstructed as the original light field, obtaining the hologram (see **Figure 2.2-13**). The vertical resolution of this instrument depends on the wavelength of the light. A value down to 0.1 nm can be obtained since there is no mechanical scan. Furthermore, the system is insensitive to vibrations, it provides high speed measurement and allows for measurement of transparent specimens. On the other hand, it is subject to parasitic interference and noise, and it is limited by the scattering, above all from thin surfaces of the specimen under measurement [10].

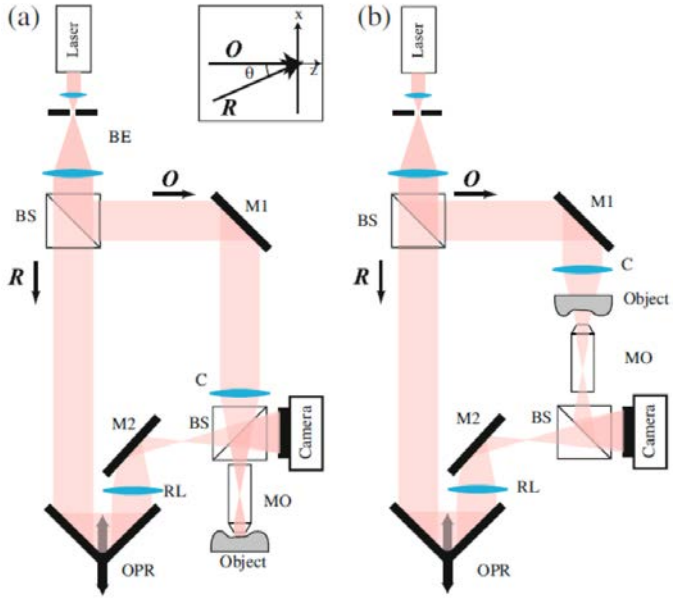

Figure 2.2-13. Basic DHM architectures in (a) reflection and (b) transmission configurations. BE, beam expander; BS, beam-splitters;M1,M2 mirrors; OPR, optical path retarder; C, condenser lens; RL, lens in the reference arm; camera, digital camera (CCD, CMOS); MO, microscope objective; ***R***, the reference wave and ***O*** the object wave. Inset, details of the off-axis geometry defined by the angle θ between ***R*** and ***O*** [10].

Phase-Shifting Interferometry (PSI)

Measurement by interferometric technologies involves the analysis of interference fringes between incident light from the specimen under measurement and reference light.

Many instruments use phase detection in their working principles. In particular, interference methods, both homodyne and heterodyne methods, are used by Phase-Shifting Interferometry (PSI) and Coherence Scanning Interferometry (CSI).

PSI consists of an interferometer integrated into a microscope (see **Figure 2.2-14**) [2], [10]. Within the interferometer, a beam-splitter directs one beam to a reference path, which has a number of optical elements including an ideally flat and smooth mirror from which the light is reflected. A second beam is directed to the specimen surface where it is reflected. The two beams return to the beam-splitter where they recombine and form on the imaging sensor array (camera) an image of the measured surface with a superimposed interference pattern.

PSI instruments can have two different configuration, Mirau and Linnik interferometers, depending on the microscope objective, (see **Figure 2.2-15**). Mirau is more compact and needs less adjustment than Linnik. However, in Linnik configuration, the central area of the objective is not blocked and no space underneath the objective is needed for attaching an extra mirror and beam splitter. Therefore, with the Linnik objective, magnifications and resolutions are the highest among standard optical microscope objectives. PSI instruments can have sub-nanometre

resolution and repeatability. Nonetheless, it is very difficult to determine their accuracy, which is greatly dependent on the surface under measurement.
Many PSI instruments usually require adjacent points on a surface with a height difference of at least $\lambda/4$. The range of PSI is limited to one fringe, or approximately half the central wavelength of the light source, so PSI instruments are usually used for measuring approximately flat surfaces (as a rule of thumb, only surfaces with an *Ra* or *Sa* less than $\lambda/10$ would be measured using PSI) [2], [10].

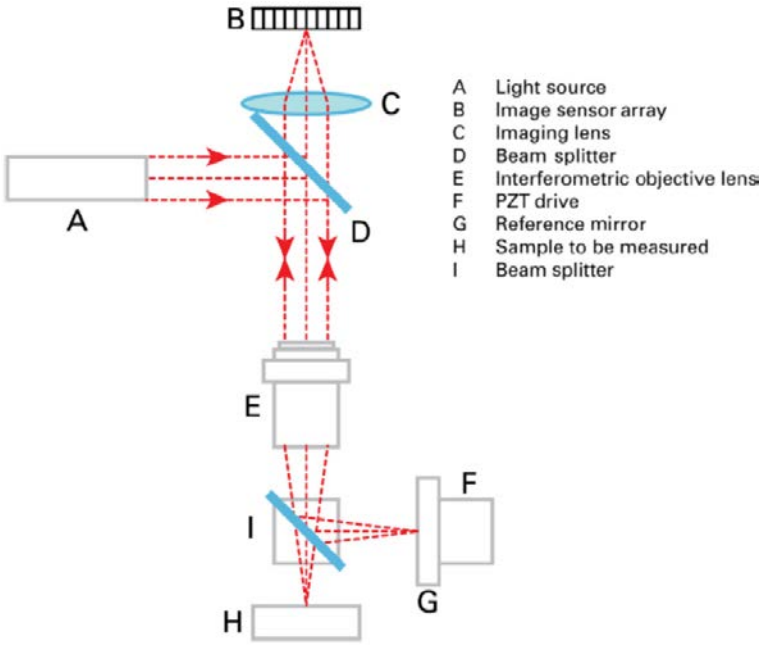

Figure 2.2-14. Schema of a phase shifting interferometer [2].

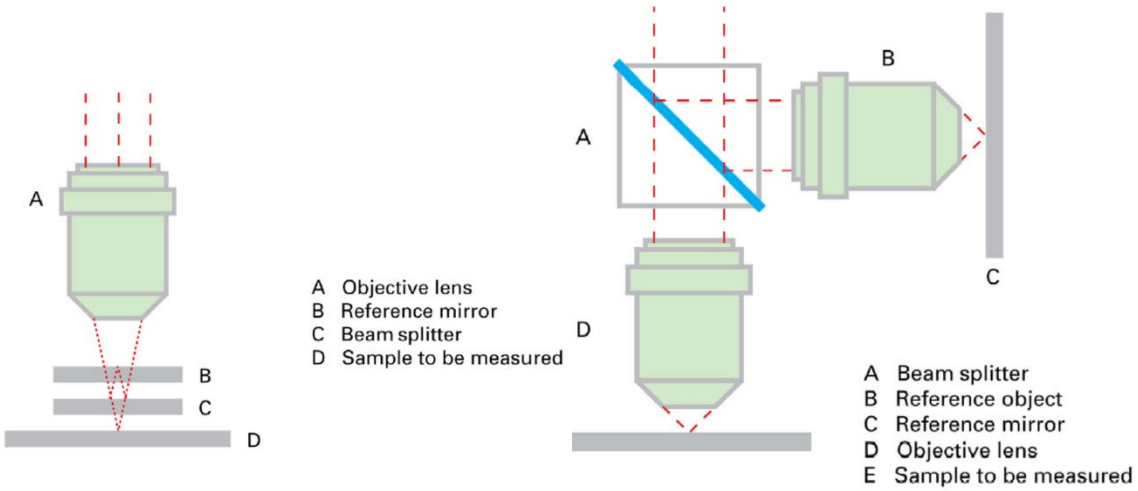

Figure 2.2-15. PSI different configuations [2]. Left: chematic diagram of a Mirau objective. Right: schematic diagram of a Linnik objective.

Coherence scanning interferometry (CSI)

CSI is also known as scanning white light interferometry. Due to the low coherence of the source (non-monochromatic), to observe interference, the length of the optical path to the specimen and the reference must be almost identical. The detector measures the intensity of the interference fringes as the optical path is varied in the vertical direction and finds the interference maximum (see **Figure 2.2-16**). CSI instruments can have sub-nanometre resolution and repeatability but, again, it is very difficult to determine their accuracy, which is dependent on the surface under measurement. Advantage of this system is a high vertical resolution. In addition, it can produce a complete 3D areal surface dataset by a single vertical scan using a Charge-Coupled Device (CCD) imaging sensor. Conversely, objective lenses have small A_N. Other limitations are reviewed elsewhere [17].

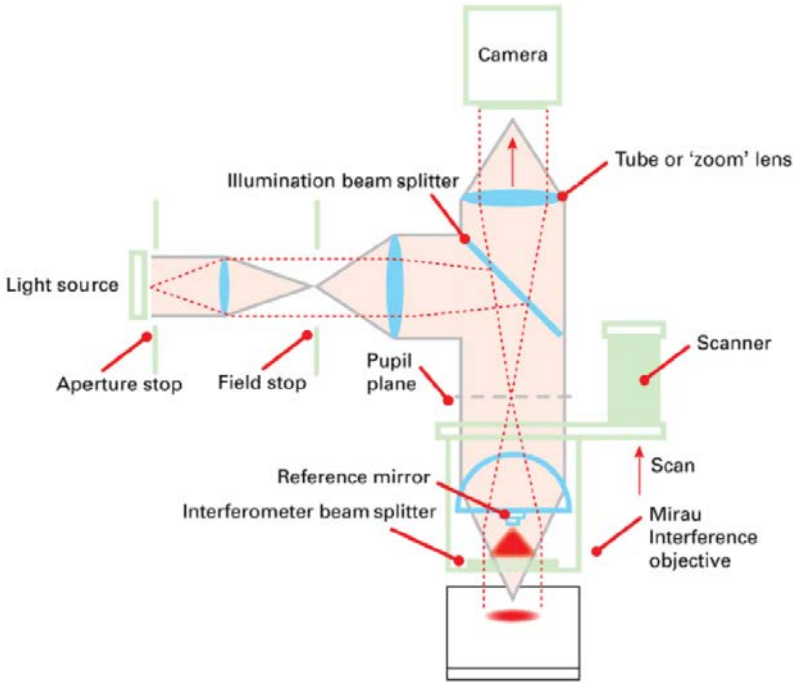

Figure 2.2-16. Schema of a coherence scanning interferometer [2].

2.2.5 Coordinate metrology

A Coordinate Measuring Machine (CMM) is commonly an instrument with a probe that measures single points on a specimen surface or scans a selected surface in order to continuously collect data as the probe is dragged across the part. The acquired points are then fitted in geometric entities. The probe in contact with the surface is usually a synthetic ruby ball and typical diameter dimensions are in the range of (0.5-10) mm [12].

In recent years smaller CMMs have been developed to enable 3D measurements of nanometre features, typically with ranges of tens of millimetres and tens of nanometres accuracy in *x*, *y* and *z* directions. Different micro/nano CMMs are described in [1]:

- Vermeulens Machine—Abbe principle (i.e., the measuring system of the displacement should be in line with the functional point, whose displacement is to be measured. If this is not possible, the slide-ways that transfer the displacement must be used to calculate the consequences of the offset [18]) is satisfied in two axis, the use of linear scales is enabled by using an intermediate body. Air bearings are involved. The measuring volume is 100 mm × 100 mm × 100 mm [19]].
- NPL Machine—it uses the movement scales of a conventional CMM with a high-accuracy probe with six degree of freedom. The working volume is 50 mm × 50 mm × 50 mm with a volumetric accuracy of 50 nm [20].

- Ruyls Machine—Abbe principle is satisfied in three axes. The measurement reference is a solid *zerodur* block that moves with the workpiece in three directions, while being measured by three-flat-mirror-laser interferometer systems. The measuring volume is 100 mm × 100 mm × 40 mm [21].
- Van Seggelens Machine (Eindhoven University)—it is a further improvement and miniaturization of the Vermeulens Machine.
  The measuring volume is 50 mm × 50 mm × 4 mm [22].
- Ilmenau Machine—it is equipped with three laser interferometers like the Ruyls Machine [23], [24].
- PTB Machine—it allows coordinate measurements on microstructures to be carried out with an uncertainty less than 100 nm.
  The measuring volume is 25 mm × 40 mm × 25 mm. It is available on the market [25].
- University of Tokyo—this device uses an optical scale to achieve high stability. It has a measuring range of 10 mm × 10 mm × 10 mm and a resolution of 10 nm [26].

Most micro CMMs usually have standard probe tips with a diameter of 0.3 mm, which is too large to measure MEMS structures or micro holes. Therefore, smaller probes have been developed. Silicon flexures, meshes or membranes are used to suspend the probe shaft in order to reduce the probing force. Probes consisting of multiple layers of electrical connections, strain gauges flexures, meshes or membranes are made using chemical etching or vapour deposition processes [2]. Probes equipped with piezoelectric strain sensors have been developed at the Eindhoven University of Technology (TUE) and at PTB, see **Figure 2.2-17** on the left. In this type of probes, a voltage signal is produced when a membrane deformation occurs. Due to high sensitivity of the membrane, they must be moved at very slow speed in order to avoid false readings [27], [25].
In a further attempt, probes which take optical measurements from illuminated glass fibres have been developed in order to reduce the surface damage caused by probe interactions, see **Figure 2.2-17** on the right. However, due to the surface forces, the probe tends to hold the head on the surface, even while the CMM head is retracting [28].

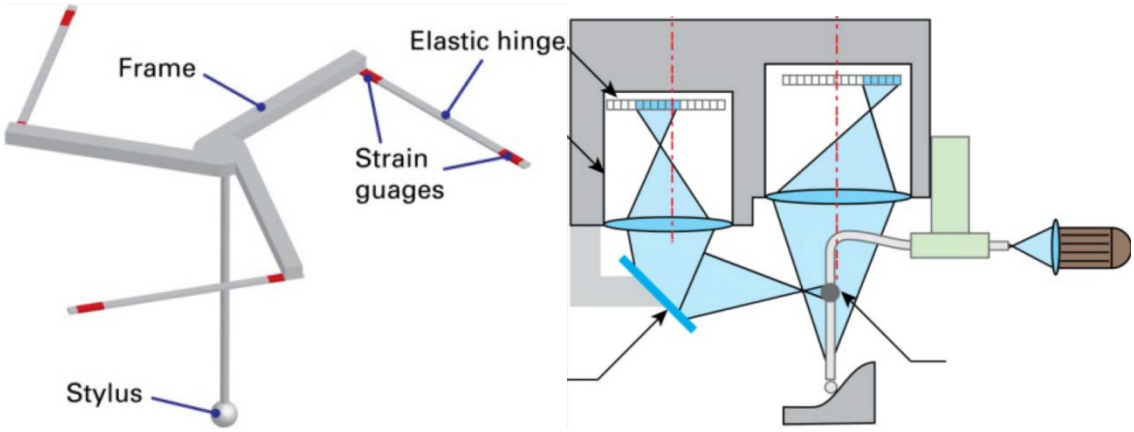

Figure 2.2-17. Left: Silicon micro-scale probe [12]. Right: A fibre probe [12].

Other probes are the vibrating probes that are forced to vibrate at a specific frequency. Any contact made with the surface under measurement produces a frequency shift, detected by a piezoelectric sensor, see **Figure 2.2-18** [29].

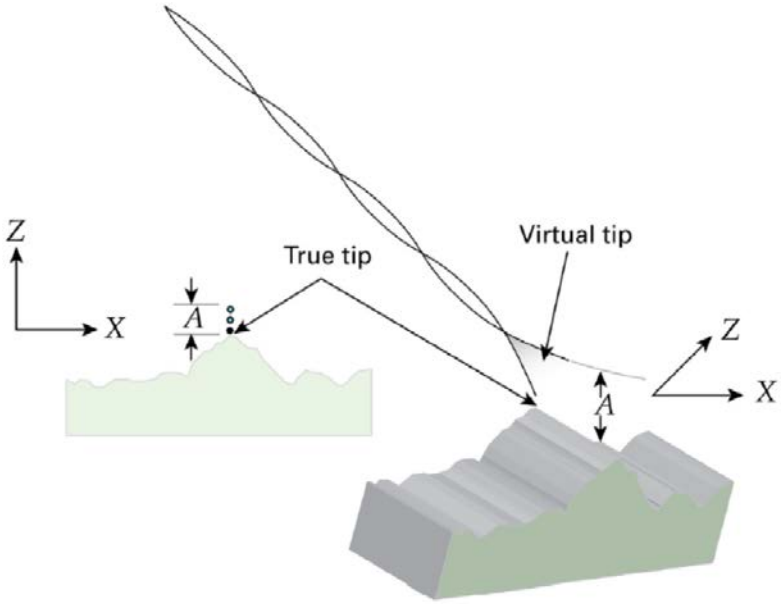

Figure 2.2-18. A vibrating fibre probe [2].

Further investigations were

- The National Physical Laboratory (NPL) three axis vibrating probe with isotropic probing forces [30].
- PTB high resolution, self-sensing and self-actuated probe was proposed for CMM and scanning force microscopy [31].
- Ilmenau University of Technology proposed a 3D tactile microscope with an optical detection system [32].

2.2.6 Computer tomography

In micro Computer Tomography (CT), a micro-focused x-ray source illuminates a specimen during the image acquisition. The specimen is rotated stepwise of 180° and images are recorded at each position, see **Figure 2.2-19**. Resolution down to 0.15 µm can be reached [12].
Recently, CT systems have been developed to replace classical CMMs or to be integrated in multisensory CMMs [33]. Machines' uncertainty has not been completely quantified, yet, due to their complexity, while some measurement uncertainties contributions have been assessed in [33] and [34].
These technologies give precise quantitative information on the whole structure of a body without destroying it within a short period of time [35]. This is what has made CT very interesting for testing and inspecting manufactured components like engine blocks, gear-boxes or even injection nozzles [36]. Hence, their main applications were for non-destructive testing and for dimensional measurements [37]. Other interesting industrial applications for CT are the analysis of fluid flows, fat content determination of meat and the analysis of the germination capacity of crops in the food industry [38].

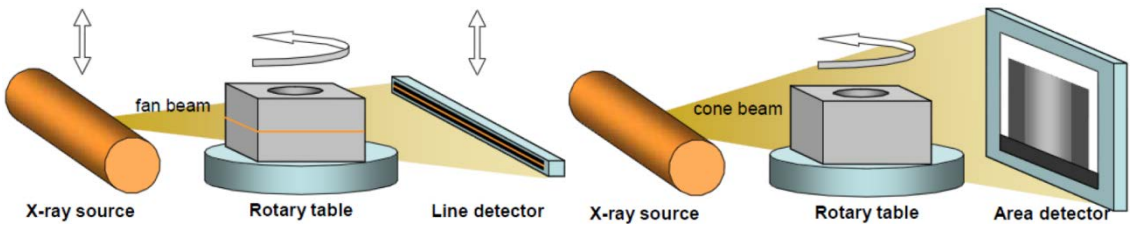

Figure 2.2-19. Schematic representation of industrial CT systems. Left: 2D CT using line detector. Right: 3D CT with flat panel detector [12]-[33].

2.3 Calibration, traceability and uncertainty evaluation

Traceability and calibration and are essential to verify and assure the consistency and the accuracy of the measurements [12].

Calibration is defined as "*operation that, under specified conditions, in a first step, establishes a relation between the quantity values with measurement uncertainties provided by measurement standards and corresponding indications with associated measurement uncertainties and, in a second step, uses this information to establish a relation for obtaining a measurement result from an indication*" [39]. The measurement uncertainty has a fundamental role and it is the information that differentiates "calibration" from "adjustment". The adjustment is a mechanical adjustment of the instrument itself or a software change. It consists in tuning some parameters in order to provide an indication that is closer to a known value [2]. "*A calibration may be expressed by a statement, calibration function, calibration diagram, calibration curve, or calibration table. In some cases, it may consist of an additive or multiplicative correction of the indication with associated measurement uncertainty*" [39].

Metrological traceability is in close connection with calibration. It is "*property of a measurement result whereby the result can be related to a reference through a documented unbroken chain of calibrations, each contributing to the measurement uncertainty*" [39], with the final purpose of achieving traceability to SI (International System of Units). Hence, uncertainty is an essential concept for ensuring traceability, too.

As an example, the metrological traceability to SI of a micrometer requires its calibration by a more accurate instrument or by a calibrated artefact (transfer standard or measurement standards or material measures), so that "*a documented unbroken chain of calibrations*" is established as shown in **Figure 2.3-1**. The chain consists of the following [4], [10]-[12]:

- The micrometer has to be calibrated using a gauge block.
- The gauge block was previously calibrated by a mechanical length comparator.
- This comparator would be calibrated by a more accurate gauge block which has been calibrated using an optical interferometer with a laser source.
- This laser source was calibrated by an iodine-stabilised laser that realises the definition of the meter.

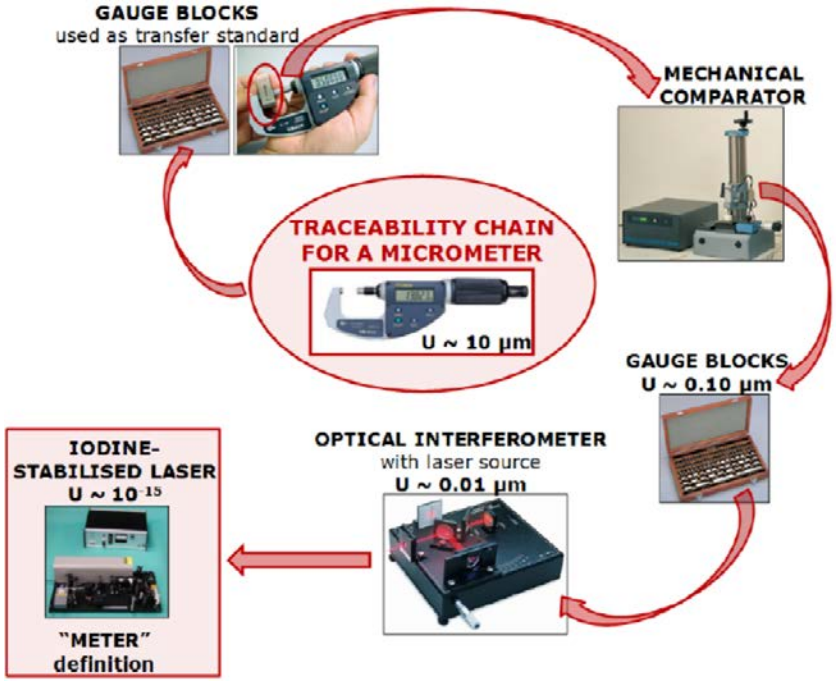

Figure 2.3-1. Traceability chain for a micrometer through primary meter, primary gauge block and workshop gauge block [12].

Different calibration artefacts are available in the micro- and nanoscale for both profile and areal methods. They are normally calibrated by primary instruments. Indication about the calibration of material measures can be found in

- ISO 5436-1:2000 [40]. It defines types of material measure according to the profile method.
- ISO 25178-701:2010 [41]. It defines types of measurement standard for the calibration of contact instruments for areal surface texture measurement.
- ISO 25178-70:2014 [42]. It defines types of material measure according to the areal method.

Furthermore, ISO 12179: 2000 [43] defines the methodologies to be applied for the calibration of contact instrument (repeated measurements, general instrument set-up and calibration certificate). Indication for the calibration of optical instruments are not available, yet. Nevertheless, such instruments can be used in a number of different measurement conditions, involving several uncertainty contributors. Therefore, an approach is to the calibration of optical instruments can be the so called "*task related*" uncertainty evaluation [44] which aim to establish the traceability for individual measurement tasks, where measurements strategy and conditions are specified [4]. The calibration of the *metrological characteristics* (MCs) of an optical instrument allow for the evaluation of an uncertainty contributor that can be related to a specific instrument and that can be used to establish a *task related* traceability. MCs are defined in ISO/DIS 25178-600:2016 [45]. When this thesis is being written, ISO 25178 part 600 is a draft not issued, yet. However, the same definitions can be found in the following ISO-standards related to specific optical working principles

- ISO 25178-602:2010 [46]. It specifies the design and metrological characteristics of a particular non-contact instrument for measurement surface texture using a confocal chromatic probe based on axial chromatic dispersion of white light.
- ISO 25178-603:2013 [47]. It describes the metrological characteristics of phase-shifting interferometric (PSI) profile and areal surface texture measurement microscopes.
- ISO 25178-604:2013 [48]. It specifies the metrological characteristics of coherence scanning interferometry (CSI) systems for 3D mapping of surface height.
- ISO 25178-605:2014 [49]. It describes the metrological characteristics of a non-contact instrument for measuring surface texture using point autofocus probing.
- ISO 25178-606:2015 [50]. It defines the metrological characteristics of a particular non-contact method measuring surface texture using a focus variation (FV) sensor.

Eventually, a review of available artefacts for micro-CMMs and method for verification, calibration and traceability can be found elsewhere [51].

2.3.1 Uncertainty evaluation

Different general approaches for the uncertainty evaluation are listed in the following [4], [12]. A review of the method available for areal surface texture measurement instruments is in [52]. Furthermore, specific approaches to the uncertainty evaluation for micro/nano geometrical and dimensional measurement are mentioned in the next § 4.1.

1. JCGM 100 [53]. The method is known as "Guide to the expression of Uncertainty in Measurement" (GUM). It is based on the well-known *frequentist approach*. It is usually considered a rigorous metrological method but, also, complex and time consuming and, for this reason, it is believed to be a method for calibration laboratories and National Metrology Institutes (NMIs).
   A completed procedure for micro/nano geometrical and dimensional measurement, based on the frequentist approach, is proposed and validated in the next Chapter 4.

2. ISO 14253-2:2011 [54]. The procedure is known as "Procedure for Uncertainty MAnagement (PUMA). It is an iterative and simplified approach of the GUM method. It can be summarised
   - Upper bound strategy (overestimation).
   - "Approximated uncertainty".
   - Intended for industrial users.
3. ISO 15530-3:2011 [55]. It is known as "substitution method" and it is intended for CMM. The following can be summarised
   - A number of calibrated measurement standards are needed.
   - Repeated measurements on calibrated measurement standards, in the same conditions of the actual measurands (alignament, handling, etc.), for estimating the influence of the instrument.
   - Repeated measurements on the actual measurands.
   - Calculation of uncertainty by simple formula.
   - Intended for industrial users.

   This method was modified, adapting it to optical instruments, and applied in the following Chapter 5, Chapter 6, Chapter 7 and Chapter 8.
4. Other approaches can be
   - Expert judgment.
   - Statistical estimation from measurement history.
   - Computer simulation.

Uncertainty budget according to GUM

According to the GUM, the ideal method for evaluating and expressing the uncertainty of a measurement result should be:

- Universal: the method should be applicable to all kinds of measurements and to all types of input data used in measurements.

The actual quantity used to express uncertainty should be:

- Internally consistent: it should be directly derivable from the components that contribute to it, as well as independent of how these components are grouped and of the decomposition of the components into subcomponents;
- Transferable: it should be possible to use directly the uncertainty evaluated for one result as a component in evaluating the uncertainty of another measurement in which the first result is used.

This method involves the identification of all sources of uncertainty, which has to be estimated and combined in order to the final uncertainty.
The contributors should be related to a model equation

$$Y = f(X_1, \cdots, X_n) \tag{2.3-1}$$

where Y is the measurand and X_i are the input quantities.
The contributors of each source of uncertainty in Equation (2.3-1) and other possible influence factors not in the model equation can be evaluated according to two approaches:

1. Contributors estimated by statistical analysis of the observations (usually from repeated readings): *Type A evaluation*.
   The mean value $\bar{x}$ of a number n of measurement results x_i is an estimate of the true value of the mean μ of the distribution

   $$\bar{x} = \frac{1}{n}\sum_{i=1}^{n} x_i \tag{2.3-2}$$

   The experimental standard deviation of the distribution based on n repeated measurements u_x is an estimate of the standard deviation of the distribution σ

   $$u_x = \sqrt{\frac{\sum_{i=1}^{n}(\bar{x}-x_i)^2}{n-1}} \tag{2.3-3}$$

The standard deviation of the mean value u_x is equal to the standard deviation of the distribution divided by the square root of the number of measurements n

$$u_{\bar{x}} = \sqrt{\frac{\sum_{i=1}^{n}(\bar{x}-x_i)^2}{n\,(n-1)}} = \frac{u_x}{\sqrt{n}} \tag{2.3-4}$$

The experimental standard deviation in Equation (2.3-3) is used characterize the variability of the observed values x_i (single observation of n repeated measurements).
The experimental standard deviation of the mean in Equation (2.3-4) is used in the uncertainty budget when the measurement result is obtained using the mean of n independent repeated observations $X_{i,k}$.

2. Contributors calculated from assigned probability distributions: *Type B evaluation*. The probability distribution can be identified from past measurements experience, calibration certificates, manufacture's specifications, calculations, published information and from common sense.
In **Figure 2.3-2** some common distribution are given together with the corresponding uncertainty contributor.

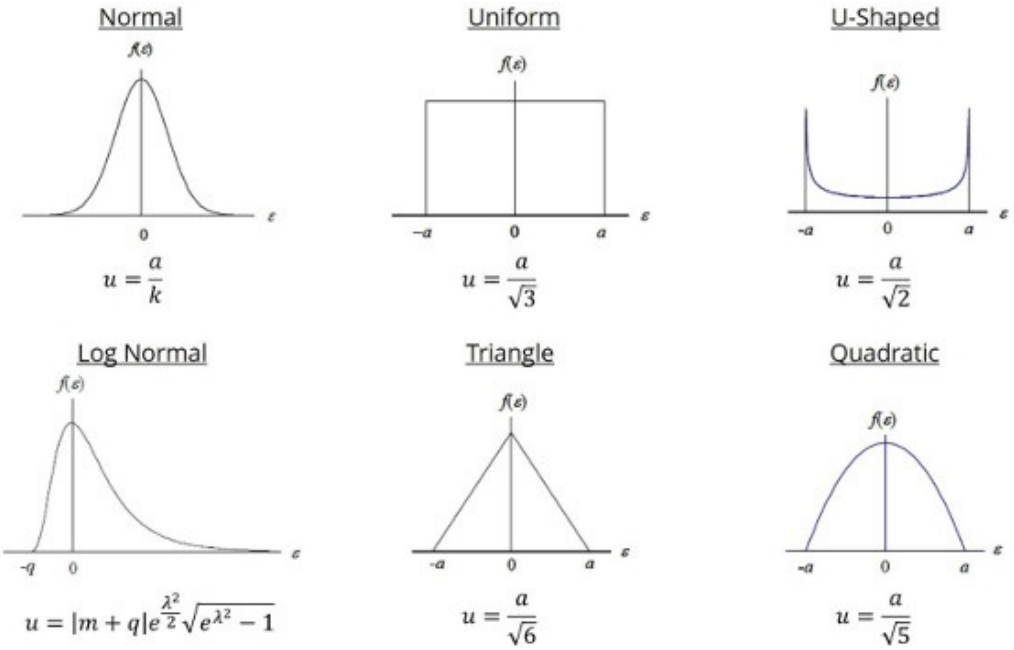

Figure 2.3-2. Experimental distributions for the type *B* uncertainty evaluation.

The combined standard uncertainty associated with the result is the positive square root of the combined variance, i.e., the variance obtained by combination of the all variances of the considered uncertainty contributors, using the law of the propagation of uncertainty.
The combined variance for uncorrelated quantities is

$$u_c^2(y) = \sum_{i=1}^{n}\left(\frac{\partial f}{\partial x_i}\right)^2 u^2(x_i) \tag{2.3-5}$$

while the combined variance for correlated quantities is

$$u_c^2(y) = \sum_{i=1}^{N}\left(\frac{\partial f}{\partial x_i}\right)^2 u^2(x_i) + 2\sum_{i=1}^{N-1}\sum_{j=i+1}^{N}\frac{\partial f}{\partial x_i}\frac{\partial f}{\partial x_j}u(x_i, x_j) \tag{2.3-6}$$

Eventually, an expanded uncertainty U can be evaluated so that it *is interpreted as defining an interval about the measurement result that encompasses a large fraction p of the probability*

distribution characterized by that result and its combined standard uncertainty, and p is the coverage probability or level of confidence of the interval.
Hence, *U* is obtained by multiplying the combined standard uncertainty u_c by a *coverage factor k*, corresponding to the desired *level of confidence*.
The estimate *y* of the measurand *Y* and its expanded uncertainty *U* are expressed as

$$y \pm U = y \pm (k \cdot u_c) \tag{2.3-7}$$

2.4 Tolerance intervals specification

The manufacturing of mechanical parts and related functional behaviour are to be safeguarded by appropriate tolerance rules. Assembly of two or more elements, sliding and rolling capabilities (e.g., coupling shaft-hole), different surfaces polishing are just few examples [56]. In the technical drawings, these functions are represented by "tolerances" or "specifications", which are given in terms of maximum deviations from an ideal geometric entity.
International standards (Geometrical Product Specification—GPS) aims to provide rules for the specifications, considering design, manufacture and tolerance verification. The following characteristics can be recognised [4], [12]:

- The classification of all the GPS standards is summarised in ISO 14638:2015 [57] which is commonly known as Masterplan.
- The approach is based on a detailed description of geometrical features linked to functional properties.
- No perfect geometry can be achieved in reality. However, a large number of points can give a realistic picture of the geometry of an object. This idea is called *skin model* [58]-[59].
- The Golden Rule of Metrology, stating that the measurement instrument should have a resolution which is one tenth of the tolerance to verify and the measurement uncertainty should be (10-20) % of the tolerance range, is not valid anymore.
  ISO 14253-1:2013 [60] asserts that the measurement uncertainty is to be accounted in tolerance verification.

In the micro- nanoscale, some problems can also be recognised related to the use of GPS standards [1], [61]:

- The absolute dimensions at micro- nanoscale are small and so should be the tolerances. These facts implicitly require that (a) the measurement method adopted must be suitable to measure the components and that (b) the measurement uncertainty must be sufficiently small to verify the tolerance. A large measurement uncertainty becomes comparable to the tolerance interval to be verified, leaving a small conformance zone for process variations [60]. Consequently, a larger tolerance is to be specified (see **Figure 2.4-1**).
- Tolerance grades are not defined in the sub-millimetre scale. The GPS system was, in fact, targeted to the millimetre scale.

Other problems are related to the manufacturing processes. The technologies used for manufacturing micro/nano components are quite different from those used for macro components. The integration of the parts in assemblies is obtained by different methods [1], [63].
According to [56], three different integration techniques may be distinguished in micro and nano technology:

1. Hetero integration—geometric tolerances are required to achieve the functionality of the assembly.
2. Hybrid integration— the most important parameter is the accuracy in the positioning of a micro component on a substrate. The micro part is placed, fixed and assembled, resulting a fully functioning micro system.
3. Monolithic integration—all the process steps of the micro component are integrated in a single substrate. The geometric measurements are not of primary importance. The most

important variables to be taken into account are the parameters of the process itself. For instance, in the case of an etching processes, the etching time is strictly related to the dimensions of the component.

In [64], a function-oriented tolerance specification model is proposed. According to this model, a tolerance is associated to the overall function of the micro component. If the calculated performance deviations during the various process steps are larger than the product tolerances, the parameters of the currently active manufacturing step are corrected, so that the final product is situated within the expected product tolerances, as defined by the functional behaviour.

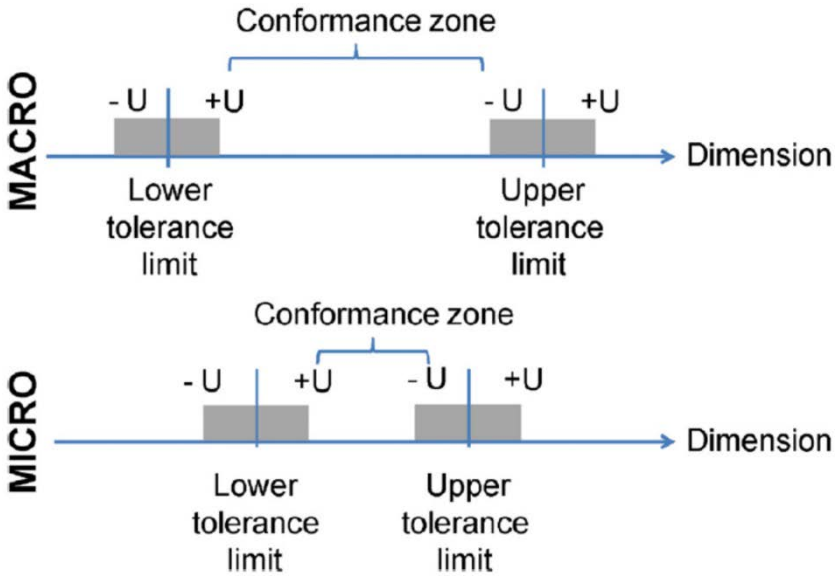

Figure 2.4-1. Illustration of the relationship between tolerance and measurement uncertainty. In this representation the measurement uncertainty was kept constant and the tolerance zone decreased [12]-[62].

2.5 Surface texture parameters

Areal surface texture parameter are defined in [65]. In the following, the definition for the parameter used in the thesis are briefly reported. Equivalent parameter for profile method assessment are in [66] and [67].

Arithmetic mean height of the scale-limited surface

The *Sa* roughness parameter is defined as the arithmetic mean of the absolute of the ordinate values within a definition area *A*. The corresponding equation is

$$S_a = \frac{1}{A}\iint_A \left|z(x,y)\right| dx\, dy \tag{2.5-1}$$

Root mean square height of the scale-limited surface

The *Sq* roughness parameter [44]is defined as the root mean square value of the ordinate values within a definition area *A*. The corresponding equation is

$$S_q = \sqrt{\frac{1}{A}\iint_A z^2(x,y)\, dx\, dy} \tag{2.5-2}$$

Maximum height of the scale-limited surface

The *Sz* roughness parameter is defined as the sum of the maximum peak height value and the maximum pit height value within a definition area *A*.

Root mean square gradient of the scale-limited surface

The *Sdq* roughness parameter [44]is defined as the root mean square of the surface gradient within the definition area *A* of a scale-limited surface

$$S_{dq} = \sqrt{\frac{1}{A}\iint_A \left[\left(\frac{\partial z(x,y)}{\partial x} \right)^2 + \left(\frac{\partial z(x,y)}{\partial y} \right)^2 \right] dx\, dy} \qquad (2.5\text{-}3)$$

References

[1] Hansen H N, Carneiro K, Haitjema H and De Chiffre L 2006 Dimensional Micro and Nano Metrology *CIRP Ann. – Manuf. Technol.* **55** 721-43

[2] Leach R 2014 *Fundamental principle of engineering nanometrology* (Elsevier)

[3] ISO 25178-6: 2012 Geometrical product specification (GPS)—Surface texture: Areal – Part 6: Classification of methods for measuring surface texture. ISO 25178 part 6 (Geneva: International Organization for Standardization)

[4] Chiffre L De 2011 *Geometrical metrology and machine testing* (Technical University of Denmark)

[5] Whitehouse D 2011 *Handbook of Surface and Nanometrology, Second Edition* (CRC Press)

[6] Dai G, Wolff H, Pohlenz F and Danzebrink H-U 2009 A metrological large range atomic force microscope with improved performance *Rev. Sci. Instrum.* **80** 43702

[7] Marinello F, Savio E, Bariani P and Carmignato S 2009 Coordinate metrology using scanning probe microscopes *Meas. Sci. Technol.* **20** 84002

[8] Rai-Choudhury P 1997 *Handbook of microlithography, micromachining, and microfabrication: Volume I* (SPIE Optical Engineering Press)

[9] Goodhew J. P, Humphrey J and Beanland R 2001 *Electron microscopy and analysis*

[10] Leach R 2011 *Optical Measurement of Surface Topography* ed R Leach (Berlin, Heidelberg: Springer Berlin Heidelberg)

[11] ISO 25178-6: 2010 Geometrical product specification (GPS)—Surface texture: Areal – Part 6: Classification of methods for measuring surface texture. ISO 25178 part 6 (Geneva: International Organization for Standardization)

[12] Gasparin S 2012 *Verification of Tolerance Chains in Micro Manufacturing* PhD thesis, Department of Mechanical Engineering, Technical University of Denmark

[13] Calaon M 2014 *Process chain validation in micro and nano replication* PhD thesis, Department of Mechanical Engineering, Technical University of Denmark

[14] Xu B, Cuminato D F and Keyes N M 1998 Evaluating Fabric Smoothness Appearance with a Laser Profilometer *Text. Res. J.* **68** 900-6

[15] Laurent J, Talbot M and Doucet M 1997 Road surface inspection using laser scanners adapted for the high precision 3D measurements of large flat surfaces *Proceedings. International Conference on Recent Advances in 3-D Digital Imaging and Modeling (Cat. No.97TB100134)* (IEEE Comput. Soc. Press) 303-10

[16] Danzl R, Helmli F, Rubert P and Prantl M 2008 Optical roughness measurements on specially designed roughness standards *Proceedings of SPIE* vol 7102, ed A Duparré and R Geyl 71020M

[17] Gao F, Leach R K, Petzing J and Coupland J M 2008 Surface measurement errors using commercial scanning white light interferometers *Meas. Sci. Technol.* **19** 15303

[18] Bryan J B 1979 The Abbé principle revisited: An updated interpretation *Precis. Eng.* **1** 129-32

[19] Vermeulen M M P a., Rosielle P C J N and Schellekens P H J 1998 Design of a High-Precision 3D-Coordinate Measuring Machine *CIRP Ann. – Manuf. Technol.* **47** 447-50
[20] Peggs G N, Lewis A J and Oldfield S 1999 Design for a Compact High-Accuracy CMM *CIRP Ann. – Manuf. Technol.* **48** 417-20
[21] Ruijl T 2001 *Ultra Precision Coordinate Measuring Machine: Design, Calibration and Error Compensation* (Delft University of Technology)
[22] Seggelen J K v., Rosielle P C J N, Schellekens P H J, Spaan H A M, Bergmans R H and Kotte G J W L 2005 An Elastically Guided Machine Axis with Nanometer Repeatability *CIRP Ann. – Manuf. Technol.* **54** 487-90
[23] Jaeger G, Manske E, Haussote T and Schott W 2002 Operation and analysis of a Nanopositioning and Nanomeasuring Machine *ASPE Annual Proceedings* vol St. Louis pp 299-304
[24] Hüser D, Petersen R and Rothe H 2006 Coordinate Measurements in Microsystems by Using AFM-Probing: Problems and Solutions *Nanoscale Calibration Standards and Methods* (Weinheim, FRG: Wiley-VCH Verlag GmbH & Co. KGaA) pp 60-72
[25] Brand U, Kleine-besten T and Schwenke H 2000 Development of a special CMM for dimensional metrology on microsystem components *Proceedings of ASPE* p 5
[26] Fujiwara M, Takamasu K and Ozono S 2003 Evaluation of properties of Nano-CMM by thermal drift and tilt angle *Proc. XVII IMEKO World Congress* vol Dubronik pp 1794-7
[27] Haitjema H, Pril W O and Schellekens P H J 2001 Development of a Silicon-based Nanoprobe System for 3-D Measurements *CIRP Ann. – Manuf. Technol.* **50** 365-8
[28] Schwenke H, Wäldele F, Weiskirch C and Kunzmann H 2001 Opto-tactile Sensor for 2D and 3D Measurement of Small Structures on Coordinate Measuring Machines *CIRP Ann. – Manuf. Technol.* **50** 361-4
[29] Weckenmann A, Estler T, Peggs G and McMurtry D 2004 Probing Systems in Dimensional Metrology *CIRP Ann. - Manuf. Technol.* **53** 657-84
[30] Claverley J D and Leach R K 2010 A novel three-axis vibrating micro-CMM probe with isotropic probing forces *Proceedings of the 11th euspen* **1** 59-62
[31] Hidaka K, Danzebrink H-U, Illers H, Saito A and Ishikawa N 2010 A high-resolution, self-sensing and self-actuated probe for micro- and nano-coordinate metrology and scanning force microscopy *CIRP Ann. – Manuf. Technol.* **59** 517-20
[32] Balzer F G, Dorozhovets N, Hofmann N, Hausotte T, Manske E, Jäger G, Büttgenbach S, 2010 3-D microprobe with optical detection system *Proceedings of the 10th euspen* **1** 104-107
[33] Carmignato S 2007 Traceability of dimensional measurements in computed tomography *Proceedings of 8th A.I.Te.M. Conference*
[34] Weckenmann A, Kramer P 2009 Predetermination of measurement uncertainty in the application of computed tomography *11th CIRP Int. Conf. Computer Aided Tolerancing*
[35] Kak A C and Slaney M 1988 *Principles of computerized tomographic imaging* (IEEE press)
[36] Bartscher M, Hilpert U, Goebbels J and Weidemann G 2007 Enhancement and Proof of Accuracy of Industrial Computed Tomography (CT) Measurements *CIRP Ann. – Manuf. Technol.* **56** 495-8
[37] Schwenke H, Neuschaefer-Rube U, Pfeifer T and Kunzmann H 2002 Optical Methods for Dimensional Metrology in Production Engineering *CIRP Ann. – Manuf. Technol.* **51** 685-99
[38] Bartscher M, Neuschaefer-Rube U and Wäldele F 2004 Computed tomography a highly potential tool for industrial quality control and production near measurements *VDI Berichte* (VDI Berichte)
[39] JCGM 200: 2012 International vocabulary of metrology—Basic and general concepts and associated terms (VIM), Joint Committee for Guides in Metrology (Sèvres: Bureau International des Poids et Mesures, BIPM)
[40] ISO 5436-1: 2000 Geometrical product specification (GPS)—Surface texture: Profile method; Measurement standards – Part 1: Material measures. ISO 5436 part 1 (Geneva: International Organization for Standardization)

[41] ISO 25178-701: 2010 Geometrical product specification (GPS)—Surface texture: Areal – Part 701: Calibration and measurement standards for contact (stylus) instruments. ISO 25178 part 701 (Geneva: International Organization for Standardization)
[42] ISO 25178-70: 2014 Geometrical product specification (GPS)—Surface texture: Areal – Part 70: Material measures. ISO 25178 part 70 (Geneva: International Organization for Standardization)
[43] ISO 12179: 2000 Geometrical product specification (GPS)—Surface texture: Profile method – Calibration of contact (stylus) instruments. ISO 12179 (Geneva: International Organization for Standardization)
[44] Wilhelm R G, Hocken R and Schwenke H 2001 Task Specific Uncertainty in Coordinate Measurement *CIRP Ann. – Manuf. Technol.* **50** 553-63
[45] ISO/DIS 25178-600: 2016 Geometrical product specification (GPS) — Surface texture: Areal – Part 600: Nominal characteristics of non-contact (variable focus) instruments. ISO DIS 25178 part 600 (Geneva: International Organization for Standardization)
[46] ISO 25178-602: 2010 Geometrical product specification (GPS) — Surface texture: Areal – Part 602: Nominal characteristics of non-contact (confocal chromatic probe) instruments. ISO 25178 part 602 (Geneva: International Organization for Standardization)
[47] ISO 25178-603: 2013 Geometrical product specification (GPS) — Surface texture: Areal – Part 603: Nominal characteristics of non-contact (phase-shifting interferometric microscopy) instruments. ISO 25178 part 603 (Geneva: International Organization for Standardization)
[48] ISO 25178-604: 2013 Geometrical product specification (GPS) — Surface texture: Areal – Part 604: Nominal characteristics of non-contact (coherence scanning interferometry) instruments. ISO 25178 part 604 (Geneva: International Organization for Standardization)
[49] ISO 25178-605: 2014 Geometrical product specification (GPS) — Surface texture: Areal – Part 605: Nominal characteristics of non-contact (point autofocus probe) instruments. ISO 25178 part 605 (Geneva: International Organization for Standardization)
[50] ISO 25178-606: 2015 Geometrical product specification (GPS) — Surface texture: Areal – Part 606: Nominal characteristics of non-contact (focus variation) instruments. ISO 25178 part 606 (Geneva: International Organization for Standardization)
[51] Claverley J D and Leach R K 2015 A review of the existing performance verification infrastructure for micro-CMMs *Precis. Eng.* **39** 1-15
[52] Leach R K, Giusca C L, Haitjema H, Evans C and Jiang X 2015 Calibration and verification of areal surface texture measuring instruments *CIRP Ann. – Manuf. Technol.* **64** 797-813
[53] JCGM 100: 2008 Evaluation of measurement data—Guide to the expression of uncertainty in measurement, Joint Committee for Guides in Metrology (Sèvres: Bureau International des Poids et Mesures, BIPM)
[54] ISO 14253-2: 2011 Geometrical product specification (GPS) — Inspection by measurement of workpieces and measuring equipment – Part 2: Guidance for the estimation of uncertainty in GPS measurement, in calibration of measuring equipment and in product verification. ISO 14253 part 2 (Geneva: International Organization for Standardization)
[55] ISO 15530-3: 2011 Geometrical product specifications (GPS)—Coordinate measuring machines (CMM): Technique for determining the uncertainty of measurement – Part 3: Use of calibrated workpieces or measurement standards ISO 15530 part 3 (Geneva: International Organization for Standardization)
[56] Weckenmann A 2000 Studies on new tolerancing rules for micro- and nanotechnology *Proceedings of the 1st topical conference on fabrication and metrology in nanotechnology, Copenhagen, Denmark*, pp 214–21
[57] ISO 14638: 2015 Geometrical product specification (GPS) — Matrix model. ISO 14638 (Geneva: International Organization for Standardization)
[58] ISO 17450-1: 2011 Geometrical product specification (GPS) — General concepts – Part 1: Model for geometrical specification and verification. ISO 17450 part 1 (Geneva: International Organization for Standardization)

[59] ISO 22432: 2011 Geometrical product specification (GPS) — Features utilized in specification and verification. ISO 22432 (Geneva: International Organization for Standardization)
[60] ISO 14253-1: 2013 Geometrical product specification (GPS) — Inspection by measurement of workpieces and measuring equipment – Part 1: Decision rules for proving conformity or nonconformity with specifications. ISO 14253 part 1 (Geneva: International Organization for Standardization)
[61] Weckenmann A and Wiedenhoefer T 2005 The use of the GPS-Standard in Nanometrology *Proc. of 5th euspen international conference* pp 169-72
[62] Tosello G, Hansen H N and Gasparin S 2009 Applications of dimensional micro metrology to the product and process quality control in manufacturing of precision polymer micro components *CIRP Ann. – Manuf. Technol.* **58** 467-72
[63] Alting L, Kimura F, Hansen H N and Bissacco G 2003 Micro Engineering *CIRP Ann. – Manuf. Technol.* **52** 635-57
[64] Weckenmann A, Ernst R and Hornfeck R 2001 Tolerancing of micromechanical monolithic components *Proc. of 2nd euspen international conference* **2** 786-8
[65] ISO 25178-2: 2012 Geometrical product specification (GPS)—Surface texture: Areal – Part 2: Terms, definitions and surface texture parameters. ISO 25178 part 2 (Geneva: International Organization for Standardization)
[66] ISO 4287: 1997 Geometrical Product Specifications (GPS)—Surface texture: Profile method – Terms, definitions and surface texture parameters. ISO 4287 (Geneva: International Organization for Standardization)
[67] ISO 4288: 1996 Geometrical Product Specifications (GPS)—Surface texture: Profile method – Rules and procedures for the assessment of surface texture. ISO 4288 (Geneva: International Organization for Standardization)

Chapter 3

Advanced precision injection moulding technologies

3.1 Introduction

Injection moulding is the most commonly used manufacturing process for the replication of polymer parts. It requires the use of an injection moulding machine, raw plastic material and a mould. The plastic is melted in the injection moulding machine and then injected into the mould, where it cools and solidifies into the final part [1]-[2]. An overview of an injection moulding machine and of a mould is given, respectively, in **Figure 3.1-1** and **Figure 3.1-2**.

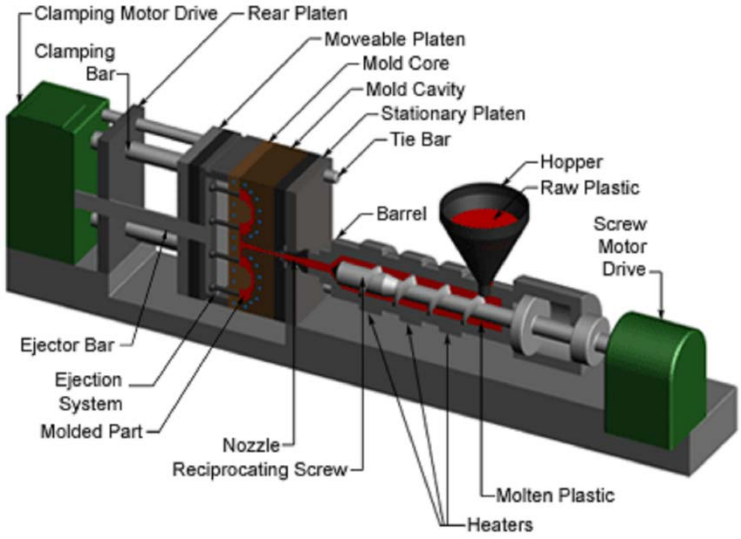

Figure 3.1-1. Injection moulding machine and principal mechanical components [3].

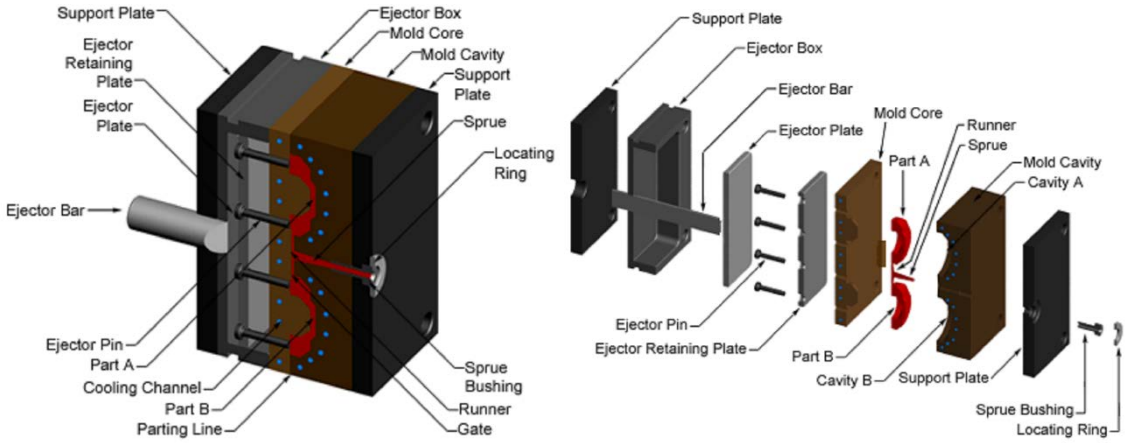

Figure 3.1-2. Overview of a mould and principal mechanical components [3].

The injection moulding process is characterised by a high volume of the production and a wide variety of manufactured components, which largely vary in size, complexity and application. Reason for a demand of high production volume can also be related to the sunk costs of the investment necessary to start up such production. Beyond the cost of an injection moulding machine, the mould has also a large impact on the final cost and on the functional design, which both increase with the complexity of the production [1].
In recent years, the tendency towards miniaturization established injection moulding as one of the key technologies for micro manufacturing because of its mass production capability and relatively low production cost but, also, high flexibility of integration with other micro/nano polymer replication technologies (UV lithography, nano imprint lithography, e-beam lithography, hot embossing, UV embossing) [4]-[10].
Hence, nowadays, a distinction is made between *precision* injection moulding and *micro* injection moulding:

- *precision* injection moulding is used to designate injection moulding processes of parts of conventional size, mass in the order of (1-100) g, and containing dimensional and/or surface features to be replicated with range of tolerances between (10-50) µm (e.g., plastic medical devices) down to (10-20) nm (e.g. blu-ray discs).
- *micro* injection moulding is the technology for the production of micro moulded parts, i.e., those parts having overall size below (3-5) mm down to less than 1 mm, mass of less than 1 g (e.g., microfluidic systems) down to (0.5-1) mg (e.g., micro gears), features in the order of 100 µm down to less than 1 µm, and dimensional tolerances between (10-20) µm down to (10-20) nm.

A comprehensive review on the replication of micro and nano geometries [13] has highlighted the typical replication capability of polymer moulding processes. In particular, precision injection moulding, micro injection moulding and injection compression moulding of thermoplastic polymers allow the replication of features having vertical size between (50-100) nm and (100-500) µm, and lateral size between (100-1000) nm and (100-500) µm (see **Figure 3.1-3**).

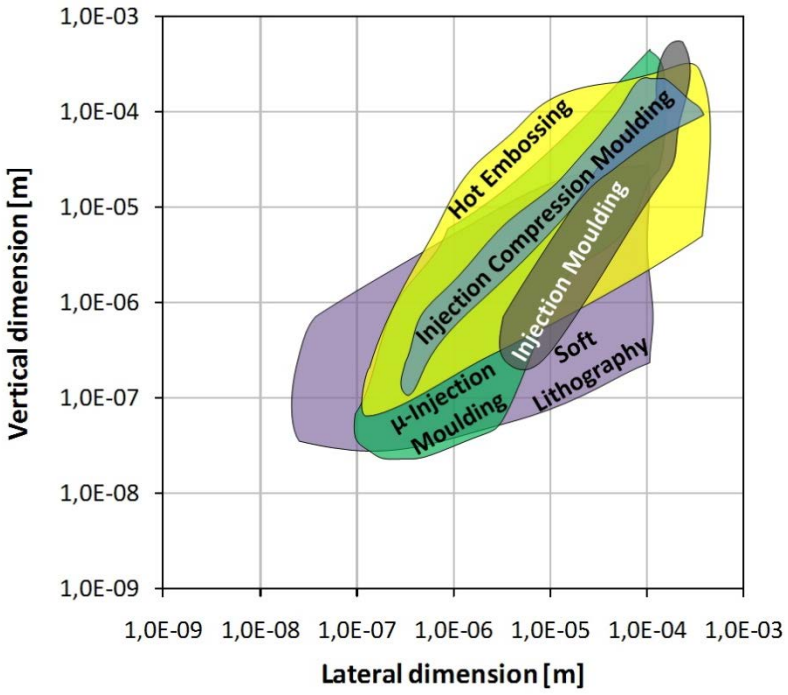

Figure 3.1-3. Polymer processing capabilities in terms of micro/nano features vertical replication at different features' lateral dimensions according to state-of-the-art research [13].

3.2 Injection molding

A typical injection moulding process is made of the following phases, which are outlined in **Figure 3.2-1** ([1], [2], [11]):

1. Plastification—during the plastification phase, the screw is rotating to build up the melt polymer necessary for the injection phase. The material melts under the effect of the created friction of the screw and heater bands. The pressure pushes the screw backwards. When sufficient polymer has built up (metering) the rotation stops.
2. Injection and filling—when the mould is closed, the screw is pushed (injection) so that the melt polymer fills the sprue, the runners and the mould cavity (filling).
3. Packing phase and cooling—the screw begins rotating again to build up more polymer (packing) in order to compensate both viscoelastic forces of the compressed melt polymer and the reduction of volume due to the cooling.
4. Demoulding and ejection—after the polymer is solidified (cooling), the mould opens and ejector pins remove the moulded part (ejection).

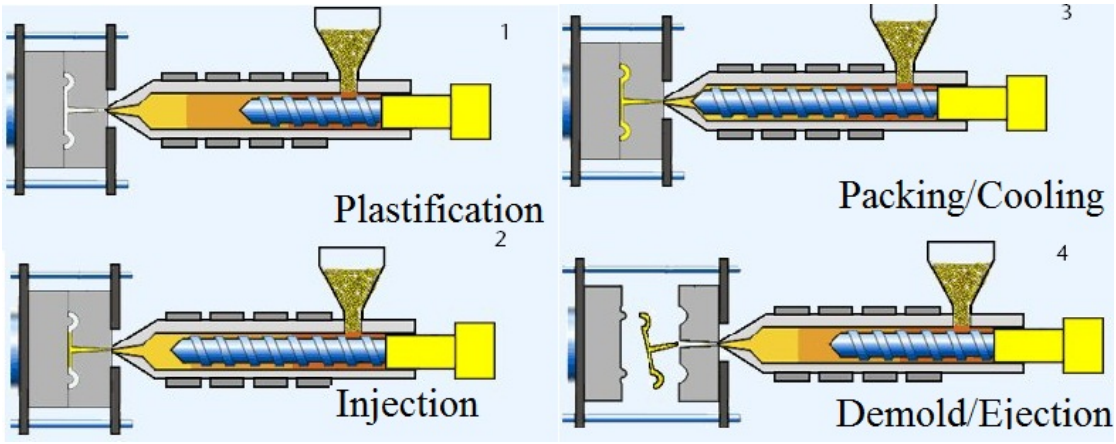

Figure 3.2-1. Phases of an injection moulding process [11].

3.2.1 Micro injection moulding

The production of micro moulded components by conventional injection moulding machines raises some issues related to the reciprocating screw [2]. In fact, it combines four function (plastification and homogenisation, metering, locking, injection) and in conventional injection moulding machine it normally has a diameter down to 14 mm. Hence,

- it is difficult to control the melt metering accuracy as a result of the screw structure and the limitation to reduce screw size;
- because of the channel configuration there is a melt back-flow when high injection pressure is applied to fill small and micro cavities.

To adapt such machines to the replication of small parts, a big sprue is necessary to achieve the minimum shot weight and perform properly the process. As a consequence there is a waste up to 90% of polymer. Moreover, the big sprue increases the cooling time and, consequently, the cycle time.

For further downscaling of the injection moulding process, to control metering accuracy and homogeneity of very small quantities of melt, these issues were solved by assigning the four functions of the screw to at least two different units (see **Figure 3.2-2**) [2]:

- A screw for plasticising and homogenising. The very small amount of plastics needed is plasticised either by a plasticising screw (diameter of 14 mm) or in an electrically heated cylinder, and then fed into the injection cylinder by a plunger (diameter of 5 mm).

- A piston for metering and injection. A second plunger with a diameter of just 5 mm down to 2 mm depending on the machine configuration injects the molten material into the cavity. It is driven by an electric motor and a precise linear drive. Typically, the shot weight can be varied between 5 mg and 300 mg.

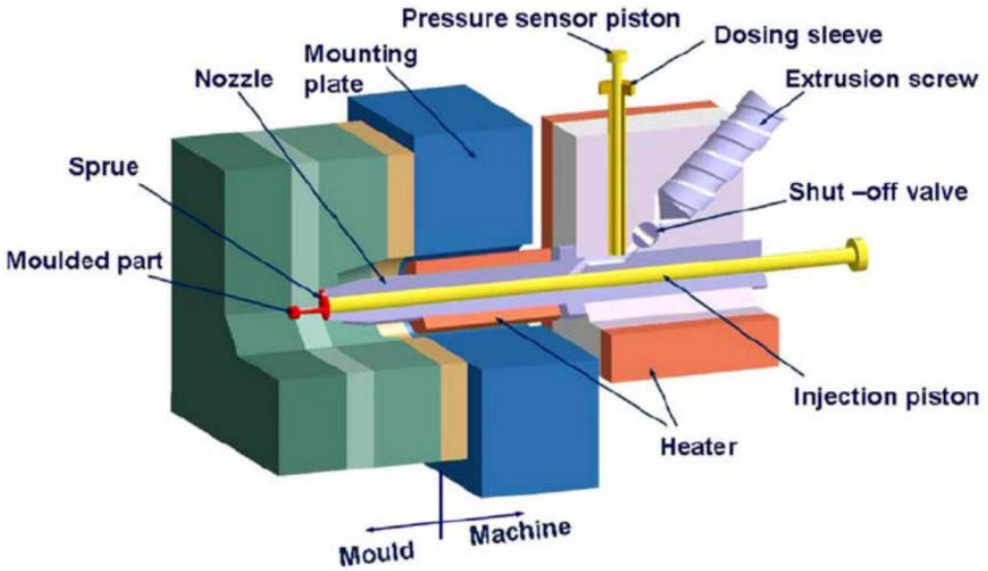

Figure 3.2-2. Injection unit of a micro injection moulding machine [2].

Eventually, the micro injection moulding process steps are the following:

1. Plastic pellets are plasticised by the fixed extruder screw and fed into the metering chamber.
2. The shut-off valve closes in order to avoid back-flow from the metering chamber.
3. Once the shot volume has been achieved, the plunger, in the dosage barrel, delivers the shot volume to the injection barrel.
4. The injection plunger then pushes the melt into the mould.
5. Once the plunger injection movement is completed, a holding pressure may be applied to the melt. This is achieved by a slight forward movement (maximum 1 mm) of the injection plunger.

3.3 Powder injection moulding

Powder injection moulding is a moulding process for the production of the metal or ceramic components (see Chapter 5).

The feedstock is a compound of powder of the selected material and a binder. The most widely used binder materials are thermoplastics like Polyethylene (PE), Polypropylene (PP), Polyoxymethylene (POM) and Polyethylene glycol (PEG). The binder is required to give to the compound the necessary mechanical properties for being injected (flow ability). The flow ability is important for rapid filling of the mould without solidification of the material, considering the high thermal conductivity of the feedstock (especially metal powders).

The size of the particles can be a critical parameter and it is recommended not to exceed 0.05-0.1 times the size of the smallest dimension of the cavity. In addition, the homogeneity and the shape of the particles (preferably globular or spherical) can influence the process.

The reinforcement of the feedstock is another important parameter. The material after solidifying must have mechanical properties to make a demoulding possible.

The injected parts, normally called *green parts*, need to be purged of the binder. Hence, after the injection moulding, they are subjected to a de-binding and to a sintering process for achieving the final mechanical properties. The consequence is a change in the dimension due to a considerable shrinkage. In addition, consequence of the sintering process is a grain growth that can cause anisotropy of the material. The grain growth can be especially harmful for the mechanical properties of micro components. To prevent it, heating and cooling rates may be increased. On the other side, higher heating and cooling rates may increase the risk of warpage.
A micro powder injection moulding process will be described in details in the next Chapter 5.

3.4 Compression injection moulding

Injection compression moulding is the leading process technology for the mass manufacturing of high precision polymer optics. The process leads to high accuracy in the replication of micro structures and to a surface finishing suitable for optical applications [13], [14]. It can be considered a natural extension of the traditional injection moulding process, characterised by the same process cycle operations with a difference in the injection phase and in the last process step (compression). The principal phases of injection compression moulding are summarised in **Figure 3.4-1**.

- Injection—during the injection phase the mould cavity is kept partially open to facilitate the flow of plastic inside the cavity. Mechanical design solutions are implanted for the closure of the cavity in order to prevent the spillage of the polymer outside the mould.

- Compression—during the injection phase or at the end of the injection phase, the machine closing force reduces the thickness of the mould cavity to the real thickness of the component and the polymer is driven inside the empty region of the cavity. This phase produces a uniform distribution of the pressure into the mould cavity, unlike conventional injection moulding where a gradient of pressure occurs.

Despite the more complex tooling design and process development, a number of crucial advantages can be attained by the injection compression moulding, making the process particularly interesting for optical parts [13]:

- Homogeneous material properties due to reduced and more uniformly distributed residual stresses.
- Lower volumetric shrinkage with respect to conventional injection moulding due to the optimal packing effect during the compression phase.
- Improved dimensional stability and lower warpage (i.e., component deflection) sustained by an effective shrinkage compensation during the compression phase.
- Improved mould cavity replication with respect to moulding technology due to the shorter flow length pattern of the molten plastic into the surface micro structures.
- Lower injection pressure than in conventional injection moulding due to the fact that the filling phase is performed when the mould is slightly open decreasing the air flow resistance (a typical gap is in the range of 0.1 mm-0.4 mm).
- Possibility to use a smaller machine with a lower tonnage due to reduced injection pressure and hence decreased clamping force required.

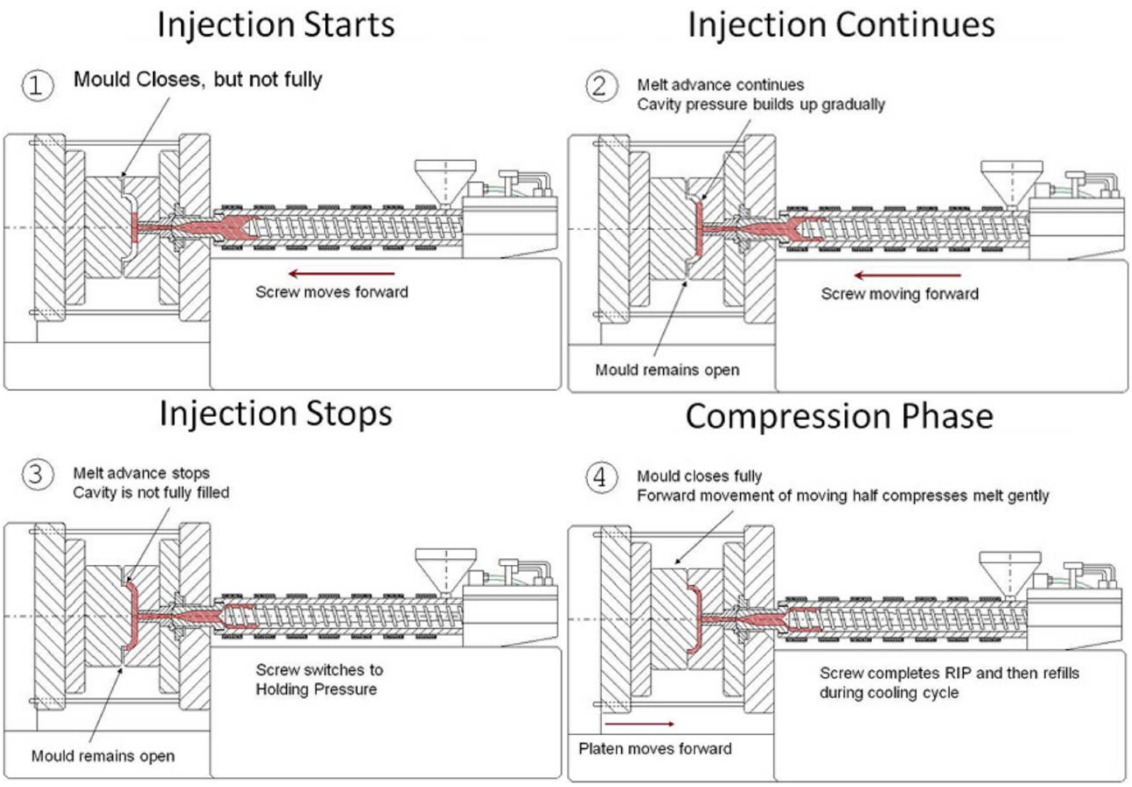

Figure 3.4-1. Phases of a compression injection moulding process [12].

References

[1] Heckele M and Schomburg W K 2004 Review on micro molding of thermoplastic polymers *J. Micromechanics Microengineering* **14** R1–14

[2] Tosello G 2008 *Precision moulding of polymer micro components* PhD thesis, Department of Mechanical Engineering, Technical University of Denmark

[3] CustomPartNet, www.custompartnet.com

[4] Chou S Y, Krauss P R and Renstrom P J 1995 Imprint of sub-25 nm vias and trenches in polymers *Appl. Phys. Lett.* **67** 3114-6

[5] Kuo J-N, Hsieh C-C, Yang S-Y and Lee G-B 2007 An SU-8 microlens array fabricated by soft replica molding for cell counting applications *J. Micromechanics Microengineering* **17** 693-9

[6] Worgull M, Hétu J F, Kabanemi K K and Heckele M 2008 Hot embossing of microstructures: Characterization of friction during demolding *Microsyst. Technol.* **14** 767-73

[7] Worgull M 2009 *Hot Embossing: Theory and Technology of Microreplication (Micro and Nano Technologies)*

[8] Yun D, Son Y, Kyung J, Park H, Park C, Lee S and Kim B 2012 Development of roll-to-roll hot embossing system with induction heater for micro fabrication *Rev. Sci. Instrum.* **83** 15108

[9] Calaon M, Hansen H N, Tosello G Garnaes J, Norregard J, Wei L. 2013 A capability study of micromolding for nano moulding for nano fluidic systems manufacture *Proceeding of the 13th euspen International Conference*, page pp. 4

[10] Chen K S, Lin I K and Ko F H 2005 Fabrication of 3D polymer microstructures using electron beam lithography and nanoimprinting technologies *J. Micromechanics Microengineering* **15** 1894-903

[11] Xie L, Shen L and Jiang B 2011 Modelling and Simulation for Micro Injection Molding Process *Computational Fluid Dynamics Technologies and Applications* (InTech)
[12] www.plastemart.com
[13] Hansen H N, Hocken R J and Tosello G 2011 Replication of micro and nano surface geometries *CIRP Ann. – Manuf. Technol.* **60** 695-714
[14] Michaeli W, Heßner S, Klaiber F and Forster J 2007 Geometrical Accuracy and Optical Performance of Injection Moulded and Injection-compression Moulded Plastic Parts *CIRP Ann. – Manuf. Technol.* **56** 545-8

Chapter 4

Uncertainty assessment for micro nano dimensional and topographic measurements

4.1 Introduction

Traditional techniques for the uncertainty assessment in manufacturing engineering appear to be outdated and not adequate any longer when considering the incessant scaling down of critical dimensions of micro and nano production [1]-[4]. Furthermore, as the technology progresses, the interest for three-dimensional areal characterization also increases [5]-[6]. Surfaces of manufactured components, which are natural interfaces to the environment, become more and more complex.

If, on one hand, this trend improves many products we use in everyday life, allowing for incorporating more and more functionalities in one single micro part, on the other hand, it poses new challenges in assessing the quality of the production. Tolerances verification requires, e.g., an adequate assessment of the measurement uncertainty and the establishment of traceability.

In this context, optical instruments appear more adequate; though, the influence of the measurement process can have severe impact on measurement uncertainty and it should be kept under reasonable limits [7]-[8].

In this view, a procedure for statistical analysis and uncertainty evaluation is proposed. It is based on the well-known frequentist approach and consistent with [9].

The uncertainty evaluation of areal acquisitions is, in fact, at an early stage, yet [10]. Some indications are given in the recent ISO 25178 series (International Organization for Standardization) but the suggested contributors are mostly related to the instruments metrological characteristics [11] and there are no suggestions about the measurand.

Some work is worth to be mentioned.

In [12], a correction of systematic effects is proposed in an uncertainty evaluation achieved by the use of metrological characteristics. In [13] the uncertainty is evaluated by the Monte Carlo method.

Attempts of using the approach suggested in [9], instead, can be found in [14], limited to the propagation of the uncertainty of correlated filtered profile roughness measurements, and in [15]. In this last work, the *type A* uncertainty defined in [9] was directly considered for the height (*z*-values) of each pixels of surface texture measurements, arriving to final equations difficult to be managed because of the excessive amount of data.

The methodology proposed here, on the contrary, is intended for results extracted from areal acquisitions (areal parameters included) and, to the best of the author's knowledge, it is completely new to micro, nano dimensional and topography areal measurements.

The methodology was investigated through three different study cases and aims to

- Provide a comprehensive structure for micro/nano dimensional and surface topography measurements.
- Reduce the evaluated uncertainty.
- Avoide the use of filters and exploiting the potentialities of statistical processing.

The study cases are reported in the following. They states the procedure, highlighting *caveat* and possible applications in micro/nano dimensional and topography areal measurements.

4.2 Metrology of micro tool insert

The first study case [16] aims to establish the general method for analysing and eventually correcting possible divergences among dimensional and surface topography measurements acquired by different optical instruments.

The challenge to compare surface texture measurements from different instruments has already been emphasised in a past work [17], where Mattsson et al. showed that agreement among surface roughness measurements is limited mostly by (a) inaccuracies in repositioning the different instruments in the same measurement area and by (b) the data set evaluation or post-processing.

The proposed method intends to reduce those systematic differences, which are commonly due to the chain operator-instrument.

In the following, dimensions and surface micro topographies of proof-of-technology (PoT) for micro mould inserts are case in point for the description of the method. They have been realised in the context of the project Hi-Micro [18]. It is an EU project aimed to improve high precision micro production technologies, in the European Commission's 7th Framework Program.

PoT micro mould inserts are four micro cavities (**Figure 4.2-1**) two made of aluminium and two made of steel, which have been produced by additive manufacturing and successively structured by Jet Electro-chemical Machining (Jet-ECM) [19]. The main Jet-ECM process parameters are specified in **Table 4.2-1**.

Table 4.2-1. Jet-ECM process parameters.

Parameters	*Values*
Electrolyte (mass fraction)	$NaNO_3$ (30% in water)
Process voltage	60 V
Pump delivery rate	10 ml/min
Nozzle diameter	100 µm
Nozzle speed	1 mm/s
Initial working gap	100 µm
Movements pitch (max)	20 µm
Number of crossing	1 (2 in limited areas)

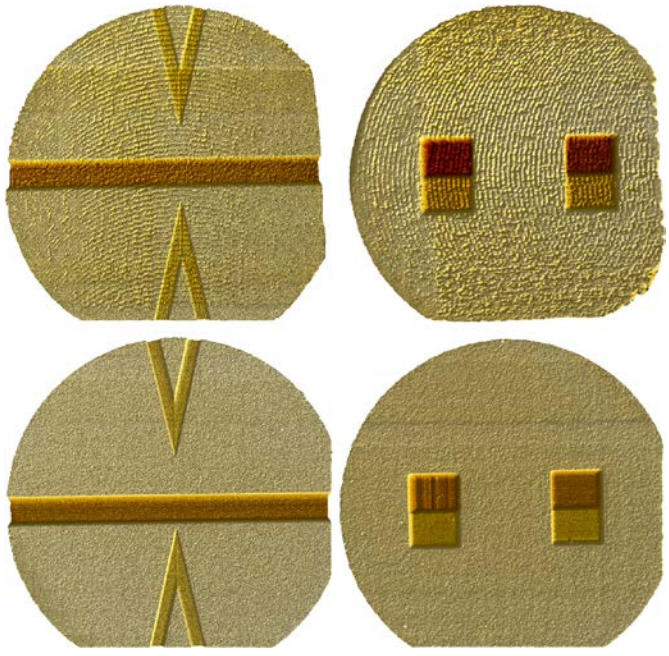

Figure 4.2-1. Overview of the proof-of-technology (PoT) for micro mould inserts. Top: Aluminium PoTs. Bottom: Steel PoTs. Left: straight-lined grooves. Right: Sectioned surfaces at different heights.

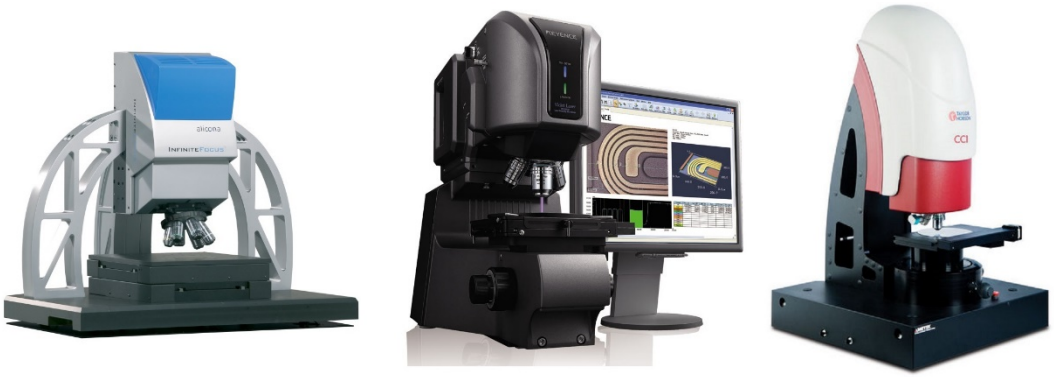

(a) (b) (c)

Figure 4.2-2. Optical instruments used in the investigation. (a): Alicona InfiniteFocus G4 (focus-variation microscope – FVM). (b): Keyence VK 9700 (laser scanning confocal microscope – CM). (c): Taylor Hobson Talysurf CCI HD (Coherent Scanning Interferometer – CSI).

Figure 4.2-3. Reference instrument: Taylor Hobson Form Talysurf series 2 Inductive 50.

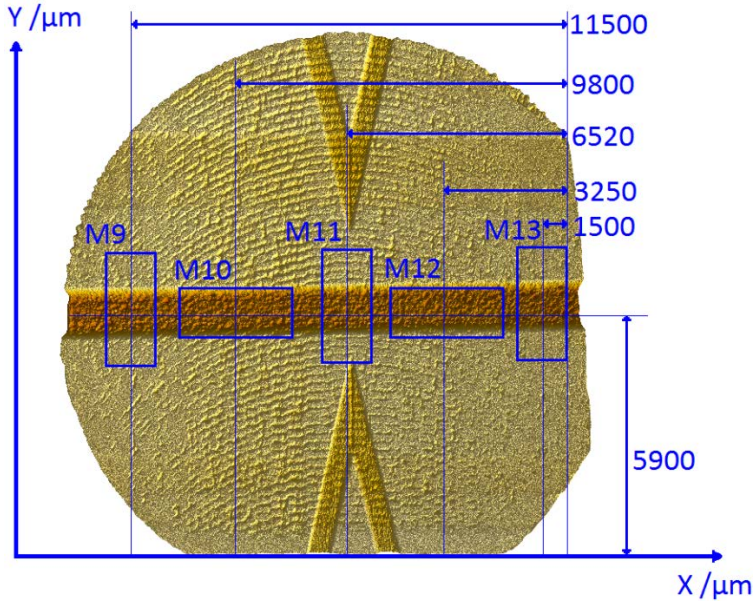

Figure 4.2-4. Acquisition areas on the micro mould inserts machined with straight-lined grooves. In particular, M9, M11, M13 are intended for step height measurements; M10, M12 are intended for roughness measurements.

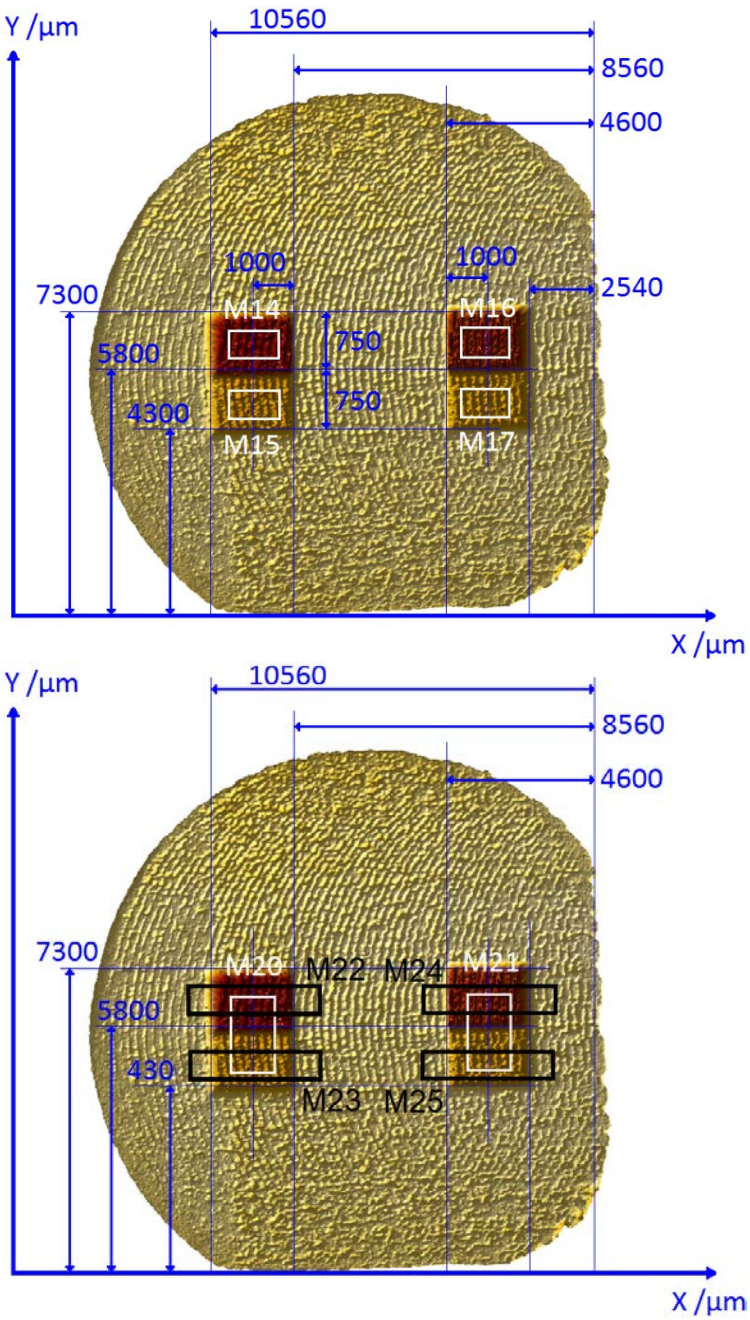

Figure 4.2-5. Acquisition areas on the micro mould inserts machined with sectioned surfaces. M14-M17 are intended for roughness measurements (top); M20-M25 are intended for step height measurements (bottom).

4.2.1 Measurements processing

Knowledgeable expert operators, following best practice procedures, in micro manufacturing metrology laboratory conditions, have carried out measurements of the micro-machined cavities using a focus-variation microscope (FVM), a laser scanning confocal microscope (CM) and a coherent scanning interferometer (CSI) (**Figure 4.2-2**). Furthermore, measurements by a contact instrument (CI) (**Figure 4.2-3**) were used as reference for indirectly achieving traceability. In fact, the measurement uncertainty was evaluated as the discrepancy between the optical instruments measurements and the contact ones (references; see § 4.2.2.2).

Subject of the investigation were step heights and *Sa* and *Sq* roughness parameters (see § 2.5 and [20]). Hence, several areal acquisitions were performed in different regions, identified over the

specimens by precisely defining (a) the acquisition area size and (b) their positions with respect to a univocal and reproducible reference system. The acquisition areas were denominated from M9 to M25. They are defined in **Figure 4.2-4** and in **Figure 4.2-5**.
Despite this caution, several areal acquisitions, performed using three different optical technologies, also require considering a number of critical aspects in order to perform a correct treatment of the measurement data sets and to allow for an effective comparison among the different instruments.
In particular, pre-processing of data sets, presence of noise and void pixels, influence of filtering and waviness are considered and discussed in the following.

Data set pre-processing

The raw measurements were analysed using the same image processing tool to reduce software influences [21].
As a preparatory activity, the raw measurement data were pre-processed with a common levelling strategy and sub-areas unsuitable for the processing (due to the presence of noise, spikes, general defects, etc.) were discarded. However, in some cases, disturbances were so extended on the acquired surfaces that this operation was not possible without compromising the entire result. Under such circumstances, completely distorted measurements were eliminated (see below).
It is important to state that heterogeneous measurements should have the same discretisation level or, referring to the discrete Fourier transform theory, the same bandwidth [22]. This can be achieved when the areal acquisitions have about the same sampling width or, equivalently, the same field of view and number of pixels. Consequently, it is important to plan heterogeneous measurement sessions with this ultimate purpose. Nevertheless, the intension here was to test the capability of the method checking if discrepancies related to different instruments/operators (magnification, discretisation levels, etc.) could be corrected against a reference.

Influence of noise

The disturbances shown in **Figure 4.2-6** are such to turn not meaningful the comparison of the related measurement with the other results. The example, in fact, shows a surface texture completely altered by anomalous and sharp changes in the measured signal that are probably due to interactions of the optical radiation with the material of the specimen, beyond the working principle of the related optical instruments (so called “spikes”). In addition, the calculated values or parameters cannot be usually detected by exclusion principles as outliers (see § 4.2.2) because such methods act on the calculated values but, in cases like the one shown, even though the disturbances amplitude can be reduced by filtering (see § 8.3.1), it is impossible to restore the original surface topography. Therefore, it was not appropriate to retain similar measurements for the statistical analysis.

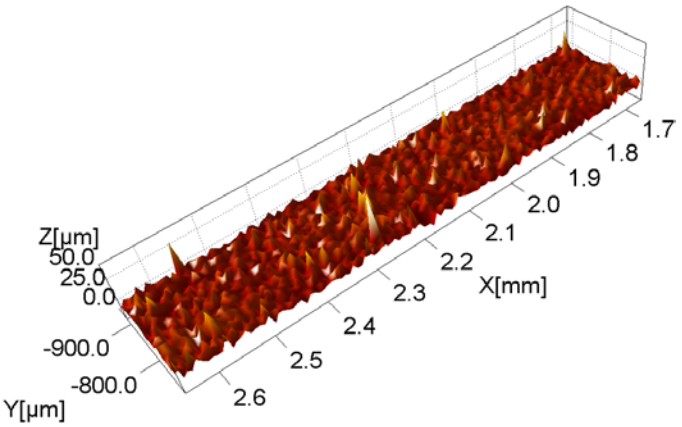

Figure 4.2-6. Example of surface in which disturbances are completely blended with the surface texture.

Presence of void pixels

When the image acquisition was not complete over limited areas on the surfaces (voids) the null pixels were reconstructed by interpolation using surface prediction values from available neighbouring pixels. This operation is not critical for the measurement. Nonetheless, both voids and the reconstructed corresponding parts are to be avoided as far as possible because they may result in an underestimation of the measured value and, consequently, contribute to the so called systematic effects in the experimental distribution of the data (see § 4.2.2.2).
In general, extended disturbances should be recognised during the measurement session, stored and replaced by a new measurement so that they can be successively further analysed and the natural sequence of events (see § 4.3) can be respected by the new acquisition, in order to allow the detection and correction of possible systematic behaviour (see § 4.2.2.2 and § 4.3).

Filtering and cut-off

Eventually, no filtering was applied. The reason is that, at this short scale (i.e. sub-mm), the cut-off wavelengths normally used for filtering become comparable with the quantities to be measured. Consequently, filters can jeopardize the results (see § 8.3.1). The ambition is to use a statistical analysis and other mathematical tools in order to replace filtering (see, e.g., the sub-section below).

Effect of Waviness

A substantial waviness, which in some cases would have required filtering, was only observed in the M14 sectioned surface of the steel specimen (see **Figure 4.2-1**, bottom-right). Here, the waviness was put in connection with a *Pq* parameter of an average profile (2-D roughness) using the Fourier transform. Any periodic signal can be identified by a spectrum consisting of a given number of discrete wavelength (or harmonic) components [23], with certain amplitudes, which can be usefully related to a *Pq* parameter (defined in [24] and [25]) and, subsequently, compared with *Sq* parameter (defined in [20]) and associated to 3-D surface measurements.
When dealing with surface roughness 2-D spectra of pure sine signals, *Pq* is equivalent to the height of a single peak (root mean square value – RMS). For more complex spectra of periodic signals, *Pq* can still be estimated from the spectrum by squared values summation of the corresponding harmonic components at discrete frequencies (peaks) [23].
Figure 4.2-7 shows the Fourier transform of the surface under evaluation calculated along the direction orthogonal to the dominant texture and averaged along the direction parallel to the dominant texture; whilst the amplitudes of the first three peaks H_1, H_2, H_3 and the corresponding spatial periods are reported in **Table 4.2-2**.

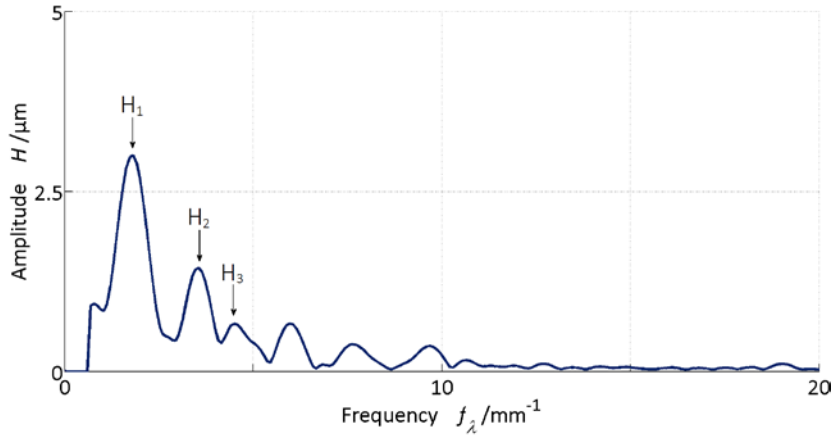

Figure 4.2-7. Spectrum of the surface affected by waviness. Three harmonic components are indicated as H_1, H_2, H_3. The relative values are reported in **Table 4.2-2**.

Table 4.2-2. Amplitude and wavelength for the first three peaks in the spectrum of Fig. 3.

λ_1 /µm	H_1 /µm	λ_2 /µm	H_2 /µm	λ_3 /µm	H_3 /µm
550.1	3.0	281.8	1.4	222.2	0.7

The estimate of the RMS value of the periodic distortion of the surface from the first three peaks of the spectrum is $H_w = (H_1^2 + H_2^2 + H_3^2)^{½} = 3.4$ µm, which is close to the value of the single first peak H_1 in **Table 4.2-2**. This means that the distortion due to the periodic roughness (waviness) is dominant. Furthermore, if the surface is sufficiently regular along the direction parallel to the dominant texture, *Pq* and *Sq* calculations should not differ in large amounts. Hence, comparing the RMS value that only contains the periodic roughness with the *Sq* value (see **Table 4.2-25** in § 4.2.3) referred to the overall surface, the waviness is about 65 % in terms of RMS height. In other words, differences between estimated RMS value of the periodic distortion and measured *Sq* might be due to non-homogeneities along the direction parallel to the dominant texture but, above all, to a random roughness, also due to machining, flanked by the peaks of the spectrum of the surface, i.e., on the flanks of the periodic texture [23].
This estimation clearly shows that the waviness affects this measurement for the most of the result. In this particular example, it was estimated at least 65 % of the result, in terms of RMS value. For a general result, this procedure can be applied to average values and Fourier transform of averaged topographies.
Furthermore, the sought functional requirements determine what kind of assessment is to be done. In this case, the choice was to evaluate the entire distortion of the texture because of the nature of the surfaces under evaluation. For example, in a tool insert for micro injection moulding application, the insert surface is to be completely transferred to the replicated surface.

4.2.2 Statistical analysis

A statistical analysis was applied to the metrology results of PoT micro mould inserts. The method followed is consistent with [9] and is summarised in **Figure 4.2-8**, including the uncertainty evaluation. Description and details of the techniques used can be found elsewhere [26]. The statistical analysis was performed on the results from the optical instruments, retaining the ones related to the tactile instrument as a reference for the uncertainty calculation. The evaluated uncertainty, in fact, was a consequence of the least square method used to compare optical and contact measurements results. Examples of acquired surfaces and related results are shown in **Figure 4.2-9**.

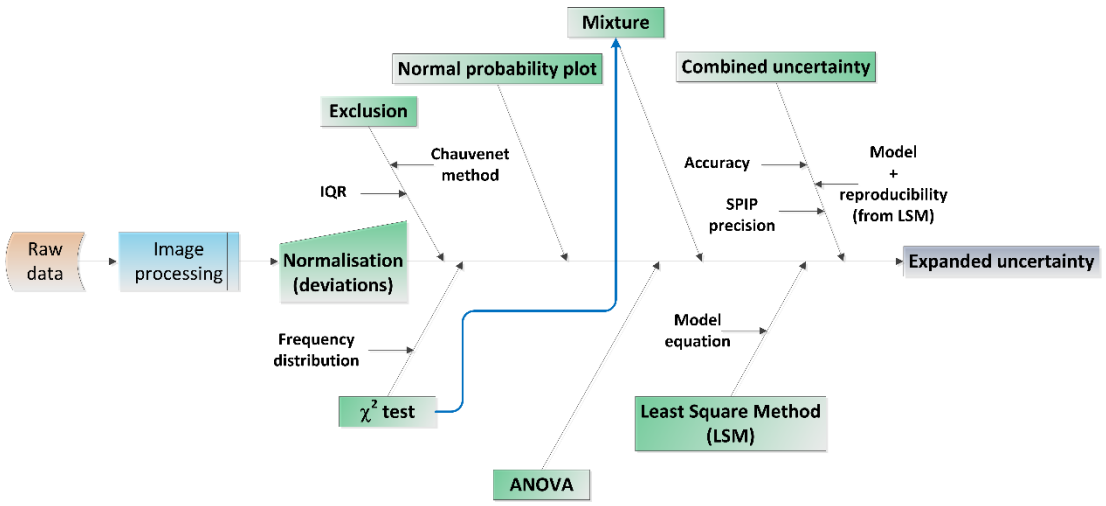

Figure 4.2-8. Diagram summarising the overall analysis and uncertainty evaluation.

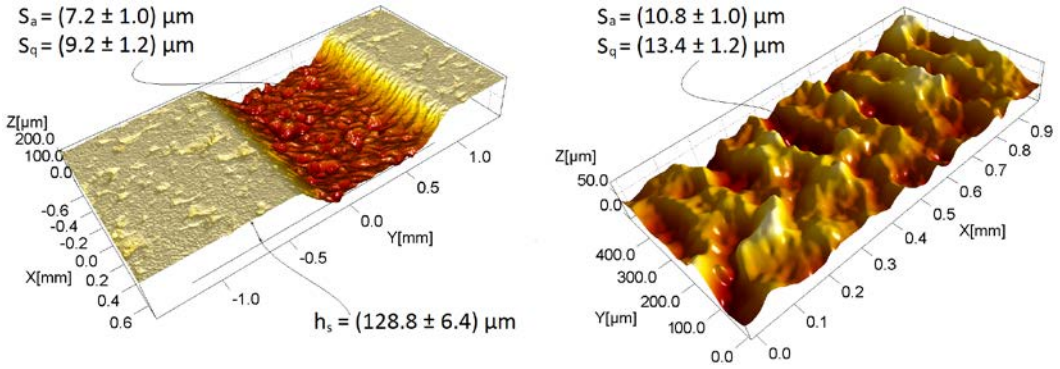

(a) (b)

Figure 4.2-9. Examples of acquired surfaces (3D view) and related results: M9, M10 (a) and M16 (b) (respectively **Table 4.2-15**, **Table 4.2-16**, **Table 4.2-17** and **Table 4.2-18**, **Table 4.2-19** in § 4.2.3).

Normalisation

A sufficient number of replications of a measured quantity is necessary for a statistical analysis to be effective in shedding light on all the aspects related to the measuring sessions and, at the same time, for the resulting estimated uncertainty to be representative of the dispersion of the values which could be reasonably attributed to the measurand § 4.4.

In this investigation, even though the measurement data were available in large number when considering the areal acquisitions over the specimens, they were limited in terms of replications of each measurand. To obtain a consistent number of data, the results of the image processing were normalised (subtracted) to their respective areal averages (M9, M10, M11…). Three groups of deviations, for each specimen material (aluminium and steel), were obtained, respectively associated to step heights (depth) and to *Sa* and *Sq* parameters of the optical measurements.

The numbers of deviations in each group is reported in **Table 4.2-3**, after applying an exclusion principle (see § 4.2.2.1 for further details). The experimental data were heterogeneous in terms of repeated measurements, i.e. there were not the same number of repeated measurements for each measurand (this circumstance is described in statistics as unbalanced set of data).

Table 4.2-3. Number of replications after the exclusion principle according to the groups of deviations.

Specimens	*depth dev.*	*Sa dev.*	*Sq dev.*
Aluminium	37	41	42
Steel	41	37	38

4.2.2.1 Outliers detection

The presence of outliers (accidents of measure or, in general, discordant observations), i.e., values unsuitable for the statistical analysis, was examined by the well-known Chauvenet's criterion, which assigns to the entire experiment a probability of 50 % of measurement accident occurrence [27]. According to this exclusion principle the data in the following table have been discarded (**Table 4.2-4**):

Table 4.2-4. Measurement results detected as outliers by the Chauvenet's criterion and discarded from the datasets.

	Aluminium			**Steel**		
Area	*depth*	*Sa*	*Sq*	*depth*	*Sa*	*Sq*
M12		CM 50×, CM 100×, FVM 50×	CM 50×, FVM 50×			
M13				CM 50× - 1		
M14					CM 50×, CM 100×, FVM 50×	CM 50×, CM 100×, FVM 50×

Exclusion

Values that are evidently outside the experimental distribution can be eliminated using an exclusion principle [27]. In this operation, it is helpful to graphically representing data by boxplots and histograms:

- Boxplots, based on the interquartile range of each homogeneous group of measurands, can assist to inspect agreement among the data.
- Histograms are helpful to visualise the distribution of the experimental data. The most favourable situation for the evaluation of uncertainty is, in fact, a normal distribution, which means that the data are randomly distributed (see § 4.4).

The exclusion of outliers supported the successive analysis of normality inspection of the experimental distribution and for the correction of possible systematic behaviour. Nonetheless, excluding some measurement values inevitably involves the risk of also excluding some suitable result. Therefore, a deep knowledge of the experimental data was also necessary before considering a result as an outlier.

Aluminium specimen

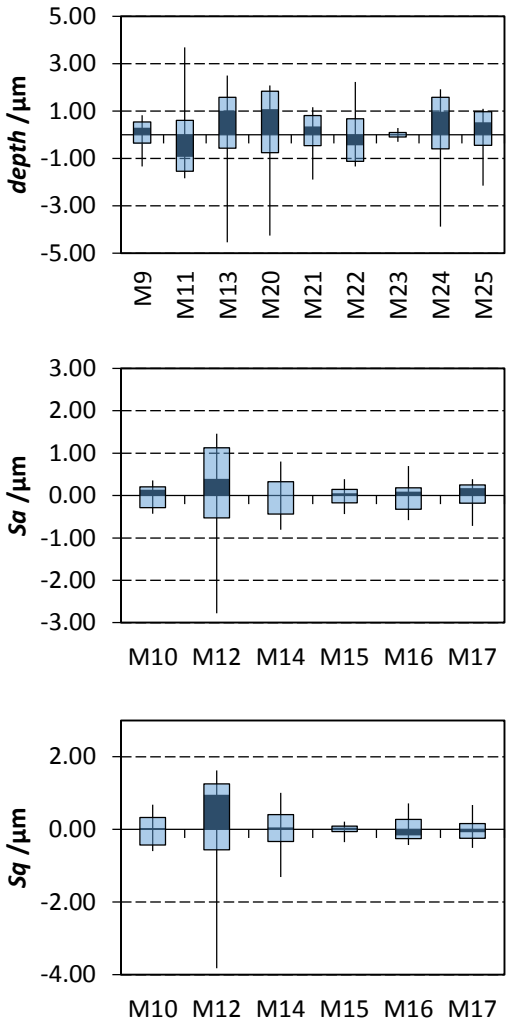

Figure 4.2-10. Aluminium specimen: boxplots of deviations with interquartile range, maximum, minimum and median (before outliers elimination).

Steel specimen

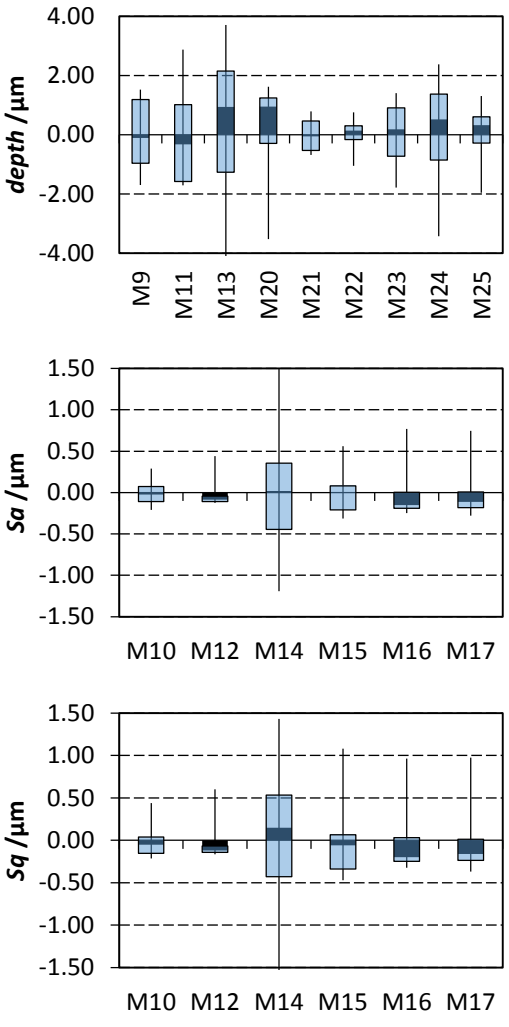

Figure 4.2-11. Steel specimen: boxplots of deviations with interquartile range, maximum, minimum and median (before outliers elimination).

The research of outliers was an iterative procedure, monitoring the boxplots (**Figure 4.2-10** to **Figure 4.2-13**) and the histograms (**Figure 4.2-14** and **Figure 4.2-15**) at each iteration. So, not all the outliers highlighted by the exclusion principle were discarded; above all when no evidence of disturbances was found in the corresponding raw measurement file or the related value was in agreement with the reference one (contact measurement). The data corresponding to each sub-group of areal acquisition were graphically represented by boxplots. A box equals a sub-group interquartile range (IQR), the "whiskers" are the corresponding maximum and minimum values and the column inside each box is the median. The deviations are reported in **Figure 4.2-10** and **Figure 4.2-11**, before the elimination of outliers, and in **Figure 4.2-12** and **Figure 4.2-13**, after the elimination of outliers.
After the elimination, almost all the IQRs were in good agreement in each respective group, which means that the exclusion was effective. Few exceptions were M14 area in *Sa* and *Sq* sub-groups of steel specimen and M12 area in *Sq* sub-group of Aluminium specimen. As already explained, M14 area in steel specimen was affected by waviness. Regarding the other exception, looking in the raw measurements files, disturbances were evident but not so diffused to justify an elimination. In addition, no further value was evidenced by the exclusion principle.

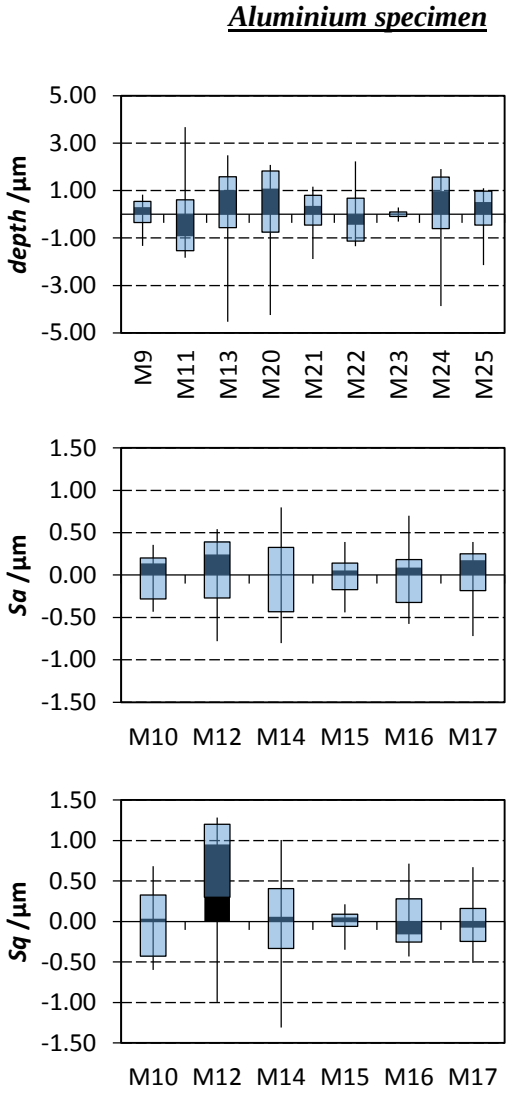

Figure 4.2-12. Aluminium specimen: boxplots of deviations with interquartile range, maximum, minimum and median (after outliers elimination).

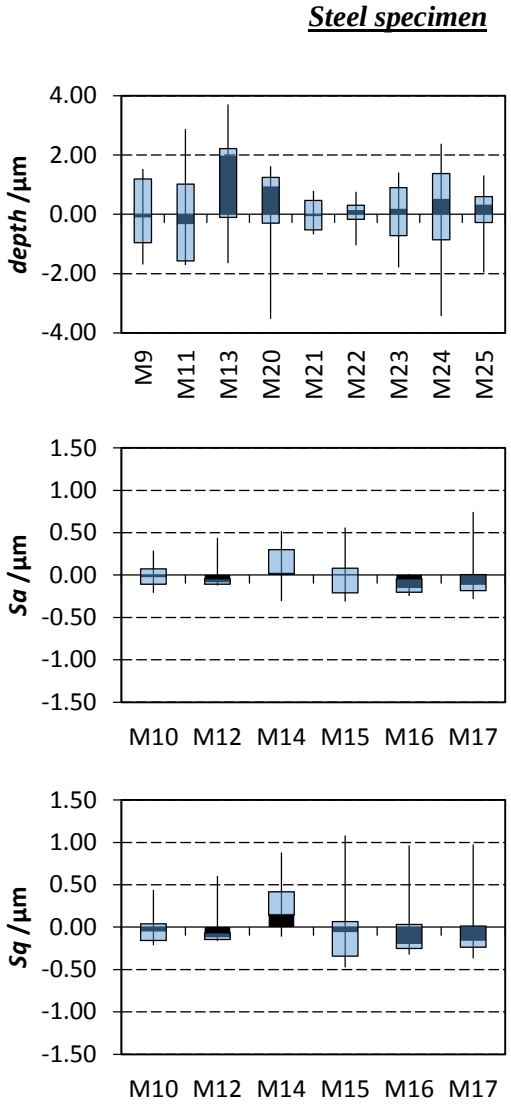

Figure 4.2-13. Steel specimen: boxplots of deviations with interquartile range, maximum, minimum and median (after outliers elimination).

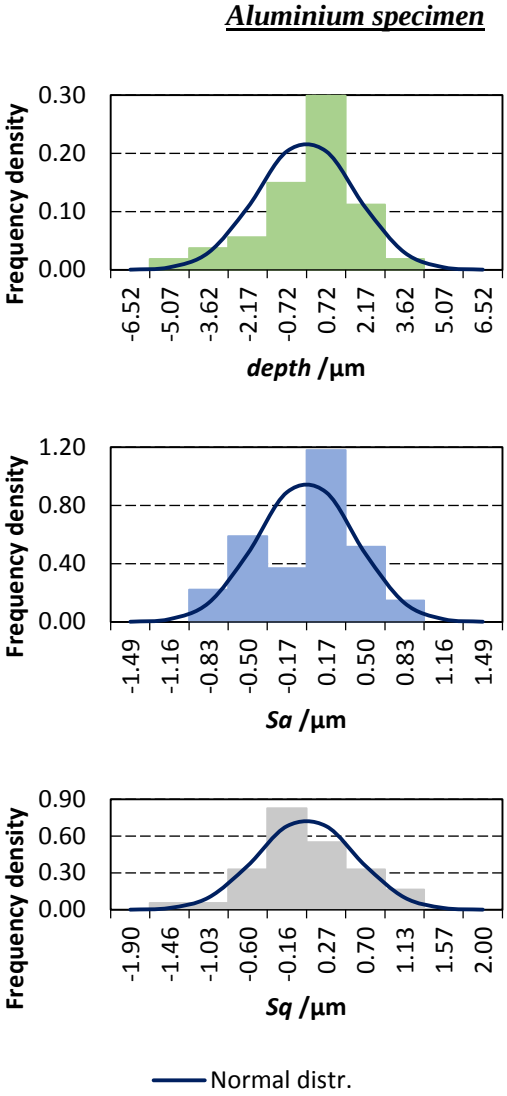

Figure 4.2-14. Aluminium specimen: histograms of experimental distributions and curve of the normal distributions.

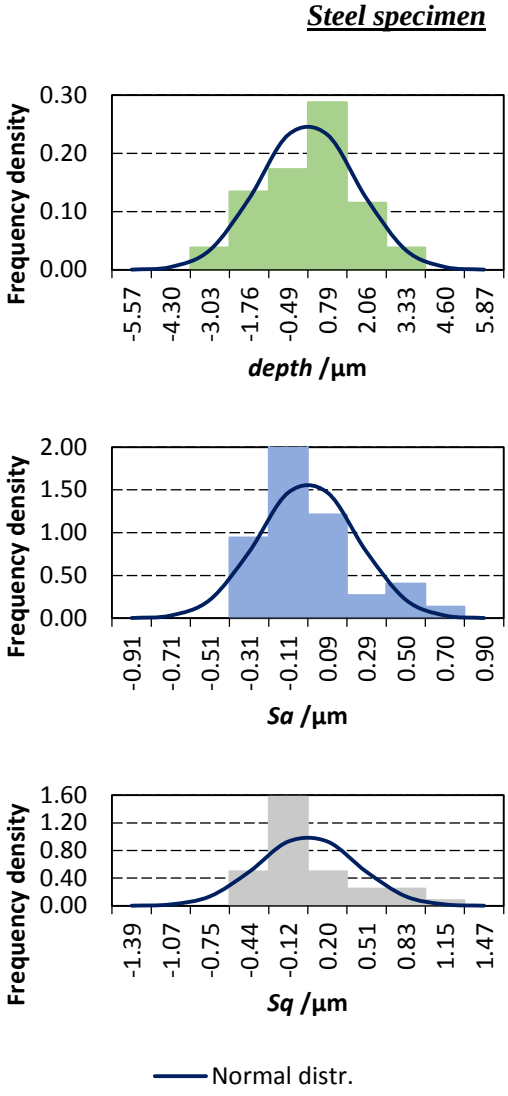

Figure 4.2-15. Steel specimen: histograms of experimental distributions and curve of the normal distributions.

4.2.2.2 Systematic effects

What is graphically represented by the histograms can be examined by running several statistical normality tests. Deviances from the normal distribution can be evidenced and then corrected (see § 4.2.2.2 , § 4.3 and § 4.4). Such deviances are called systematic effects and can be related to the factors involved in the measurements. They are, in fact, consequences of the measurement operations, due to the non-ideal behaviour and use of the measurement instruments in the actual environmental conditions. Hence, the time sequence of the measurement events (occurrences) is strictly related to the generation of such effects (see § 4.3). They can be identified as a difference from the random effects when the Theorem of Central Limit has its validity (i.e. when an adequate number of data is generated—see § 4.4).

Organising the data in the exact time sequence allows to evidence systematic behaviours, mathematically describing and correcting them using regression models.

The tendencies are highlighted in **Figure 4.2-16** and in **Figure 4.2-17**. On the top, step height measurements are distributed in such a way that an overall correction can be achieved. Instead, roughness measurements can be corrected by piecewise regressions (i.e. per instruments).
Therefore, statistical tests aimed to characterise the experimental data were carried out on the groups of deviations and, eventually, the least square method was implemented onto the un-normalised values.

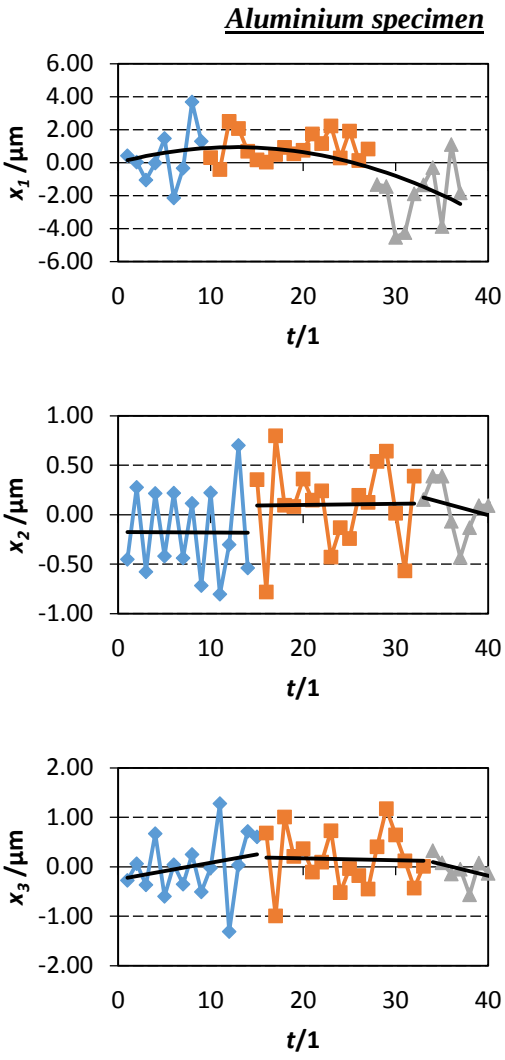

Figure 4.2-16. Aluminium specimen: sequence of deviations. First on the left, in blue, is CM; in the middle, in red, is CSI and on the right, in green, is FVM. x_1 stands for depth, x_2 for Sa and x_3 for Sq.

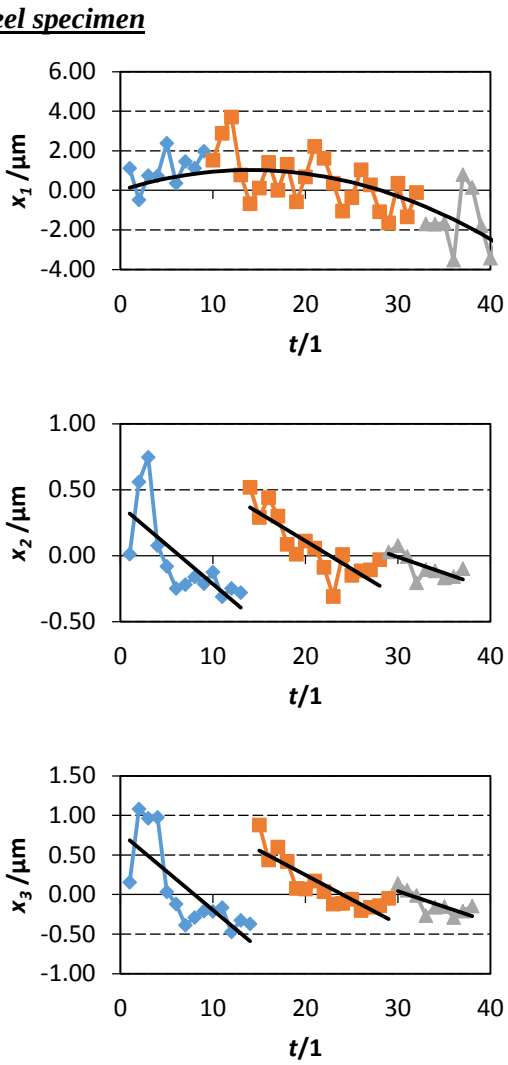

Figure 4.2-17. Steel specimen: sequence of deviations. First on the left, in blue, is CM; in the middle, in red, is CSI and on the right, in green, is FVM. x_1 stands for depth, x_2 for Sa and x_3 for Sq.

χ^2 test

The deviations were statistically grouped in histograms (**Figure 4.2-14** and **Figure 4.2-15**) and compared with the respective theoretical normal distributions. A chi-square test was performed accordingly, with the statistical null hypothesis that the experimental distributions were normal. The confidence level was stated to 80 %, i.e. accepting a risk of error of 20 %. The choice of such confidence level was considered conservative. In fact, it is normally related to the consequences of rejecting the null hypothesis. In other words, a high risk of error (of first type) could result in getting an answer of systematic effects even though they were absent.

In this particular case, the consequence would be a possible re-examination of the measurement process, which was done anyway by other normality tests.
The test rejected the null hypothesis of normal distribution only in the cases of depth and *Sq* sub-groups of the steel specimen. In all the other sub-groups no systematic effects were evidenced. However, looking at the histograms, none of them is suitable to be represented by their respective normal distributions.

Aluminium specimen

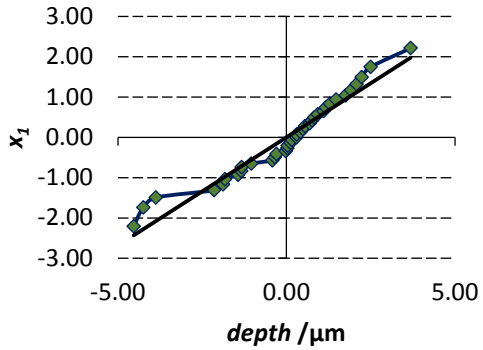

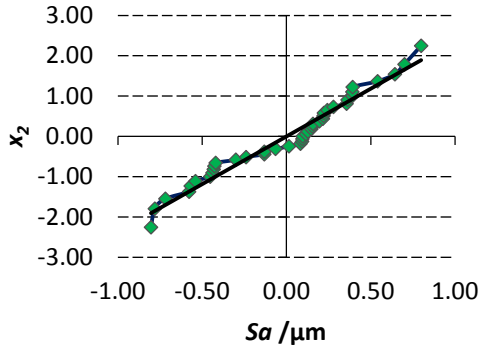

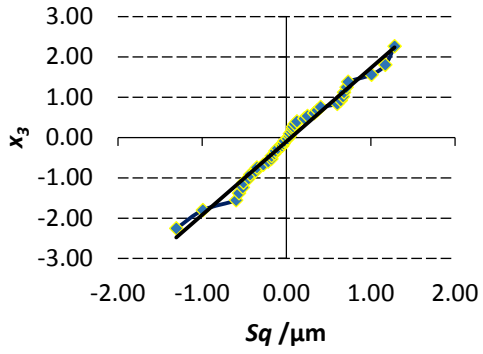

Figure 4.2-18. Aluminium specimen: NPP of deviations.

Steel specimen

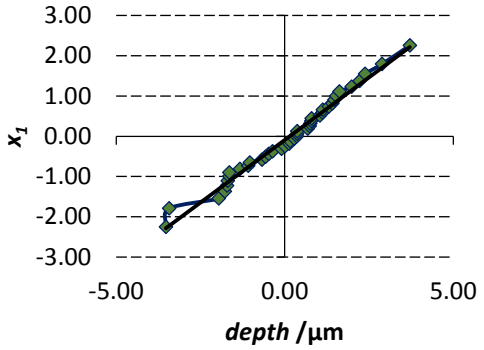

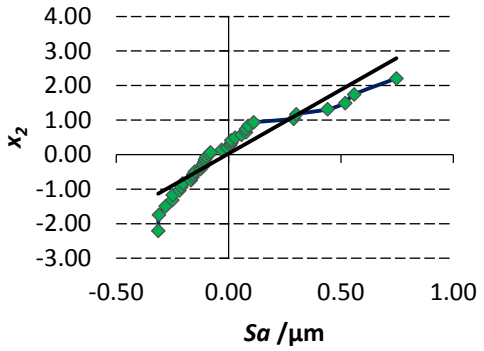

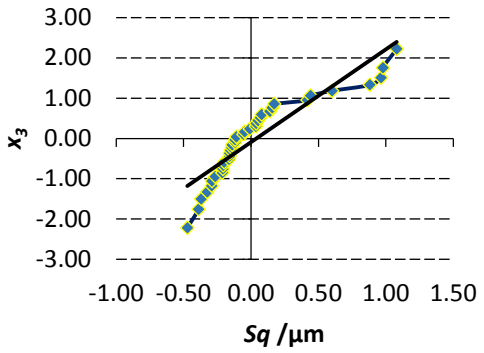

Figure 4.2-19. Steel specimen: NPP of deviations.

Normal Probability Plot (NPP)

NPP is the representation of the cumulative normal distribution with the ordinate deformed so that its typical "S" shape becomes a straight line.
NPP diagrams for the deviations under evaluation are reported in **Figure 4.2-18** and **Figure 4.2-19**. Each NPP has a trend, which is clearly far from a straight line.
Deviances with respect to the straight line lead to a hypo-normal distribution when the slope of the curve is higher at the extremes and lower in the middle, resulting in a reversed "S" shape.

Conversely, deviances with respect to the straight line lead to a hyper-normal distribution when the slope of the curve is lower at the extremes and higher in the middle, resulting in an "S" shape. Looking at the extremes of the curves, aluminium specimen distribution x_2 can be considered hypo-normal. However, the slope is not confirmed in the middle where an arc is present.
More difficult is to analyse the other curves in which the two extremes show different trend of slope (one higher and the other lower than the straight line). This is the case of distribution x_1 and x_3 of both aluminium and steel specimens. Steel specimen distribution x_3 shows a concave arc in the middle, which evidences a right asymmetric distribution (right-skewed; see also histograms in **Figure 4.2-14** and **Figure 4.2-15**). The same can be said for distribution x_2 of the steel specimen. Hence, systematic effects are evident. However, a better understanding of the curves can be achieved if different slopes piecewise can be recognised (multimodal distributions) presuming, therefore, systematic effects due to different factors.

ANOVA

The analysis of variance (ANOVA) is a test based on the ratio between two different calculations of the experimental data variance: one should not contain effects of any systematic factor while the other should contain only the effect of the examined factor.
ANOVA test was performed to connect systematic effects to the factors involved in the measurements.
Being the data sets unbalanced, a general linear model was used to implement the ANOVA test, considering the three factors *instrument*, *magnification* and *acquisition area*. The experimental data were not enough for also considering the interactions among the factors.
The results, reported in **Table 4.2-5** and **Table 4.2-6**, were obtained using adjusted sum of squares, which means that the results were not considered dependent on the order the factors are entered into the model.

Aluminium specimen

Table 4.2-5. ANOVA: general linear model, adjusted sum of squares.

	depth	*Sa*	*Sq*
Instr.	Influence (p-val <0.001)	No infl.	No infl.
Mag.	No influence	No infl.	No infl.
Area	No influence	No infl.	No infl.
R^2	55 %	12 %	14 %

Steel specimen

Table 4.2-6. ANOVA: general linear model, adjusted sum of squares.

	depth	*Sa*	*Sq*
Instr.	Influence (p-val <0.001)	No infl.	No infl.
Mag.	Influence (p-val 0.030)	Influence (p-val <0.001)	Influence (p-val <0.001)
Area	No infl.	No infl.	No infl.
R^2	61 %	78 %	84 %

In the case of aluminium specimen, the coefficients of determination associated to the ANOVA model were very low which means that the model was not well fitted. In the case of steel specimen, instead, the coefficients of determination were more robust. Nonetheless, repeating the analysis using sequential sum of squares (results depending on the order of the factors entered into the model) the instrument became an influence factor for *Sq* sub-group, too. Since no information was available about the sequence in which the data were acquired, the given order was an arbitrary one.
In conclusion, the ANOVA test was not completely reliable, too.
In **Figure 4.2-16** and **Figure 4.2-17**, examples of deviations are represented according to the sequence arbitrarily chosen for the current investigation. Their distributions clearly show tendencies that could be identified by regression models and successively corrected. Changing the sequence of the data the tendencies also change. This can affect the results of ANOVA test but not the systematics correction. In fact, the particular mathematical model used for correcting the sequences is not influential of the results if the data are always referred to that specific model.

In addition, in the proposed procedure, the correction is to be achieved against the reference measurements.

Mixture

When different, even though few, systematic effects are existent in the experimental data it is likely that the statistical methods based on the hypothesis of normal distribution fail. In this situation, the joint effects of random and systematic factors can be described as a mixture of normal distributions [28].

Figure 4.2-20 to **Figure 4.2-23** show a mixture of three normal distributions for each group of deviations and the comparison between the estimated mixture and the kernel distribution. The kernel represents here the probability density estimation of the experimental data and corresponds to the envelope of the histograms in **Figure 4.2-14** and **Figure 4.2-15**. As shown in the figures, the mixtures describes the kernel distributions shapes with a good faithfulness. The estimates of the parameters (average, standard deviation and percentage of incidence) of the normal distributions in the mixtures were obtained by an optimisation of the chi-square test and are given in **Table 4.2-7** to **Table 4.2-12**.

Aluminium specimen

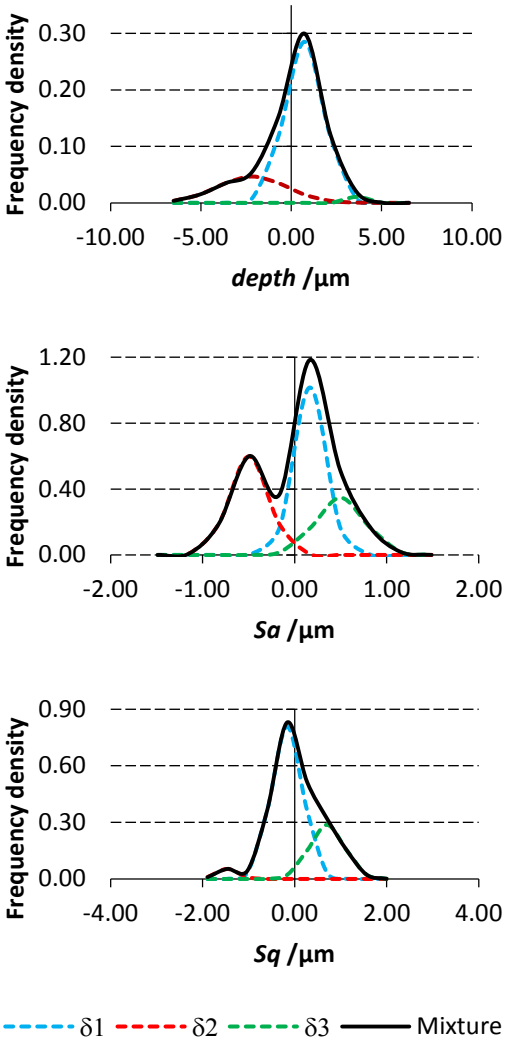

Figure 4.2-20. Mixture of three normal distributions (values in **Table 4.2-7** to **Table 4.2-9**).

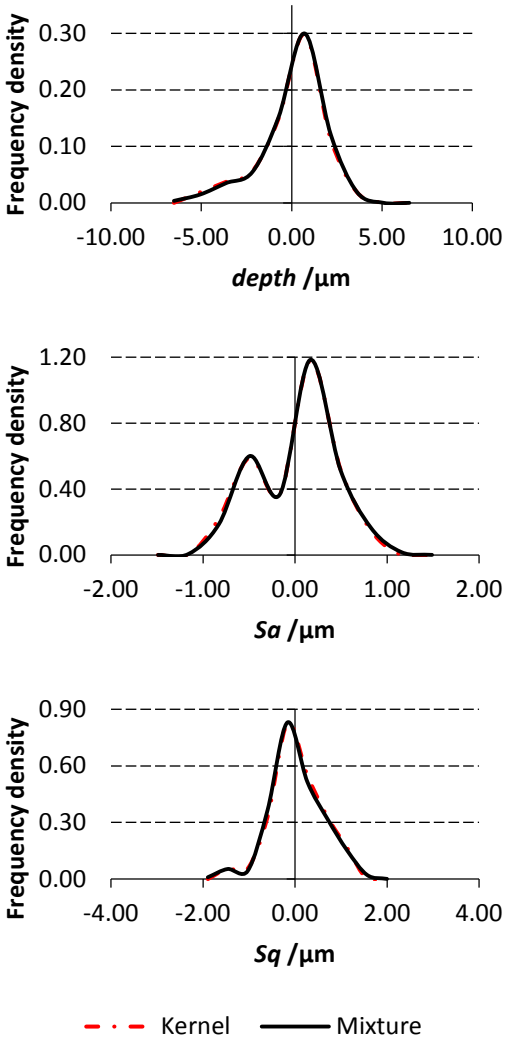

Figure 4.2-21. Comparison between mixture and probability density estimation of the experimental data (kernel).

Table 4.2-7. Depth group: parameters of three normal distributions (optimised χ^2 statistics is 0.52).

Distribution	*Average /µm*	*STD /µm*	*Percentage /%*
1	0.72	1.08	77.4
2	-2.17	1.91	22.3
3	3.62	0.11	0.3

Table 4.2-8. Sa group: parameters of three normal distributions (optimised χ^2 statistics is 0.98).

Distribution	*Average /µm*	*STD /µm*	*Percentage /%*
1	0.17	0.17	44.1
2	-0.50	0.22	32.5
3	0.50	0.27	23.4

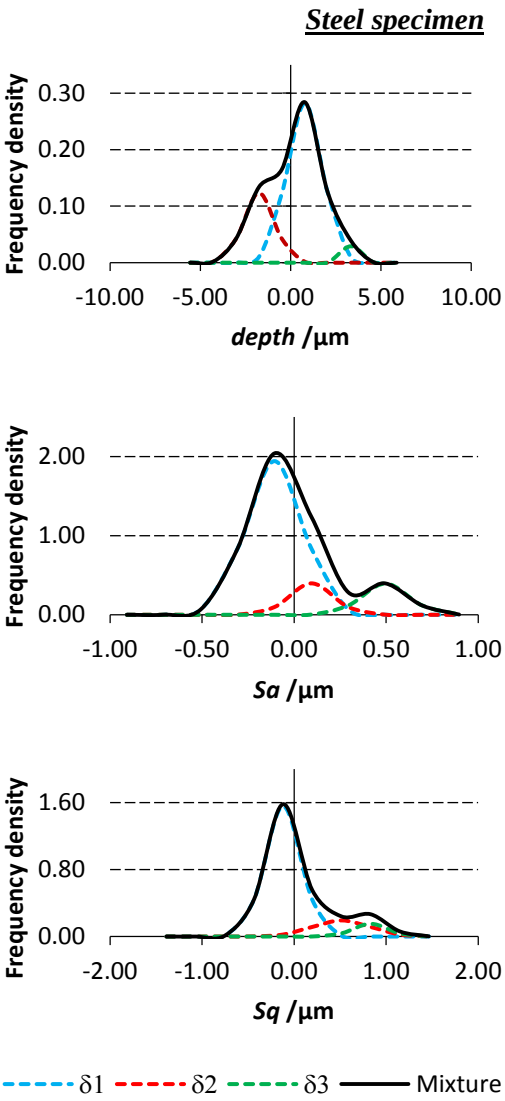

Figure 4.2-22. Mixture of three normal distributions (values in **Table 4.2-10** to **Table 4.2-12**).

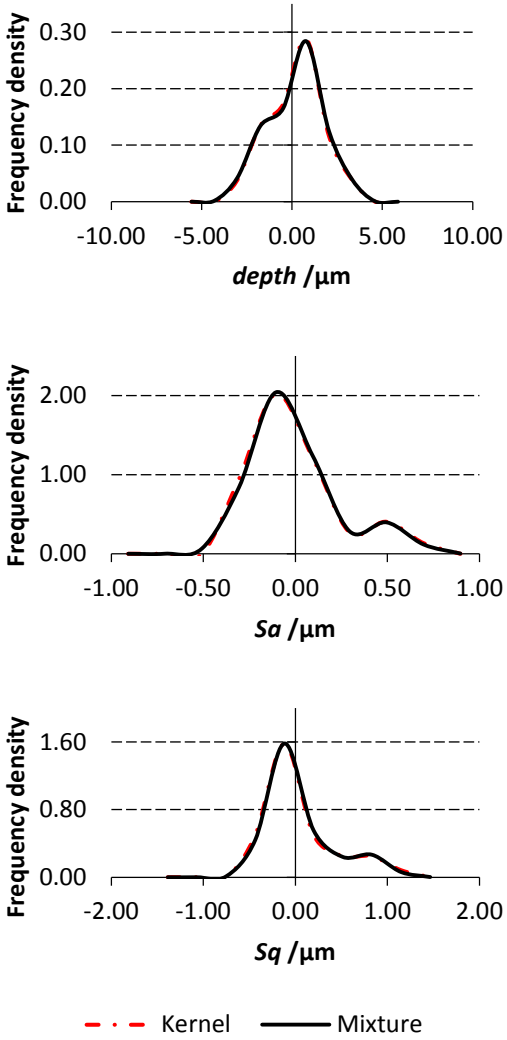

Figure 4.2-23. Comparison between mixture and probability density estimation of the experimental data (kernel).

Table 4.2-9. Sq group: parameters of three normal distributions (optimised χ^2 statistics is 0.95).

Distribution	*Average /µm*	*STD /µm*	*Percentage /%*
1	-0.16	0.34	69.5
2	-1.46	0.23	3.1
3	0.70	0.38	27.4

Table 4.2-10. Depth: parameters of three normal distributions (optimised χ^2 statistics is 0.55).

Distribution	*Average /µm*	*STD /µm*	*Percentage /%*
1	0.79	0.99	69.9
2	-1.76	0.87	26.9
3	3.33	0.45	3.3

Table 4.2-11. Sa group: parameters of three normal distributions (optimised χ^2 statistics is 0.99).

Distribution	*Average /µm*	*STD /µm*	*Percentage /%*
1	-0.11	0.15	75.3
2	0.09	0.12	11.9
3	0.50	0.13	12.8

Table 4.2-12. Sq group: parameters of three normal distributions (optimised χ^2 statistics is 0.77).

Distribution	*Average /µm*	*STD /µm*	*Percentage /%*
1	-0.12	0.20	77.8
2	0.51	0.31	15.0
3	0.83	0.19	7.2

Least square method

The method of least squares was implemented onto the un-normalised values (the deviations un-normalised after the statistical analysis by their respective areal averages) to evaluate discrepancies between the optical and the contact measurements, i.e., the reference. On one side, the contact techniques are, in fact, well established as well as the calibration of the instruments used. On the other side, the optical instruments strongly depend on the physical working principle and the relative calibrations are not completely defined.

The model equation which was found consistent with the experimental data is a straight line passing by the origin. Ideally, if different instruments measure the same quantity the results should be equal (unitary angular coefficient). Hence, the best fit evaluated the mismatch with respect to the unitary slope

$$y_{opt} = q \cdot x_t \tag{4.2-1}$$

where y_{opt} refers to the optical values and x_t to the tactile ones.

The results of the regressions are summarised in **Table 4.2-13** and **Table 4.2-14**.

Equation (4.2-1) was found consistent with the experimental data to mathematically describe the best-fit regression. Nonetheless, from a metrological point of view, factors influencing the calculation are to be added into the equation.

Eventually, the complete model equation used for the uncertainty evaluation was

$$y_{opt} = q \cdot x_t \pm Rep \pm Res \quad (4.2\text{-}2)$$

in which the reproducibility *Rep*, i.e., the standard deviation of the regression results, and the resolution *Res* were added.
The resolution is the one of the reference instrument and its effect is usually estimated by the reproducibility. Nevertheless, this does not happen with rough instruments where it should be evaluated separately. It is also true that, when this is not the case, counting the resolution twice does not affect the final uncertainty values because it is very low for quality instruments.
In addition, separate values for reproducibility and resolution may be considered when they refer to heterogeneous contributors, which is, actually, the case considered in this section. Here, the resolution should be the one of the stylus instrument, which is a quality instrument and the resolution can be considered included into the reproducibility. However, the raw measurements acquired by CI were successively analysed with the post-processing software [21]. For this reason, the resolution was set equal to the precision of the post-processing software *Res* = 1 nm. This is a conservative choice because, even though unlikely, the software significative digits may limit the instrument resolution.

Aluminium specimen

Table 4.2-13. Parameters of the least square regressions (first order). Slope *q*, standard deviation of the slope s_q, reproducibility (standard deviation of the residuals), degrees of freedom.

	q /1	s_q /1	*Repr.* /µm	*Deg. of freed.*	R^2 /%
Depth	1.013	0.004	3.112	36	99.9
Sa	1.029	0.008	0.449	40	99.7
Sq	1.028	0.008	0.548	41	99.8

Steel specimen

Table 4.2-14. Parameters of the least square regressions (first order). Slope *q*, standard deviation of the slope s_q, reproducibility (standard deviation of the residuals), degrees of freedom.

	q /1	s_q /1	*Repr.* /µm	*Deg. of freed.*	R^2 /%
Depth	0.998	0.002	2.092	40	99.9
Sa	1.032	0.026	0.252	36	93.9
Sq	1.038	0.033	0.405	37	88.8

4.2.3 Uncertainty evaluation

Equation (4.2-2) is the calibration equation of the optical measurements with respect to the contact ones. The standard uncertainty was calculated, in association with this equation, applying the usual method for the combination of variances of uncorrelated quantities

$$u(y) = \sqrt{\sum_q \left(\frac{\partial f}{\partial x_q} \right)^2 u_q^2(x_q)} \quad (4.2\text{-}3)$$

where *f* is the Model Equation (4.2-2) and x_q each of the following considered contributions:

- The accuracy of the CI (U = 0.112 µm, unfiltered), i.e. its uncertainty stated in the calibration certificate [29] for the range of interest.
- The standard deviations of the coefficient of the model equation defined for the best fit regression (s_q in **Table 4.2-13** and **Table 4.2-14**).
- The reproducibility values out-coming from the regressions (**Table 4.2-13** and **Table 4.2-14**)
- The image processing software precision (1 nm) [21].

Finally, according to [9], the expanded uncertainty was evaluated as the confidence interval corresponding to the conventional confidence level of 95 % (no further information available to choose a different confidence level), which is equivalent to accept a risk of error of the first type of 5 %.
The related coverage factor was calculated using the *t*-distribution with degrees of freedom ν_y evaluated by the Welch-Satterthwaite formula

$$\nu_y = \frac{u^4(y)}{\sum_j \frac{u_j^4(y)}{\nu_j}} \tag{4.2-4}$$

where $u^2(y)$ is the combined variance from Equation (4.2-3), $u_j^2(y)$ and ν_j are respectively the variance of each single contributor and the related degrees of freedom. Hence,

$$U = k\, u(y) \tag{4.2-5}$$

with *k* ranging from 2.0 to 2.3.
The expanded uncertainty is referred to Equation (4.2-2), so that

$$Y_{opt} = q \cdot X_t \pm U \tag{4.2-6}$$

with X_t any measurement acquired with the CI and Y_{opt} the corresponding optical estimates. Equation (4.2-6) is normally used inverted. The stated expanded uncertainty is also inverted with the equation.
The main results are instead summarised in the following, from **Table 4.2-15** to **Table 4.2-26**, with reference, optical measurements and evaluated expanded uncertainties.
In the same tables, an expanded uncertainty related to each optical instrument is also given. Such uncertainties were evaluated considering piecewise regressions (per instrument), i.e., considering separate least squares regressions for the values corresponding to each optical instrument. These values are not intended to be used as expanded uncertainty but rather like a trend: to understand how each optical instrument would have contributed if it were used alone. In other words, these values are only proposed to highlight the role of each optical instrument in the current analysis and how it would have performed alone.

Aluminium specimen

Table 4.2-15. Aluminium specimen: height results for M9, M11 and M13 surfaces and expanded uncertainty.

	Depth /µm										
	Tact	*CM 10×*	*CSI 10×*	*CSI 20×*	*CSI 50×*	*FVM 20×*	*FVM 50×*	*U*	U_{CM}	U_{CSI}	U_{FVM}
M9	128.8	130.5	131.1	131.4	131.6	129.5		6.4	6.8	5.8	6.6
M11	131.4	132.8	128.7			127.7	127.3	6.4	6.8	5.8	6.7
M13	126.8	132.1	133.3	131.6		126.3		6.4	6.8	5.8	6.6

Table 4.2-16. Aluminium specimen: *Sa* roughness results for M10 and M12 surfaces and expanded uncertainty.

	Groove's roughness – ***Sa*** /µm										
	Tact	*CM 50×*	*CM 100×*	*CSI 10×*	*CSI 20×*	*CSI 50×*	*FVM 50×*	*U*	U_{CM}	U_{CSI}	U_{FVM}
M10	7.21	6.95	7.59	7.73	7.52	7.50	6.94	0.98	1.09	1.11	0.72
M12	8.52			7.50	8.53	8.82		0.98	1.09	1.12	0.73

Table 4.2-17. Aluminium specimen: *Sq* roughness results for M10 and M12 surfaces and expanded uncertainty.

Groove's roughness – ***Sq*** /µm

	Tact	*CM 50×*	*CM 100×*	*CSI 10×*	*CSI 20×*	*CSI 50×*	*FVM 50×*	*U*	U_{CM}	U_{CSI}	U_{FVM}
M10	9.15	8.72	9.30	10.01	9.42	9.73	8.76	1.17	1.22	1.39	1.01
M12	11.24		12.25	9.97	11.70	12.14		1.17	1.22	1.41	1.02

Table 4.2-18. Aluminium specimen: *Sa* roughness results for M14-M17 surfaces and expanded uncertainty.

Roughness in basins – ***Sa*** /µm

	Tact	*CM 5×*	*CM 50×*	*CM 100×*	*CSI 10×*	*CSI 20×*	*CSI 50×*	*FVM 20×*	*FVM 50×*	*U*	U_{CM}	U_{CSI}	U_{FVM}
M14	10.50	10.59	11.26	10.23	11.84	10.61	11.68	11.19	10.91	0.99	1.11	1.13	0.74
M15	7.27	7.78	7.06	7.20	7.59	7.37	7.51	7.89	7.59	0.98	1.09	1.12	0.72
M16	10.78	10.50	11.19	11.78	11.16	10.84	10.51	11.47	11.17	0.99	1.11	1.13	0.74
M17	6.11	6.39	5.46	5.64	6.54	6.37	6.57	6.11	6.33	0.98	1.08	1.11	0.72

Table 4.2-19. Aluminium specimen: *Sq* roughness results for M14-M17 surfaces and expanded uncertainty.

Roughness in basins – ***Sq*** /µm

	Tact	*CM 5×*	*CM 50×*	*CM 100×*	*CSI 10×*	*CSI 20×*	*CSI 50×*	*FVM 20×*	*FVM 50×*	*U*	U_{CM}	U_{CSI}	U_{FVM}
M14	12.71	13.09	13.40	12.05	14.37	12.84	14.01	13.69	13.44	1.18	1.24	1.41	1.03
M15	8.97	9.27	8.86	9.24	9.42	9.17	9.33	9.29	9.08	1.17	1.22	1.39	1.01
M16	13.41	13.15	13.77	14.23	13.88	13.34	13.09	13.37	13.30	1.18	1.24	1.42	1.03
M17	7.75	8.73	7.55	8.66	7.95	7.61	8.07	8.01	7.88	1.17	1.21	1.39	1.00

Table 4.2-20. Aluminium specimen: height results for M20–M25 surfaces and expanded uncertainty

Depth /µm

	Tact	*CM 5×*	*CSI 10×*	*CSI 20×*	*FVM 20×*	*U*	U_{CM}	U_{CSI}	U_{FVM}
M20	134.0	133.8	135.5	135.1	129.1	6.4	6.8	5.8	6.7
M21	108.8	115.3	115.9	116.4	113.4	6.4	6.7	5.7	6.6
M22	213.9	215.2	216.4	218.5	214.9	6.5	7.0	6.0	6.9
M23	80.5	80.4	80.5	80.7	80.1	6.4	6.7	5.7	6.6
M24	188.4	193.8	192.8	194.2	188.4	6.5	6.9	5.9	6.8
M25	79.8	77.3	80.4	79.6	80.6	6.4	6.7	5.7	6.6

Steel specimen

Table 4.2-21. Steel specimen: height results for M9, M11 and M13 surfaces and expanded uncertainty.

Depth /µm

	Tact	*CM 10×*	*CSI 10×*	*CSI 20×*	*CSI – 1 50×*	*CSI – 2 50×*	*FVM 20×*	*U*	U_{CM}	U_{CSI}	U_{FVM}
M9	162.6	162.1	162.1	160.0	159.5	161.0	158.9	4.3	3.0	4.1	5.5
M11	162.3	163.9	165.7	163.5	161.1	161.4	161.1	4.3	3.0	4.1	5.5
M13	164.2	167.3	169.0	167.6		165.2	163.7	4.3	3.0	4.1	5.5

Table 4.2-22. Steel specimen: *Sa* roughness results for M10 and M12 surfaces and expanded uncertainty.

Groove's roughness – ***Sa*** /µm

	Tact	*CM 50×*	*CM 100×*	*CSI 20×*	*CSI – 1 50×*	*CSI – 2 50×*	*FVM 50×*	*U*	U_{CM}	U_{CSI}	U_{FVM}
M10	0.84	0.88	0.59	1.09	0.86	0.69	0.70	0.63	0.81	0.60	0.46
M12	0.79	0.64	0.60	1.16	0.63	0.69	0.61	0.63	0.81	0.60	0.46

Table 4.2-23. Steel specimen: *Sq* roughness results for M10 and M12 surfaces and expanded uncertainty.

Groove's roughness – ***Sq*** /µm

	Tact	*CM 50×*	*CM 100×*	*CSI 20×*	*CSI – 1 50×*	*CSI – 2 50×*	*FVM 50×*	*U*	U_{CM}	U_{CSI}	U_{FVM}
M10	1.10	1.06	0.81	1.47	1.06	0.89	0.87	0.90	1.33	0.72	0.52
M12	0.98	0.80	0.76	1.52	0.80	0.87	0.77	0.90	1.33	0.72	0.52

Table 4.2-24. Steel specimen: *Sa* roughness results for M14-M17 surfaces and expanded uncertainty.

Roughness in basins – ***Sa*** /µm

	Tact	*CM 5×*	*CM 50×*	*CM 100×*	*CSI 10×*	*CSI 20×*	*CSI 50×*	*FVM 20×*	*FVM 50×*	*U*	U_{CM}	U_{CSI}	U_{FVM}
M14	4.12	4.18			4.68	4.47	3.86	4.19		0.66	0.99	0.64	0.52
M15	0.62	1.15	0.35	0.28		0.68	0.60	0.67	0.43	0.63	0.81	0.60	0.46
M16	0.40		0.36	0.33		0.59	0.43	0.57	0.42	0.63	0.80	0.60	0.46
M17	0.36	1.22	0.31	0.19		0.58	0.36	0.27	0.37	0.63	0.80	0.60	0.46

Table 4.2-25. Steel specimen: *Sq* roughness results for M14-M17 surfaces and expanded uncertainty.

Roughness in basins – ***Sq*** /µm

	Tact	*CM 5×*	*CM 50×*	*CM 100×*	*CSI 10×*	*CSI 20×*	*CSI 50×*	*FVM 20×*	*FVM 50×*	*U*	U_{CM}	U_{CSI}	U_{FVM}
M14	5.19	5.25			5.97	5.51	4.98	5.23		0.95	1.66	0.77	0.60
M15	0.78	1.91	0.44	0.36		0.91	0.77	0.88	0.54	0.90	1.33	0.71	0.51
M16	0.49	1.69	0.44	0.41		0.80	0.53	0.72	0.52	0.89	1.32	0.71	0.51
M17	0.44	1.58	0.40	0.24		0.78	0.45	0.34	0.47	0.89	1.32	0.71	0.51

Table 4.2-26. Steel specimen: height results for M20–M25 surfaces and expanded uncertainty.

	Depth /µm								
	Tact	*CM 5×*	*CSI 10×*	*CSI 20×*	*FVM 20×*	*U*	U_{CM}	U_{CSI}	U_{FVM}
M20	97.3	96.2	95.9	96.7	91.6	4.3	2.9	4.1	5.4
M21	84.8	83.9	83.7	84.8	85.2	4.3	2.9	4.0	5.4
M22	177.2	177.8	177.1	176.0	177.2	4.3	3.0	4.1	5.6
M23	85.2	85.6	86.3	84.5	83.1	4.3	2.9	4.1	5.4
M24	163.1	163.9	161.5	162.6	158.1	4.3	3.0	4.1	5.5
M25	80.2	80.9	81.9	80.8	78.6	4.3	2.9	4.1	5.4

4.3 Correction of the systematic behaviour vs. time sequence

In the previous study case (see § 4.2), the correction of the systematic behaviour was achieved in consequence of the regression against the reference (contact measurements), matching correspondent measurements. This was required for indirectly achieving traceability through a calibrated instrument.

Indeed, the correction of the systematic behaviour is independent from any reference. As already emphasised in § 4.2.2.2, such effects act as a result of the non-ideal behaviour and use of the measurement instruments in the actual environmental conditions. Hence, the time sequence of the measurement events (occurrences) is strictly related to the generation of such effects. In order to better point out this matter, two areas of the same specimens in the previous study case were re-measured and corrected according to the time sequence of acquisition [30]. Furthermore, two issues that influenced the results of the previous analysis were modified in this second study case:

- Several repeated measurements were performed, including repeated measurements for each possible influence factor.
- The time sequence of the acquisitions was stored and considered during the analysis.

Metrology

Measurements of the steel specimens were repeated by FVM (**Figure 4.2-2-(a)**) for the step height defined in area M11 (**Figure 4.2-4**) and for the surface texture (*Sa* parameter) of area M14 (**Figure 4.2-5**, top):

- The step height was measured in M11 by twenty-five repeated areal acquisitions. Different magnifications were considered (5×, 10×, 20×, 50× and 100×), performing five acquisitions by each objective. The Chauvenet's criterion did not evidence any outlier.
- The *Sa* roughness was calculated by thirty repeated areal acquisitions in M14. Five ones by 5× objective and other five with 10×; fifteen by 20×; three by 50×; two by 100×. The Chauvenet's criterion evidenced one outlier that was excluded.

Two examples of areal acquisitions are shown in **Figure 4.3-1**. Average values and expanded uncertainties are also given in the figure.

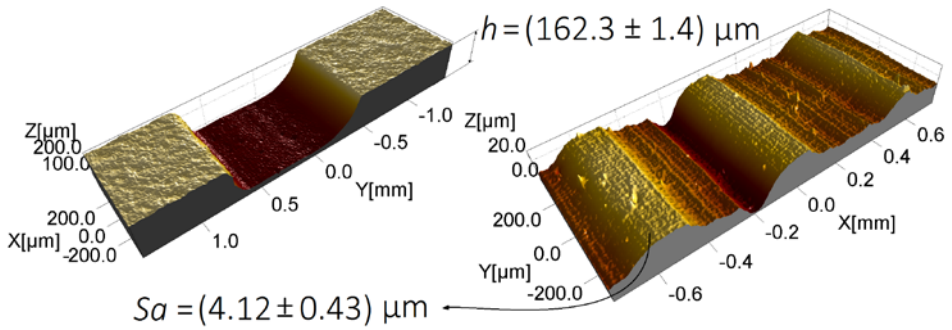

Figure 4.3-1. Illustration in 3-D of two examples of acquired surfaces. Average values and related expanded uncertainties are also indicated.

Table 4.3-1. ANOVA: general linear model, sequential sum of squares.

	depth	*Sa*
Day	Influence (p-value < 0.001)	Influence (p-value < 0.001)
Mag.	Influence (p-value < 0.001)	Influence (p-value < 0.001)
R^2	76 %	91 %

Area M11 – step height

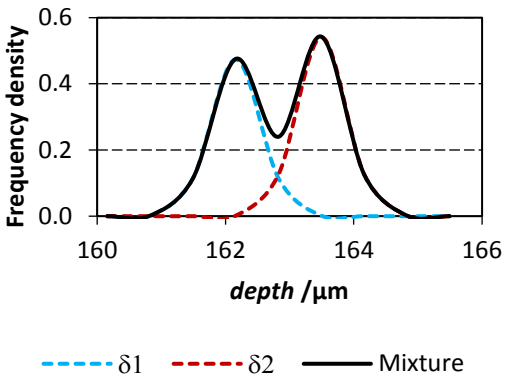

Figure 4.3-2. Mixture of two normal distributions (values in **Table 4.3-2**).

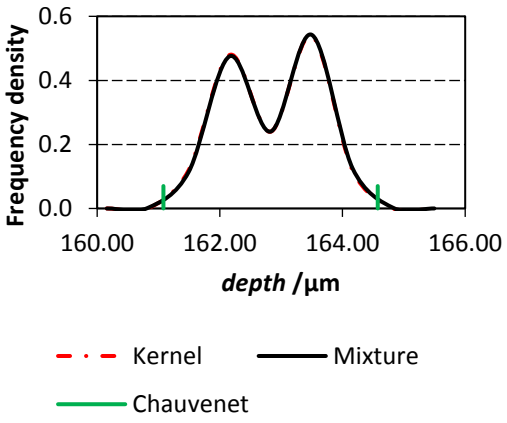

Figure 4.3-3. Comparison between mixture (**Figure 4.3-2**) and probability density estimation of the experimental data (kernel). The limits corresponding to the Chauvenet criterion are also indicated (vertical green segments).

Area M14 – Sa roughness

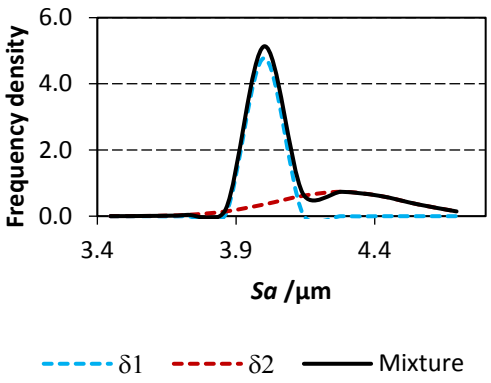

Figure 4.3-4. Mixture of two normal distributions (values in **Table 4.3-3**).

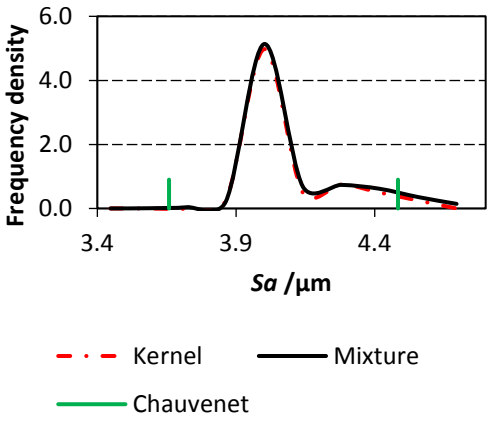

Figure 4.3-5. Comparison between mixture (**Figure 4.3-4**) and probability density estimation of the experimental data (kernel). The limits corresponding to the Chauvenet criterion are also indicated (vertical green segments).

Systematics

After the exclusion of one outlier, the ANOVA test was used to investigate two influence factors in the measurement sessions, namely, the *magnification* and the *day* in which the acquisitions were performed. The acquisitions, in fact, were completed in six days, spending three days per each specimen. Therefore, the measurements related to a specific day or to a definite magnification were compared with the ones of all the other corresponding factors, for each of the two quantities examined. A general linear model was used with sequential sum of squares.
The results of ANOVA test are in **Table 4.3-1**. Both factors influence the measurements in all the quantities examined. The fit of the models was acceptable (R^2 = 76 % for depth measurements and R^2 = 91% for *Sa* ones), even though not completely adequate for the depth measurements.

Mixtures of normal distributions successively confirmed the systematic behaviour investigated by the ANOVA (**Figure 4.3-2** to **Figure 4.3-5**). In particular, both experimental distributions (step height and *Sa*) are bivariate normal distributions. In addition, being available several repeated measurements, it was possible to associate the factors to their corresponding marginal distributions calculating the averages related to each factor. The parameters of the marginal distributions in the mixtures are in **Table 4.3-2** and **Table 4.3-3**.

Table 4.3-2. Depth: parameters of two normal distributions (optimised χ^2 statistics is 0.62).

Distribution	*Average /µm*	*STD /µm*	*Percentage /%*
1 (*day*)	162.16	0.40	47.0
2 (*magnification*)	163.49	0.39	53.0

Table 4.3-3. *Sa*: parameters of three normal distributions (optimised χ^2 statistics is 2.80).

Distribution	*Average /µm*	*STD /µm*	*Percentage /%*
1 (*day*)	4.00	0.05	57.5
2 (*magnification*)	4.28	0.23	42.5

Regression

Unlike the previous study case (see § 4.2 and § 4.2.2.2), the reference did not contribute to the regression and the correction of the systematic factors was performed with respect to the time sequence of the repeated measurements. Therefore, the traceability was achieved correcting the accuracy with respect to the contact measurements, i.e., correcting by the average distance of the experimental distribution from the average trend of the contact measurements x_t^{ref}. The metrological model equation for the correction was

$$y_{opt}^{corr} = x_t^{ref} + x_{opt} - x_{regression} \pm Rep \pm Res \qquad (4.3\text{-}1)$$

where y_{opt}^{corr} are the optical measurements corrected for accuracy and systematics; x_{opt} are the optical measurements; $x_{regression}$ is $y_{opt} = q \cdot t$, ans t is the time sequence of acquisition [2].

[2] For the sake of clarity, it should be noted that Equation (4.3-1) is different from Equation (4.2-2). Equation (4.2-2), if inverted, gives an estimate of a reference measurement and the related uncertainty is the consequence of the regression model. Equation (4.3-1), instead, achieves the correction of the systematic behaviour, function of the time sequence, and the accuracy from the reference. See also Equation (4.4-1) in § 4.4.2.

Table 4.3-4. Parameters of the least square regressions.

	Intercept *a* /µm	Slope *b* /µm	Quadratic *c* /µm	St Dev s_a /µm	St Dev s_b /µm	St Dev s_c /µm	*Repr.* /µm	*Deg. of freed.*	R^2 /%
Depth	162.827	-0.058	–	0.127	0.018	–	0.633	23	31.9
Sa	3.945	-0.011	0.002	0.027	0.002	0.0003	0.449	40	71.2

A first order regression was found for the step height and a second order one for the *Sa* roughness. The parameters are in **Table 4.3-4**.
Figure 4.3-6 shows the experimental distribution for the step height together with the least squares regression model used for the correction. **Figure 4.3-7** shows the same distribution after correcting for the systematic behaviour, together with the expanded uncertainty interval evaluated per each repeated measurement. The corresponding reference value (CI) and the related expanded uncertainty interval are also in **Figure 4.3-7**.
Identical quantities for *Sa* are respectively in **Figure 4.3-8** and in **Figure 4.3-9**.

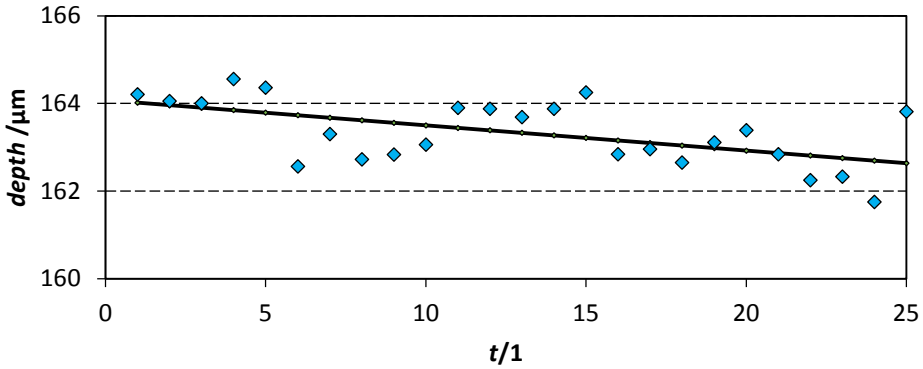

Figure 4.3-6. Graph of the experimental distribution of the M11 step height (lozenges) and least squares regression model (first order line).

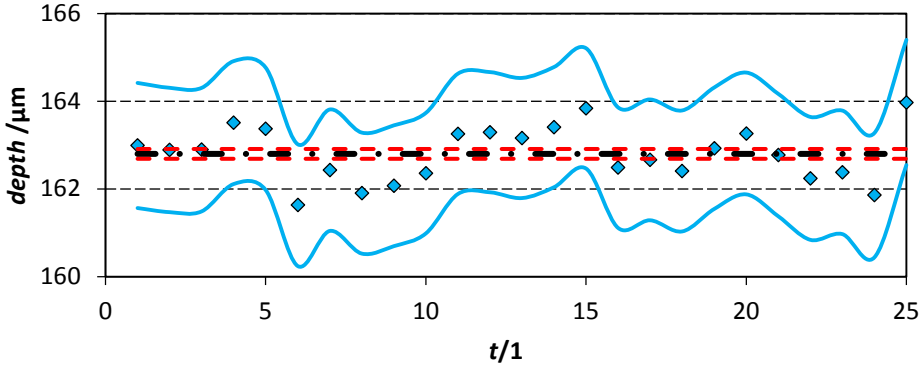

Figure 4.3-7. Graph of the experimental distribution of the M11 step height after the correction (lozenges) and reference value (dotted-dashed straight black line in the middle). The limits related to the expanded uncertainty are also indicated for the reference (dashed red lines) and for the corrected experimental distribution (external blue lines).

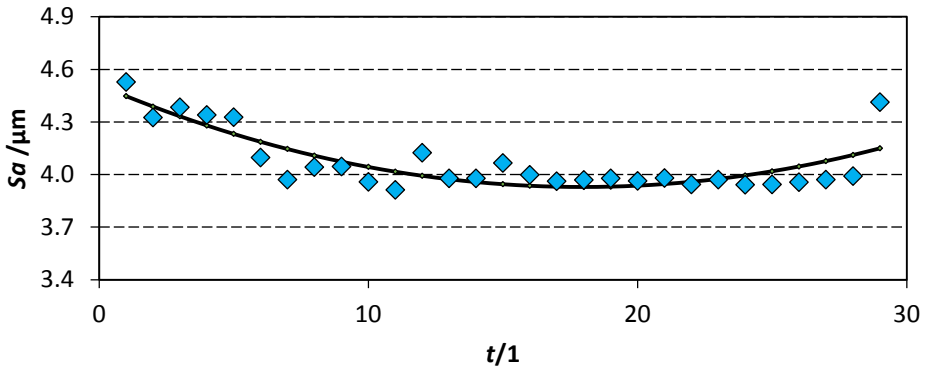

Figure 4.3-8. Graph of the experimental distribution of the M14 roughness *Sa* parameter (lozenges) and least squares regression model (second order line).

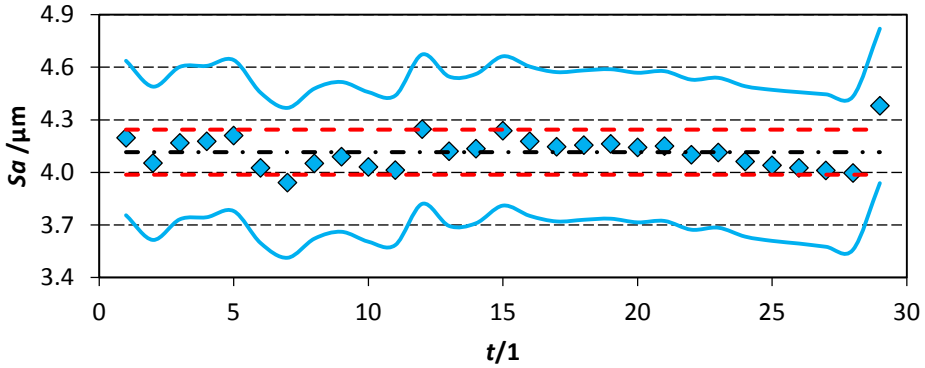

Figure 4.3-9. Graph of the experimental distribution of the M14 roughness *Sa* parameter after the correction (lozenges) and reference value (dotted-dashed straight black line in the middle). The limits related to the expanded uncertainty are also indicated for the reference (dashed red lines) and for the corrected experimental distribution (external blue lines).

Uncertainty evaluation

Eventually, similarly to § 4.2.3, the expanded uncertainty was evaluated according to Equation (4.3-1) and to Equations (4.2-3), (4.2-4) and (4.2-5). The following contributors were considered:

- The accuracy of the CI (U = 0.112 µm, unfiltered), i.e. its uncertainty stated in the calibration certificate [29] for the range of interest.
- The standard deviations of the coefficients of the model equation defined for the best fit regression (s_a, s_b, s_c in **Table 4.3-4**).
- The reproducibility values out-coming from the regressions (**Table 4.3-4**).
- The image processing software precision (1 nm) [21].

The main results are instead summarised in the following **Table 4.3-5** and **Table 4.3-6**, with reference, optical measurements related to the influence factors and assessed expanded uncertainties.

Table 4.3-5. Step height results for M11 after the correction. The values are the reference, averages grouped according to magnifications and days, related expanded uncertainties.

	Tact	*5×*	*10×*	*20×*	*50×*	*100×*	*Day 1*	*Day 2*	*Day 3*
depth /µm	162.30	162.63	162.89	161.58	162.25	162.14	162.38	162.32	162.11
U /µm	0.112	1.41	1.38	1.37	1.38	1.41	1.41	1.38	1.41

Table 4.3-6. *Sa* roughness results for M14 after the correction. The values are the reference, averages grouped according to magnifications and days, related expanded uncertainties.

	Tact	*5×*	*10×*	*20×*	*50×*	*100×*	*Day 1*	*Day 2*	*Day 3*
Sa /µm	4.12	4.16	4.03	4.13	4.01	4.38	4.10	4.14	4.09
U /µm	0.112	0.44	0.43	0.43	0.43	0.44	0.43	0.43	0.44

4.4 Correction of systematic behaviour in topographical surface analysis

The last study case [31] in this chapter aims to present a possible application of the correction of the systematic behaviour and to better define its validity.

As it was stated in § 4.1, the evaluation of the uncertainty has central importance in manufacturing engineering. Regardless of the instrument used, the influence of the measuring process on the sought parameters of the topographical characterisation should be kept below reasonable limits [7]-[8]. In this view, the method was applied to topographic measurements characterising four different surfaces. The influence of the instrument on the measurement uncertainty was reduced by correcting the systematic effects. The achievement was validated comparing with the measurement uncertainty evaluated when the systematic behaviour was not corrected.

4.4.1 Metrology

The measured specimens were four steel components of cylindrical shape and height about 1 cm. They had different polished flat surfaces in the sub-micrometre range, with nominal diameter of 2.54 cm (two examples are in **Figure 4.4-1**). The nominal characteristics, provided by the manufacturer [32], are in **Table 4.4-1**.

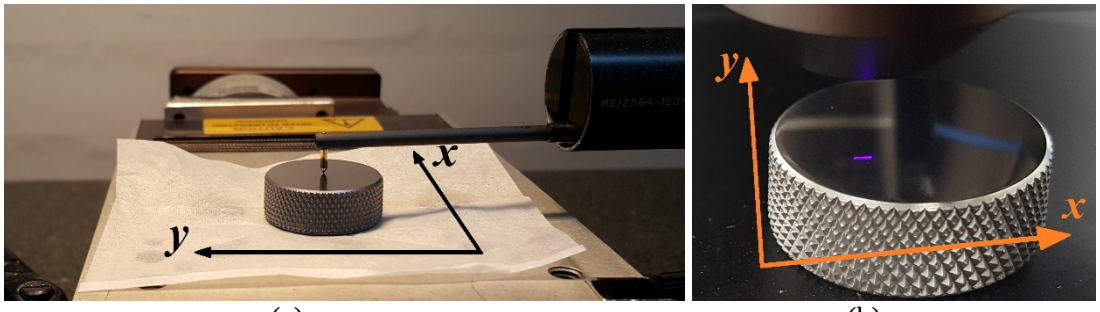

(a) (b)

Figure 4.4-1. Example of the investigated tools. (a): Specimens measured by Talysurf 50 (CI, **Figure 4.2-3**). (b): Specimens measured by Olympus Lext OLS 4100 (CM, **Figure 4.4-3**)

Table 4.4-1. Specifications of the specimens under investigation and nominal *Ra* roughness intervals, provided by the manufacturer of the specimens [32].

Sample	*Surface finish*	*Nominal interval, Ra* /nm
T1	Diamond buff (grade 15)	51–76
T2	320 Grit paper	229–254
T3	400 Stone	635–711
T4	400 Dry blast (glass bead 11)	254–305

Reference measurements

The specimens were initially measured by the contact instrument Talysurf 50 (CI – **Figure 4.2-3**), performing five areal acquisitions in the centre of the surface of each sample under evaluation.
According to a local reference system defined on the sample, as shown in **Figure 4.4-2-(a)**, an evaluation area 4 mm × 10 mm was acquired as 8200 pixels along the *y*-axis and 21 profiles along the *x*-axis. When it was possible to recognise a dominant texture, it was oriented orthogonally to the scanning direction (**Figure 4.4-1-(a)** and **Figure 4.4-2-(a)**).
Such results were the reference for the optical measurements, according to what presented in § 4.2. Nevertheless, being the surface texture of the specimens in the sub-micrometre range, it was not used the same calibrated expanded uncertainty as in § 4.2. In fact, different values are stated in calibration certificate [29]. For the range of interest, the expanded uncertainty stated for CI is 10 nm, for *Ra* values up to 229 nm, and 24 nm, for *Ra* values up 604 nm. These values and the average of the reference results for *Sa* and *Sq* parameters are in **Table 4.2-2**.

Table 4.4-2. Average of *Sa* and *Sq* parameters calculated from the reference measurements (CI). These values are associated with the expanded uncertainties stated in the calibration certificate [29] for the range of interest.

	Sa_{REF} /nm	Sq_{REF} /nm	*U* /nm
T1	48	61	10
T2	133	179	10
T3	232	313	10
T4	510	646	24

Although the reference expanded uncertainty was referred to *Ra*, the parameter chosen for this investigation was *Sq*. Indeed, *Sq* is the root mean square value of the height ordinates in the evaluation area and is related somehow to the variance of the pixels distribution (after the subtraction of the least square plane). Since the investigation deals with optical measurements, often subjected to noise, *Sq* was deemed more challenging for the correction of the systematic behaviour. At this regard, some remarks are needed:

- Measurements of *Ra* in the calibration certificate led to evaluate the ability of the reference stylus instrument to measure average height variations on a surface within a confidence interval (expanded uncertainty). For this reason, the uncertainty of CI related to *Ra* measurements was consider compatible with measurements of *Sa*.
- *Sa* and *Sq* are both amplitude parameters and strongly correlated (they measure the same quantity in different ways). The related uncertainties are normally in the same order of magnitude. Therefore, it is an estimation of the uncertainty based on previous knowledge, which is in agreement with [9].
- The uncertainty contributor related to the calibration uncertainty is constant for all cases, both related to the correction of the systematic effects and not. Hence, it is a common constant value and may affect the final evaluated uncertainty but not the investigation itself (correction of systematic behaviour).

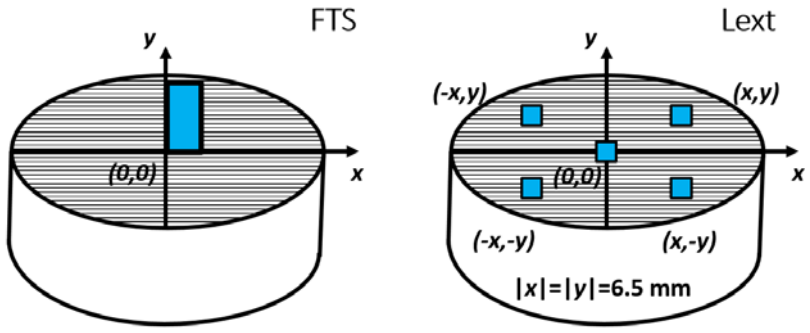

(a) (b)

Figure 4.4-2. Specimens local reference system and definition of the acquisition areas.

Optical measurements

Optical measurements were performed by Olympus Lext laser scanning confocal microscope (CM – **Figure 4.4-3**), using the 100× objective lens (same discretisation level).

Considering the surfaces under evaluation of circular shape, the centre of each circle was defined as the origin (0,0) of a local reference system, integral to the specimens. Each sample was oriented on the stage of the instrument so that the laser scanning movement was orthogonal to the dominant texture (when it was possible to recognise a dominant texture – **Figure 4.4-1-(b)** and **Figure 4.4-2-(b)**). Hence, the direction of the laser scanning movement was chosen to identify the *y*-axis of the specimens' reference system. The *x*-axis was set in order to have a right-handed reference system.

With reference to the local reference system (**Figure 4.4-2-(b)**), ten repeated measurements were performed, in the central position (0,0), and in the peripheral positions (x,y), (x,-y), (-x,y), (-x,-y), where $|x| = |y| = 6.5$ mm.

Figure 4.4-3. Optical instrument used in the investigation: Olympus Lext OLS 4100 (laser scanning confocal microscope – CM).

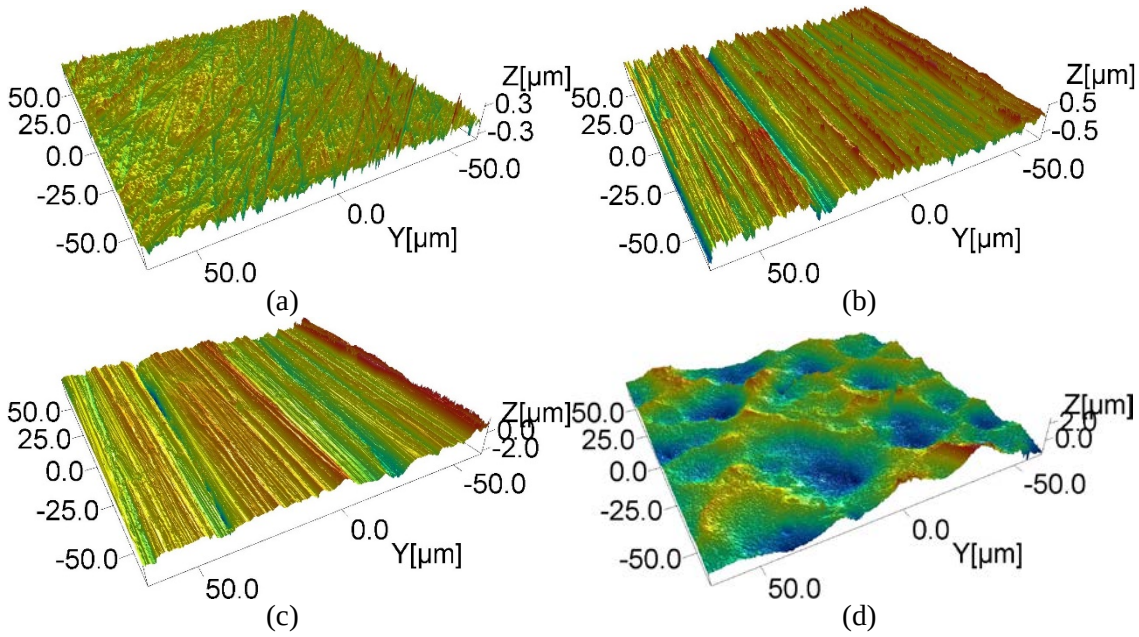

Figure 4.4-4. Three dimensional view of acquired surfaces. Examples of T1 (a), T2 (b), T3 (c), T4 (d).

It should be noted that the sampling on the surfaces was defined in a different way for the reference and the optical measurements. The reason is that, when using an optical instrument, the motorised stage and the visualisation system are in line and it is relatively easy to assign the machine coordinates to a specific spot on the specimen under measurement. Using a contact instrument, instead, it is the tip of the stylus that defines a specific spot on the surface. This makes difficult or impossible to identify an origin on the specimen, which can be univocal and repeatable. Hence, it would anyway be not possible to match the same sampling areas for the two instruments. Since CI can scan relatively faster on a surface, the choice was to acquire a larger area even though not so resolute. Averaging on a larger area allowed reducing the indeterminacy of the origin. This choice may influence the results but it also made possible some useful consideration.

4.4.2 Results

The investigation was carried out inspecting for amplitude variations by *Sq* areal parameter. Data extraction was performed by [21], after correcting for the least square plane. No filter was used. Examples of areal acquisitions, one for each type of polishing, are in **Figure 4.4-4** (3D view). The dataset was successively examined for outliers by Chauvenet's criterion. Four outliers were removed. They were all related to T3 specimen, one in each peripheral area.

The correction for systematics was carried out by a least square fit of the optical measurements as function of the reference measurements, according to what already shown in § 4.2.2.2. The model equation found consistent for best fitting the experimental data was a straight line with null constant term. The final equation used for achieving traceability and correcting the systematic behaviour is

$$y_{opt}^{corr} = x_{opt} + x_{opt}^{ave} - x_{regression} \pm Rep =$$

$$= x_{opt} + x_{opt}^{ave} - q \cdot x_t^{ref} \pm Rep \qquad (4.4\text{-}1)$$

where y_{opt}^{corr} are the optical measurements corrected for accuracy and systematics; x_{opt} are the optical measurements with average value x_{opt}^{ave}; x_t^{ref} are the reference measurements (CI) [3]. Being the image processing software precision negligible, it was not added anymore.

[3] Analogously to Equation (4.3-1) in § 4.3, Equation (4.4-1) is different from Equation (4.2-2). Equation (4.2-2), if inverted, gives an estimate of a reference measurement and the related uncertainty is the consequence of

When the correction of the systematic behaviour was not performed, the accuracy was corrected as the mismatch ('distance') between optical and contact measurements, leading to the following equation

$$y_{opt}^{d} = x_{opt} - \left(x_{opt}^{ave} - x_{t}^{ref}\right) \tag{4.4-2}$$

According to Equation (4.4-1) (correction of systematic behaviour) and to Equations (4.2-3), (4.2-4) and (4.2-5), the uncertainty was evaluated considering the following contributors (see **Table 4.4-10** to **Table 4.4-13** for the complete uncertainty budget)

- u_{repr}: reproducibility values out-coming from the regressions;
- u_{slope}: standard deviations of the coefficient of the model equation defined for the best fit regression;
- u_{repea}: standard deviations of optical measurements (repeatability);
- u_{cal}: accuracy of the CI, i.e. its uncertainty stated in the calibration certificate [29] (see **Table 4.4-2** for the range of interest).

According to Equation (4.4-2) (no correction of systematic behaviour) and to Equations (4.2-3), (4.2-4) and (4.2-5), the uncertainty was evaluated considering the following contributors (see **Table 4.4-10** to **Table 4.4-13** for the complete uncertainty budget)

- u_{repr}: maximum deviation of optical measurements (uniformly distributed);
- u_{repea}: standard deviations of optical measurements (repeatability);
- $u_{repea,ref}$: standard deviations of reference measurements (CI) (reference repeatability);
- u_{cal}: accuracy of the CI, i.e. its uncertainty stated in the calibration certificate [29] (see **Table 4.4-2** for the range of interest).

Regarding the contributors relative to Equation (4.4-2), normally, the reproducibility (u_{repr}) includes the repeatability (u_{repea}). Nonetheless, in this particular case, they refer to two different quantities that both appear in Equation (4.4-2), being the first accounting for the variability of the optical measurements and the latter for the average of optical measurements.
Furthermore, when the correction was performed, the quantity $u_{repea,ref}$ was normally considered included into the reproducibility of the regression. This assumption is allowed when the reference is a more accurate or a quality instrument. However, without regression, it should be considered into the uncertainty budget.

Average results and evaluated expanded uncertainties for the data corrected for systematic behaviour are in **Table 4.4-3**, for the measurements in the central area of the surfaces, and in **Table 4.4-5**, for the measurements in the peripheral areas. In the same tables, the values for the coefficient q of the model equation are also given. Furthermore, in **Table 4.4-5**, the deviations ΔSq of the averages of the peripheral areas with respect to the averages in the central areas of the surfaces are indicated. These quantities are intended for showing the variability of the peripheral areas with respect to the central one.
Deviations are defined as

$$\Delta Sq(\pm x, \pm y) = Sq(\pm x, \pm y) - Sq(0,0) \tag{4.4-3}$$

Analogous average results and evaluated expanded uncertainties for the data without correction are in **Table 4.4-4** and **Table 4.4-6**, respectively for the central area and for the other peripheral areas. No model equation was fitted in this circumstance. This condition is indicated in the tables as $q = 0$.

the regression model. Equation (4.4-1), instead, achieves the correction of the systematic behaviour and the accuracy from the reference. However, conversely to Equation (4.3-1), Equation (4.4-1) contains Equation (4.2-2).

Table 4.4-3. Results of the surface analysis in the central area of the surfaces. Data corrected for systematic behaviour: q is the slope of the model equation. U is the expanded uncertainty.

	$q(0,0)$	$Sq(0,0)$/nm	$U(Sq(0,0))$/nm
T1	0.8	49	28
T2	0.9	160	32
T3	1.2	388	43
T4	0.9	576	74

Table 4.4-4. Results of the surface analysis in the central area of the surfaces. Data not corrected for systematic behaviour: no model equation coefficient is specified ($q = 0$). U is the expanded uncertainty.

	$q(0,0)$	$Sq(0,0)$/nm	$U(Sq(0,0))$/nm
T1	0	49	35
T2	0	160	36
T3	0	388	35
T4	0	576	84

Table 4.4-5. Results of the surface analysis in the peripheral areas of the surface. Data corrected for systematic behaviour: q is the slope of the model equation. U is the expanded uncertainty.
Values are in nanometre.

	$q(x,y)$	$Sq(x,y)$	$\Delta Sq(x,y)$	$U(Sq(x,y))$
T1	0.8	47	-2	28
T2	1.0	176	16	35
T3	1.3	407	19	46
T4	0.8	491	-85	65

	$q(x,-y)$	$Sq(x,-y)$	$\Delta Sq(x,-y)$	$U(Sq(x,-y))$
T1	0.8	48	-1	28
T2	1.1	193	33	38
T3	1.0	306	-81	36
T4	0.9	569	-7	74

	$q(-x,y)$	$Sq(-x,y)$	$\Delta Sq(-x,y)$	$U(Sq(-x,y))$
T1	0.7	45	-5	26
T2	0.9	154	-6	30
T3	0.7	223	-165	25
T4	0.8	525	-51	68

	$q(-x,-y)$	$Sq(-x,-y)$	$\Delta Sq(-x,-y)$	$U(Sq(-x,-y))$
T1	0.9	53	4	32
T2	0.8	140	-20	28
T3	0.7	221	-166	25
T4	0.9	594	18	78

Table 4.4-6. Results of the surface analysis in the peripheral areas of the surface. Data not corrected for systematic behaviour: no model equation coefficient is specified in this case ($q = 0$). U is the expanded uncertainty. Values are in nanometre.

	$q(x,y)$	$Sq(x,y)$	$U(Sq(x,y))$
T1	0	47	35
T2	0	176	35
T3	0	407	36
T4	0	491	85

	$q(x,-y)$	$Sq(x,-y)$	$U(Sq(x,-y))$
T1	0	48	35
T2	0	193	35
T3	0	306	37
T4	0	569	84

	$q(-x,y)$	$Sq(-x,y)$	$U(Sq(-x,y))$
T1	0	45	36
T2	0	154	35
T3	0	223	35
T4	0	525	83

	$q(-x,-y)$	$Sq(-x,-y)$	$U(Sq(-x,-y))$
T1	0	53	36
T2	0	140	35
T3	0	221	35
T4	0	594	85

Table 4.2-3 to **Table 4.2-6** show the regressions in each spot defined in **Figure 4.4-2-(b)**. The general trend in the tables is a lower expanded uncertainty evaluated when the systematic behaviour was corrected. Exceptions to this trend are the uncertainties of T3(0,0), T3(x,y) and T2($x,-y$). The uncertainty budget related to the measurements in these three spots are in the following **Table 4.4-7**, **Table 4.4-8** and **Table 4.4-9**. Unlike to what expected, in this specific

cases, the correction of the systematic behaviour is responsible for higher values of the sensitivity coefficients[4] relative to the calibration uncertainty, which amplified the related contributors.

Table 4.4-7. Uncertainty budget of the measurements in the central area of the specimen T3.

T3(0,0)							
	Correction				*No correction*		
	$\|c_j\|$	$u(x_j)$ /nm	$u_j(y)$ /nm		$\|c_j\|$	$u(x_j)$ /nm	$u_j(y)$ /nm
u_{cal}	1.2	16	19	u_{cal}	1.0	16	16
$u_{repea,opt}$	1.0	2.8	2.8	$u_{repea,opt}$	1.0	2.8	2.8
u_{slope}	312.6	0.003	0.98	$u_{repea,ref}$	1.0	0.46	0.46
$u_{repr,fit}$	1.0	3.1	3.1	$u_{repr,meas}$	1.0	2.5	2.5
k(95 %)			2.18	*k(95 %)*			2.18
U			43	*U*			35

Table 4.4-8. Uncertainty budget of the measurements in the peripheral (*x*,*y*) area of the specimen T3.

T3(x,y)							
	Correction				*No correction*		
	$\|c_j\|$	$u(x_j)$ /nm	$u_j(y)$ /nm		$\|c_j\|$	$u(x_j)$ /nm	$u_j(y)$ /nm
u_{cal}	1.3	16	20	u_{cal}	1.0	16	16
$u_{repea,opt}$	1.0	3.6	3.6	$u_{repea,opt}$	1.0	3.6	3.6
u_{slope}	312.6	0.004	1.2	$u_{repea,ref}$	1.0	0.46	0.46
$u_{repr,fit}$	1.0	3.7	3.7	$u_{repr,meas}$	1.0	3.1	3.1
k(95 %)			2.18	*k(95 %)*			2.16
U			46	*U*			36

Table 4.4-9. Uncertainty budget of the measurements in the peripheral (*x*,-*y*) area of the specimen T2.

T2(x,-y)							
	Correction				*No correction*		
	$\|c_j\|$	$u(x_j)$ /nm	$u_j(y)$ /nm		$\|c_j\|$	$u(x_j)$ /nm	$u_j(y)$ /nm
u_{cal}	1.1	16	17	u_{cal}	1.0	16	16
$u_{repea,opt}$	1.0	1.7	1.7	$u_{repea,opt}$	1.0	1.7	1.7
u_{slope}	177.1	0.003	0.59	$u_{repea,ref}$	1.0	1.2	1.2
$u_{repr,fit}$	1.0	1.9	1.9	$u_{repr,meas}$	1.0	1.4	1.4
k(95 %)			2.20	*k(95 %)*			2.20
U			38	*U*			35

It is well known that the correction of systematic behaviour, achieved by the frequentist approach, is based on the Theorem of the Central Limit (TLC).
One of the possible formulation of TLC is

> ***Theorem (4.4-1)*** *(Central limit). A normalised sum or an arithmetic mean of a LARGE number of independent random variables APPROXIMATELY converges to a normal distribution, regardless of the underlying distributions of the random variables.*

If the **Theorem (4.4-1)** can be considered under valid hypotheses, the experimental distribution x_i, which is not normal, cannot be considered a distribution of "independent random variables". Nonetheless, since random factors always influence the results of a measurement session, the experimental distribution y_i can be decomposed in an part x_i of 'independent random variables'

[4] They are the partial derivatives in Equation (4.2-3).

and in a part $f(x_i)$ characterised by a relationships among the variables. $f(x_i)$ is normally called systematic behaviour of the experimental distribution.
In other words, if the hypotheses of the **Theorem (4.4-1)** are met, it would be possible to correct the experimental distribution to a random one subtracting an estimate $f'(x_i)$ of the systematic behaviour, resulting

$$y_i = x_i + f(x_i) - f'(x_i) \tag{4.4-4}$$

Even though the systematic behaviour cannot completely be recognised, i.e. $f(x_i) - f'(x_i) \neq 0$, the correction is still effective when the unrecognised systematic effects have zero expectation and they are 'randomised' in the experimental distribution

$$E\{f(x_i) - f'(x_i)\} = 0 \tag{4.4-5}$$

Failure in the validity of the starting hypotheses of **Theorem (4.4-1)** may lead to a correction with a non-zero expected value of the 'randomised' systematic components. Therefore, the non-zero expected value becomes a bias that increases the overall evaluated uncertainty [33].

The uncertainties previously shown were assessed on each of the spots defined on the surfaces, meaning that only ten repeated measurements were used in the regressions. Hence, the measurements in this circumstance do not satisfy the **Theorem (4.4-1)** hypothesis, in the way they were considered.

Inspecting the **Table 4.4-7**, **Table 4.4-8** and **Table 4.4-9**, the following can be observed:

- Ten repeated measurements are not enough to apply the frequentist approach.
- The bias affects u_{cal}, thus affecting the way the traceability is achieved.
- $u_{repr,fit}$ and $u_{repr,meas}$ are not directly comparable because $u_{repr,fit}$ also contains $u_{repea,ref}$.
- The standard deviation of the slope has central importance in the correction, meaning that a quality reference allows controlling the spread of the uncertainty. Furthermore, it is not enough to have a good coefficient of determination (R^2) for the choice of a model regression; it is also important that the standard deviation of the coefficients in the regression is sufficiently low.

In addition, from **Table 4.4-3** to **Table 4.4-6** , it can be deduced that:

- The surface of T3 is especially uneven with respect to the central area.
- The larger uncertainty of T4 is due to the different calibrated expanded uncertainty of CI (different roughness range).
- The average values of the measurements are the same whether the correction of the systematic behaviour was performed or not. In other words, in the study case examined, the correction did not influence the average values.

Conversely, when all the areas were considered together, fifty repeated measurements were available for each specimen (46 for T3 because of the outliers), which is a number of 'variables' certainly satisfying the **Theorem (4.4-1)**. Therefore, the investigation was repeated in this circumstance, too. The results are in **Table 4.4-10** to **Table 4.4-13**.
About the correction of the systematics, it can be remarked that:

- The coefficients of sensitivity of u_{cal} were reduced with respect to the previous evaluation and with respect to the case of *no correction* of the systematic behaviour.
- The coefficient of sensitivity of u_{cal} in the measurements of T3 was not reduced with respect to the case of *no correction*; however, it remained the same, in the two cases of *correction* and *no correction*, as well as it was the expanded uncertainty. This happened because the measurements related to T3 were particularly problematical. In fact, they were the only dataset in which an exclusion of outliers was necessary.

Table 4.4-10. Uncertainty budget of the measurements of the specimen T1, averaging in all areas.

T1

Correction				*No correction*			
	$\|c_j\|$	$u(x_j)$ /nm	$u_j(y)$ /nm		$\|c_j\|$	$u(x_j)$ /nm	$u_j(y)$ /nm
u_{cal}	0.8	16	12	u_{cal}	1.0	16	16
$u_{repea,opt}$	1.0	1.7	1.7	$u_{repea,opt}$	1.0	1.7	1.7
u_{slope}	60.9	0.009	0.6	$u_{repea,ref}$	1.0	0.4	0.4
$u_{repr,fit}$	1.0	1.8	1.8	$u_{repr,meas}$	1.0	1.6	1.6
k(95 %)			2.20	*k(95 %)*			2.20
U			28	*U*			35

Table 4.4-11. Uncertainty budget of the measurements of the specimen T2, averaging in all areas.

T2

Correction				*No correction*			
	$\|c_j\|$	$u(x_j)$ /nm	$u_j(y)$ /nm		$\|c_j\|$	$u(x_j)$ /nm	$u_j(y)$ /nm
u_{cal}	0.9	16	15	u_{cal}	1.0	16	16
$u_{repea,opt}$	1.0	1.5	1.5	$u_{repea,opt}$	1.0	1.5	1.5
u_{slope}	177.0	0.003	0.5	$u_{repea,ref}$	1.0	1.2	1.2
$u_{repr,fit}$	1.0	1.5	1.5	$u_{repr,meas}$	1.0	1.4	1.4
k(95 %)			2.20	*k(95 %)*			2.20
U			32	*U*			35

Table 4.4-12. Uncertainty budget of the measurements of the specimen T3, averaging in all areas.

T3

Correction				*No correction*			
	$\|c_j\|$	$u(x_j)$ /nm	$u_j(y)$ /nm		$\|c_j\|$	$u(x_j)$ /nm	$u_j(y)$ /nm
u_{cal}	1.0	16	16	u_{cal}	1.0	16	16
$u_{repea,opt}$	1.0	1.8	1.8	$u_{repea,opt}$	1.0	1.8	1.8
u_{slope}	312.6	0.002	0.6	$u_{repea,ref}$	1.0	0.5	0.5
$u_{repr,fit}$	1.0	1.8	1.8	$u_{repr,meas}$	1.0	1.7	1.7
k(95 %)			2.20	*k(95 %)*			2.20
U			35	*U*			35

Table 4.4-13. Uncertainty budget of the measurements of the specimen T4, averaging in all areas.

T4

Correction				*No correction*			
	$\|c_j\|$	$u(x_j)$ /nm	$u_j(y)$ /nm		$\|c_j\|$	$u(x_j)$ /nm	$u_j(y)$ /nm
u_{cal}	0.8	38	32	u_{cal}	1.0	38	38
$u_{repea,opt}$	1.0	1.8	1.8	$u_{repea,opt}$	1.0	1.8	1.8
u_{slope}	648.7	0.001	0.6	$u_{repea,ref}$	1.0	0.1	0.1
$u_{repr,fit}$	1.0	1.8	1.8	$u_{repr,meas}$	1.0	1.5	1.5
k(95 %)			2.20	*k(95 %)*			2.20
U			71	*U*			83

Considering the large amount of data, to summarise the overall trend, a general linear model *design of experiment* (DOE) was implemented on the entire dataset collected from **Table 4.4-3** to **Table 4.4-6**, with influence factors:

- Correction: "*Yes*", "*No*".
- Evaluation area: "(0,0)", "(*x*,*y*)", "(*x*,-*y*)", "(-*x*,*y*)", "(-*x*,-*y*)".
- Polishing; "T1", "T2", "T3", "T4".

The main effects plot is in **Figure 4.4-5** and the interactions plot in **Figure 4.4-6**.

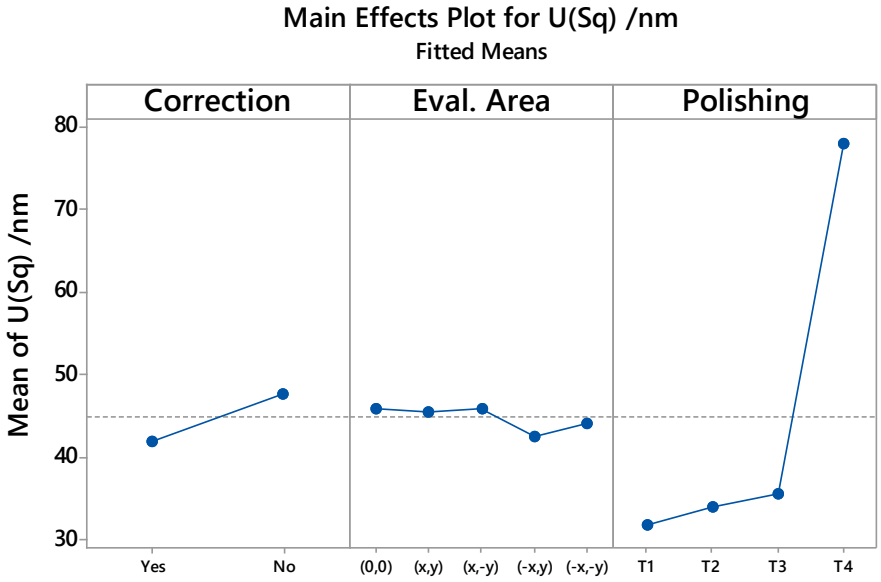

Figure 4.4-5. Main effects plot of the *design of experiment* of the expanded uncertainty evaluated in the different areas of measurement, with and without of the systematic behaviour.

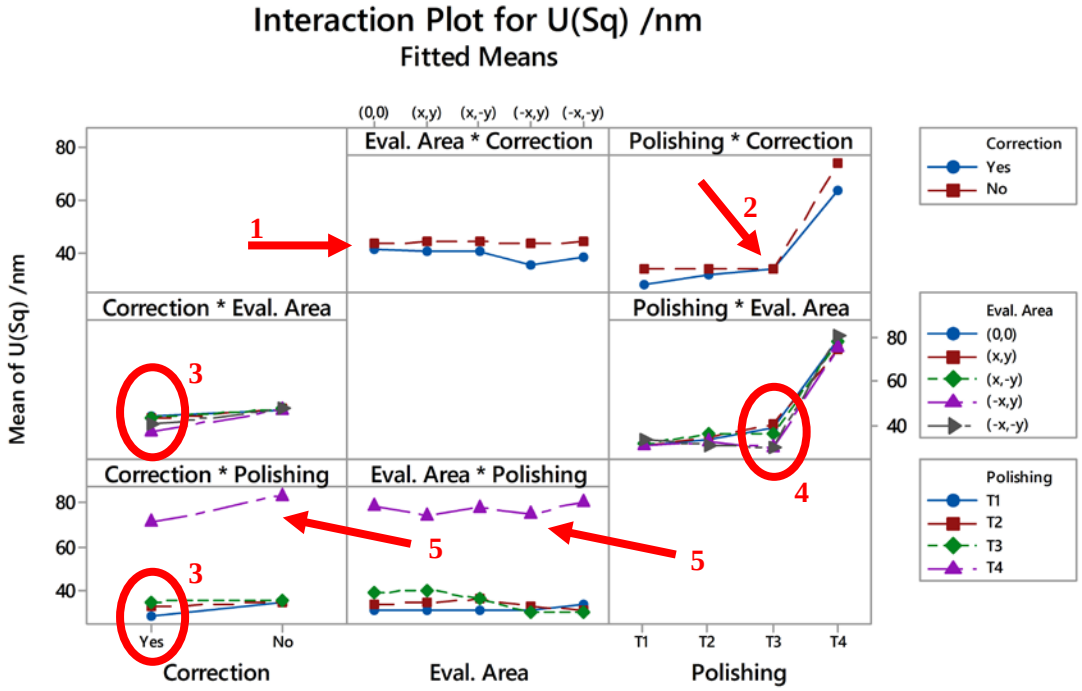

Figure 4.4-6. Interaction plot of the *design of experiment* of the expanded uncertainty evaluated in the different areas of measurement, with and without correction of the systematic behaviour.

Comments to the analysis of the main effects (**Figure 4.4-5**):

- The evaluated expanded uncertainty is lower after the correction of the systematic behaviour.
- Small differences exist connected to the evaluation areas. As already stated, higher values are related to the bias generated after the correction of the systematic effects, under not valid hypothesis of the **Theorem (4.4-1)**.
- The lowest uncertainty was stated for T1 ('Diamond buff' polishing), whilst the highest was for the T4 ('Dry blast' polishing). Nonetheless, it is an obvious result influenced by a higher uncertainty available in the calibration certificate for the roughness range of T4 specimen.

Comments to the analysis of the interactions (**Figure 4.4-6**):

1. The evaluated uncertainty is lower after the correction of the systematic effects, independently of the evaluation area.
2. When systematic effects are corrected, a lower uncertainty can be obtained for all the specimens except for T3.
3. The correction produces different evaluated uncertainties, depending on the evaluation areas and on the surfaces.
4. The largest spread of uncertainty values is on the evaluation areas of T3.
5. As already stated, the higher uncertainty of T4 is due to the different uncertainty available in the calibration certificate for its roughness range.

4.5 Discussion

The sequence of the proposed study cases successful implemented the method. They clearly highlighted the potentialities of the overall procedure and the precautions that are to be addressed and planned, before the measurement sessions, in order to make the method effective and to reduce or eliminate the influence of several factors.

In the first study, the correction of the systematics was possible because of the large number of deviations. Despite this, it was not possible to associate the three marginal distributions in the mixture to any of the influence factors involved. They remained undefined because not enough repeated measurements were associated to the influence factors. This is a central point. When comparing different instruments, if the measurements are properly planned with enough repeated measurements, the mixture can be exploited to identify the deviations introduced by each instrument.

This issue was explained in the second study where the measurements were enough to define all the factors influencing the experimental distribution, accounted in their natural sequence of acquisition. Nonetheless, the discretisation level was still different among the measurements and, even though it was possible to correct its effect, the coefficients of determination in the least square regressions were not completely satisfactory. It means that the reproducibility could further be reduced when the same discretisation level (or bandwidth [22]) is chosen for the areal acquisitions.

The measurement day as influence factor was also an interesting outcome in the second study. The instrument, in fact, is normally restarted at the beginning of a daily session and switched off at the end. Therefore, some of the conditions responsible for the systematic behaviour are restored or changed at the beginning of each session. Hence, the systematics should be related to and corrected for every single continuous measurement session. For effectively applying the method when there are long lasting acquisitions, it is necessary to plan the measurements in homogeneous groups that can be corrected together.

These indications were observed in the third study. The method was effective to reduce the evaluated uncertainty, inherently compensating the influence of the instrument when it was properly implemented, i.e., when it was possible to use **Theorem (4.4-1)**.

It was also shown that a favourable situation for applying the method can be when characterising a surface, sampling it in several spots. Few repeated measurements acquired in each single spot

become all together enough for satisfying **Theorem (4.4-1)** and correcting the influence of the instrument.
Nonetheless, the validity itself of **Theorem (4.4-1)** can pose some limitation to the method. Optical measurements are relatively long lasting measurements. With some instruments the time of a single acquisition is so long that they would give unacceptable lasting times for acquiring enough repeated measurements, making impossible to apply the approach.
Furthermore, the contact measurements were useful for defining the method and achieving the traceability but they were provisional in this research. In fact, it emerged clearly that the contact instrument was not adequate to be used as reference, above all in nanometre range.
In the first study, even though the measured quantities spread over several length scales, the related uncertainties were limited in almost one order of magnitude. This suggests that the main impact on the uncertainty was due to the reference instrument and to the reproducibility (see, e.g., **Table 4.4-10** to **Table 4.4-13**).
On one hand, the calibration of tactile instruments is well established by the ISO standards. But on the other, establishing the traceability of optical instruments using contact measurements inevitably leads to an overestimated uncertainty, which can be additionally dependent on their results. Indeed, implicit hypothesis was that the contact measurements were not affected by systematic errors but it is known that, at least, they are affected by the finite radius tip of the stylus. In addition, further problems may arise when micro and especially nano features are not accessible by the stylus. This advises that new progresses of the method are possible.

4.6 Conclusion

The statistical approach presented in this chapter is normally used in many fields of science. The implemented study cases established (for the first time, to the best of the author's knowledge) that such statistics is also suitable for micro, nano dimensional and topographic measurements.
The correction of the systematic behaviour in the experimental distribution allowed to reduce the evaluated uncertainty when it was properly implemented. At this regard, measurements should be planned in well-matched sessions and with a sufficient number of replications. If so, the **Theorem (4.4-1)** can conveniently be applied for correcting the systematic behaviour and other useful tools, like the mixture, can be exploited to separate the systematic effects (comparison of different instruments, sampling over the surface, etc.).
There is still room to improve the method.
Besides the need of a relatively high number of repeated measurements, the main drawback of the method was related to the reference. A further reduction of the measuring uncertainty is envisaged in a stand-alone calibration of the optical instruments. Since it seems to be a long way until a direct calibration is achieved, an intermediate passage is to modify the method for referencing the traceability to material measures (calibrated artefacts).

4.7 Outlook

The method will be further developed using material measures for achieving the traceability. Inspiring to the substitution method normally used with measurements of coordinate measuring machines (ISO 15530 series), material measures will be used for determining one or more calibration equations, related to the optical instruments under examination, in the range of interest. The advantage is that the systematic behaviour, if any, would be related to the same instrument and corrected in the same evaluation.
Furthermore, a software implementation of the procedure is also on schedule. The software implementation would allow the use of the procedure to a larger number of users and, especially, in combination with automated instruments.
Eventually, the use of the mixture (multivariate normal distribution) will be investigated deeper for specific applications, e.g., in the comparison of different instruments or for inspecting unevenness of surfaces with respect to a reference spot.

References

[1] Tosello G, Hansen H N, Marinello F, Gasparin S 2010 Replication and dimensional quality control of industrial nanoscale surfaces using calibrated AFM measurements and SEM image processing *CIRP Annals – Manufacturing Technology* **59-1** 563-568

[2] Hansen H N, Hocken R, Tosello G 2011 Replication of micro/nano surface geometries *CIRP Annals – Manufacturing Technology* **60-2** 695-714

[3] Tosello G, Marinello F, Hansen H N 2012 Characterisation and analysis of microchannels and submicrometre surface roughness of injection moulded microfluidic systems using optical metrology *Plastics, Rubber and Composites: Macromolecular Engineering* **41-1** 29-39

[4] Tosello G, Hansen H N, Calaon M, Gasparin S 2014 Challenges in high accuracy surface replication for micro optics and micro fluidics manufacture *Int. J. Precision Technology* **4** 122-144

[5] Hansen HN, Carneiro K, Haitjema H, De Chiffre L 2006 Dimensional Micro and Nano Metrology *CIRP Annals – Manufacturing Technology* **55-2** 721-743

[6] Leach R 2013 *Characterisation of Areal Surface Texture* (Berlin, Heidelberg: Springer Berlin Heidelberg)

[7] Kunzmann H, Pfeifer T, Schmitt R, Schwenke H and Weckenmann A 2005 Productive Metrology – Adding Value to Manufacture *CIRP Ann. – Manuf. Technol.* **54** 155-68

[8] Weckenmann A and Rinnagl M 2000 Acceptance of processes: do we need decision rules? *Precis. Eng.* **24** 264-9

[9] JCGM 100: 2008 Evaluation of measurement data—Guide to the expression of uncertainty in measurement, Joint Committee for Guides in Metrology (Sèvres: Bureau International des Poids et Mesures, BIPM)

[10] Leach R K, Giusca C L, Haitjema H, Evans C and Jiang X 2015 Calibration and verification of areal surface texture measuring instruments *CIRP Ann. – Manuf. Technol.* **64** 797-813

[11] ISO/DIS 25178-600: 2016 Geometrical product specification (GPS)—Surface texture: Areal – Part 600: Nominal characteristics of non-contact (variable focus) instruments. ISO DIS 25178 part 600 (Geneva: International Organization for Standardization)

[12] MacAulay G D and Giusca C L 2016 Assessment of uncertainty in structured surfaces using metrological characteristics *CIRP Ann. – Manuf. Technol.* **65** 533-6

[13] Leach R K, Giusca C L and Naoi K 2009 Development and characterization of a new instrument for the traceable measurement of areal surface texture *Meas. Sci. Technol.* **20** 125102

[14] Krystek M 2001 Measurement uncertainty propagation in the case of filtering in roughness measurement *Meas. Sci. Technol.* **12** 63-7

[15] Haitjema H 2015 Uncertainty in measurement of surface topography *Surf. Topogr. Metrol. Prop.* **3** 35004

[16] Quagliotti D, Tosello G, Islam A M, Hansen H N, Zeidler H, Martin A, Schubert A, Brandao C and Riemer O 2015 A method for dimensional and surface optical measurements uncertainty assessment on micro structured surfaces manufactured by Jet-ECM *4M 2015 Proc. of the International Conference on Micro-Manufacturing* Milan, Italy, 31 March – 2 April

[17] Mattsson L, Bolt P, Azcarate S, Brousseau E, Fillon B, Fowler C, Gelink E, Griffiths C, Khan Malek C, Marson S, Retolaza A, Schneider A, Schoth A, Temun A, Tiquet P and Tosello G 2008 How reliable are surface roughness measurements of micro-features? - Experiences of a Round Robin test within nine 4M laboratories *4M 2008 Proc. of the International Conference on Micro-Manufacturing* Cardiff, UK, 9-11 September

[18] Internet site: www.hi-micro.eu.

[19] Hackert-Oschätzchen M, Meichsner G, Zeidler H, Zinecker M and Schubert A 2011 Micro Machining of Different Steels with Closed Electrolytic Free Jet *AIP Conference Proceedings* **1337** 1337–43

[20] ISO 25178-2: 2012 Geometrical product specification (GPS)—Surface texture: Areal – Part 2: Terms, definitions and surface texture parameters. ISO 25178 part 2 (Geneva: International Organization for Standardization)
[21] SPIP™, www.imagemet.com
[22] Leach R and Haitjema H 2010 Bandwidth characteristics and comparisons of surface texture measuring instruments *Meas. Sci. Technol.* **21** 1-9
[23] Broke M 1983 Surface Roughness Analysis *Bruel & Kjaer Instruments Inc.* Technical Review 3
[24] ISO 4287: 1997 Geometrical Product Specifications (GPS)—Surface texture: Profile method – Terms, definitions and surface texture parameters. ISO 4287 (Geneva: International Organization for Standardization)
[25] ISO 4288: 1996 Geometrical Product Specifications (GPS)—Surface texture: Profile method – Rules and procedures for the assessment of surface texture. ISO 4288 (Geneva: International Organization for Standardization)
[26] Barbato G, Genta G and Germak A 2013 Measurements for Decision Making (Società Editrice Esculapio)
[27] Barbato G, Barini E M, Genta G and Levi R 2011 Features and performance of some outlier detection methods *J. Appl. Stat.* **38** 2133-49
[28] Aggogeri F, Barbato G, Genta G and Levi R 2014 Statistical modelling of industrial process parameters *Procedia CIRP* 9th CIRP Conference on Intelligent Computation in Manufacturing Engineering 23rd-25th July, Capri (Italy)
[29] CGM (Center for Geometrical Metrology), DANAK Calibration certificate n.RUM11011, Taylor Hobson Form Talysurf Series 2 50 i, date of issue 31-12-11
[30] Quagliotti D, Tosello G, Islam A M, Hansen H N, Zeidler H, Martin A, Schubert A, Brandao C and Riemer O 2015 Optical micro-metrology of structured surfaces micro-machined by jet-ECM *Proc. of the 15th international conference of the european society for precision engineering and nanotechnology (euspen)* (Leuven: Richard Leach) 167-168 Leuven, Belgium, 1-5 June (ISBN: 978-0-9566790-7-9)
[31] Quagliotti D, Baruffi F, Tosello G, Gasparin S, Annoni M, Parenti P, Sobiecki R and Hansen H N 2016 Correction of systematic behaviour in topographical surface analysis *Proc. of the 4M/IWMF2016 Conference* (Copenhagen: Tosello G, Hansen H N, Kornel E and Dimov S) 277-80 Copenhagen, DK, 13-15 September (ISBN: 978-981-11-0749-8)
[32] DME Mold Finish Comparison Kit – DME Company, www.dme.net
[33] Pavese F and Forbes A 2009 *Data modeling for metrology and testing in measurement science* ed F Pavese and A B Forbes (Boston: Birkhäuser Boston)

Chapter 5

Shrinkage calibration method for formulation of multiscale dimensional tolerance specifications

5.1 Introduction

Quality assurance has undoubtedly need of an adequate assessment of the measurement uncertainty and the establishment of traceability. They are properties of the measurements that depend on the procedures adopted for uncertainty assessment but also on the measurement equipment used. On the other side, the specifications of the produced parts are the essential requirements for defining the quality in accordance with the production. Mutual dependences of production variability on these two aspects have deeply been considered (see, e.g., [1]-[3]). In [1], following the pragmatic *golden rule* of metrology, that advises an expanded uncertainty lower than 10 % when verifying tolerances, a number of errors related to different measurement instruments, influence factors and examples of typical uncertainty evaluation have been reported. Costs and benefits about metrology are discussed in [2], as a tool for gaining information and generating knowledge, according to the following tenets: "1) The measurand shall be defined unambiguously. 2) The measurand shall reflect the functional requirements. 3) The result of a measurement shall be utilizable for making decisions". Beyond the *golden rule*, the concept of measurement process uncertainty combined to the one of the production process is introduced in [3] and dealt with the process capability indices.

Nowadays, general indications to deal with the conformance verification can be found in official documents, like [4] and [5], but no official documents are available for addressing the inverse problem of the formulation of a specification zone. Nonetheless, several specific works exist in literature for allocating tolerances, even though predominantly for assemblies. They include different methods, from traditional ones (proportional scaling, minimum-cost function, Lagrange multipliers, etc.) e.g., [6]-[9], to more recent ones (cost/risk estimation, fuzzy logic, specifications based on Monte Carlo method) e.g. [10]-[13].

In this chapter, a novel method for the formulation of a specification interval is given in the specific case of a micro-powder injection moulding production.

Micro-powder injection moulding (µPIM) is considered an interesting manufacturing process for complex micro parts or micro structured parts. In fact, i) miniaturised manufacture at a relatively low cost, ii) chances to have mass production and, finally, iii) assembly steps integrated into the process (co-injection and co-sintering) [14]-[16] turn µPIM into a particularly attractive technology. Nevertheless, there are some limitations related to this manufacturing technology [16] and the quality control is included.

Past works already investigated the µPIM dimensions replication [15], [17]-[18], the achievable surface topography [15], [19]-[21] and the influence of moulding parameters on dimensional accuracy [15], [22]. In the current study, taking advantage from the specific study case, a method for the formulation of specification intervals as a function of the shrinkage was developed considering the following aspects: 1) Impact of the shrinkage on the dimensions. 2) Conformance verification of the specifications stated by the manufacturer. Nevertheless, they are intended for the purpose of introducing the method. A complete investigation on product conformance with specifications in the micro scale can be found elsewhere [23]. A discussion about the performance and influence of two instruments in relation to the quality of the measurement process was also

included. Furthermore, a different evaluation of the uncertainty was adopted. It is based on the ISO 15530 part 3 [24] and it is deemed an effective and faster alternative to the optimised solution proposed in Chapter 4, when enough repeated measurements are not possible.

5.2 Ceramic injection moulding manufactured parts

The project HiMicro (EU project for high precision micro production technologies—European Commission's 7th Framework Program [25]) was also the context of this study [26]. One of the developed demonstrators was, in fact, a critical functional component in a high-accuracy miniaturised mechanism. This micro mechanical part was subject of the investigation. Examples of a final product and of an intermediate part (after injection moulding) are in **Figure 5.2-1**.

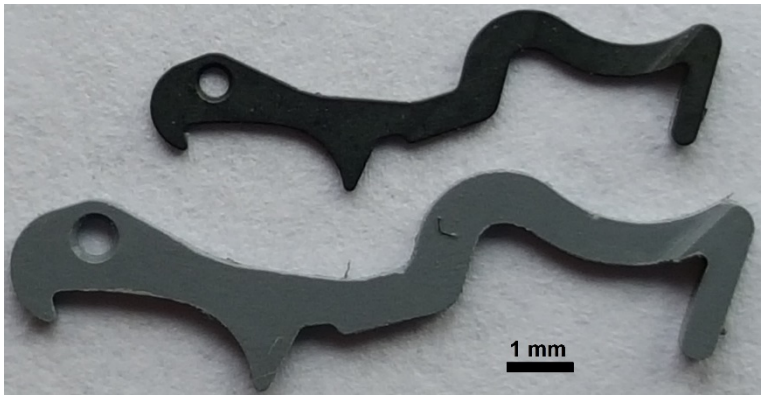

Figure 5.2-1. Examples of final product (top) and intermediate component (bottom).

The components were produced by µPIM. In detail, intermediate parts (commonly called *green parts*) were obtained by ceramic injection moulding (CIM). The process was performed by an Arburg Allrounder 270 S 250-60, with a diameter of the reciprocating screw of 15 mm, a diameter of the nozzle of 2 mm and a maximum clamping force of 250 kN.
The ceramic feedstock used for CIM was Catamold® TZP-F 315 produced by BASF SE, i.e., a compound of zirconium dioxide (ZrO_2), stabilised by diyttrium trioxide (Y_2O_3), with polyoxymethylene (POM) as binder. Parameters and settings of the CIM process are summarised in **Table 5.2-1**. Material properties can be found in [27].

Table 5.2-1. Parameters and settings of the ceramic injection moulding process.

Parameter	*Setting*
Material type	ceramic feedstock (ZrO^2)
Barrel temperature /°C	164-172
Mould temperature /°C	140
Injection speed /cm^3 s^{-1}	8
Switch-over pressure /MPa	152
Cushion /cm^3	1.1
Packing pressure (pressure profile vs time)	0 s: 120 MPa, 1 s: 90 MPa, 2 s: 7.5 MPa
Total packing time /s	2
Machine	Arburg Allrounder 270 S 250-60 (15 mm)

The green parts were exposed to a de-binding process (at 110 °C by nitric acid), with a minimum loss of 17.5 %, and, successively, to a sintering cycle, performed in air (mild purge of air up to 600 °C, sintering support Al_2O_3 with a purity of 99.6 %), consisting of the following typical steps:

- Heating from room temperature to 270 °C with rate 3 K/min; hold on 1 hour.
- Heating from 270 °C to 1500 °C with rate 3 K/min; hold on 1 hour.
- Cooling from 1500 °C to 600 °C with rate 5 K/min.

- Furnace cooling.

The final parts were obtained after the sintering process (commonly called *sintered parts*), in which the ceramic feedstock was converted into polycrystalline yttria-stabilised tetragonal zirconia, with a typical composition of about

- 89 % of zirconium dioxide (ZrO_2)
- 5 % of diyttrium trioxide (Y_2O_3)
- 6 % of unspecified material(s) (not disclosed by the producer[5]).

A considerable shrinkage can be subsequent to the curing process (de-binding and sintering). It is normally accounted oversizing the mould dimensions. To obtain the desired sizes of the final sintered parts, the material producer specified an *oversizing factor* in the range 1.285 ÷ 1.292.

5.3 Metrology for quality assurance

The inspection of the quality assurance of the parts requires to consider the specific manufacturing process and, in particular, the accuracy of the curing process and the mould repeatability. For doing so, as a general indication [2]-[3], twenty-five batches are normally selected, extracting five parts from each of them. Furthermore, the green parts are not stable. To characterise the curing process, the same period of time after the CIM process is to be considered.

Even so, as already stated, the interest was to provide a method rather than to characterise the production itself. Hence, only five green and five sintered parts of the micro mechanical component were inspected. Sintered and green parts were chosen independently from each other. As a consequence, the analysis of this specific manufacturing process is to be considered in reproducibility conditions.

A sketch of the micro mechanical part, with a legend of the measured features of size, is shown in **Figure 5.3-1**. The nominal values are summarised in **Table 5.3-1** and **Table 5.3-2**. These values refer to the final dimensions after the curing process. **Table 5.3-3** instead reports the tolerances specified by the manufacturer, according to the ISO 2768 part 1 (class *m*) [28].

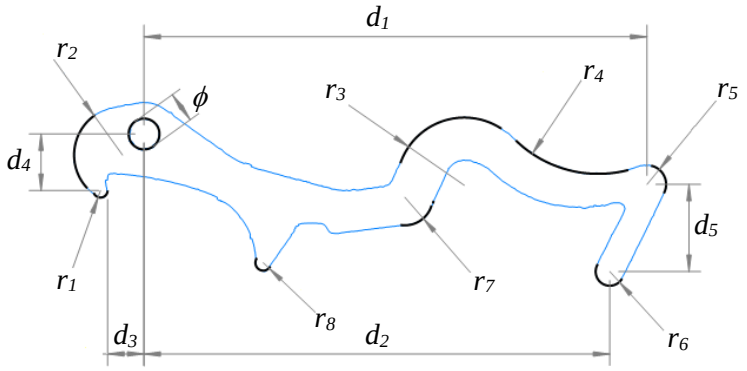

Figure 5.3-1. Legend of the dimensions in **Table 5.3-1** and **Table 5.3-2**.

Table 5.3-1. Nominal values in millimetres of the linear features in **Figure 5.3-1** (sintered components).

d_1	d_2	d_3	d_4	d_5	ϕ
7.939	7.515	0.612	0.984	1.438	0.40

Table 5.3-2. Nominal values in millimetres of the two-dimensional features in **Figure 5.3-1** (sintered components).

r_1	r_2	r_3	r_4	r_5	r_6	r_7	r_8
0.08	0.75	1.06	1.82	0.30	0.22	0.40	0.10

[5] In similar compounds the producer specified dialuminium trioxide (Al_2O_3).

Table 5.3-3. Tolerances specified by the manufacturer, in the range of interest, according to ISO 2768 part 1, class *m* [116].

	Linear Dimension			*Radii*
Dimension	$d \leq 3$ /mm	$3 < d \leq 6$ /mm	$6 < d \leq 30$ /mm	$r \leq 3$ /mm
Tolerance	± 0.1	± 0.1	± 0.2	± 0.2

The size of the features of the micro component ranges from several millimetres to tens of micrometres. This is challenging when the measurements are to be performed, although, it is particularly useful for examining dimensions and tolerance chains, at different scales, in the same process. The impact of the different scales on the measurement instrument is analysed below and in the following § 5.5.

Measurements and evaluation of the uncertainty

All the features of size in **Figure 5.3-1**, of both green and sintered parts, were measured using an optical coordinate measuring machine (OCMM – magnification 2×, lateral resolution 4 µm) (**Figure 5.3-2**). Successively, the expanded uncertainties of the measured dimensions were evaluated for each single part as well as for the overall parts. The uncertainty model was inspired to the ISO 15530 part 3 [24], even though no correction of the final values was performed. It is summarised in the diagram of **Figure 5.3-3**. Average values and related expanded uncertainties for green and sintered parts are in **Table 5.3-4** to **Table 5.3-13**.

Figure 5.3-2. Optical coordinate measuring machine (DeMeet 220 – OCMM) used in the investigation.

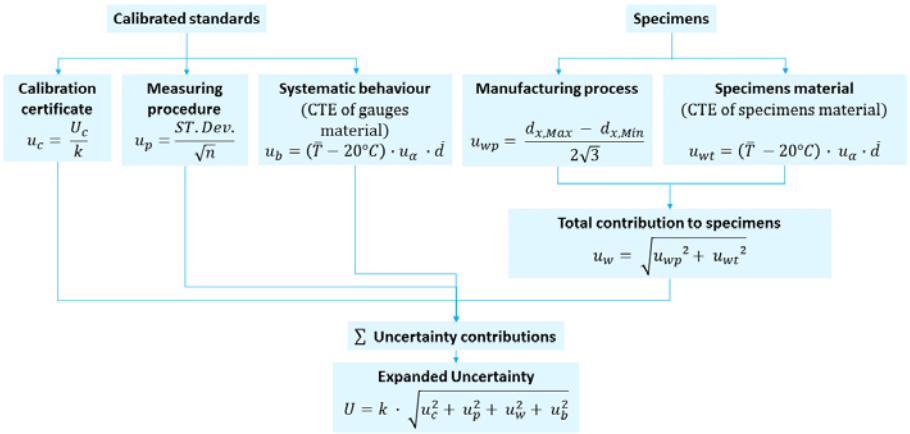

Figure 5.3-3. Diagram of the uncertainty model used in the investigation.

Table 5.3-4. Average values (first row) and expanded uncertainties (second row) of the green parts (lengths).

d_1 /mm	d_2 /mm	d_3 /mm	d_4 /mm	d_5 /mm	ϕ /mm
10.210	9.703	0.783	1.233	1.779	0.605
0.067	0.035	0.033	0.029	0.075	0.010

Table 5.3-5. Average values (first row) and expanded uncertainties (second row) of the sintered parts (lengths).

d_1 /mm	d_2 /mm	d_3 /mm	d_4 /mm	d_5 /mm	ϕ /mm
7.958	7.517	0.599	0.963	1.369	0.482
0.099	0.023	0.016	0.040	0.038	0.003

Table 5.3-6. Lower and upper limits of the conformance zones for the sintered parts.

d_1 /mm	d_2 /mm	d_3 /mm	d_4 /mm	d_5 /mm	ϕ /mm
7.838	7.338	0.528	0.834	1.376	0.203
8.040	7.692	0.696	0.954	1.500	0.597

Table 5.3-7. Lower and upper limits of the specification intervals for the sintered parts.

d_1 /mm	d_2 /mm	d_3 /mm	d_4 /mm	d_5 /mm	ϕ /mm
7.739	7.315	0.512	0.794	1.338	0.200
8.139	7.715	0.712	0.994	1.538	0.600

Table 5.3-8. Measured oversizing factors.

d_1	d_2	d_3	d_4	d_5	ϕ
1.283	1.291	1.308	1.280	1.300	1.256

Table 5.3-9. Average values (first row) and expanded uncertainties (second row) of the green parts (radii).

r_1 /mm	r_2 /mm	r_3 /mm	r_4 /mm	r_5 /mm	r_6 /mm	r_7 /mm	r_8 /mm
0.119	0.942	1.361	2.412	0.415	0.279	0.509	0.137
0.015	0.024	0.089	0.188	0.083	0.027	0.073	0.012

Table 5.3-10. Average values (first row) and expanded uncertainties (second row) of the sintered parts (radii).

r_1 /mm	r_2 /mm	r_3 /mm	r_4 /mm	r_5 /mm	r_6 /mm	r_7 /mm	r_8 /mm
0.073	0.765	1.122	1.799	0.272	0.215	0.397	0.098
0.021	0.077	0.021	0.163	0.046	0.051	0.020	0.019

Table 5.3-11. Lower and upper limits of the conformance zones for the sintered parts.

r_1 /mm	r_2 /mm	r_3 /mm	r_4 /mm	r_5 /mm	r_6 /mm	r_7 /mm	r_8 /mm
0.021	0.627	0.881	1.783	0.146	0.071	0.220	0.019
0.259	0.873	1.239	1.857	0.454	0.369	0.580	0.281

Table 5.3-12. Lower and upper limits of the specification intervals for the sintered parts.

r_1 /mm	r_2 /mm	r_3 /mm	r_4 /mm	r_5 /mm	r_6 /mm	r_7 /mm	r_8 /mm
0.000	0.550	0.860	1.620	0.100	0.020	0.200	0.000
0.280	0.950	1.260	2.020	0.500	0.420	0.600	0.300

Table 5.3-13. Measured oversizing factors.

r_1	r_2	r_3	r_4	r_5	r_6	r_7	r_8
1.619	1.230	1.213	1.341	1.525	1.293	1.282	1.394

The expanded uncertainty U was evaluated according to the uncertainty contributors shown in **Figure 5.3-3** . In particular:

- u_c: uncertainty stated in the calibration certificates of the references.
- u_p: instrument repeatability (seven repeated measurements per reference).
- u_w: two contributions. Effect of temperature on specimens and variability due to manufacturing process (reproducibility—seven repeated measurements per specimen)
- u_b: effect of temperature on references.
- Coverage factor $k = 2$, i.e., an approximated expanded interval of 95 %.
- Measurement result d_x and its expanded uncertainty U were expressed as $d_x \pm U$.

From the inspections of the tables, the following can be said:

- The conformity to the specifications can be proved for all the dimensions except d_4 and d_5.
- Neither the conformity nor the nonconformity to the specifications can be proved for d_4 and d_5.
- The oversizing factors are all outside the interval provided by the producer of the feedstock, except the one of d_2. However, the oversizing factors of d_1, d_4, d_5, r_6 and r_7 are very close to the nominal interval provided.

Measurements capability

Ideally, if the variability expressed by the expanded uncertainty is intrinsic to the production, the results can be considered an acceptable estimation. Conversely, if it is influenced by the measurement process the results cannot directly be related to the manufacturing process [1]-[3]. For this reason, in order to understand if the evaluation could rely on the measurement process, the evaluated expanded uncertainty was separated in two contributions, one related to the instrument *U(instr)* and another one related to the production *U(μPIM)* [3]. Considering *U(instr)* as the average of the expanded uncertainties related to each single part (results in **Table 5.3-14**, **Table 5.3-15**, **Table 5.3-16** and **Table 5.3-17**), and *U* the one evaluated on all parts (**Table 5.3-4**, **Table 5.3-5**, **Table 5.3-9** and **Table 5.3-10**), *U(μPIM)* was estimated, for both green and sintered parts, as [3]

$$U^2(\mu PIM) = U^2 - U^2(instr) \tag{5.3-1}$$

Eventually, an indication of the measuring process capability was given as the ratio

$$\frac{U(instr)}{U(\mu PIM)} < R_P \tag{5.3-2}$$

Table 5.3-14. Green parts (lengths): expanded uncertainties related to the single components, *U(instr)*, *U(μPIM)* and capability ratio in Equation (5.3-2).

	d_1 /mm	d_2 /mm	d_3 /mm	d_4 /mm	d_5 /mm	ϕ /mm
U_1	0.023	0.001	0.011	0.011	0.012	0.001
U_2	0.038	0.023	0.010	0.010	0.018	0.001
U_3	0.009	0.017	0.016	0.013	0.045	0.001
U_4	0.018	0.015	0.017	0.012	0.015	0.001
U_5	0.013	0.002	0.015	0.012	0.043	0.002
U(instr)	0.020	0.012	0.014	0.012	0.027	0.001
U(μPIM)	0.064	0.033	0.030	0.026	0.070	0.010
Ratio	32 %	36 %	47 %	45 %	38 %	15 %

Table 5.3-15. Green parts (radii): expanded uncertainties related to the single components, *U(instr)*, *U(μPIM)* and capability ratio in Equation (5.3-2).

	r_1 /mm	r_2 /mm	r_3 /mm	r_4 /mm	r_5 /mm	r_6 /mm	r_7 /mm	r_8 /mm
U_1	0.004	0.004	0.005	0.013	0.018	0.004	0.003	0.002
U_2	0.002	0.002	0.006	0.003	0.037	0.018	0.003	0.003
U_3	0.006	0.002	0.008	0.017	0.008	0.009	0.014	0.004
U_4	0.003	0.004	0.008	0.012	0.004	0.007	0.016	0.004
U_5	0.005	0.003	0.007	0.018	0.029	0.015	0.004	0.004
U(instr)	0.004	0.003	0.007	0.012	0.019	0.010	0.008	0.003
U(μPIM)	0.014	0.023	0.089	0.188	0.081	0.025	0.073	0.012
Ratio	28 %	14 %	8 %	7 %	24 %	41 %	11 %	27 %

Table 5.3-16. Sintered parts (lengths): expanded uncertainties related to the single components, *U(instr)*, *U(μPIM)* and capability ratio in Equation (5.3-2).

	d_1 /mm	d_2 /mm	d_3 /mm	d_4 /mm	d_5 /mm	ϕ /mm
U_1	0.018	0.009	0.010	0.010	0.020	0.002
U_2	0.004	0.003	0.015	0.034	0.011	0.002
U_3	0.014	0.001	0.011	0.011	0.011	0.001
U_4	0.005	0.002	0.010	0.011	0.012	0.001
U_5	0.091	0.008	0.011	0.011	0.038	0.001
U(instr)	0.026	0.005	0.011	0.015	0.018	0.002
U(μPIM)	0.096	0.023	0.012	0.037	0.034	0.002
Ratio	27 %	20 %	97 %	41 %	55 %	78 %

Table 5.3-17. Sintered parts (radii): expanded uncertainties related to the single components, *U(instr)*, *U(μPIM)* and capability ratio in Equation (5.3-2).

	r_1 /mm	r_2 /mm	r_3 /mm	r_4 /mm	r_5 /mm	r_6 /mm	r_7 /mm	r_8 /mm
U_1	0.003	0.012	0.005	0.004	0.028	0.050	0.003	0.004
U_2	0.003	0.003	0.005	0.007	0.002	0.002	0.004	0.003
U_3	0.003	0.004	0.009	0.010	0.019	0.003	0.004	0.004
U_4	0.003	0.005	0.003	0.003	0.002	0.003	0.003	0.002
U_5	0.004	0.014	0.010	0.008	0.028	0.009	0.008	0.016
U(instr)	0.003	0.008	0.006	0.006	0.016	0.013	0.004	0.006
U(μPIM)	0.020	0.077	0.020	0.163	0.044	0.049	0.019	0.018
Ratio	15 %	10 %	33 %	4 %	36 %	28 %	23 %	32 %

As a general trend for both green and sintered parts, the ratios between the expected uncertainties *U(instr)* and the estimated uncertainties of the process *U(μPIM)* were larger than the 10 % stated by the *golden rule* of metrology, with few exceptions. It means that the measurement process influenced the evaluation of the uncertainty and, consequently, the conformance verification.
The reason concerns the software equipped on the used OCMM. It identifies the geometrical entities in a specimen under measurement by an algorithm based on edge detection: an edge is recognised as sharp transition between a dark and a light area in the formed image. Unfortunately, many defects were found along the edges of the parts, which explain the poor performance of the instrument.
The presence of defects on such manufactured parts is quite common. Two examples are in **Figure 5.3-4**. Besides the measured dimensions, such defects could locally change and counteract the "light to dark" transition. This behaviour raises questions on the choice of a suitable measurement instrument that will be taken up in § 5.5, where two different working principles will be discussed.
Even so, this poor outcome was concealed by the large tolerances stated by the producer: the lengths were specified with a precision of 1 μm, the radii with a precision of 10 μm whilst tolerances had a precision of 100 μm. This also emphasises a lack of *tolerancing* rules at the sub-mm scale.

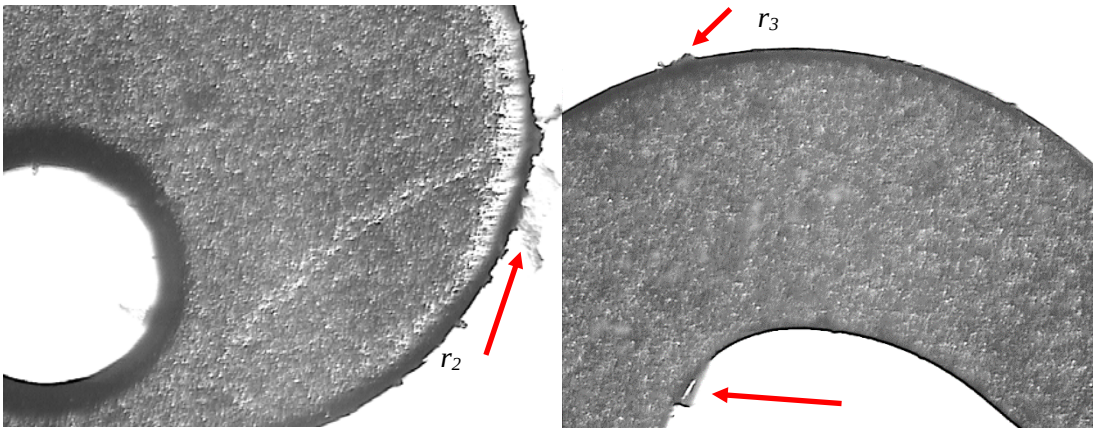

Figure 5.3-4. Example of defects on the edges of features r_2 and r_3.

Evaluation of the shrinkage and uncertainty propagation

The shrinkage due to the j^{th} green part $\delta L_{\%,j} = f\left(d_{x_j,g}, \bar{d}_{x,s}\right)$ was estimated, for each dimension $d_{x_j,g}$, as the relative deviation from the corresponding average dimension $\bar{d}_{x,s}$ of all sintered parts.

The average dimensions of all sintered parts (stable parts) were, in fact, considered the reference for the achieved production:

$$\delta L_{\%,j} = f\left(d_{x_j,g}, \bar{d}_{x,s}\right) = \frac{d_{x_j,g} - \bar{d}_{x,s}}{\bar{d}_{x,s}} \times 100 \quad (5.3\text{-}3)$$

where

- $f\left(d_{x_j,g}, \bar{d}_{x,s}\right)$ is the shrinkage of the j^{th} green part, expressed in percentage;
- $d_{x_j,g}$ is a generic dimension of a generic green part;
- $\bar{d}_{x,s}$ is the average value for a generic dimension considering all sintered parts.

For evaluating the uncertainty of the shrinkage due to the sintering process, the uncertainty was propagated considering green and sintered parts correlated. According to the non-linear second order Taylor series of the shrinkage (see § 2.3.1 and [29]), the approximated expression used for the correlated quantities was:

$$u_{x,j}^2 = \left(\frac{\partial f}{\partial d_{x_j,g}}\right)^2 \Delta d_{x_j,g}^2 + \left(\frac{\partial f}{\partial \bar{d}_{x,s}}\right)^2 \Delta \bar{d}_{x,s}^2 + 2\frac{\partial f}{\partial d_{x_j,g}}\frac{\partial f}{\partial \bar{d}_{x,s}}\rho_{g,s}\Delta d_{x_j,g}\Delta \bar{d}_{x,s} \quad (5.3\text{-}4)$$

where

- $u_{x,j}$ is the uncertainty of the shrinkage propagated for the j^{th} green part, expressed in percentage;
- $\frac{\partial f}{\partial d_{x_j,g}}$ and $\frac{\partial f}{\partial \bar{d}_{x,s}}$ are respectively the partial derivative of the shrinkage with respect to the generic dimension of the j^{th} green part and the one with respect to the average value of the generic dimension considering all sintered parts;
- $\Delta d_{x_j,g}$ and $\Delta \bar{d}_{x,s}$ are respectively the variability of $d_{x_j,g}$ (j^{th} green part) and the variability of $\bar{d}_{x,s}$ (all sintered parts) due to the measurement process. These quantities were considered correlated with a degree of dependence given by the Pearson's correlation coefficient $\rho_{g,s}$. Furthermore, they are normally standard uncertainties. However, as anticipated, they were subjected to the purpose of introducing the method in § 5.4, where a different choice will be justified in § 5.4.

The results about the evaluation of the shrinkage are in the following **Figure 5.3-5** to **Figure 5.3-18**. The propagated uncertainties of the shrinkage are in **Table 5.3-18**, evaluated for the dimensions of each green part with respect to the average dimensions of all sintered parts, and in **Table 5.3-19**, evaluated for the average dimensions of both green and sintered parts.

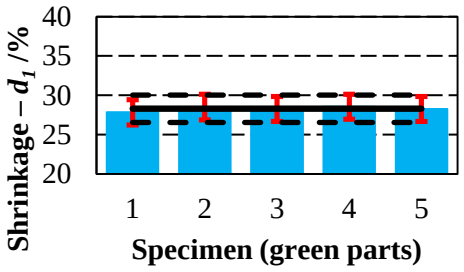

Figure 5.3-5. Shrinkage of d_1 for each green part. The bars represent the estimated uncertainty of the shrinkage for each sample. The solid line is the shrinkage considering average values (both green and sintered) and the dashed lines indicate the uncertainty interval estimated on the overall samples.

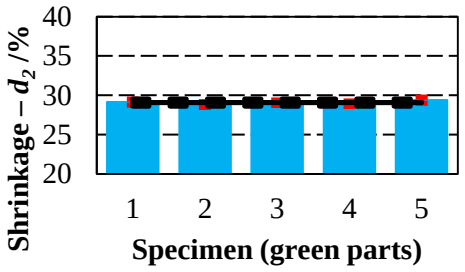

Figure 5.3-6. Shrinkage of d_2 for each green part. The bars represent the estimated uncertainty of the shrinkage for each sample. The solid line is the shrinkage considering average values (both green and sintered) and the dashed lines indicate the uncertainty interval estimated on the overall samples.

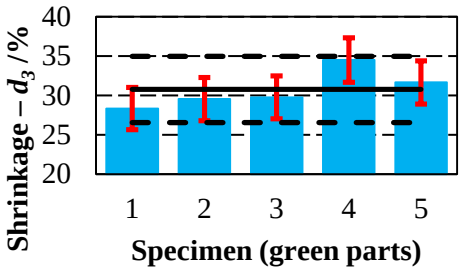

Figure 5.3-7. Shrinkage of d_3 for each green part. The bars represent the estimated uncertainty of the shrinkage for each sample. The solid line is the shrinkage considering average values (both green and sintered) and the dashed lines indicate the uncertainty interval estimated on the overall samples.

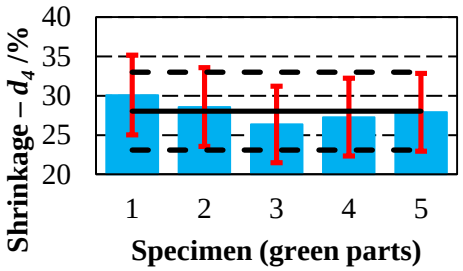

Figure 5.3-8. Shrinkage of d_4 for each green part. The bars represent the estimated uncertainty of the shrinkage for each sample. The solid line is the shrinkage considering average values (both green and sintered) and the dashed lines indicate the uncertainty interval estimated on the overall samples.

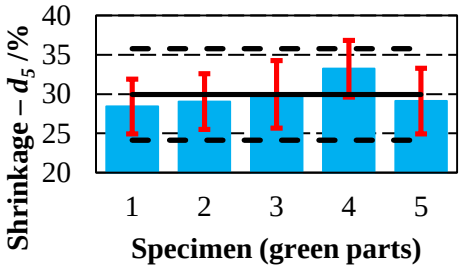

Figure 5.3-9. Shrinkage of d_5 for each green part. The bars represent the estimated uncertainty of the shrinkage for each sample. The solid line is the shrinkage considering average values (both green and sintered) and the dashed lines indicate the uncertainty interval estimated on the overall samples.

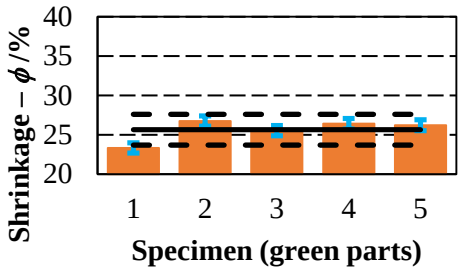

Figure 5.3-10. Shrinkage of ϕ for each green part. The bars represent the estimated uncertainty of the shrinkage for each sample. The solid line is the shrinkage considering average values (both green and sintered) and the dashed lines indicate the uncertainty interval estimated on the overall samples.

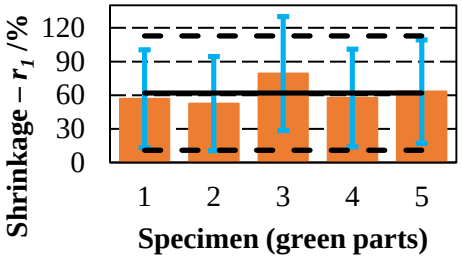

Figure 5.3-11. Shrinkage of r_1 for each green part. The bars represent the estimated uncertainty of the shrinkage for each sample. The solid line is the shrinkage considering average values (both green and sintered) and the dashed lines indicate the uncertainty interval estimated on the overall samples.

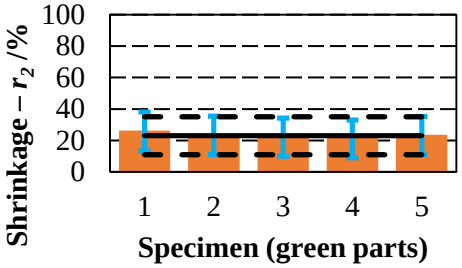

Figure 5.3-12. Shrinkage of r_2 for each green part. The bars represent the estimated uncertainty of the shrinkage for each sample. The solid line is the shrinkage considering average values (both green and sintered) and the dashed lines indicate the uncertainty interval estimated on the overall samples.

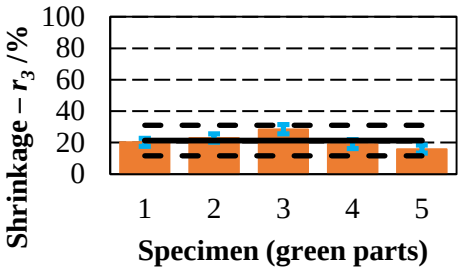

Figure 5.3-13. Shrinkage of r_3 for each green part. The bars represent the estimated uncertainty of the shrinkage for each sample. The solid line is the shrinkage considering average values (both green and sintered) and the dashed lines indicate the uncertainty interval estimated on the overall samples.

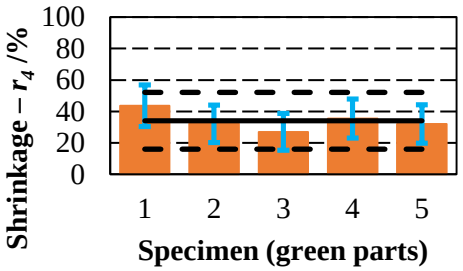

Figure 5.3-14. Shrinkage of r_4 for each green part. The bars represent the estimated uncertainty of the shrinkage for each sample. The solid line is the shrinkage considering average values (both green and sintered) and the dashed lines indicate the uncertainty interval estimated on the overall samples.

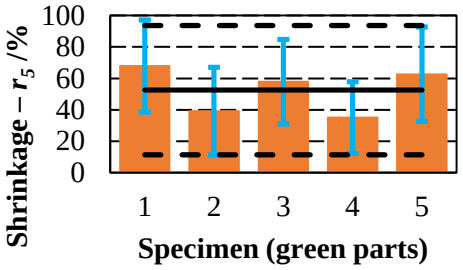

Figure 5.3-15. Shrinkage of r_5 for each green part. The bars represent the estimated uncertainty of the shrinkage for each sample. The solid line is the shrinkage considering average values (both green and sintered) and the dashed lines indicate the uncertainty interval estimated on the overall samples.

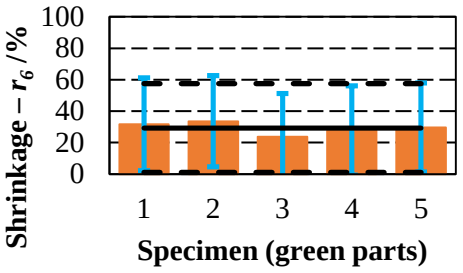

Figure 5.3-16. Shrinkage of r_6 for each green part. The bars represent the estimated uncertainty of the shrinkage for each sample. The solid line is the shrinkage considering average values (both green and sintered) and the dashed lines indicate the uncertainty interval estimated on the overall samples.

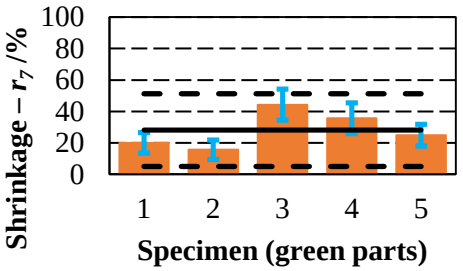

Figure 5.3-17. Shrinkage of r_7 for each green part. The bars represent the estimated uncertainty of the shrinkage for each sample. The solid line is the shrinkage considering average values (both green and sintered) and the dashed lines indicate the uncertainty interval estimated on the overall samples.

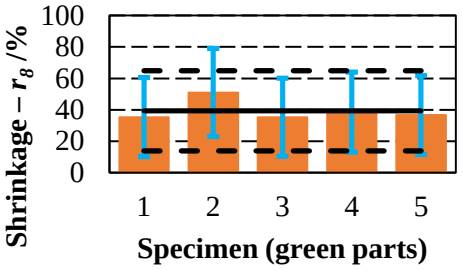

Figure 5.3-18. Shrinkage of r_8 for each green part. The bars represent the estimated uncertainty of the shrinkage for each sample. The solid line is the shrinkage considering average values (both green and sintered) and the dashed lines indicate the uncertainty interval estimated on the overall samples.

Table 5.3-18. Shrinkage propagated uncertainty for each green part.

$u_{d1,j}$ /%	$u_{d2,j}$ /%	$u_{d3,j}$ /%	$u_{d4,j}$ /%	$u_{d5,j}$ /%	$u_{\phi,j}$ /%	$u_{r1,j}$ /%	$u_{r2,j}$ /%	$u_{r3,j}$ /%	$u_{r4,j}$ /%	$u_{r5,j}$ /%	$u_{r6,j}$ /%	$u_{r7,j}$ /%	$u_{r8,j}$ /%
1.6	0.4	2.7	5.1	3.5	0.6	43.6	12.4	2.5	13.1	29.4	29.6	6.5	25.1
1.6	0.4	2.7	5.0	3.5	0.7	41.9	12.2	2.6	11.9	27.9	29.0	6.2	28.0
1.6	0.3	2.7	4.9	4.3	0.7	50.7	12.1	3.0	11.7	26.9	27.3	9.9	24.8
1.6	0.3	2.8	4.9	3.6	0.7	43.5	12.0	2.8	12.4	22.8	28.4	9.8	25.4
1.6	0.4	2.7	4.9	4.2	0.7	46.0	12.2	2.6	12.2	30.0	28.3	6.9	25.1

Table 5.3-19. Shrinkage propagated uncertainty considering the average of all green parts.

$u_{d1,Av}$ /%	$u_{d2,Av}$ /%	$u_{d3,Av}$ /%	$u_{d4,Av}$ /%	$u_{d5,Av}$ /%	$u_{\phi,Av}$ /%	$u_{r1,Av}$ /%	$u_{r2,Av}$ /%	$u_{r3,Av}$ /%	$u_{r4,Av}$ /%	$u_{r5,Av}$ /%	$u_{r6,Av}$ /%	$u_{r7,Av}$ /%	$u_{r8,Av}$ /%
1.7	0.4	4.2	5.0	5.8	2.0	50.9	12.1	9.7	18.1	41.1	28.2	23.1	25.5

5.4 Formulation of specification intervals

The analysis of the shrinkage in § 5.3 showed a different behaviour of the linear and bi-dimensional features which can be accounted more efficiently with respect to the specifications.
In the following, a method is proposed, in which the specifications are formulated as function of the variability of the production both before (CIM process) and after (sintering process) the dimensional progression of the shrinkage [30].
The method allocates two-sided tolerance intervals in agreement with the guarded acceptance decision rule, defined in [4], with guard bands corresponding to a length parameter equal to the expanded uncertainty characterising the production. In the same way, it is in agreement with the conformance zone defined in [5] and obtained reducing a specification zone (tolerance interval) by the expanded uncertainty characterising the production.
Key point of the method, in fact, is the assumption of propagating a coverage interval.
As already stated concerning $\Delta d_{x_j,g}$ and $\Delta \bar{d}_{x,s}$ in Equation (5.3-4), their variability in the propagation of the uncertainty related to the shrinkage was fixed to non-conventional quantities.
The specifications were formulated propagating a coverage interval, evaluated according to a confidence level of the same amount of the desired conformance probability. This gives to the producer a risk of rejecting a part, in future evaluations, established according to a desired conformance probability. Having no specific indications, the choice was here a conformance probability of 95 %. Therefore, tolerance intervals could be estimated setting $\Delta d_{x_j,g}$ and $\Delta \bar{d}_{x,s}$ to the corresponding expanded uncertainties in the propagation of the shrinkage.
Two sets of contributions can be propagated according to Equation (5.3-4): $u_{x,j}$, which is the propagated uncertainty of each single sample in percentage of the shrinkage (**Table 5.3-18**), and $u_{x,Av}$, which is the propagated uncertainty in percentage of the average shrinkage (**Table 5.3-19**— the average of all green parts $\bar{d}_{x,g}$ instead of $d_{x_j,g}$ in Equation (5.3-4)).
Analogously to what done in § 5.3 [3], a formula similar to Equation (5.3-1) can be specified, where the shrinkage uncertainty $u_{x,j}$ of each green part (variability of the instrument) is square subtracted from $u_{x,Av}$ (total variability), which gives an estimation of the process uncertainty:

$$u^2_{proc,x_j} = u^2_{x,Av} - u^2_{x_j} \tag{5.4-1}$$

In some case the difference in Equation (5.4-1) was a negative number, meaning that the influence of the instrument was dominant for some parts (as already explained in § 5.3, due to defects on parts edges). In such cases, it was considered $u^2_{proc,x_j} = u^2_{x,Av}$, i.e., no estimation of the process uncertainty was possible.
Eventually, the specification limits were calculated as the average of all the process uncertainties u^2_{proc,x_j}. Nonetheless, conversely to what considered for the process capability in § 5.3, the

arithmetic average of the uncertainties (expected uncertainties) was considered a too weak assessment. A quadratic average was, instead, performed (average of the variances):

$$U_{proc,x} = h_S \times 2 \times \sqrt{\frac{1}{n}\sum_{j=1}^{n} u_{proc,x_j}^2} \tag{5.4-2}$$

where n is the number of green parts considered and $h_S \geq 1$ is a safety factor. It was added into the equation to satisfy the conformance interval with a certain margin (see conformance limits in Equations (5.4-4-a) and (5.4-4-b) below).
Hence, the specification intervals were calculated as[6]

$$\bar{d}_{x,s} - U_{x,process} < \bar{d}_{x,s} < \bar{d}_{x,s} + U_{x,process} \tag{5.4-3}$$

and the conformance zones were identified by the following limits

$$T_{x,L} = \bar{d}_{x,s} - U_{x,process} + U_{x,S} \tag{5.4-4-a}$$
$$T_{x,U} = \bar{d}_{x,s} + U_{x,process} - U_{x,S} \tag{5.4-4-b}$$

where $U_{x,S}$ were the expanded uncertainties of the sintered parts, reported in **Table 5.3-5** and **Table 5.3-10**.
The method is a dimensional characterisation that should be performed on several samples of green and sintered parts in order to be representative of the entire production. Consequently, the average values and the limits of the conformance zones, resulting from the characterisation, become the nominal values and the limits of the specification intervals (tolerances) of the produced components, respectively. Results are summarised in **Table 5.4-1**. In the same table, an indication of the measurements capability of the characterisation is given according to the formula [4]

$$C_m = \frac{T_{x,U} - T_{x,L}}{2 \times U_{x,S}} \tag{5.4-5}$$

Table 5.4-1. Results related to the dimensions of the final component (sintered parts): nominal values $\bar{d}_{x,s}$ (averages of the dimensional characterisation), tolerances and specification limits T_{xL}, T_{xU} (conformance zones of the dimensional characterisation). Safety factors h_S, process uncertainty estimations $U_{x,process}$ are also reported. Lastly, the expanded uncertainties of the sintered parts in **Table 5.3-5** and **Table 5.3-10** are rewritten here for convenience.

	d_1 /mm	d_2 /mm	d_3 /mm	d_4 /mm	d_5 /mm	ϕ /mm	r_1 /mm	r_2 /mm	r_3 /mm	r_4 /mm	r_5 /mm	r_6 /mm	r_7 /mm	r_8 /mm
h_S	1.1	1.0	1.0	1.0	1.0	1.0	1.0	1.0	1.0	1.0	1.0	1.0	1.0	1.3
$T_{x,L}$	7.939	7.504	0.577	0.942	1.287	0.466	0.060	0.677	0.934	1.487	0.152	0.156	0.245	0.086
$\bar{d}_{x,s}$	7.958	7.517	0.599	0.963	1.369	0.482	0.073	0.765	1.122	1.799	0.272	0.215	0.397	0.098
$T_{x,U}$	7.978	7.530	0.621	0.984	1.450	0.497	0.087	0.854	1.311	2.111	0.392	0.275	0.549	0.110
$\pm tol$	0.020	0.013	0.022	0.021	0.082	0.015	0.014	0.088	0.189	0.312	0.120	0.059	0.152	0.012
$U_{x,pro}$	0.119	0.036	0.038	0.061	0.120	0.018	0.034	0.166	0.209	0.476	0.166	0.110	0.172	0.031
$U_{x,S}$	0.099	0.023	0.016	0.040	0.038	0.003	0.021	0.077	0.021	0.163	0.046	0.051	0.020	0.019
C_m	0.2	0.6	1.4	0.5	2.1	5.7	0.7	1.1	9.1	1.9	2.6	1.2	7.7	0.6

[6] The quantity in Equation (5.4-2) is expressed in percentage so, before using it, the following should be calculated

$$U_{x,process} = \bar{d}_{x,s} \cdot {}^{U_{proc,x}}/_{100}$$

The values in **Table 5.4-1** are pictured in the following **Figure 5.4-1** to **Figure 5.4-4**.
The defined specification zones are intended as minimum values possible in relations to the dimensional characterisation. Nonetheless, such intervals can be further extended tuning the safety factors h_S.
Eventually, it should be noted that the contributions due to the measurement and manufacturing processes might also have been separated before the propagation of the uncertainties (see Equation (5.4-1)). Even so, the suggested procedure is a more stringent choice. Equation (5.4-1) is, in fact, an approximated estimation. Such approximation may have been enlarged propagating the uncertainties.

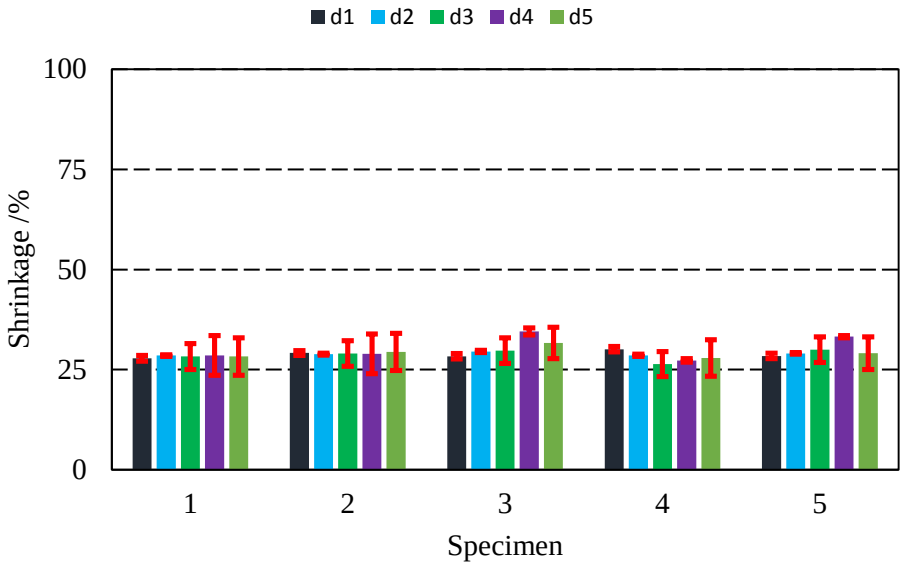

Figure 5.4-1. Shrinkage of the linear feature per each green part. Error bars indicate the estimated $u_{proc,xj}$.

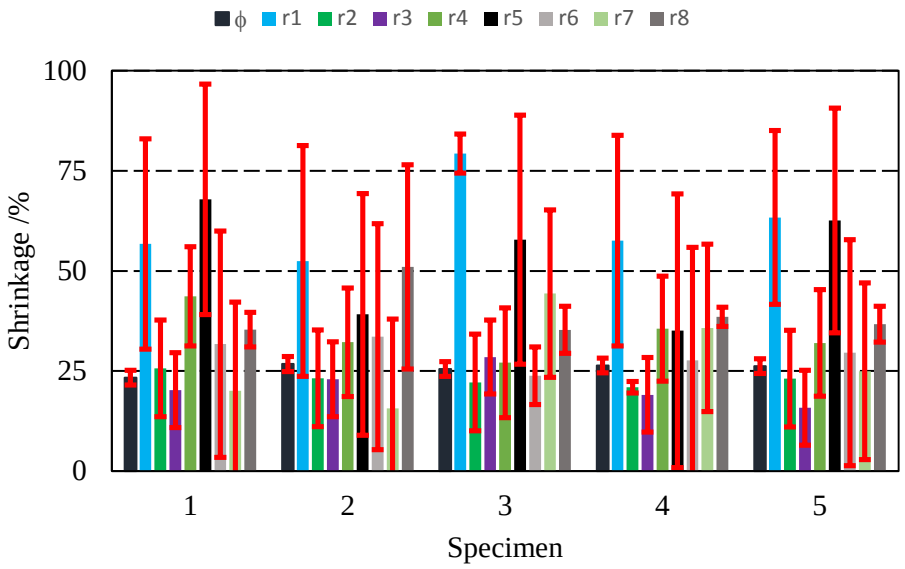

Figure 5.4-2. Shrinkage of the two dimensional features per each green part. Error bars indicate the estimated $u_{proc,xj}$.

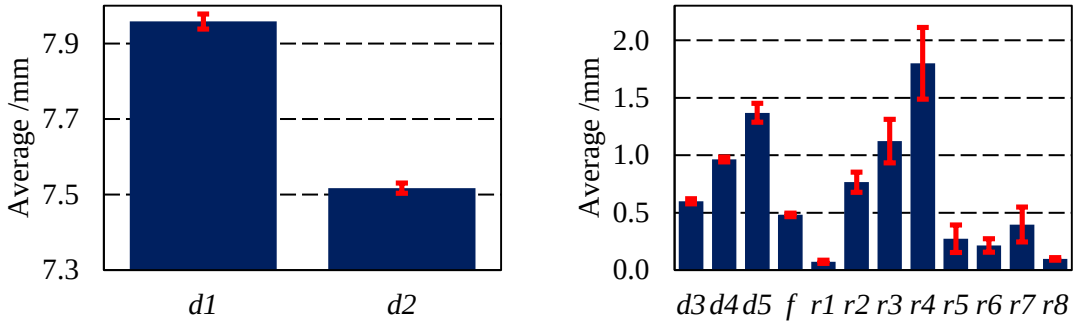

Figure 5.4-3. Nominal values for all the features after the dimensional characterisation. The error bars represents the specification limits.

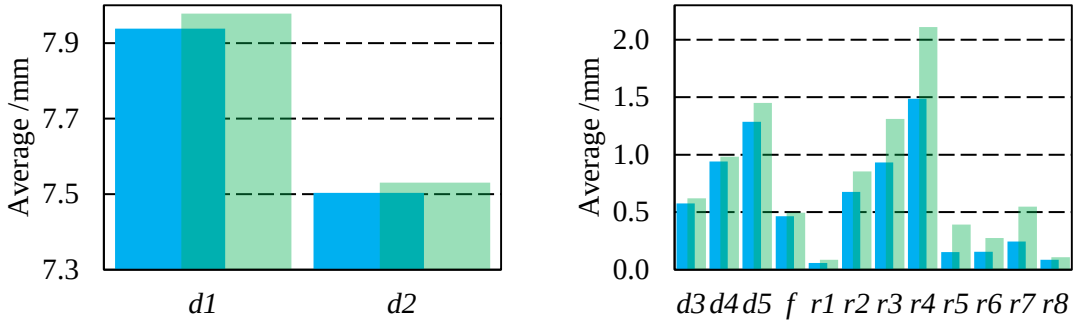

Figure 5.4-4. Specification limits for all the features after the dimensional characterisation.

5.5 Assessment of multiscale measurements by two working principles

The selection of the measurement instrument to be used for inspecting the parts is a fundamental aspect for the success of the quality assurance operations. It has already been emphasised in this chapter that defects along the edges of the parts made particularly problematic the measurements by OCMM. Furthermore, difficulties in measurements are enhanced when multiscale specimens are under evaluation and features of size are close to a limit of the operating range of a measurement technology.

To highlight challenges in the choice of a measurement instrument, the same specimens already presented in § 5.3 (five green and five sintered parts of a µPIM manufacture), have been re-measured by a different operator and successively compared using again DeMeet 220 OCMM (magnification 2×, lateral resolution 4 µm – **Figure 5.3-2**), commonly used in an industrial environment, and Alicona G4 focus variation microscope (FVM), suitable for laboratory use (magnification 5×, vertical resolution 500 nm, optical lateral resolution 2.2 µm – Figure 4.2-2-(a)).

The on-instrument software [32] provided the values of the measurements by OCMM. An image processing software [33] was instead used to extract the measurements values from the FVM acquisitions, by a routine for contour fitting in the *xy*-plane based on least square method. Datum was defined as the support (stage of the instruments). In fact, the resting points of the specimens on the support are supposed to be same on both instruments. Hence, the levelling was performed on the partitioned and extracted surface of the support.

The expanded uncertainty was evaluated for each features of size according to the same uncertainty model shown in **Figure 5.3-3**. The processing was instead performed by the same operator in charge of the measurements. Results of average values and expanded uncertainties of green and sintered parts, measured by both OCMM and FVM, are in **Table 5.5-1** to **Table 5.5-8**.

Table 5.5-1. Average values (first row) and expanded uncertainties (second row) of the green parts (lengths), results of OCMM.

d_1 /mm	d_2 /mm	d_3 /mm	d_4 /mm	d_5 /mm	ϕ /mm
10.206	9.707	0.783	1.228	1.775	0.605
0.081	0.035	0.033	0.062	0.086	0.010

Table 5.5-2. Average values (first row) and expanded uncertainties (second row) of the green parts (lengths), results of FVM.

d_1 /mm	d_2 /mm	d_3 /mm	d_4 /mm	d_5 /mm	ϕ /mm
10.250	9.586	0.849	1.195	1.804	0.622
0.066	0.174	0.073	0.052	0.040	0.028

Table 5.5-3. Average values (first row) and expanded uncertainties (second row) of the green parts (radii), results of OCMM.

r_1 /mm	r_2 /mm	r_3 /mm	r_4 /mm	r_5 /mm	r_6 /mm	r_7 /mm	r_8 /mm
0.123	0.940	1.341	2.427	0.420	0.285	0.506	0.147
0.047	0.053	0.468	0.500	0.083	0.073	0.168	0.199

Table 5.5-4. Average values (first row) and expanded uncertainties (second row) of the green parts (radii), results of FVM.

r_1 /mm	r_2 /mm	r_3 /mm	r_4 /mm	r_5 /mm	r_6 /mm	r_7 /mm	r_8 /mm
0.131	0.980	1.391	2.363	0.398	0.290	0.606	0.160
0.038	0.016	0.022	0.160	0.024	0.020	0.110	0.024

Table 5.5-5. Average values (first row) and expanded uncertainties (second row) of the sintered parts (lengths), results of OCMM.

d_1 /mm	d_2 /mm	d_3 /mm	d_4 /mm	d_5 /mm	ϕ /mm
7.894	7.516	0.599	0.965	1.367	0.479
0.086	0.037	0.038	0.059	0.056	0.003

Table 5.5-6. Average values (first row) and expanded uncertainties (second row) of the sintered parts (lengths), results of FVM.

d_1 /mm	d_2 /mm	d_3 /mm	d_4 /mm	d_5 /mm	ϕ /mm
7.948	7.461	0.634	0.945	1.413	0.478
0.052	0.086	0.051	0.039	0.024	0.012

Table 5.5-7. Average values (first row) and expanded uncertainties (second row) of the sintered parts (radii), results of OCMM.

r_1 /mm	r_2 /mm	r_3 /mm	r_4 /mm	r_5 /mm	r_6 /mm	r_7 /mm	r_8 /mm
0.074	0.808	1.094	1.824	0.324	0.216	0.629	0.101
0.045	0.066	0.067	0.159	0.081	0.012	0.259	0.024

Table 5.5-8. Average values (first row) and expanded uncertainties (second row) of the sintered parts (radii), results of FVM.

r_1 /mm	r_2 /mm	r_3 /mm	r_4 /mm	r_5 /mm	r_6 /mm	r_7 /mm	r_8 /mm
0.097	0.758	1.063	1.788	0.301	0.229	0.483	0.123
0.022	0.015	0.011	0.031	0.024	0.015	0.031	0.015

Results related to the two instruments were successively compared expressing the relative deviations between the averages of the measured values and the upper and lower limits of the variability intervals due to the expanded uncertainty. In other words, being d the generic dimension and considering green and sintered parts, the following was evaluated

$$\Delta d = \left|\frac{d_{OCMM} - d_{FVM}}{d_{FVM}}\right| \times 100 \tag{5.5-1}$$

for the average values $\bar{d}_{OCMM}$, $\bar{d}_{FVM}$ and for the quantities

1) $\bar{d}_{OCMM} - U_{d,OCMM}$, $\bar{d}_{FVM} - U_{d,FVM}$
2) $\bar{d}_{OCMM} + U_{d,OCMM}$, $\bar{d}_{FVM} + U_{d,FVM}$

where $U_{d,x}$ is the expanded uncertainty evaluated for each dimension and each instrument. Furthemore, FVM measurements were considered as reference because they showed a lower trend for the average uncertainty (the indication was given by a quadratic average of the uncertainties related to all the measured dimensions). The results are summarised in **Figure 5.5-1** for the green parts and in **Figure 5.5-2** for the sintered parts. In the same figures the relative deviations between the lower limits $\bar{d}_{OCMM} - U_{d,OCMM}$, $\bar{d}_{FVM} - U_{d,FVM}$ and the upper limits $\bar{d}_{OCMM} + U_{d,OCMM}$, $\bar{d}_{FVM} + U_{d,FVM}$ are also given.

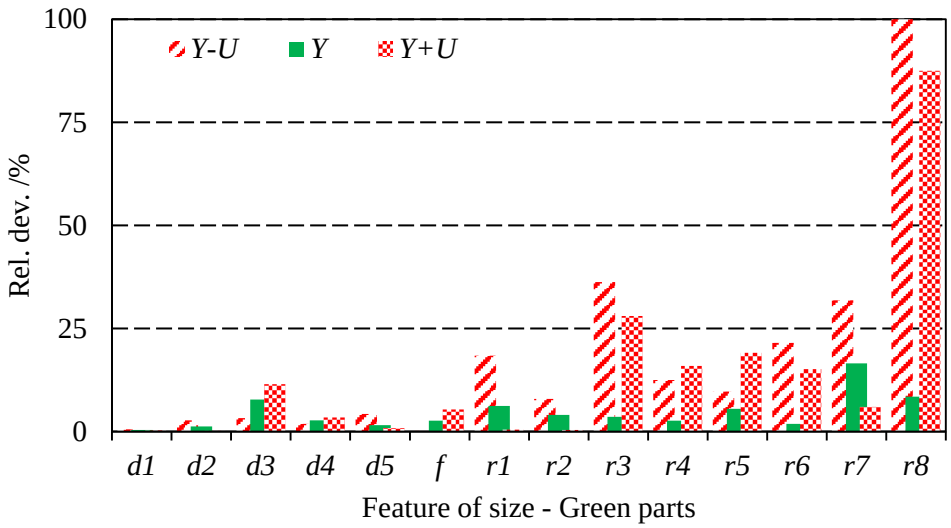

Figure 5.5-1. Relative deviations between the measurements of the green parts performed by OCMM and FVM (green solid columns). FVM is considered the reference. Considering the expanded uncertainty *U*, the red-dashed columns (▨) are the relative deviations between the lower limits of the uncertainty intervals ($\bar{d}_{OCMM} - U_{d,OCMM}$ and $\bar{d}_{FVM} - U_{d,FVM}$); while, the red-dotted columns (▩) are the relative deviations between the upper limits of the uncertainty intervals ($\bar{d}_{OCMM} + U_{d,OCMM}$ and $\bar{d}_{FVM} + U_{d,FVM}$).

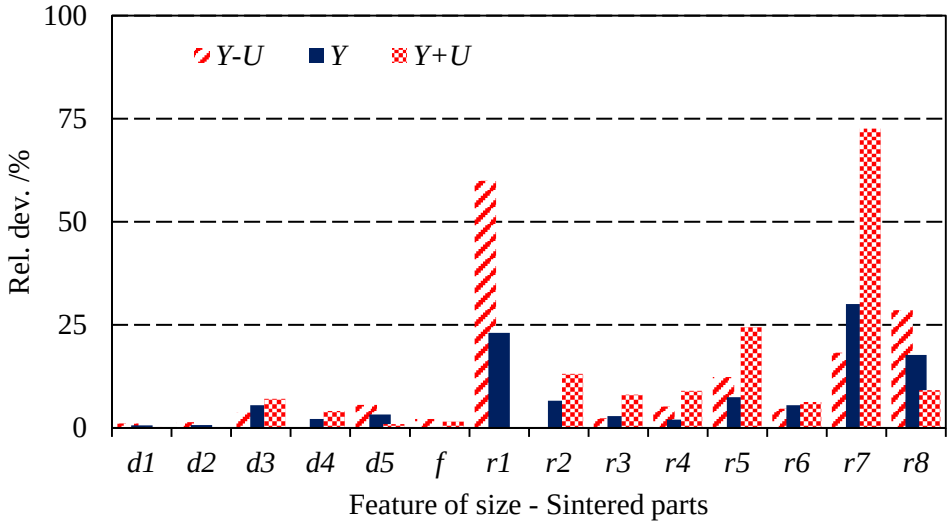

Figure 5.5-2. Relative deviations between the measurements of the sintered parts performed by OCMM and FVM (blue solid columns). FVM is considered the reference. Considering the expanded uncertainty *U*, the red-dashed columns (▨) are the relative deviations between the lower limits of the uncertainty intervals ($\bar{d}_{OCMM} - U_{d,OCMM}$ and $\bar{d}_{FVM} - U_{d,FVM}$); while, the red-dotted columns (▩) are the relative deviations between the upper limits of the uncertainty intervals ($\bar{d}_{OCMM} + U_{d,OCMM}$ and $\bar{d}_{FVM} + U_{d,FVM}$).

Measurements of the green parts by OCMM showed maximum relative deviations from the ones performed by FVM of 17 % for radii and 8 % for linear dimensions. Minimum relative deviations

were 2 % for radii and below 1 % for linear dimensions. Regarding the sintered parts, instead, maximum relative deviations were 30 % for radii and 6 % for linear dimensions. Minimum relative deviations observed were below 1 % for both.
Nonetheless, much larger relative deviations between the two sets of measurements were obtained when considering the limits of the corresponding uncertainty intervals.

Finally, the datasets from the two instruments were both used to verify the specifications formulated for the sintered parts in the previous § 5.4 (**Table 5.4-1**). The results are in the following **Table 5.5-9** to **Table 5.5-10**.

From the inspections of **Table 5.5-9** (OCMM), the following can be said:

- The conformity to the specifications can be proved for ϕ, d_5, r_3, r_4 and r_6.
- Neither the conformity nor the nonconformity to the specifications can be proved for d_2, d_3, d_4, r_1, r_2, r_5 and r_8.
- The nonconformity to the specifications can be proved for d_1, and r_7.

From the inspections of **Table 5.5-9** (FVM), the following can be said:

- The conformity to the specifications can be proved for d_5, r_2, r_3, r_4, r_5, r_6 and r_7.
- Neither the conformity nor the nonconformity to the specifications can be proved for ϕ, d_1, and d_4.
- The nonconformity to the specifications can be proved for d_2, d_3, r_1 and r_8.

In order to have the conformity verified for all the features measured by both instruments, the safety factors were modified to enlarge the specification intervals. The new conformance zones, safety factors and corresponding tolerances are in **Table 5.5-11** and **Table 5.5-12**.

Table 5.5-9. Conformance intervals and average values of the measurements performed by OCMM (sintered parts). The conformance intervals are calculated considering the specification zones in **Table 5.4-1** and the expanded uncertainties in **Table 5.5-5** and **Table 5.5-7**.

	d_1 /mm	d_2 /mm	d_3 /mm	d_4 /mm	d_5 /mm	ϕ /mm	r_1 /mm	r_2 /mm	r_3 /mm	r_4 /mm	r_5 /mm	r_6 /mm	r_7 /mm	r_8 /mm
$d_{x,L}$	8.025	7.541	0.614	1.001	1.343	0.470	0.104	0.743	1.000	1.646	0.233	0.168	0.504	0.110
$\bar{d}_{x,s}$	7.894	7.516	0.599	0.965	1.367	0.479	0.074	0.808	1.094	1.824	0.324	0.216	0.629	0.101
$d_{x,U}$	7.892	7.493	0.583	0.925	1.394	0.493	0.042	0.788	1.244	1.952	0.311	0.263	0.290	0.086
	out	*undet*	*undet*	*undet*	*OK*	*OK*	*undet*	*undet*	*OK*	*OK*	*undet*	*OK*	*out*	*undet*

Table 5.5-10. Conformance intervals and average values of the measurements performed by FVM (sintered parts). The conformance intervals are calculated considering the specification zones in **Table 5.4-1** and the expanded uncertainties in **Table 5.5-6** and **Table 5.5-8**.

	d_1 /mm	d_2 /mm	d_3 /mm	d_4 /mm	d_5 /mm	ϕ /mm	r_1 /mm	r_2 /mm	r_3 /mm	r_4 /mm	r_5 /mm	r_6 /mm	r_7 /mm	r_8 /mm
$d_{x,L}$	7.991	7.589	0.628	0.981	1.311	0.479	0.082	0.692	0.945	1.518	0.176	0.171	0.276	0.101
$\bar{d}_{x,s}$	7.948	7.461	0.634	0.945	1.413	0.478	0.097	0.758	1.063	1.788	0.301	0.229	0.483	0.123
$d_{x,U}$	7.925	7.445	0.570	0.945	1.427	0.484	0.065	0.839	1.300	2.080	0.368	0.260	0.518	0.095
	undet	out	out	undet	OK	undet	out	OK	OK	OK	OK	OK	OK	out

Table 5.5-11. Conformance intervals and average values of the measurements performed by OCMM (sintered parts). The conformance intervals are calculated considering the specification zones in **Table 5.4-1** extended by the safety factors h_S reported in the table and the expanded uncertainties in **Table 5.5-5** and **Table 5.5-7**. The corresponding tolerances are also reported.

	d_1 /mm	d_2 /mm	d_3 /mm	d_4 /mm	d_5 /mm	ϕ /mm	r_1 /mm	r_2 /mm	r_3 /mm	r_4 /mm	r_5 /mm	r_6 /mm	r_7 /mm	r_8 /mm
h_S	2.40	4.60	2.70	1.70	1.00	1.10	2.00	1.20	1.00	1.00	1.10	1.00	3.00	2.60
$d_{x,L}$	7.884	7.410	0.549	0.958	1.343	0.468	0.070	0.710	1.000	1.646	0.217	0.168	0.160	0.079
$\bar{d}_{x,s}$	7.894	7.516	0.599	0.965	1.367	0.479	0.074	0.808	1.094	1.824	0.324	0.216	0.629	0.101
$d_{x,U}$	8.033	7.624	0.648	0.968	1.394	0.495	0.076	0.821	1.244	1.952	0.328	0.263	0.634	0.117
$\pm tol$	0.165	0.145	0.090	0.065	0.085	0.020	0.050	0.125	0.190	0.315	0.140	0.060	0.500	0.045

Table 5.5-12. Conformance intervals and average values of the measurements performed by FVM (sintered parts). The conformance intervals are calculated considering the specification zones in **Table 5.4-1** extended by the safety factors h_S reported in the table and the expanded uncertainties in **Table 5.5-6** and **Table 5.5-8**. The corresponding tolerances are also reported.

	d_1 /mm	d_2 /mm	d_3 /mm	d_4 /mm	d_5 /mm	ϕ /mm	r_1 /mm	r_2 /mm	r_3 /mm	r_4 /mm	r_5 /mm	r_6 /mm	r_7 /mm	r_8 /mm
h_S	2.40	4.60	2.70	1.70	1.00	1.10	2.00	1.20	1.00	1.00	1.10	1.00	3.00	2.60
$d_{x,L}$	7.851	7.458	0.563	0.938	1.311	0.477	0.048	0.659	0.945	1.518	0.160	0.171	0.000	0.070
$\bar{d}_{x,s}$	7.948	7.461	0.634	0.945	1.413	0.478	0.097	0.758	1.063	1.788	0.301	0.229	0.483	0.123
$d_{x,U}$	8.066	7.576	0.635	0.987	1.427	0.486	0.099	0.872	1.300	2.080	0.385	0.260	0.862	0.126
$\pm tol$	0.165	0.145	0.090	0.065	0.085	0.020	0.050	0.125	0.190	0.315	0.140	0.060	0.500	0.045

5.6 Discussion

The conformity to the specifications in § 5.3 was almost verified mostly because the tolerance intervals were large and not adequate to the third and second decimal in the nominal values that was instead specified by the manufacturer.

The proposed method for the allocation of tolerances aimed to optimise the specifications considering the different impact of the shrinkage on the different features and, hence, accounting for them independently.

The shrinkage was, in fact, constant for the linear dimensions while pretty uneven for the curved features (**Figure 5.3-5** to **Figure 5.3-18** and **Figure 5.4-1**, **Figure 5.4-2**). In this last case, a dependence of the shrinkage on the dimensions was also noticed, perhaps because of an anisotropic curing of two-dimensional features (**Figure 5.4-2**).

The impact of the measurement process on the investigation could not be considered negligible. The ratio defined in Equation (5.3-2) was mostly worse for the linear dimensions (**Table 5.3-14** to **Table 5.3-17**). An explanation of this contradiction might be that linear dimensions were indirectly measured using the centres of the curvatures of curved features as inputs, propagating the measurement errors. Therefore, the linear features had tendency to constant shrinkage and, even though the evaluated expanded uncertainty was not excessive, the portion of variability due to the instrument, inside the uncertainty, was large.

Samples of green and sintered components should be representative of the production for a fruitful formulation of the specifications. This means that a large number of samples are to be considered and, also, in ideal circumstances, the green parts should be measured before sintering and the same parts re-measured after the sintering process. For a correct description of the shrinkage, in fact, the correlation among the parts should be exploited.

In addition, the influence of the instrument on the variability of the sintered parts (they are the reference in the propagation of the uncertainty) can affect the estimated variability of the green parts, leading to the formulation of wrong specifications.
The effect of the influence of the measurement process was investigated in § 5.5. Three measurement sessions by two different operators gave different results. Looking carefully into the **Table 5.3-4**, **Table 5.3-5**, **Table 5.3-9**, **Table 5.3-10** and **Table 5.5-1** to **Table 5.5-8**, the problem could be related not much to the specifications or the evaluated expanded uncertainties but rather to the different averages resulting from the three different sessions. It means that, in some cases, the intervals were centred on distant reference values.
This was a complex behaviour, dependent on different causes, which resulted in inaccuracy of the measured values:

- Some features were small and measured by the OCMM at the lower limit of the measurement range of the instrument (lack of accuracy).
- Defects (burrs and splinters) on the edges of the parts affected the "light to dark" transition algorithm in OCMM measurements. The unrecognised edge led to poor repeatability/reproducibility of the measurements.
- Defects on the edges of the parts influenced the contour fitting of the post processing software in FVM measurements.
- The operator of the second evaluation decided to acquire only two repeated measurements for each part by FVM, while performing seven repeated measurements per part by OCMM.

5.7 Conclusion

The evaluation of quality assurance in a micro powder injection moulding production highlighted a constant shrinkage of the lengths and a non-uniform one of the radii that suggested a possible optimisation of the specifications. A method for the synthesis of tolerance intervals, based on the evaluation of the shrinkage, was developed on purpose.
The shrinkage calibration procedure that the author developed was applied and validated in the case of micro powder injection moulding. However, it is of general validity for ANY moulding process, i.e., any process in which the material undergoes a change in dimensions from the mould cavity, due to a phase transformation.
It was not possible to reduce the impact of the measurement process that influenced the entire investigation. The measurements by an optical coordinate measuring machine (OCMM) were particular critical due to the presence of defects on the edges.
To put in evidence the importance of the choice of the instrument in relation to the specimens under evaluation and to the range of the dimensions to be inspected, the same components were re-measured by a focus-variation microscope (FVM). The extraction of the results obtained from FVM was less critical because performed with a dedicated post-processing software which allowed to better define the contour to be measured, but equally affected by inaccuracy: Differences among the average values of three different measurement sessions were evident. The reduction of the dimensions after the curing process resulted in increased relative deviations between the measurements from the two different instruments.
The chance to measure other geometrical features, such as surface texture and flatness, may depict FVM measurements as more attractive. Nevertheless, measurements should be optimised for *in-line* quality control, in a production environment, where a fast inspection time is required and measuring times are more compatible to those of the OCMM.
In conclusion, both instruments, with two different working principles, were affected by inaccuracy. Defects on the measured components made not possible to define the dimensions with the desired degree of accuracy. In this specific case, the quality of the measurement process could be improved improving the quality of the parts. A cleaning treatment, like a mild ultrasonic vibration machining, would eliminate burrs and splinters and allow to better define the

dimensions. In other words, a mutual dependence of the quality of the measurement process on the quality of the production was a strong outcome of the investigation: the measurement process influenced the quality assurance, but the lack of quality of the parts influenced the measurement process.

5.8 Outlook

The proposed investigation has the ambition to be independent from specific process conditions, whenever a shrinkage can be specified, because based on a statistical approach.
Furthermore, it is deemed independent on the used uncertainty model. Other approaches for uncertainty evaluation can be used, e.g., the well-known PUMA method or the frequentist approach.
The method will be proved in a more conventional micro injection moulding production where the shrinkage can be defined on the injected polymer parts with respect to the dimensions of the tool insert. In addition, the method defined in Chapter 4 will be used for the evaluation of the uncertainty and compensating the influence of the measurement process by correcting the systematic behaviour.

References

[1] Knapp W 2001 Tolerance and uncertainty *Laser Metrology & Machine Performance V* (G. N. Peggs, National Physical Laboratory, United Kingdom) **34** 357–66
[2] Kunzmann H, Pfeifer T, Schmitt R, Schwenke H and Weckenmann A 2005 Productive Metrology – Adding Value to Manufacture *CIRP Ann. – Manuf. Technol.* **54** 155-68
[3] Weckenmann A and Rinnagl M 2000 Acceptance of processes: do we need decision rules? *Precis. Eng.* **24** 264-9
[4] JCGM 106: 2012 Evaluation of measurement data—The role of measurement uncertainty in conformity assessment, Joint Committee for Guides in Metrology (Sèvres: Bureau International des Poids et Mesures, BIPM)
[5] ISO 14253-1: 2013 Geometrical product specification (GPS)—Inspection by measurement of workpieces and measuring equipment – Part 1: Decision rules for proving conformity or nonconformity with specifications. ISO 14253 part 1 (Geneva: International Organization for Standardization)
[6] Chase K W, Greenwood W H, Loosli B G and Hauglund L F 1990 Least cost tolerance allocation for mechanical assemblies with automated process selection *Manuf. Rev.* **3** 49–59
[7] Weiss P 1993 *A Discussion of Scientific Methods for Setting Manufacturing Tolerances* Uniersity of Wiscounsin Report 98
[8] Chase K W 1999 *Minimum-Cost Tolerance Allocation* Brigham Young University Report 99-5
[9] Chase K W 1999 *Tolerance Allocation Methods for Designers* Brigham Young University Report 99-6
[10] Ji S, Li X, Ma Y and Cai H 2000 Optimal Tolerance Allocation Based on Fuzzy Comprehensive Evaluation and Genetic Algorithm *Int. J. Adv. Manuf. Technol.* **16** 461–8
[11] Kumar A, Choi S-K and Goksel L 2011 Tolerance allocation of assemblies using fuzzy comprehensive evaluation and decision support process *Int. J. Adv. Manuf. Technol.* **55** 379–91
[12] Mirdamadi S, Etienne A, Hassan A, Dantan J Y and Siadat A 2013 Cost Estimation Method for Variation Management *Procedia CIRP* **10** 44–53
[13] Hernández C and Tutsch R 2013 Statistical Dynamic Specifications Method for Allocating Tolerances *Procedia CIRP* **10** 17–22

[14] Rota A, Imgrund P and Petzoldt F 2004 Fine powders give micro producers the cutting edge *Met. Powder Rep.* **59** 14–7
[15] Li S G, Fu G, Reading I, Tor S B, Loh N H, Chaturvedi P, Yoon S F and Youcef-Toumi K 2007 Dimensional variation in production of high-aspect-ratio micro-pillars array by micro powder injection molding *Appl. Phys. A* **89** 721–8
[16] Attia U M and Alcock J R 2011 A review of micro-powder injection moulding as a microfabrication technique *J. Micromechanics Microengineering* **21** 43001
[17] Okubo K, Tanaka S, Hamada H and Ito H 2009 Compression process effects on filling density and replication properties of micro-surfaces during metal injection molding *Asia-Pacific J. Chem. Eng.* **4** 133–9
[18] Islam A, Giannekas N, Marhöfer D M, Tosello G and Hansen H N 2014 Experimental investigation on shrinkage and surface replication of injection moulded ceramic parts *Proc. 4th Int. Conf. Nanomanufacturing (nanoMan 2014)* 8–10
[19] Tay B Y, Liu L, Loh N H, Tor S B, Murakoshi Y and Maeda R 2005 Surface roughness of microstructured component fabricated by μMIM *Mater. Sci. Eng. A* **396** 311–9
[20] Islam A, Giannekas N, Marhöfer D M, Tosello G and Hansen H N 2015 The shrinkage behavior and surface topographical investigation for micro metal injection molding *AIP Conf. Proc.* **1664** 110007
[21] Islam A I, Giannekas N, Marhöfer D M, Tosello G and Hansen H N 2015 A Comparative Study of Metal and Ceramic Injection Moulding for Precision Applications *Proceedings of the 4M/ICOMM2015 Conference* (Singapore: Research Publishing Services) 538–41
[22] Mueller T, Plewa K and Piotter V 2013 Investigation of Dimensional Accuracy in Powder Injection Molding *Proceedings of the 10th International Conference on Multi-Material Micro Manufacture* (Singapore: Research Publishing Services) 243–6
[23] Tosello G, Hansen H N and Gasparin S 2009 Applications of dimensional micro metrology to the product and process quality control in manufacturing of precision polymer micro components *CIRP Ann. - Manuf. Technol.* **58** 467–72
[24] ISO 15530-3: 2011 Geometrical product specifications (GPS)—Coordinate measuring machines (CMM): Technique for determining the uncertainty of measurement – Part 3: Use of calibrated workpieces or measurement standards ISO 15530 part 3 (Geneva: International Organization for Standardization)
[25] Internet site: www.hi-micro.eu
[26] Quagliotti D, Tosello G, Agour M, Flosky C, Meier A, Riemer O and Dormann B 2015 Calibration and Metrology for Micro/Nano Dimensional Quality Control Project HiMicro: High Precision Micro Production Technologies, FP7-2012-NMP-ICT-FoF
[27] BASF SE, Catamold®, www.catamold.de
[28] ISO 2768-1: 1989 General tolerances – Part 1: Tolerances for linear and angular dimensions without individual tolerance indications ISO 2768 part 1 (Geneva: International Organization for Standardization)
[29] JCGM 100: 2008 Evaluation of measurement data—Guide to the expression of uncertainty in measurement, Joint Committee for Guides in Metrology (Sèvres: Bureau International des Poids et Mesures, BIPM)
[30] Quagliotti D, Tosello G, Salaga J and Hansen H N 2016 Shrinkage calibration method for μPIM manufactured parts *Proc. of 11th International Conference on Micro Manufacturing* Irvine, Orange County, California, USA, 29-31 March, WeCT1.4
[31] Quagliotti D, Salaga J, Tosello G and Hansen H N 2016 Comparison of measurements from optical CMM and focus-variation microscope of a μPIM mechanical part *Proc. of the 16th international conference of the european society for precision engineering and nanotechnology (euspen)* (Nottimgham: P. Bointon, R. Leach, N. Southon) 167-168 Nottingham, UK, 30 May – 3 June (ISBN 14: 978-0-9566790-8-6)
[32] Approve for DeMeet—Manual v. 1.3.3, Schut Geometrical Metrology, www.schut.com
[33] MountainsMap® Premium, www.digitalsurf.com

Chapter 6

Replication assessment of polymer surfaces at sub-micrometre scale

6.1 Introduction

In the last two decades, the manufacturing industry has been the scene of a technological revolution. The opportunity to reduce the dimensions of the products rapidly allowed for the realisation of new advanced micro and nano systems that were unthinkable just few years earlier. Precision moulding and micro injection moulding (μIM) were the main actors of this change in the production of polymer micro-parts and parts with micro and nano surfaces manufacture, where the miniaturisation of moulded parts and features required new specially developed solutions in all the steps of injection moulding processes [1].

The achievement of a full surface replication of the tool insert component when moulding the polymer melt is essential in advanced μIM technology. The notion of replication has thoroughly been dealt with [2]. A replication process requires to reproduce a master geometry by conveying it to a substrate material. It is typically induced by means of different energy sources (usually heat and force) and a direct physical contact between the master and the substrate. Furthermore, concepts of advanced products are founded on combined processes and process chains, including large variety of materials (mainly polymers, glass or metals) and different dimensional scales. Hence, it is particularly critical when dealing with increasingly small dimensions in micro and nanostructured surfaces. In addition, because of the replication nature of moulding processes, the required accuracy for the manufacture of micro moulded components must be ensured by means of a metrological approach to surface replication and dimensional control of both master geometry and replicated substrate ([3]-[4]). As a consequence, a detailed knowledge is necessary not only of the absolute dimensions and geometrical quantities, but also about the uncertainty of measurement, which is a decisive parameter to deal with the quality assurance of micro and nano manufactured components [5].

In this context, the role of metrology is presented by two study cases in which the quality of the achieved replication was assessed by the replication fidelity [2]. Specifically, the surface texture replication was investigated about the amplitude (*Sa*, *Sq*—see § 2.5 and [6]) and the slope (*Sdq*—see § 2.5 and [6]), comparing the produced parts with the tool used to replicate the geometry and evaluating the measurement uncertainty.

The specimens investigated were made of thermoplastic polymers. Nonetheless, the techniques employed are general and can be used to describe any kind of material of the replicated substrate. In the first study case, three different conditions were analysed about surface topographies in the 100 nm amplitude range: specimens with random and periodic surface examined in the same production batch and specimens with periodic surface produced in two different batches. In the second study case, the amplitude and slope replications were quantified regarding the texture of four specimens with different surface finish.

6.2 Amplitude replication of nanostructured polymer surfaces

Polymer replicated artefacts can be produced easily, at low cost and employed for precision moulding verification of medical, optical or electro-mechanical applications. This first study [7] deals with the amplitude replication assessment of some of the artefacts that were used as *transfer standards* in a recent international comparison of optical instrument for areal topography measurements (see Chapter 7 and [8]).

6.2.1 Manufacture of the sub-micro structured polymer surfaces

The investigated polymer surfaces were replicated by injection moulding using a commercially available acrylonitrile butadiene styrene (ABS) Cycolac KJY 039075 produced by Borg Warner with a grey colour. ABS is a common thermoplastic amorphous polymer with glass transition temperature of approximately 105 °C.

Nickel roughness standards, manufactured by Rubert & Co Ltd., UK, have been used as tool inserts in the mould, mounted on a conventional injection moulding machine (see **Figure 6.2-1**) (Ferromatik Milacron K60) with a reciprocating screw of 35 mm in diameter and a clamping force of 60 kN (see process parameters in **Table 6.2-1**). Two of them were used for this study, namely 503 and 529. Both have nominal *Ra* roughness of 100 nm, though 529 has sinusoidal texture and 503 has a random one. They are shown in **Figure 6.2-2**, while their type and characteristics, specified according to [9][7], are listed in **Table 6.2-2**. Replicating this standards two series of polymer specimens have been obtained. Two examples are in **Figure 6.2-3**, one for each series.

Table 6.2-1. Injection moulding process parameters used for the production of the polymer parts.

	529	**503**
Dosage	270 mm	265 mm
Injection Speed	50 mm/s	50 mm/s
Max injection pressure	41 bar	41 bar
Packing pressure (Hydraulic)	32 bar	35 bar
Packing pressure (Estimated to the nozzle)	350 bar	400 bar
Packing time	5 s	3 s
Cooling time	30 s	30 s
Total cycle time (including packing, cooling and demoulding)	≈ 60 s	≈ 60 s
Mould temperature	50 °C	50 °C
Melt temperature	230 °C	230 °C

Table 6.2-2. Nominal characteristics of the nickel standards used as masters for the production of the injection moulded parts [9].

Master number	ISO type	Nominal roughness parameter values	Shape
503	D	Ra = 0.1 µm	4 × 1.25 mm random
529	C	Ra = 0.1 µm RSm = 10 µm Pt = 0.3 µm	Sine wave

[7] This ISO standard describes types of material measures with the profile method. An ISO standard describing material measure types for areal method is [10]. However, no specific characteristics are given in [10] that specifies the features on the surface with the areal method. Hence, the specimens are defined according to profile parameters even though they are used for areal evaluations. This is not misleading here because the specimens are uniform along the lateral direction (parallel to the dominant texture).

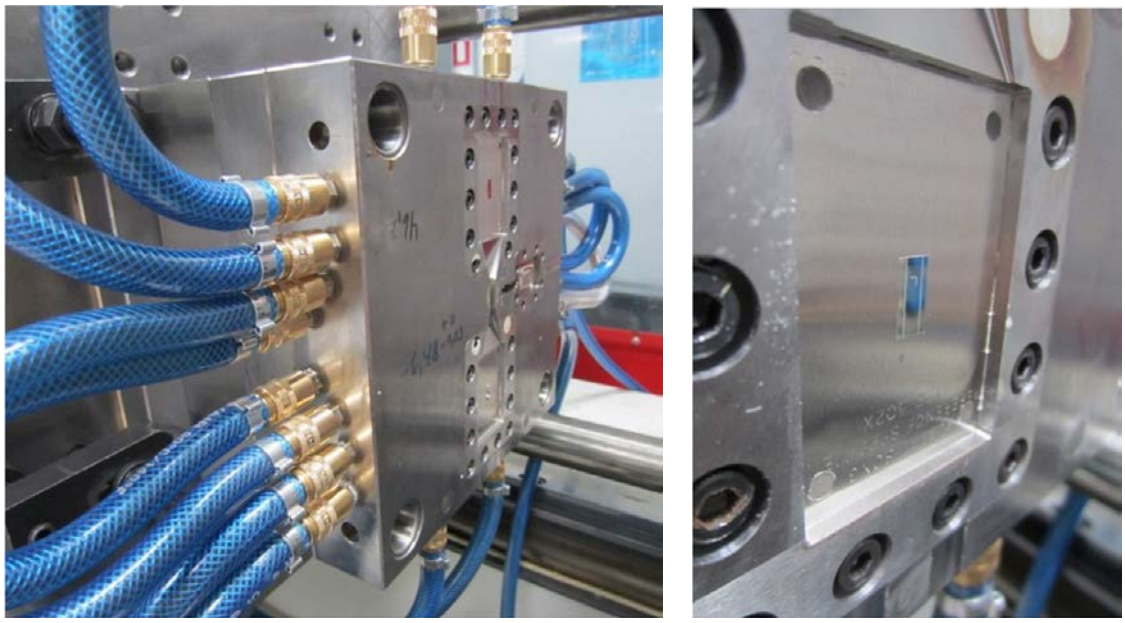

(a) (b)

Figure 6.2-1. (a): Two nickel roughness standards used together as tool inserts in a mould. (b): Detail of a tool insert.

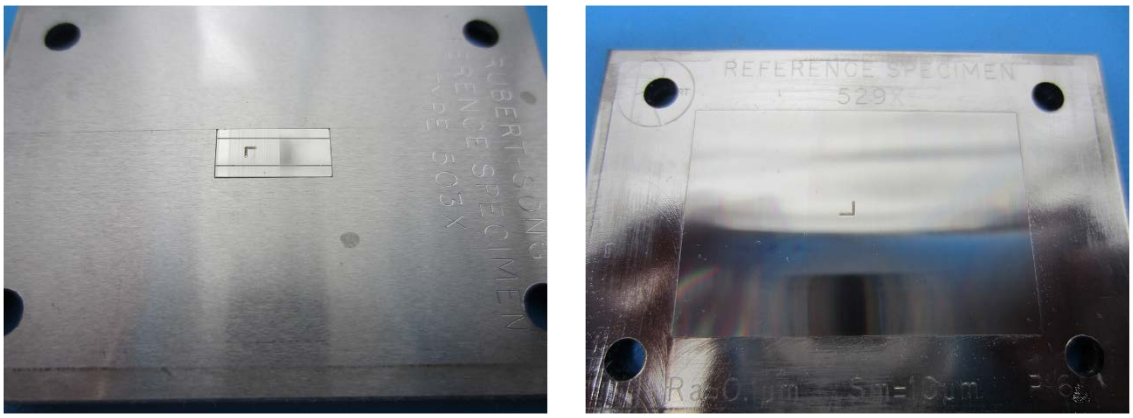

(a) (b)

Figure 6.2-2. Nickel roughness standards 503 (a) and 529 (b).

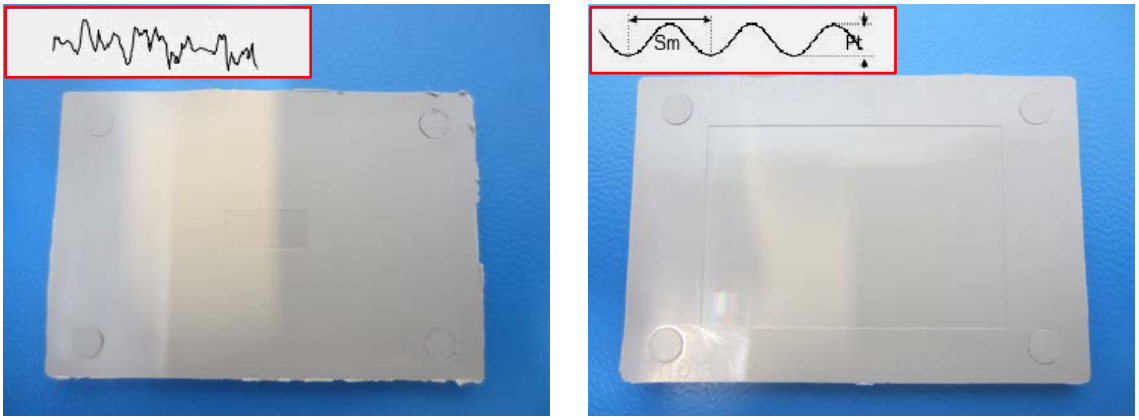

(a) (b)

Figure 6.2-3. Examples of replicated polymer specimens by roughness standards 503 (a) and 529 (b). For both specimens, a general profile is given to indicate the type of surface topography.

6.2.2 Repeatability of the replication process

The repeatability characterisation of the replication process was performed by areal surface acquisitions within the same production batch, i.e., all the inspected surfaces were generated the same day, in a short period of time.

A selection of eighteen replicated polymer specimens for each injected series (503 and 529) was measured using an atomic force microscope (AFM) [11]. Measurements of the reference standards (tool inserts) were also obtained by the same AFM. Examples of areal acquisition of the roughness standards and corresponding replicated surface are in **Figure 6.2-4** and **Figure 6.2-5** for, respectively, 503 and 529 polymer series.

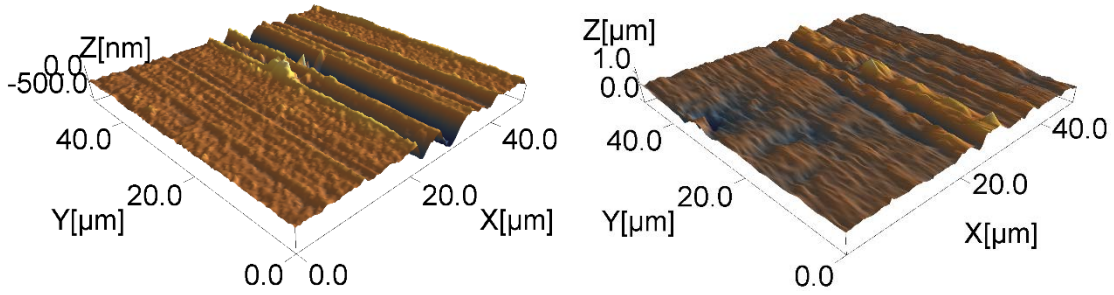

Figure 6.2-4. Examples of acquired surfaces: 503 nickel reference (left) and corresponding polymer replicated (right) surfaces.

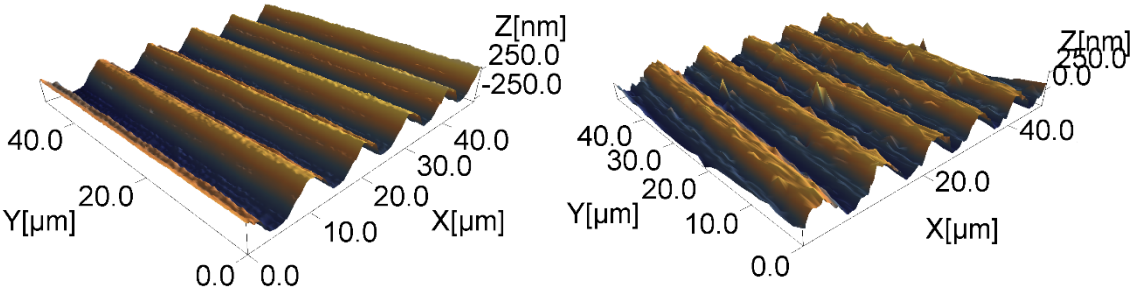

Figure 6.2-5. Examples of acquired surfaces: 529 nickel reference (left) and corresponding polymer replicated (right) surfaces.

Roughness standards have a mark on the surface that defines a univocal reference system, which was consequently transferred on the surface of the replicated specimens. Taking advantage of the mark, the measurements were acquired in the same spot of each specimen and in the same size of 250 µm × 250 µm. To evaluate the replication, in fact, it was important that the same portions of the surfaces were matched in the comparison between the master geometry and the replicated one. Furthermore, as it was clearly shown in the Chapter 4, the same discretisation level was required for comparing heterogeneous measurements: in this case, the same area in the nickel tool replicated in different components, i.e., the moulded parts. This was ensured by measuring the same area with the same amount of points [12]. Finally, a 2-D Gaussian filter according to [13] was applied (S-filter, nesting index 2.5 µm).

Regarding the replication repeatability, it must be noticed that, when a manufacturing process (an experiment in general) is replicated, information about the production of the process is obtained by the results of one or more sessions of measurements. Hence, repeatability (or reproducibility) conditions can analogously be extended to the process, too. Nevertheless, when doing so, it is important to clearly distinguish between

- the variability due to the manufacturing process (investigated by measuring different manufacturing parts)
- the variability due to the measurement process (inspected by considering several repeated measurements per each part)

These two aspects were deeply discussed in Chapter 5, even though from a different perspective. Moreover, repeatability and reproducibility both specify agreement (or disagreement) of the measurement results, generically indicated as precision of a measurement system, or of a measurement session, and expressed as uncertainty contributors. Nonetheless, they are two different uncertainty contributors because they are evaluated in different conditions. In particular, repeatability refers to the variability of the results when the measurements are performed in unchanged measurement conditions. As a consequence, repeatability can be considered a lower limit with respect to the reproducibility (best way undertaken measurements). Correspondingly, the reproducibility normally takes into account the repeatability, too.
In this study five repeated measurements in repeatability conditions were performed for each nickel standard. Conversely, one measurement for each of the replicated polymer parts were performed. In addition, considering that AFM acquisitions are time consuming, the measurements of the polymer parts were performed in several days. Hence, the measurements are to be considered acquired in reproducibility conditions. This is not in contrast with the repeatability investigation of the replication process (provided that the uncertainty contribution of the measurement process is kept below reasonable limits). Extending the idea, in fact, the process repeatability refers to unchanged process conditions. Here, the process repeatability conditions are well defined by the production of the considered parts, which were injected in one day and in unchanged process conditions.

6.2.3 Reproducibility of the replication process

The reproducibility characterisation of the replication process was performed on the polymer replicas of 529 nickel standard within two different batches. They were produced in the same day, the first one in the morning and the second one in the afternoon, meaning that the process was restarted after the production of the first batch (reproducibility conditions).
AFM measurements were performed on six samples for each batch, i.e., twelve replicated specimens of the 529 nickel standard. Three repeated measurements were acquired for each specimen and, all in all, thirty-six acquisitions. The procedure was the same explained in § 6.2.2.

6.2.4 Uncertainty model

The *Sa* roughness parameter was extracted from the acquired surfaces. The uncertainty was evaluated according to the model in **Figure 6.2-6** and inspired to [14]. The following was considered:

- u_c: uncertainty stated in the calibration certificate of the reference [15].
- u_p: instrument repeatability (three repeated measurements per reference). Because of the reduced number of repeated measurements, the standard deviation of the mean was extended from a normal distribution to a *t* distribution comparing both distributions at the same confidence interval of 95 %. This was achieved multiplying by a factor *h*.
- u_w: two contributions. Effect of temperature on specimens and variability due to manufacturing process (five repeated measurements for the nickel standards, one measurement for each of eighteen specimens for the polymer production).
- u_b: effect of temperature on references.
- Moreover, a contribution related to the environmental noise u_n (not considered in [14]) was estimated from measurements of an optical flat and considering the amplitude variations uniformly distributed.
- Coverage factor $k = 2$, i.e., an approximated expanded interval of 95 %.
- Measurement result *Sa* and its expanded uncertainty *U* were expressed as $Sa \pm U$.

Results are summarised in **Table 6.2-3** where averages, expanded uncertainties and contributors of the uncertainty budget are shown. The results are given for the filtered *Sa* values (S-filter, nesting index 2.5 µm), which are used hereinafter referred to the investigation. Nonetheless, an uncertainty budget for unfiltered values is given in **Table 6.2-4** for consideration.

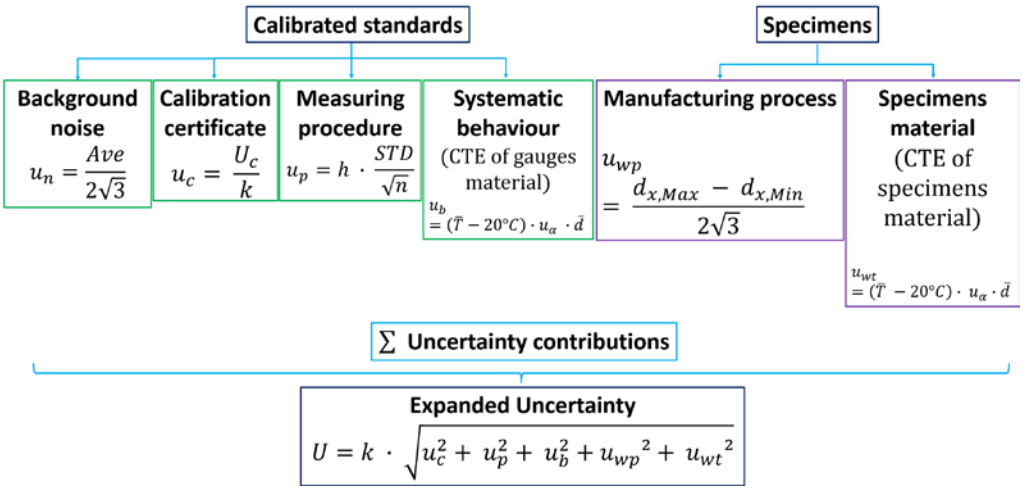

Figure 6.2-6. Uncertainty model adopted in the investigation.

Table 6.2-3. Averages, expanded uncertainties and uncertainty contributors of the S-filtered AFM measurements.

S-filter nesting index 2.5 µm		Nickel		Polymer 1 batch		Polymer 2 batches
		503 /nm	529 /nm	503 /nm	529 /nm	529 /nm
Average	*Sa*	73	112	56	103	97
Background noise	u_n	0.1	0.1	0.1	0.1	0.1
Calibration certificate	u_c	0.7	0.7	0.7	0.7	0.7
Procedure (h = 2.3)	u_p	0.3	0.3	0.3	0.3	0.3
Uncertainty due to systematics	u_b	0.0	0.0	0.0	0.0	0.0
Workpiece – manufacturing	u_{wp}	0.5	0.1	1.8	1.3	6.3
Workpiece – material	u_{wt}	0.0	0.0	0.0	0.0	0.0
Expanded uncertainty	U	2	2	4	3	13

Table 6.2-4. Averages, expanded uncertainties and uncertainty contributors of the unfiltered AFM measurements.

No filter		Nickel		Polymer 1 batch		Polymer 2 batches
		503 /nm	529 /nm	503 /nm	529 /nm	529 /nm
Average	*Sa*	83	117	64	108	103
Background noise	u_n	0.3	0.3	0.3	0.3	0.3
Calibration certificate	u_c	0.7	0.7	0.7	0.7	0.7
Procedure (h = 2.3)	u_p	1.0	1.0	1.0	1.0	1.0
Uncertainty due to systematics	u_b	0.0	0.0	0.0	0.0	0.0
Workpiece – manufacturing	u_{wp}	0.7	0.2	1.4	1.4	6.5
Workpiece – material	u_{wt}	0.0	0.0	0.0	0.0	0.0
Expanded uncertainty	U	3	3	4	4	13

6.2.5 Replication fidelity

The replication fidelity was considered the complement to 100 % of the relative deviation replicas-references and evaluated according to the following formula

$$f_R = \frac{Sa_{poly}}{Sa_{ref}} \times 100 \tag{6.2-1}$$

where Sa_{poly} is *Sa* calculated on the replicated specimens (polymer specimens) and Sa_{ref} the one calculated on the nickel standards (references). Furthermore, a replication uncertainty u_{fR} was estimated as the discrepancy between the average values of Sa_{poly} and Sa_{ref} (respectively $Sa_{ave,poly}$ and $Sa_{ave,ref}$) considering it uniformly distributed

$$u_{f_R} \cong \frac{|Sa_{ave,poly} - Sa_{ave,ref}|}{2\sqrt{3}} \tag{6.2-2}$$

The replication repeatability (or equivalently reproducibility, according to the states of the process considered for the evaluation) was assessed as the maximum deviation among the measured *Sa* values of the replicated specimens and also deemed to be uniformly distributed

$$u_r = \frac{|Sa_{max,poly} - Sa_{min,poly}|}{2\sqrt{3}} \tag{6.2-3}$$

Table 6.2-5. Average replication fidelity, process repeatability (reproducibility for the case with two batches) and estimated replication fidelity uncertainty.

		Polymer 1 batch		Polymer 2 batches
		503	529	529
Average replication fidelity	$f_R(Sa)$ /%	78	92	86[(a)]
Process repeatability/reproducibility	u_r /nm	2	1	5
Estimated replication fidelity uncertainty	u_{fR} /nm	5	3	4

[(a)] Respectively 83 % and 90 % for the first and the second batch

Average values of the replication for the three conditions investigated, process repeatability/reproducibility and estimated replication uncertainties are in **Table 6.2-5**. These results, together with the values related to each polymer specimen and to the reference, are summarised in the **Figure 6.2-7** to **Figure 6.2-12**.

By the analysis of the figures, a good replication fidelity can be assumed for the periodic polymer surfaces (529), produced in the same batch, with 92 % of replication achieved. They have congruent uncertainty intervals and the estimated uncertainty of the replication fidelity is very close to the expanded uncertainty evaluated for the polymer replicas (see **Figure 6.2-7** and **Figure 6.2-8**).

Considering the random polymer surfaces (503), the measured values are still in congruent uncertainty intervals and have close values of expanded uncertainty and replication fidelity uncertainty. However, the replication was not completely realised. In particular, 78 % of it was achieved (see **Figure 6.2-9** and **Figure 6.2-10**).

A good repeatability was observed for both 529 and 503 one single batch case.

When two different batches are considered, an overall replication fidelity of 86 % was achieved with congruent uncertainty intervals. Nevertheless, there was larger reproducibility and no agreement between the replication fidelity uncertainty and the expanded uncertainty evaluated for the polymer replicas. The latter, in fact, had an uncertainty contributor u_{wp} which revealed a larger variability of the manufacturing process. Considering the partial average values per each batch of production, the replication fidelity was 83 % and 90 %, respectively, for the first batch injected and for the second one. The variation corresponds to a different replication of about 7 % (about 10 nm). This means that, even though the same parameters for injection moulding were

considered, re-starting the process yielded a different replication. Such difference can normally be considered small in a mass production but it becomes relevant when reference artefacts are to be produced (see **Figure 6.2-11** and **Figure 6.2-12**).

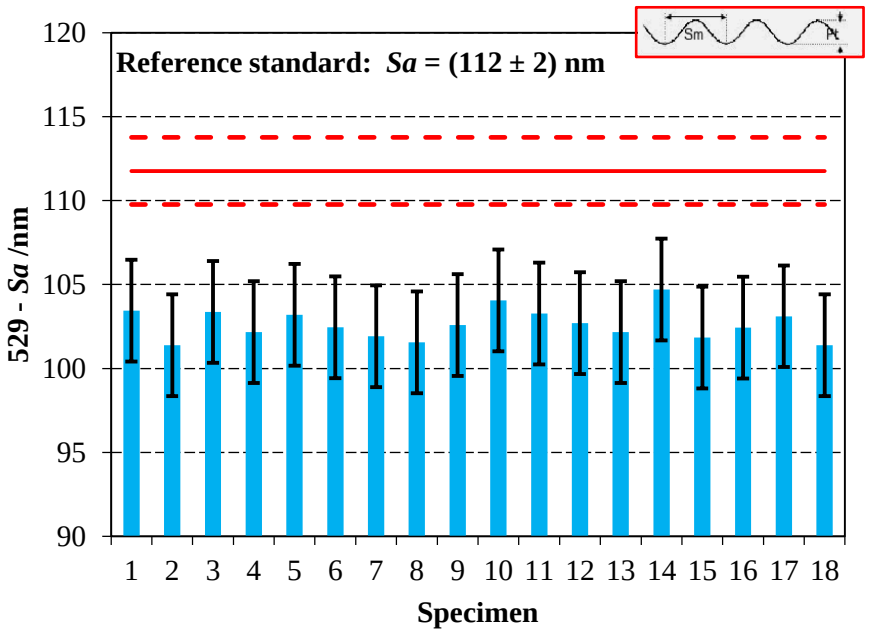

Figure 6.2-7. AFM measurements results of 529 series of replicated samples (single batch production). Results are given for *Sa* parameter (columns). The bars represent the expanded uncertainty evaluated for Sa_{poly}. AFM results (solid red line) of reference roughness standards are also in the graphs together with the expanded uncertainty intervals (dashed red lines).

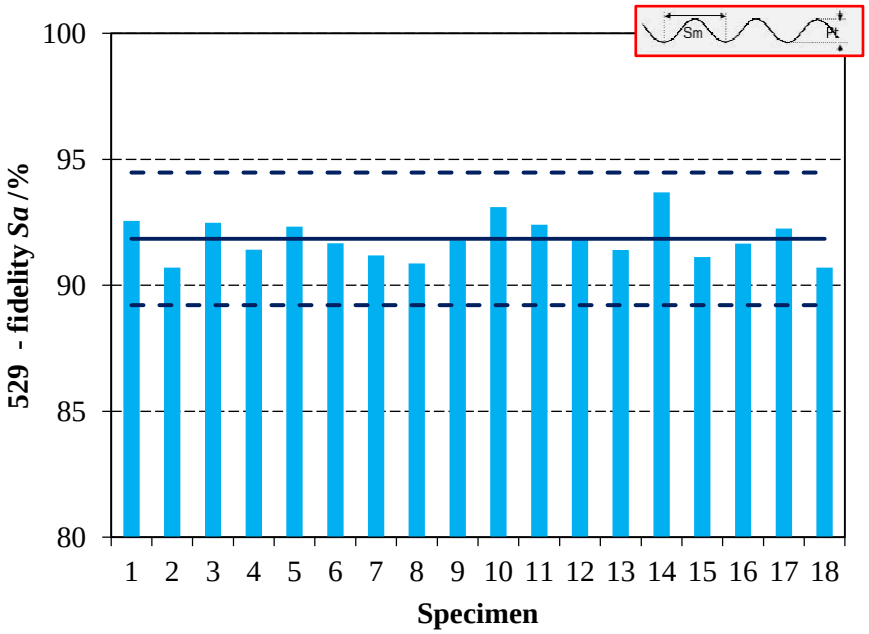

Figure 6.2-8. Replication fidelity of 529 series of replicated samples (single batch production). Results are given for *Sa* parameter (columns). The solid blue line is the average replication fidelity while the dashed blue lines represent the replication fidelity uncertainty.

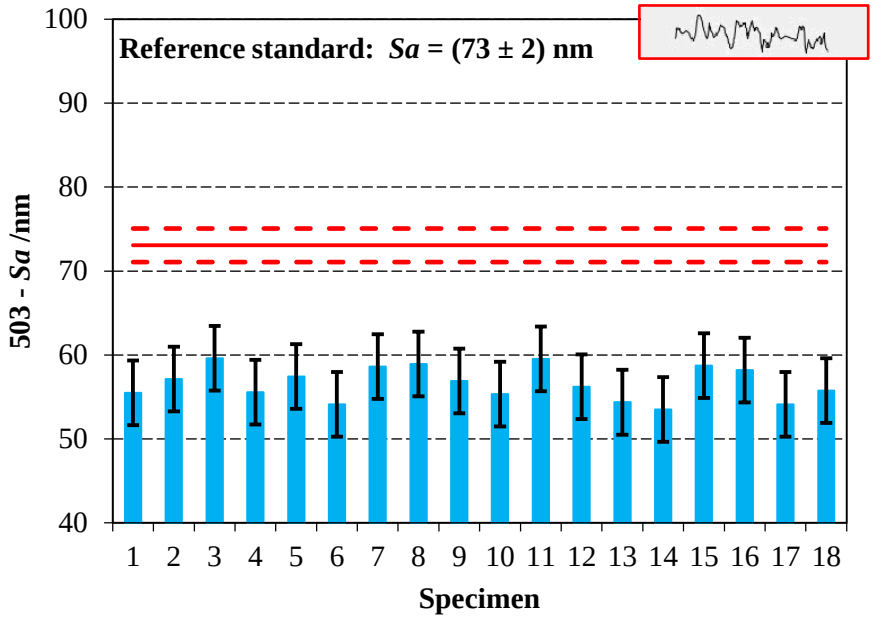

Figure 6.2-9. AFM measurements results of 503 series of replicated samples (single batch production). Results are given for *Sa* parameter (columns). The bars represent the expanded uncertainty evaluated for Sa_{poly}. AFM results (solid red line) of reference roughness standards are also in the graphs together with the expanded uncertainty intervals (dashed red lines).

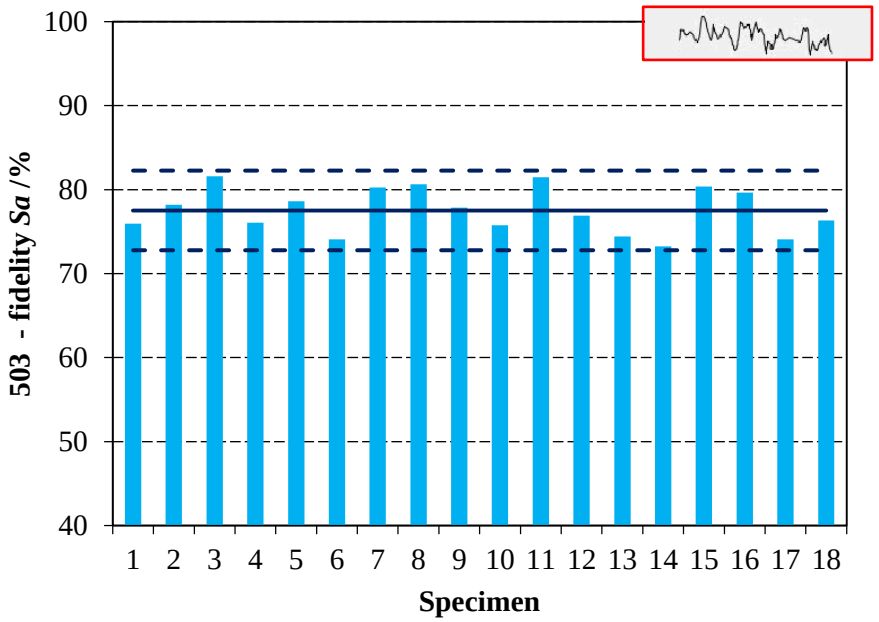

Figure 6.2-10. Replication fidelity of 503 series of replicated samples (single batch production). Results are given for *Sa* parameter (columns). The solid blue line is the average replication fidelity while the dashed blue lines represent the replication fidelity uncertainty.

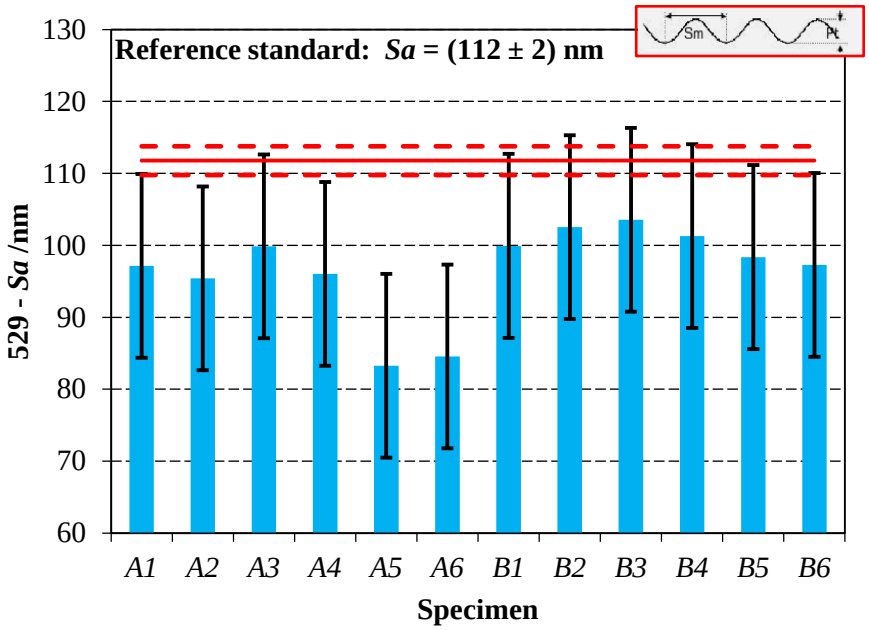

Figure 6.2-11. AFM measurements results of 529 series of replicated samples (two batches production: *A1-A6* and *B1-B6*). Results are given for *Sa* parameter (columns). The bars represent the expanded uncertainty evaluated for Sa_{poly}. AFM results (solid red line) of reference roughness standards are also in the graphs together with the expanded uncertainty intervals (dashed red lines).

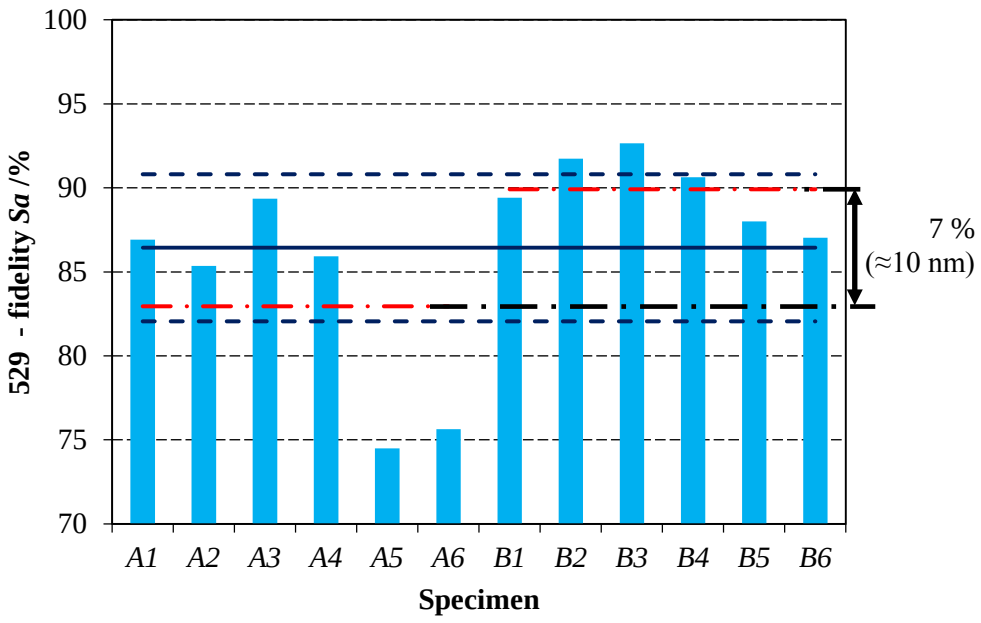

Figure 6.2-12. Replication fidelity of 529 series of replicated samples (two batches production: *A1-A6* and *B1-B6*). Results are given for *Sa* parameter (columns). The solid blue line is the average replication fidelity while the dashed blue lines represent the replication fidelity uncertainty. The dot-dashed red lines are the averages of each single batch.

6.3 Amplitude and slope replication of sub-micro polished polymer surfaces

The amplitude replication fidelity assessment, discussed in § 6.2, was extended to amplitude and slope replication in this second study case [16]. Furthermore, the uncertainty evaluation of the replication fidelity was achieved by propagating the uncertainties, instead of using the approximated expression in Equation (6.2-2).

A different group of specimens was used to carry out the study. The masters were in the set of steel specimens for mould finish comparison already investigated in § 4.4, **Table 4.4-2**. They have different polished flat surfaces (diamond buff polishing, grit paper polishing, stone polishing, dry blast polishing), in the sub-micrometre range, and nominal characteristics, provided by the manufacturer [17], reported in **Table 6.3-1**. The *Sa* measured values are reported for comparison in the same table. Regarding the specimens in **Table 4.4-2**, *T1* and *T3* are the same as *R1* and *R3* in **Table 6.3-1**, while the specimens named *R2* and *R4* are of a different range with respect to *T2* and *T4*.

The replicated surfaces were in same set of comparison artefacts and are supposed to have the same nominal characteristics in **Table 6.3-1**. No information about the replication process and the material used were provided [17].

Examples of master and replicated substrate are in **Figure 6.3-1**.

Table 6.3-1. Specifications of the specimens under investigation and nominal *Ra* roughness intervals, provided by the manufacturer of the specimens [17]. The measured *Sa* values of the masters are also in the table.

Specimen	*Surface finish*	*Nominal interval, Ra* /nm	*Measured values, Sa* /nm
R1	Diamond buff (grade 15)	51–76	35±4
R2	320 Grit paper	102–127	75±3
R3	400 Stone	635–711	291±19
R4	400 Dry blast (glass bead 11)	660–813	879±18

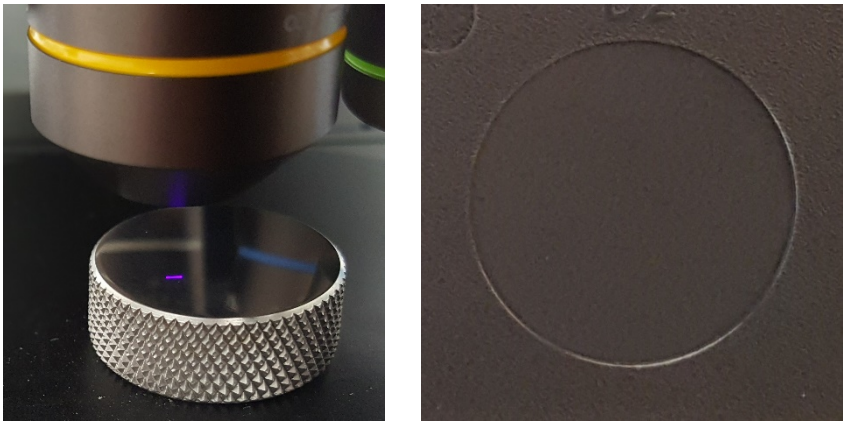

(a) (b)

Figure 6.3-1. Examples of master surface (a) and replicated substrate (b).

6.3.1 Metrology task and uncertainty evaluation

Both masters and replicated surfaces were measured in the centre, using a laser scanning confocal microscope by both 50× and 100× (CM – **Figure 4.4-3**). The acquisitions of 50× lens were cut at the same field of view of 100× lens and resampled to the same number of pixels. The amplitude[8] and the slope replications were considered calculating, respectively, *Sq* and *Sdq* areal surface

[8] It has already been pointed out in § 4.4.1 that *Sa* and *Sq* are both amplitude parameters and strongly correlated (they measure the same quantity in different ways). Their ratio is ideally constant for a certain surface and, if no noise influences the acquisitions, the replication fidelity assessed by *Sa* or *Sq* expresses the same result.

texture parameters (see § 2.5 and [6]). Examples of acquisitions of the master surface and replicated one are in **Figure 6.3-2** to **Figure 6.3-5**.

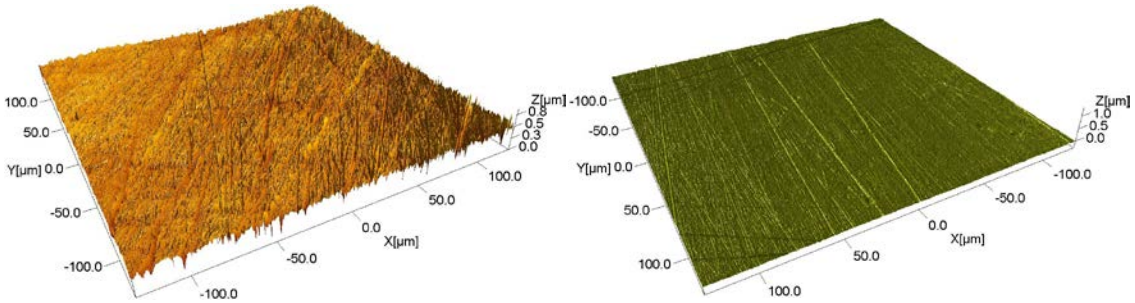

Figure 6.3-2. Diamond buff polishing. Example of acquired surfaces of the master (left) of the replicated surface (right).

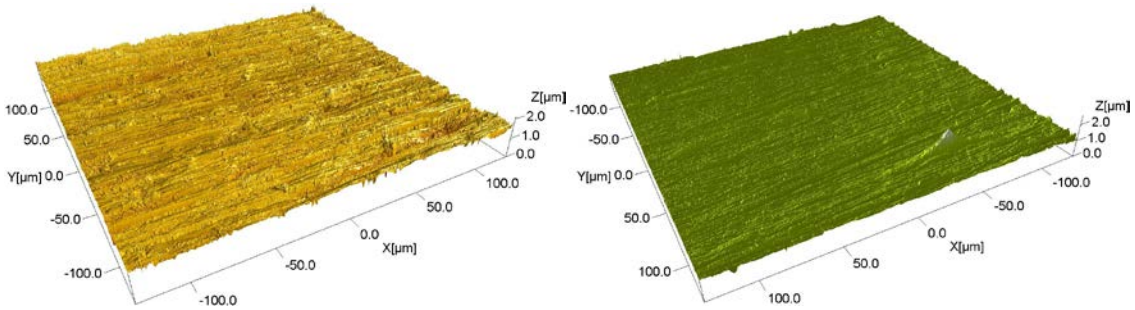

Figure 6.3-3. Grit paper polishing. Example of acquired surfaces of the master (left) of the replicated surface (right).

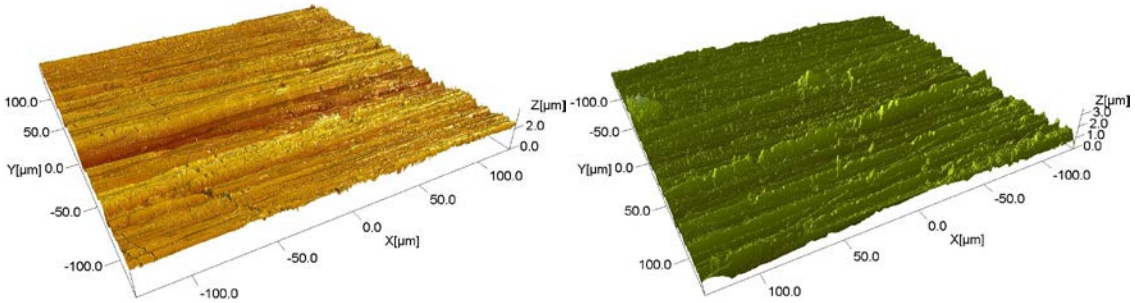

Figure 6.3-4. Stone polishing. Example of acquired surfaces of the master (left) of the replicated surface (right).

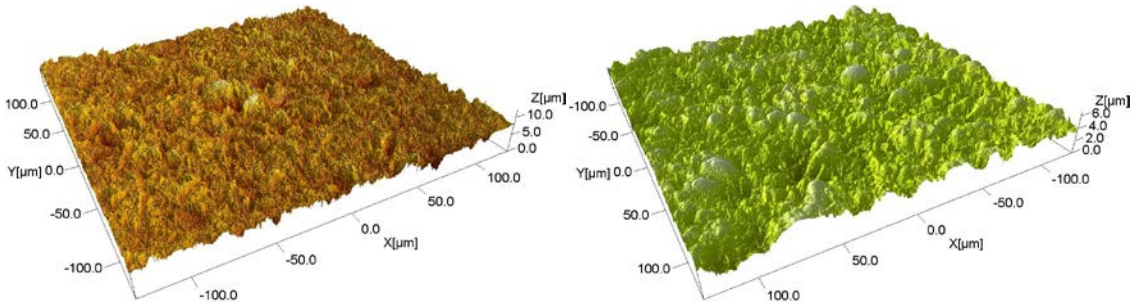

Figure 6.3-5. Dry blast polishing. Example of acquired surfaces of the master (left) of the replicated surface (right).

Table 6.3-2. Results and uncertainty budget related to the measurements of the masters.

Masters		Diamond buff		Grit paper		Stone		Dry blast	
		Sq /nm	*Sdq* /1	*Sq* /nm	*Sdq* /1	*Sq* /nm	*Sdq* /1	*Sq* /nm	*Sdq* /1
Average		48	0.16	108	0.21	379	0.46	1201	1.77
Background noise	u_n	1.1	0.005	1.1	0.005	1.1	0.005	1.1	0.005
Calibration certificate	u_c	0.7	0.001	0.7	0.001	4.7	0.002	4.7	0.002
Procedure (h = 1.0)	u_p	0.2	10^{-4}	0.2	10^{-4}	6.9	0.003	6.9	0.003
Uncertainty due to systematics	u_b	2×10^{-6}	9×10^{-10}	2×10^{-6}	9×10^{-10}	10^{-5}	9×10^{-9}	10^{-5}	9×10^{-9}
Reproducibility on workpiece	u_{wp}	2.8	0.021	1.6	0.024	9.5	0.053	5.4	0.015
Workpiece – material	u_{wt}	6×10^{-5}	2×10^{-7}	6×10^{-5}	2×10^{-7}	10^{-3}	10^{-6}	10^{-3}	10^{-6}
Expanded uncertainty	U	6	0.04	4	0.05	25	0.11	20	0.03

Table 6.3-3. Results and uncertainty budget related to the measurements of the replicas.

Replicas		Diamond buff		Grit paper		Stone		Dry blast	
		Sq /nm	*Sdq* /1	*Sq* /nm	*Sdq* /1	*Sq* /nm	*Sdq* /1	*Sq* /nm	*Sdq* /1
Average		23	0.05	60	0.11	360	0.31	843	0.89
Background noise	u_n	1.1	0.005	1.1	0.005	1.1	0.005	1.1	0.005
Calibration certificate	u_c	0.7	0.001	0.7	0.001	4.7	0.002	4.7	0.002
Procedure (h = 1.0)	u_p	0.2	10^{-4}	0.2	$0.\ 10^{-4}$	6.9	0.003	6.9	0.003
Uncertainty due to systematics	u_b	2×10^{-6}	9×10^{-10}	2×10^{-6}	9×10^{-10}	10^{-5}	9×10^{-9}	10^{-5}	9×10^{-9}
Reproducibility on workpiece	u_{wp}	2.4	0.010	3.4	0.014	15.3	0.034	13.3	0.060
Workpiece – material	u_{wt}	6×10^{-5}	2×10^{-7}	6×10^{-5}	2×10^{-7}	10^{-3}	10^{-6}	10^{-3}	10^{-6}
Expanded uncertainty	U	5	0.02	7	0.03	35	0.07	31	0.12

Once more, the uncertainty evaluation was inspired to [14], according to the model already introduced in § 6.2.4 and illustrated in **Figure 6.2-6**.
The uncertainty contributors are explained again in the following, for this specific study.

- u_c: uncertainty stated in the calibration certificate of the references. A reference with nominal *Ra* = 27 nm was used for *R1* and *R2* [18] and a reference with nominal *Ra* = 209 nm was used for *R3* and *R4* [19]. Under the same assumption in § 4.4.1, the calibrated uncertainty related to *Ra* was considered adequate for *Sq* values, too. However, a value for *Sdq* was not available. Thus, it was estimated weighting the calibration expanded uncertainty stated for *Ra* by the relevant standard deviations in the measurement sessions (*Sa*, *Sq*, *Sdq*).
- u_p: instrument repeatability (ten repeated measurements per reference). In this case, the number of repeated measurements was deemed enough to set h = 1 (see § 6.2.4 and **Figure 6.2-6**).
- u_w: two contributions. Effect of temperature on specimens and variability due to manufacturing process (fifteen repeated measurements for both the masters and the replicas).
- u_b: effect of temperature on references.
- Moreover, a contribution related to the environmental noise u_n (not considered in [14]) was estimated from measurements of an optical flat and considering the amplitude variations uniformly distributed.
- Coverage factor k = 2, i.e., an approximated expanded interval of 95 %.

- Measurement result *Sq*, *Sdq* and their respective expanded uncertainties *U* were expressed as $Sq \pm U_{Sq}$ and $Sdq \pm U_{Sdq}$.

Results and uncertainty budget are in **Table 6.3-2** for the masters and in **Table 6.3-3** for the replicated surfaces.

6.3.2 Replication fidelity

The replication fidelity was calculated according to Equation (6.2-1). The standard uncertainty of the replication fidelity was evaluated propagating the expanded uncertainties of masters and replicas, considering uncorrelated quantities, i.e., according to [20],

$$u_{f_R} = \left(\sum_j \frac{\partial f_R}{\partial Sx_j}^2 u_{Sx_j}^2\right)^{\frac{1}{2}} \tag{6.3-1}$$

where f_R is given in Equation (6.2-1), *Sx* stands for *Sq* and *Sdq*, S_{xj} stands for $Sx_{replicas}$ and $Sx_{masters}$. The expanded uncertainty was eventually

$$U_{f_R} = 2 \times u_{f_R} \tag{6.3-2}$$

Average values of the replication for the four types of polished surfaces investigated and estimated replication uncertainties are in **Table 6.3-4**. These results are summarised in **Figure 6.3-6**, for *Sq* parameter, and in **Figure 6.3-7**, for *Sdq* parameter. Furthermore, a comparison between the replication fidelity uncertainties evaluated by the approximated Equation (6.2-2) and the Equation (6.3-1) is in **Table 6.3-5**.
Eventually, the angular spectra of the four masters and corresponding replicas are in **Figure 6.3-8** for consideration.

Table 6.3-4. Results of the replication fidelities, deviations of the replicas from the masters (complement to 100 % of the replication fidelity), sensitivity coefficients in Equation (6.3-1) and propagated uncertainties.

Replication		Diamond buff		Grit paper		Stone		Dry blast	
		Sq	*Sdq*	*Sq*	*Sdq*	*Sq*	*Sdq*	*Sq*	*Sdq*
Replication fidelity	f_R /%	47	33	56	51	95	67	70	50
Shortage	R_D /%	53	67	44	49	5	33	30	50
Sensitivity coeff. (master)	$\lvert c_{S,m}\rvert$ /1	-1.0	-182.2	-0.5	-227.1	-0.3	-136.9	-0.1	-28.2
Sensitivity coeff. (replica)	$\lvert c_{S,r}\rvert$ /1	2.1	610.7	0.9	481.6	0.3	215.7	0.1	56.6
Propagated uncertainty	U_{fR} /%	13	16	7	18	11	21	3	7

Table 6.3-5. Comparison between the replication fidelity uncertainties evaluated by the approximated Equation (6.2-2) and the Equation (6.3-1).

Uncertainty replication u_{fR}[(a)]	Diamond buff		Grit paper		Stone		Dry blast	
	$u_{fR,Sq}$ /nm	$u_{fR,Sdq}$ /1	$u_{fR,Sq}$ /nm	$u_{fR,Sdq}$ /1	$u_{fR,Sq}$ /nm	$u_{fR,Sdq}$ /1	$u_{fR,Sq}$ /nm	$u_{fR,Sdq}$ /1
Estimated (Equation (6.2-2))	7	0.03	14	0.03	6	0.04	103	0.25
Propagated (Equation (6.3-1))	3	0.013	4	0.02	21	0.05	17	0.06

[(a)] In opposition to the values in **Table 6.3-4** (expanded uncertainties), here they refer to the standard uncertainties

By the analysis of the tables and figures, a good amplitude replication was achieved for stone polished surfaces with a replication fidelity larger than 95 %. The dry blast ones were evaluated with an amplitude replication fidelity of about 70 %. The worst amplitude replication was achieved for both diamond buff and grit paper polished surfaces with a replication fidelity of, respectively, 47 % and 56 %.
The tendency is almost the same for slope replication but the replication fidelity values are lower: 67 % for stone polished surfaces. 50 % for dry blast and grit paper polished surfaces. 33 % for diamond buff polished surfaces.

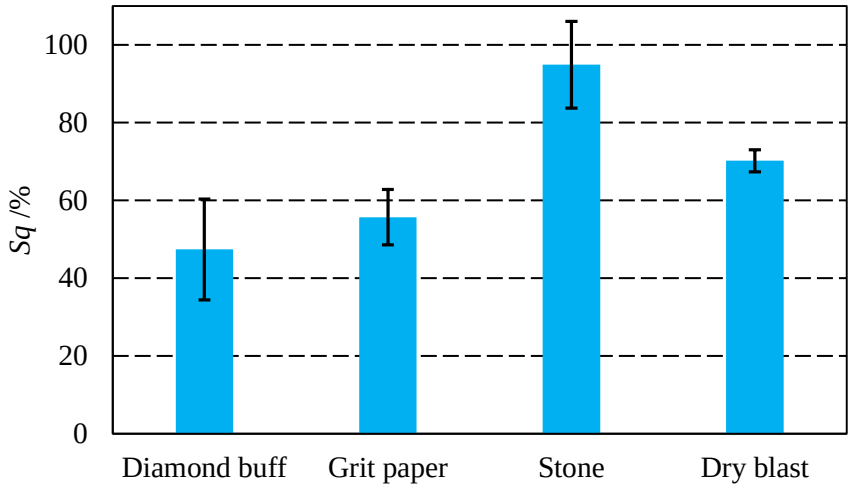

Figure 6.3-6. Replication fidelity of the amplitude of the different considered surfaces. The error bars are the propagated expanded uncertainties.

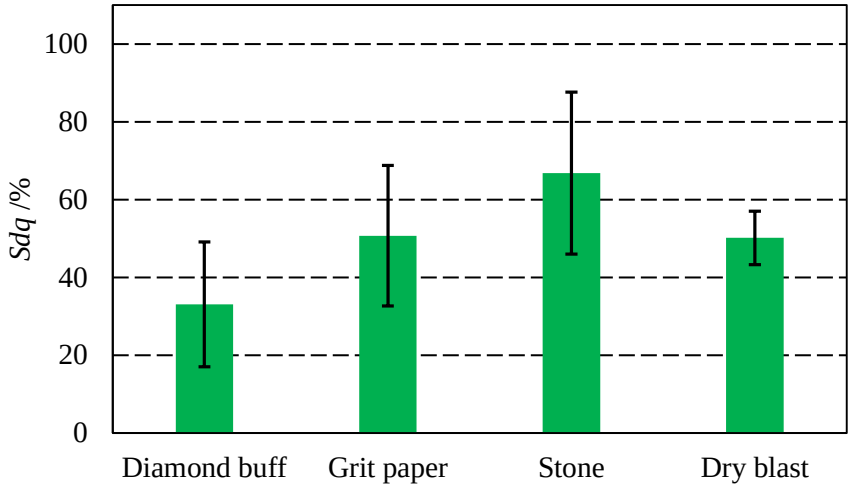

Figure 6.3-7. Replication fidelity of the slope of the different considered surfaces. The error bars are the propagated expanded uncertainties.

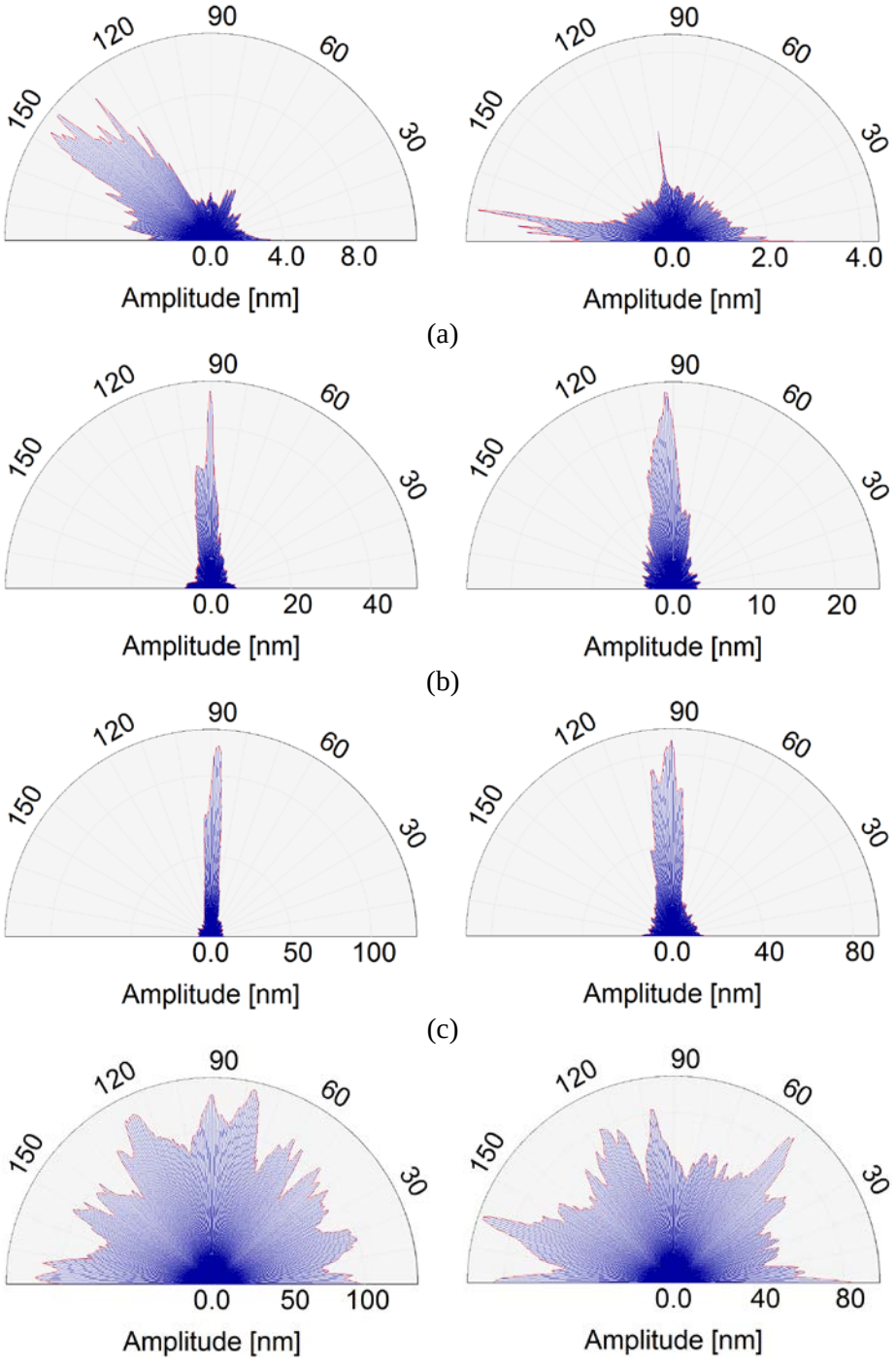

Figure 6.3-8. Angular spectrum of the masters (left side) of the replicated substrates (right side). (a): Diamond buff polishing. (b): Grit paper polishing. (c): Stone polishing. (d): Dry blast polishing.

6.4 Discussion

Master geometries and corresponding polymer replicas, replicated by two different processes, were measured by two different technologies in two different investigations. Nevertheless, a common outcome was that uneven topographies are worse replicated with respect to the regular ones. In the first study, 503 standard is not completely replicated. On the contrary, in 529 standard the uniform pattern of the periodic topography was dominant with respect to the local roughness, allowing a better performance of the replication process.

This outcome was confirmed in the second study. The inspected polished surfaces can be considered pseudo-random topographies where uniformity is introduced by the polishing itself. The replication fidelity increased when the polishing introduced uniformity in the masters in the form of a partial order of the texture direction. The behaviour has been evidenced by the angular spectra of **Figure 6.3-8**, applied to both masters and replicas. A more wide investigation would be required to extend this result to more general conclusions.

Both studies suggest metrological tools for the evaluation of a replication process. In particular, height and slope replications are obtained as average values considering, respectively, *Sa – Sq* and *Sdq* roughness parameters. Nonetheless, the assessment of the replication fidelity by means of roughness parameters is not univocally determined. For instance, the slope can locally vary considerably and a small deficit in the achieved replication can produce large differences in the local slopes (*Sdq* calculated values). Correspondingly, even though *Sa* and *Sq* are less sensitive to variations because the amplitude is unambiguously defined in the vertical direction, a similar trend can be experienced for the height assessment of irregular random substrates, where local changes among portions of the replicated uneven surface can produce large variations in the average values. In other words, if domains of somewhat uniform portions can be identified in an uneven surface, the replication assessment, by averaging many replicated specimens, would *flatten* the calculation to a certain value included in a larger variability interval.

In view of these remarks, the replication assessment of 503 polymer specimens, in the first study, might slightly be dependent on the *flattening* of the average within a larger evaluated uncertainty, with respect to 529 replication fidelity uncertainty. In the same way, the stone polishing replicas of the second study might contain such effect. In fact, the replication was pretty good but the uncertainty was also quite large.

It was not possible to estimate the *flattening effect* of the averaging parameters but it is believed to be small in the amplitude replication assessment, compared to the one related to the slope. In particular, in the second study, it may have been mixed with the poor performance of the optical instrument CM (see below).

Regarding *Sdq*, such effect can be noticed comparing the graphs in the **Figure 6.3-6** and **Figure 6.3-7**. The slope replication has a trend that follows the one of the amplitude but with smaller values of replication fidelity and larger uncertainty intervals. Hence, *Sdq* appears difficult to be managed for its tendency to large variability but also because no calibrated values are normally available in the calibration certificates.

More complete information can be provided by the angular spectrum, as already showed in **Figure 6.3-8**, because evaluated considering all the directions on a surface under investigation that can be compared between master and replica. Nonetheless, it is more complicated when quantitative information is to be extracted.

An influence on the replication assessment can also be exerted by the use of a filter. Comparing the values in **Table 6.2-3** and **Table 6.2-4**, it is possible to recognise a reducing effect on the amplitude replication of the first study. It affected above all the calculated averages but a mild influence can also be noticed on the uncertainty evaluated. Rigorously speaking, the mathematical function of a filter should be considered a model equation for the propagation of the uncertainty. This would raise difficulties in the practical implementation of the calculation. However, the worst results is on the measured values. Filtering changes the experimental distribution, adding a systematic behaviour. In the next Chapter 8, an example will clearly show the influence of the S-filter on the extracted *Sdq* parameter from an irregular surface.

Regarding the uncertainty, it should be noted that the uncertainty evaluated in the second study is quite different with respect to the one evaluated in § 4.4, although the specimens were of the same

type and two of them were exactly the same (diamond buff and stone polishing masters). The main reason is to be found in the instruments used: optical instrument CM in § 4.4 and AFM in the work exposed this chapter. Nonetheless, it was already stated in § 4.4 that it was overestimated there by the way of achieving the traceability (anyway provisional). In addition, an underestimation in the evaluation in this chapter is also likely, possibly due to the few repeated measurements available for the masters.
Comparing the replication fidelity uncertainty (**Table 6.3-5**) obtained by the usual formula for the propagation of the variances (Equation (6.3-1)) and the approximated formula (Equation (6.2-2)), there is a general agreement but also an overestimation when the approximated formula is used. Exception to this behaviour is the uncertainty of the replication of the stone polished master that is smaller with the approximated formula.
It is the same specimen whose measurements were not possible to be corrected for the systematic behaviour in § 4.4. A problem was successively found about the optical instrument CM used for measuring such specimens. The problem is described in the next Chapter 8 and it is deemed to be concurrent to the poor measurements of such specimens, enhanced by a possible interaction between the laser beam of the instrument and the black thermoplastic material the replicas are made of. The effect here was about different resulting average values related to the 50× and 100× objectives, even though cut and resampled in the same way: a small spread of the values but averages quite distant between them.

6.5 Conclusion

In this chapter an investigation of the replication fidelity of different moulded specimens allowed to introduce several metrological techniques for analysing the replication process:

- Repeatability and reproducibility to define the variability of the production, evaluated as uncertainty contributors.
- Evaluation of the amplitude and slope replication of the features on the surface described by roughness parameters.
- Approximated evaluation of the uncertainty of the replication fidelity.
- Evaluation of the uncertainty of the replication fidelity by the usual formula for the propagation of the variances, considering the expression of the replication fidelity as model equation.

Amplitude replication, calculated by *Sa* and *Sq*, was a reliable assessment of the replication. The slope replication was instead more dependent on the larger variability of *Sdq*.
The use of the uncertainty in the replication analysis was also shown. Indeed, the uncertainty has two main contributors: one is related to the variability of the replicated surface (considered by different specimens) and the other one is related to the measurement instrument (repeated measurements are needed to spot this variability). Hence, it is extremely important to properly evaluate the uncertainty so that it can be used to extract useful information from the process. If the uncertainty associated with the instrument becomes dominant, it would hide the sought variability of the manufacturing process and hence the replication would be altered by the poor measurement results. At this concern, the choice of the measurement instrument is also important. In the first study, AFM measurements were precise and accurate but also time consuming and, consequently, unsuitable for acquiring many repeated measurements. In the second study, CM had faster times of acquisition but a problem of the instrument influenced the measurement sessions. This also raises the need to have the instruments verified periodically, measuring in the range of interest and the materials of interest.

6.6 Outlook

The method described in Chapter 4 is also suitable to be used in conjunction with the replication assessment because of the possibility to reduce the influence of the measurement instrument with respect to the process variability. The method will be adopted for an optimised assessment of the replication fidelity.

Furthermore, as emerged from the discussion, new tools for the investigation of the replication may be explored. The angular spectrum and the frequency analysis, in general, can be examined. In particular, the wavelet transform would allow to relate local changes in uneven surfaces to the corresponding portion of a surface.

References

[1] Heckele M and Schomburg W K 2004 Review on micro molding of thermoplastic polymers *J. Micromechanics Microengineering* **14** R1–14

[2] Hansen H N, Hocken R J and Tosello G 2011 Replication of micro and nano surface geometries *CIRP Annals – Manuf. Technol.* **60** 695–714

[3] Tosello G, Hansen HN, Marinello F, Gasparin S 2010 Replication and dimensional quality control of industrial nanoscale surfaces using calibrated AFM measurements and SEM image processing *CIRP Annals – Manufacturing Technology* **59-1** 563-568

[4] Tosello G, Marinello F, Hansen H N 2012 Characterisation and analysis of microchannels and submicrometre surface roughness of injection moulded microfluidic systems using optical metrology *Plastics, Rubber and Composites: Macromolecular Engineering* **41-1** 29-39

[5] Hansen H N, Carneiro K, Haitjema H, De Chiffre L 2006 Dimensional Micro and Nano Metrology *CIRP Annals – Manufacturing Technology* **55-2** 721-743

[6] ISO 25178-2: 2012 Geometrical product specification (GPS)—Surface texture: Areal – Part 2: Terms, definitions and surface texture parameters. ISO 25178 part 2 (Geneva: International Organization for Standardization)

[7] Quagliotti D, Tosello G and Hansen H N 2015 *Replication assessment of nanostructured polymer surfaces using atomic force microscopy: Uncertainty evaluation in the surface replication fidelity assessment of moulded specimens at the 100 nm scale* VDI-Berichte – Messunsicherheit praxisgerecht bestimmen – Prüfprozesse in der industrielle Praxis **2269** 49-55 (ISSN: 0083-5560)

[8] Tosello G, Haitjema H, Leach R K, Quagliotti D, Gasparin S and Hansen H N 2016 An international comparison of surface texture parameters on polymer artefacts using optical instruments *CIRP Annals - Manuf. Technol.* **65** 529–32

[9] ISO 5436-1: 2000 Geometrical product specification (GPS)—Surface texture: Profile method; Measurement standards – Part 1: Material measures. ISO 5436 part 1 (Geneva: International Organization for Standardization)

[10] ISO 25178-70: 2014 Geometrical product specification (GPS)—Surface texture: Areal – Part 70: Material measures. ISO 25178 part 70 (Geneva: International Organization for Standardization)

[11] DME—Danish micro engineering, Atomic Force Microscope DS 95

[12] Leach R and Haitjema H 2010 Bandwidth characteristics and comparisons of surface texture measuring instruments *Meas. Sci. Technol.* **21** 1-9

[13] ISO 25178-3: 2012 Geometrical product specification (GPS)—Surface texture: Areal – Part 3: Specification operators. ISO 25178 part 3 (Geneva: International Organization for Standardization)

[14] ISO 15530-3: 2011 Geometrical product specification (GPS)—Coordinate measuring machines (CMM): Technique for determining the uncertainty of measurement – Part 3: Use

of calibrated workpieces or measurement standards. ISO 15530 part 3 (Geneva: International Organization for Standardization)
[15] PTB Physikalisch-Technische Bundesanstalt, Calibration certificate n. AC 10 07 31, Grating standard, TGZ2 (NT-MDT Co., Moscow)
[16] Quagliotti D, Tosello G, Salaga J, Baruffi F, Hansen H N and Gasparin S 2016 Metrology of sub-micron structured polymer surfaces *Proc. of The 3rd International Conference Polymer Replication on Nanoscale* Windisch, Switzerland, 19-20 May
[17] DME Mold Finish Comparison Kit – DME Company, www.dme.net
[18] PTB Physikalisch-Technische Bundesanstalt, Calibration certificate n. PTB-5.15-4059219, Roughness Standard ISO 5436 type D2, Serial number 6329 (manufacturer Hersteller) date of issue 26-07-2012
[19] CGM (Center for Geometrical Metrology), DANAK Calibration certificate n. Rou03032, Roughness Standard ISO 5436 type D, Serial number Mrk. 619 (manufacturer Halle) date of issue 17-12-2003
[20] JCGM 100: 2008 Evaluation of measurement data—Guide to the expression of uncertainty in measurement, Joint Committee for Guides in Metrology (Sèvres: Bureau International des Poids et Mesures, BIPM)

Chapter 7

International comparison on surface texture of polymer artefacts using optical instruments

7.1 Introduction

A comparison of surface texture measurements on the sub-micrometre scale by optical instruments was organised under the umbrella of the Scientific Technical Committee on 'Surfaces' (STC-S) of The International Academy for Production Engineering (CIRP) [1]-[2].
The comparison aimed to identify the current capability about the areal topography parameters, using optical surface measurement instruments, in laboratory conditions, by experienced operators.
Advanced precision manufacturing processes can produce structured surfaces with micro/nanoscale features and integrated functional properties [2]-[4]. Such surfaces require areal topographic measurements for their characterisation and optical instruments have a number of advantages compared to contact ones, e.g., they measure much faster without damaging the surface. The increasing use of optical instruments for areal characterization suggested the investigation of the state-of-the-art in the field, by an international comparison, to support the quality assurance of surface manufacturing [5].
Other metrological comparisons (see, e.g., [6]-[11]) have previously been carried out on surfaces in the micro- down to the nanoscale, measuring surface texture parameters with the profile method (see, e.g., [7]-[10]) and step heights (see, e.g., [6], [8] and [9]), using either contact instruments or scanning probe microscopes. Optical instruments were also used but the investigation was still limited to profile roughness parameters [10]-[11]. Conversely, the presented comparison focused for the first time on areal surface texture parameters acquired by optical instruments on polymer surfaces. It was carried out in the period from August 2012 to August 2015 and involved sixteen optical surface instruments (three focus variation microscopes (FVMs), four confocal microscopes (CMs) and nine coherence scanning interferometers (CSIs)) from thirteen research laboratories in ten countries worldwide.
A list of the laboratories involved in the comparison is in **Table 7.1-1**.
The project has been organised and coordinated by the Department of Mechanical Engineering at the Technical University of Denmark (DTU).
The coordinator was responsible for:

- Defining, receiving and measuring the surface texture standards.
- Designing and producing the mould.
- Fitting the surface texture standards into the mould.
- Choosing a polymer material stable and suitable for the process and the measurements.
- Running-in moulding process, including metrology for replication fidelity analysis.
- Producing polymer replicas of the surface texture standards.
- Measuring all polymer replicas (defining the exact measurement procedure).
- Handing over the standards to participants.
- Preparing the comparison analysis and the final report.

The participants were required to:

- Provide contact and address details to the coordinator.
- Follow the measuring procedure for each standard and specify any variation.
- Calculate the required parameters and their associated uncertainty.
- Supply to the coordinator with all results, the uncertainty evaluations and the raw data files of the measurements, mathematically unfiltered.

The entire data processing of the comparison analysis and final reporting was conducted in the context of this PhD. The key characteristics of the comparison, the results from the different instruments and an overview of the uncertainty assessment of the performed measurements is described in the following.

Table 7.1-1. Participants involved in the comparison.

Participant	Country
ETH, Swiss Federal Institute of Technology in Zurich	Switzerland
Hong Kong Polytechnic University	China
Mitutoyo Research Center Europe B.V.	Netherland
NTB, Interstaatliche Hochschule für Technik	Switzerland
Politecnico di Milano	Italy
Technical University of Denmark	Denmark
University of Bremen	Germany
University of Huddersfield	UK
University of North Carolina Charlotte	USA
University of Padova	Italy
University of Thessaloniki	Greece
University of Tianjin	China
Worcester Polytechnic Institute	USA

7.2 Transfer standards

A set of four nickel roughness standards, manufactured by Rubert & Co. Ltd., UK [12], were replicated by injection moulding. The process was already introduced in § 6.2.1 (see Figure 6.2-1 to Figure 6.2-3) for two of the roughness standards (503 and 529). The process parameters are re-copied in **Table 7.2-1** for convenience.

According to the classification of material measure types given in [13] (the comment in § 6.2.1, footnote 1 is still applicable), based on profile method, two nickel transfer standards, with serial numbers 528 and 529, were of ISO type C with nominal periodic profile of Ra = 500 nm (RSm = 50 µm) and Ra = 100 nm (RSm = 10 µm), respectively. Other two were of ISO type D, with serial numbers 502 and 503, with random texture of nominally Ra = 30 nm and Ra = 100 nm, respectively (see **Table 7.2-2**).

The polymer replicas were eighteen sets of transfer standards, produced in the same batch (repeatability process conditions). An example is in **Figure 7.2-1**. Each participant received a set of polymer replicas. Hence, the replication of the transfer standards by polymer moulding and in repeatability conditions allowed several laboratories to measure in parallel, in contrast to comparisons where a single set of specimens has to be transferred between laboratories.

Table 7.2-1. Injection moulding parameters used for the production of the polymer parts

	528, 529	**502, 503**
Dosage	270 mm	265 mm
Injection Speed	50 mm/s	50 mm/s
Max injection pressure	41 bar	41 bar
Packing pressure (Hydraulic)	32 bar	35 bar
Packing pressure (Estimated to the nozzle)	350 bar	400 bar
Packing time	5 s	3 s
Cooling time	30 s	30 s
Total cycle time (including packing, cooling and demoulding)	≈ 60 s	≈ 60 s
Mould temperature	50 °C	50 °C
Melt temperature	230 °C	230 °C

Table 7.2-2. Nominal sizes of the standards used as masters for the production of the injection moulded parts.

Master number	ISO type	Nominal roughness parameter values	Shape
502x	D	*Ra* = 0.03 µm	4 × 1.25 mm, random
503x	D	*Ra* = 0.1 µm	4 × 1.25 mm, random
528x	C	*RSm* = 50 µm, *Pt* = 1.5 µm, *Ra* = 0.5 µm	Sine wave
529x	C	*RSm* = 10 µm, *Pt* = 0.3 µm, *Ra* = 0.1 µm	Sine wave

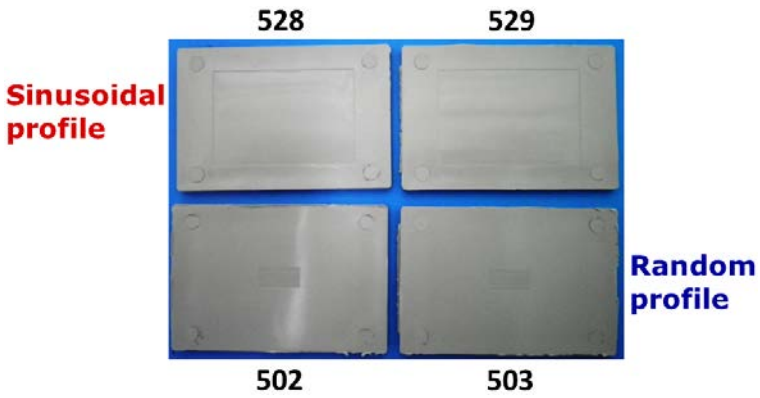

Figure 7.2-1. A set of four replicated specimens.

7.3 Measurement procedure

The measurements on the polymer transfer standards were acquired and successively analysed, according to the measurement specifications summarised in **Table 7.3-1**.

The evaluation area was 250 µm × 250 µm, from which a least-squares plane was removed before calculating and reporting the arithmetical mean height of the scale-limited surface (*Sa*), the root mean square height of the scale-limited surface (*Sq*) and the root mean square gradient of the scale-limited surface (*Sdq*) areal texture parameters (see § 2.5 and [14]). A Gaussian S-filter [15] was applied (with no L-filter).

When comparing measurements it is essential that the spatial bandwidths match. This was achieved by having all the measurements taken on the same areal width, with the same number of points and with the same filter settings [16]. Any variation from the recommended procedure was documented. The 2.5 µm nesting index S-filter was applied to reduce variation due to different numbers of points and/or the different lateral resolutions of the instruments.

Furthermore, it was also necessary that the same areas on the specimens were measured. At this purpose, a reference mark having an L shape was engraved in the centre of the measuring area in all four nickel standards (**Figure 7.3-1**). It was replicated in the polymer specimens and used as a local reference system to be aligned with the *x* and *y* axes of the instrument (**Figure 7.3-2**).
The acquisition area was identified with its left-bottom corner at a distance of 1 mm in both positive *x* and *y* directions from the origin (corner of the mark) of the local reference system (**Figure 7.3-3**).

Table 7.3-1. Measurement specifications.

	528-x	529-x	502-x	503-x
Plane correction	Least squares plane	Least squares plane	Least squares plane	Least squares plane
Measured area /(µm × µm)	250×250	250×250	250×250	250×250
S-filter /µm	2.5	2.5	2.5	2.5

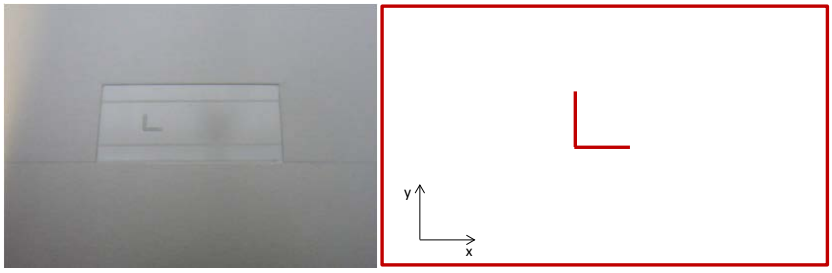

Figure 7.3-1. L-shaped mark showing the origin of the measurement area.

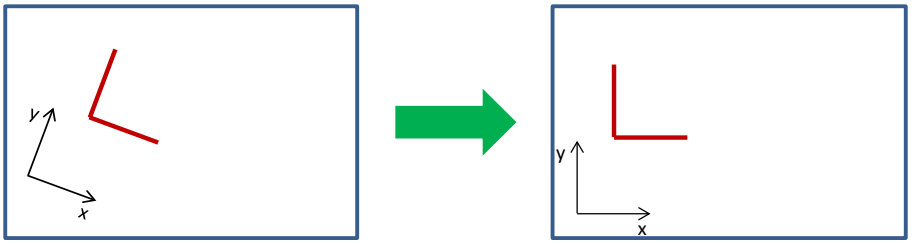

Figure 7.3-2. Alignment of measuring area in the polymer specimens.

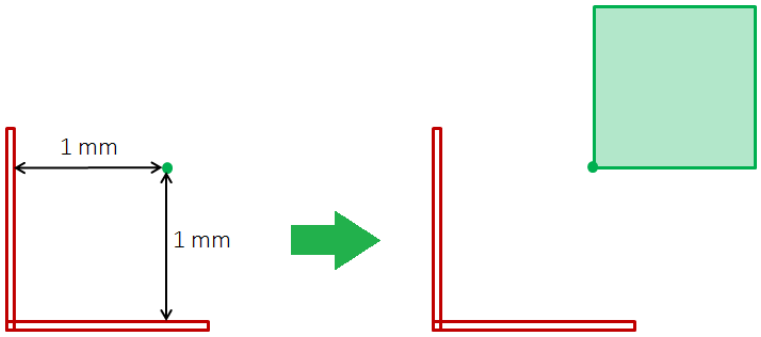

Figure 7.3-3. Positioning of the measuring 250 µm × 250 µm area with respect to the L-shaped mark.

7.4 Reference values

The replicated polymer specimens provided to the laboratories were measured before the start of the comparison using an atomic force microscope (AFM). These measurements were the reference values to which all the participants results were referred.

In **Table 7.4-1** the references are summarised according to the polymer specimen number.

The uncertainty was inspired by ISO 15530-3:2011 [17], focused on coordinate measuring machines uncertainty assessment. The evaluation procedure presented in the ISO standard was adapted to AFM measurements.

The contributors considered and computed in the uncertainty estimation were:

- Background noise of the AFM.
- Calibration uncertainty from the calibration artefact certificate.
- Measurement repeatability (including instrument, relocation, workpiece).
- Calibration uncertainty of the instrument.

Table 7.4-1. Calibrated values of the polymer specimens used by the participants. The expanded uncertainty *U*, evaluated considering the replicated polymer specimens variability, is also indicated.

No	502-x			503-x			528-x			529-x		
	Sa	*Sq*	*Sdq*	*Sa*	*Sq*	*Sdq*	*Sa*	*Sq*	*Sdq*	*Sa*	*Sq*	*Sdq*
1	38.8	48.8	0.043	55.5	73.0	0.073	229.0	258.0	0.052	103.5	114.5	0.077
2	38.9	49.1	0.044	57.1	74.9	0.072	222.4	249.7	0.048	101.4	112.2	0.076
3	38.9	48.0	0.043	59.6	78.4	0.075	213.7	240.6	0.050	103.4	114.6	0.078
4	41.3	51.6	0.042	55.6	74.3	0.074	210.8	239.1	0.048	102.2	113.1	0.077
5	38.7	47.6	0.042	57.4	74.1	0.075	224.1	251.4	0.053	103.2	114.3	0.077
6	38.7	47.6	0.042	57.4	74.1	0.075	224.1	251.4	0.053	103.2	114.3	0.077
7	35.7	44.7	0.047	55.3	72.6	0.073	211.3	239.9	0.054	100.2	110.9	0.075
8	35.7	44.7	0.047	55.3	72.6	0.073	211.3	239.9	0.054	100.2	110.9	0.075
9	35.7	44.7	0.047	55.3	72.6	0.073	211.3	239.9	0.054	100.2	110.9	0.075
10	35.7	44.7	0.047	55.3	72.6	0.073	211.3	239.9	0.054	100.2	110.9	0.075
11	37.9	47.5	0.042	59.5	78.1	0.074	208.0	234.0	0.050	103.3	115.0	0.078
12	40.3	50.0	0.046	56.2	74.7	0.072	218.7	245.6	0.050	102.7	114.5	0.079
13	39.8	50.3	0.043	54.4	71.8	0.072	211.1	239.2	0.051	102.2	114.3	0.079
14	37.7	47.6	0.043	53.5	71.7	0.075	224.2	251.9	0.054	104.7	117.7	0.081
15	39.0	48.5	0.045	58.7	78.3	0.074	221.1	248.5	0.047	101.8	112.7	0.077
16	37.5	46.6	0.042	58.2	76.1	0.075	221.1	251.0	0.051	102.4	113.6	0.077
17	40.9	50.5	0.045	54.1	71.9	0.076	229.2	256.9	0.050	103.1	114.8	0.078
18	40.2	50.5	0.048	55.8	74.3	0.076	217.3	244.6	0.055	101.4	113.1	0.077
U	3.5	4.3	0.004	3.9	4.3	0.008	13.3	15.0	0.011	3.0	4.2	0.009

7.5 Analysis of participants' data

The analysis of the participants' data was carried out considering the *Sa*, *Sq* and *Sdq* parameters, according to the procedure previously specified. All the measurements were related to the references calculating the relative deviations for all surface texture parameters. Furthermore, for all instruments and measurands, the uncertainties stated by the participants were compared to those evaluated for the references by the *En* value determination. Histograms of the deviations and participants' stated uncertainties (error bars—see next § 7.5.1) for all parameters are in **Figure 7.5-1** to **Figure 7.5-12**. In the figures, the intervals of the expanded uncertainties of the

AFM measurements are also given (red dashed lines). The corresponding values are in **Table 7.5-1**. In addition, technologies and characteristics of the instruments involved in the comparison are listed in **Table 7.5-2**.

Table 7.5-1. Average values, standard deviations between specimens and expanded uncertainties of reference AFM measurements calculated over the eighteen replicated polymer samples provided to the laboratories.

	502			503			528			529		
	Sa /nm	*Sq* /nm	*Sdq*	*Sa* /nm	*Sq* /nm	*Sdq*	*Sa* /nm	*Sq* /nm	*Sdq*	*Sa* /nm	*Sq* /nm	*Sdq*
Average	39.0	48.8	0.044	56.3	74.3	0.073	218.8	246.3	0.051	102.6	114.1	0.078
Std. dev. between specimens	1.8	2.2	0.002	1.8	2.2	0.001	6.8	6.9	0.002	1.4	1.8	0.002
Exp. meas. uncertainty (k=2)	3.5	4.3	0.004	3.9	4.3	0.008	13.3	15.0	0.011	3.0	4.2	0.009

Table 7.5-2. Instruments in the comparison and principal measurement characteristics (FVM = focus variation microscope; CSI = coherent scanning interferometer; CM = confocal microscope).

	Technology	A_N	Lens Mag.	Scanning area /µm	Number of pixels	Resolution[a]		
						X /nm	Y /nm	Z /nm
A	FVM	0.55	50×	287 × 218	1624 × 1232	176.7	176.9	20
B	FVM	0.55	50×	288 × 219	1231 × 1622	177.5	177.9	13.2
C	FVM	0.55	50×	287 × 398	816 × 1133	351.7	351.3	20
D	CSI	0.55	50×	96 × 72	1280 × 960	75.0	75.0	0.1
E	CSI	0.50	25×	250 × 250	1272 × 1272	196.5	196.5	0.1
F	CM	0.95	50×	258 × 258	4096 × 4096	62.9	62.9	10
G	CM	0.95	50×	258 × 258	4096 × 4096	62.9	62.9	10
H	CM	0.95	50×	258 × 258	1024 × 1024	251.9	251.9	10
I	CM	0.95	100×	250 × 250	1508 × 1508	165.8	165.8	2
L	CSI	0.55	50×	255 × 191	768 × 576	332.0	331.6	0.1
M	CSI	0.55	50×	250 × 250	755 × 755	331.1	331.1	1
N	CSI	0.55	50×	368 × 368	1028 × 1028	356.0	356.0	0.01
O	CSI	0.55	50×	335 × 335	1024 × 1024	327.1	327.1	0.01
P	CSI	0.40	20×	309 × 231	640 × 480	482.8	481.3	<1[b]
Q	CSI	0.40	20×	320 × 240	640 × 480	500.0	500.0	0.1
R	CSI	0.40	20×	250 × 250	614 × 614	402.2	407.2	≤3.5[c]

[a] The resolution in x and y, given in the table, is defined as actual pixel width. It is not the lateral resolution specified for the instruments.

[b] A sub-nanometric vertical resolution is declared by the manufacturer. Actual value not disclosed.

[c] Vertical resolution as declared by the manufacturer.

502 series

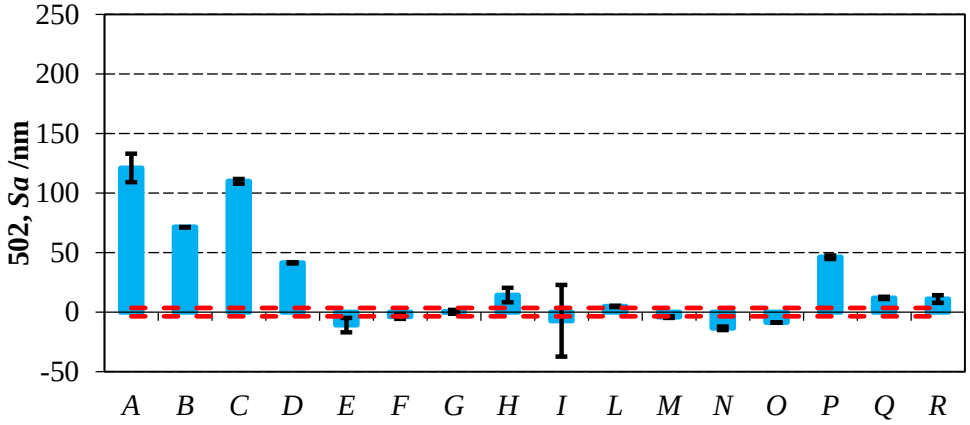

Figure 7.5-1. *Sa* deviations for 502 type specimens (random texture). Red dashed lines (– – –) indicate the expanded uncertainty of AFM reference measurements. Bars on histograms indicate the expanded uncertainty of the measurements stated by the participants.

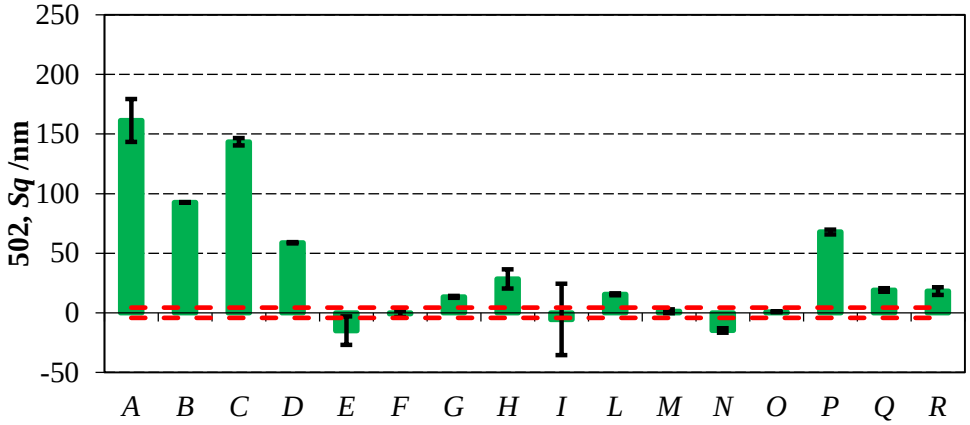

Figure 7.5-2. *Sq* deviations for 502 type specimens (random texture). Red dashed lines (– – –) indicate the expanded uncertainty of AFM reference measurements. Bars on histograms indicate the expanded uncertainty of the measurements stated by the participants.

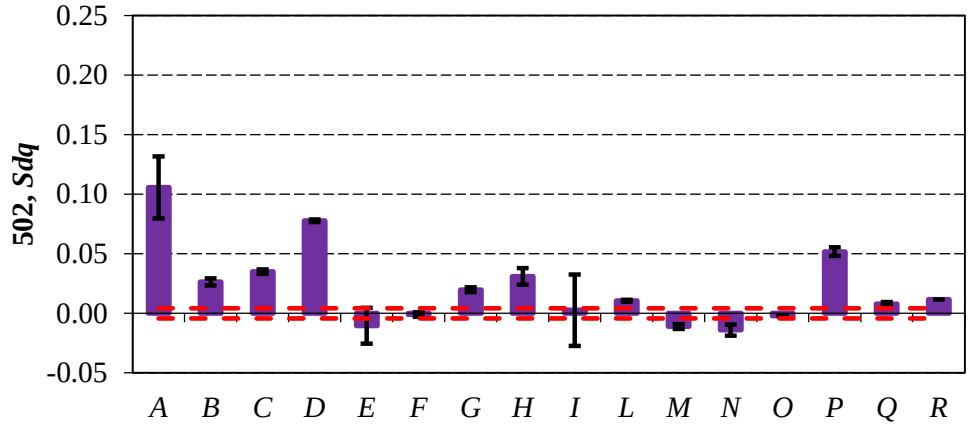

Figure 7.5-3. *Sdq* deviations for 502 type specimens (random texture). Red dashed lines (– – –) indicate the expanded uncertainty of AFM reference measurements. Bars on histograms indicate the expanded uncertainty of the measurements stated by the participants.

503 series

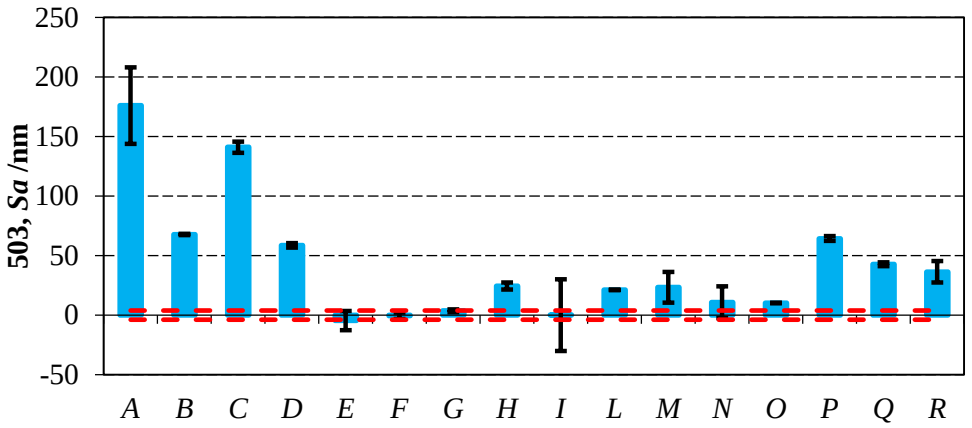

Figure 7.5-4. *Sa* deviations for 503 type specimens (random texture). Red dashed lines (– – –) indicate the expanded uncertainty of AFM reference measurements. Bars on histograms indicate the expanded uncertainty of the measurements stated by the participants.

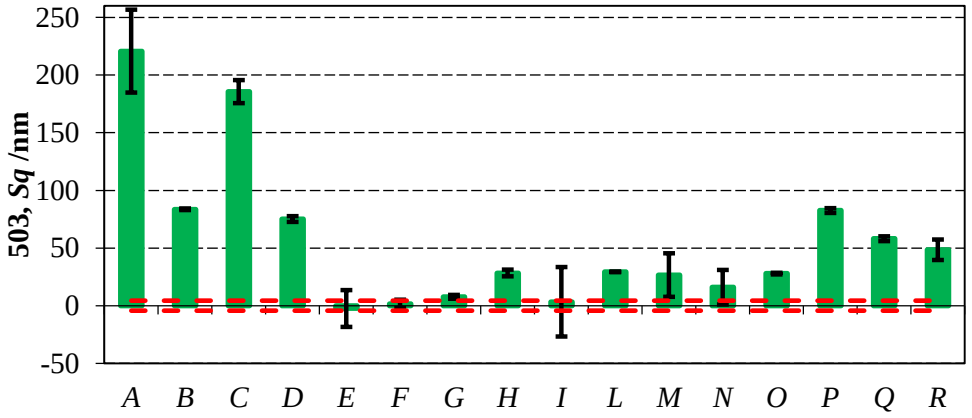

Figure 7.5-5. *Sq* deviations for 503 type specimens (random texture). Red dashed lines (– – –) indicate the expanded uncertainty of AFM reference measurements. Bars on histograms indicate the expanded uncertainty of the measurements stated by the participants.

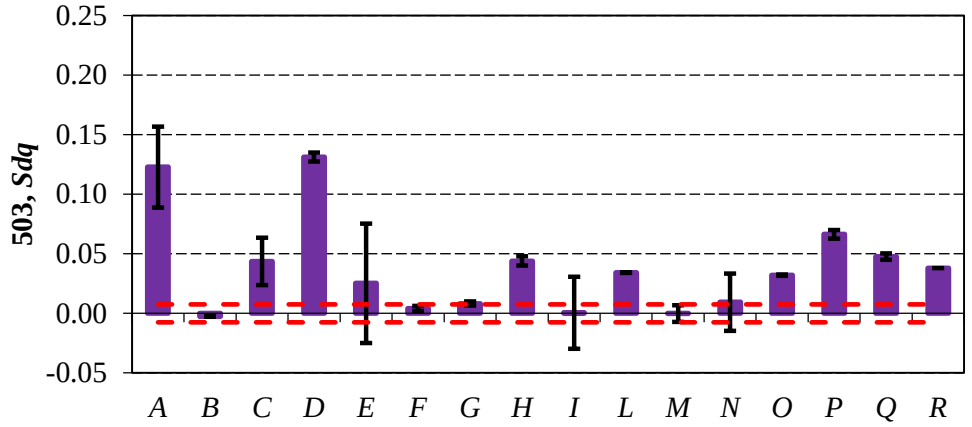

Figure 7.5-6. *Sdq* deviations for 503 type specimens (random texture). Red dashed lines (– – –) indicate the expanded uncertainty of AFM reference measurements. Bars on histograms indicate the expanded uncertainty of the measurements stated by the participants.

528 series

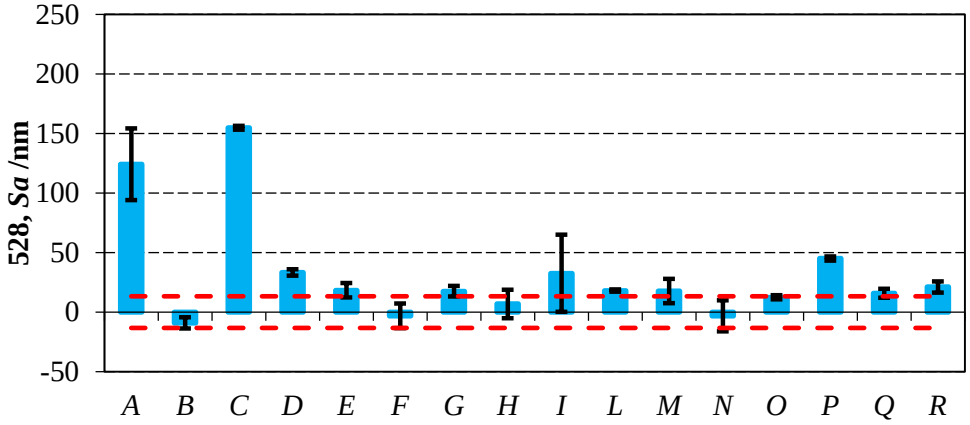

Figure 7.5-7. *Sa* deviations for 528 type specimens (random texture). Red dashed lines (– – –) indicate the expanded uncertainty of AFM reference measurements. Bars on histograms indicate the expanded uncertainty of the measurements stated by the participants.

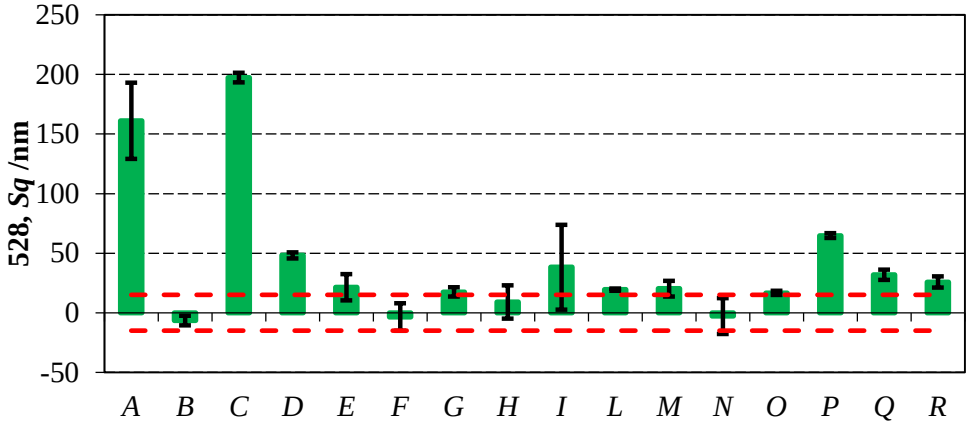

Figure 7.5-8. *Sq* deviations for 528 type specimens (random texture). Red dashed lines (– – –) indicate the expanded uncertainty of AFM reference measurements. Bars on histograms indicate the expanded uncertainty of the measurements stated by the participants.

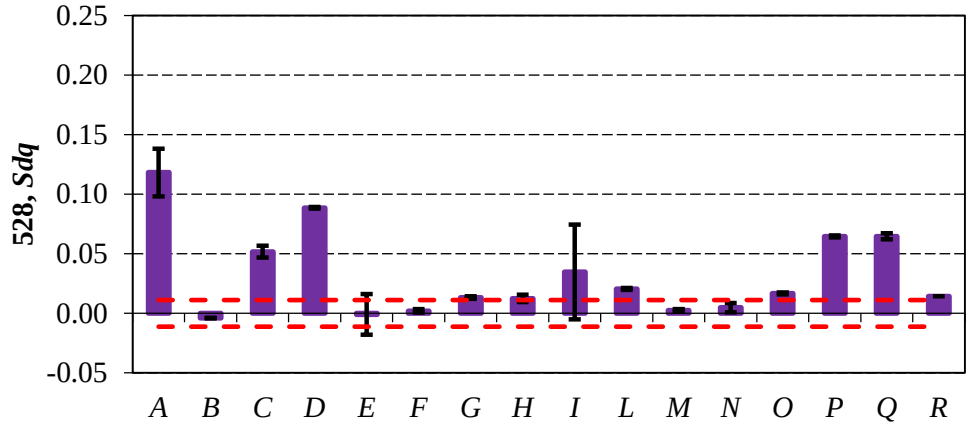

Figure 7.5-9. *Sdq* deviations for 528 type specimens (random texture). Red dashed lines (– – –) indicate the expanded uncertainty of AFM reference measurements. Bars on histograms indicate the expanded uncertainty of the measurements stated by the participants.

529 series

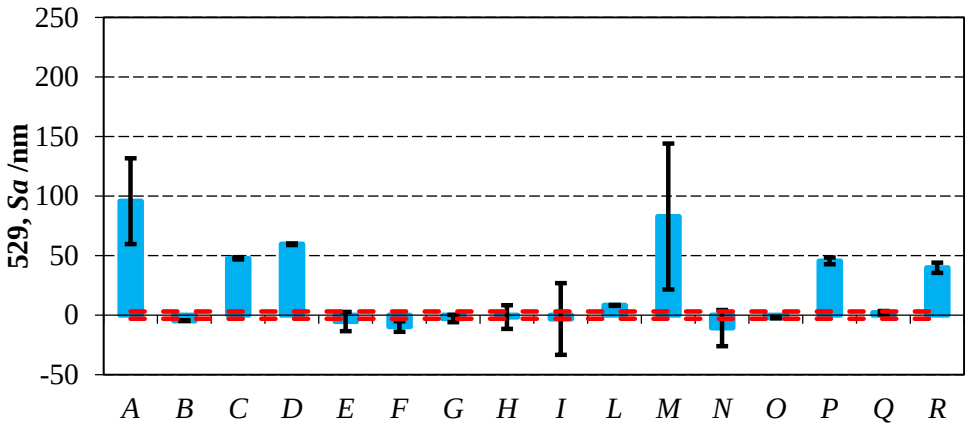

Figure 7.5-10. *Sa* deviations for 529 type specimens (random texture). Red dashed lines (– – –) indicate the expanded uncertainty of AFM reference measurements. Bars on histograms indicate the expanded uncertainty of the measurements stated by the participants.

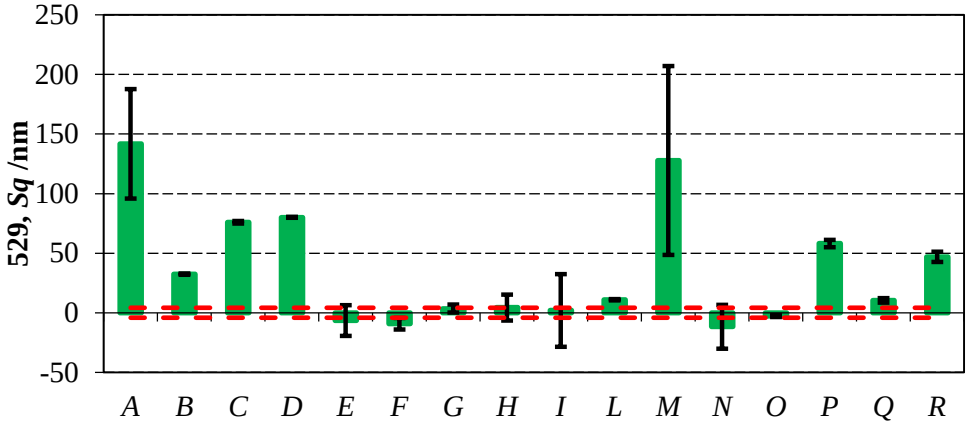

Figure 7.5-11. *Sq* deviations for 529 type specimens (random texture). Red dashed lines (– – –) indicate the expanded uncertainty of AFM reference measurements. Bars on histograms indicate the expanded uncertainty of the measurements stated by the participants.

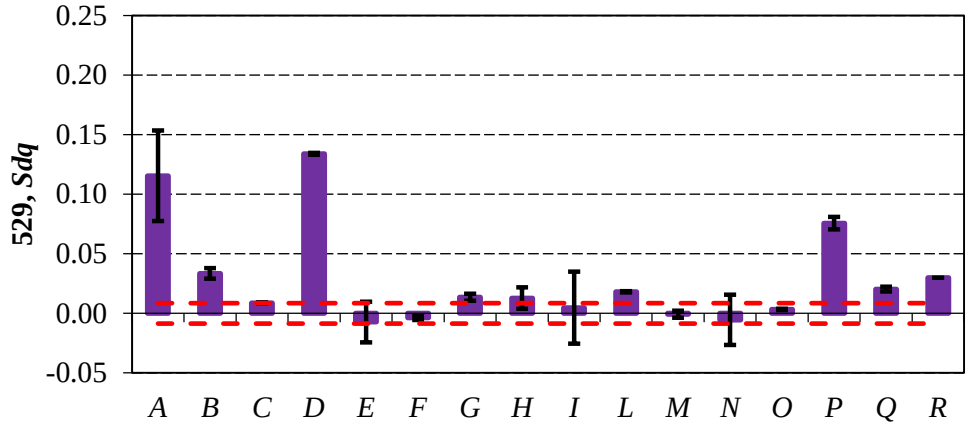

Figure 7.5-12. *Sdq* deviations for 529 type specimens (random texture). Red dashed lines (– – –) indicate the expanded uncertainty of AFM reference measurements. Bars on histograms indicate the expanded uncertainty of the measurements stated by the participants.

7.5.1 Uncertainty evaluation

The evaluation of the uncertainty was also theme of the comparison. Hence, participants were asked to evaluate the uncertainty using the method they considered appropriate. The uncertainty models employed are categorised in **Table 7.5-3** for each instrument, according to the influence factors considered relevant by the participants.
The following can be summarised:

- When the uncertainty was evaluated by repeatability only, chances of uncertainty underestimation were revealed by deviations between optical measurements and reference values which were much larger than the uncertainty itself.
- When a more complete uncertainty model was applied, a more realistic uncertainty value was obtained and agreement was observed in some cases.
- When calibrated artefacts were used to estimate the variability of the instruments, an overestimation of the uncertainty was associated to those circumstances in which the calibration uncertainty of the calibrated artefacts was of the same order of magnitude as the amplitude of the specimens under investigation.

Uncertainties stated for the instruments (histograms) and expanded uncertainties of reference AFM measurements (red dashed lines) are plotted in **Figure 7.5-13** to **Figure 7.5-24**, for each specimen.

Table 7.5-3. Uncertainty contributors related to the different instruments involved in the comparison; (■): letters refer to the instruments; (□): FVM = focus variation, CSI = coherence scanning interferometer, CM = confocal microscope.

(■)	(□)	Calibration	Resolution	Repeatability/Reproducibility	Noise	Instrument	Note
A	FVM	×	×	×			
B	FVM			× (*)			(*) reproducibility
C	FVM			× (*)			(*) standard deviation of the mean
D	CSI			×			
E	CSI					× (*)	(*) z-linearity, filter effect, dirt effect, noise, ref. flatness
F	CM	×	×	×		× (*)	(*) vertical resolution
G	CM			×			
H	CM			× (*)			(*) standard deviation
I	CM	×		×	×	× (*)	(*) different light settings considered
L	CSI			×			
M	CSI			× (*)			(*) standard deviation expanded with t-distribution
N	CSI			×		× (*)	(*) repositioning in the origin (L-shaped sign); type B uncertainty
O	CSI			expanded uncertainty declared (*)			(*) model not disclosed
P	CSI	×	× (*)	×			(*) quadratic sum of lateral and vertical resolution considered
Q	CSI	×	×	×		× (*)	(*) vertical resolution
R	CSI			× (*)		× (**)	(*) surface topography repeatability (ISO 25178-604); (**) z-axis amplification factor effect

Participants' uncertainties U(Sa)

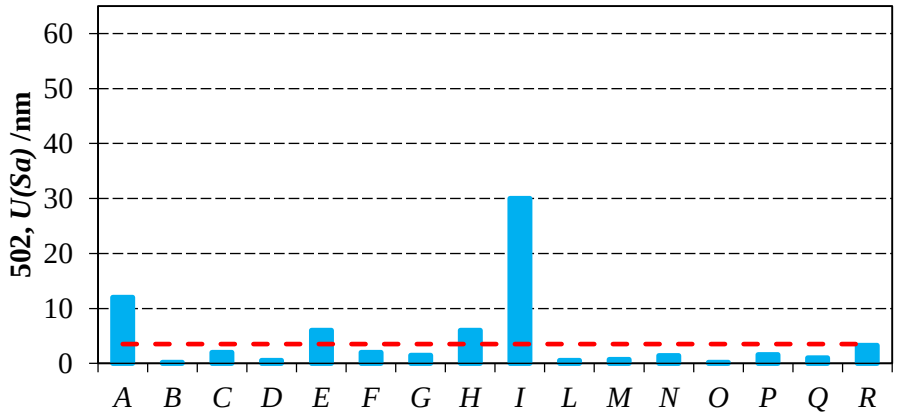

Figure 7.5-13. Instruments uncertainties for the *Sa* measurements related to 502 type specimens. The red dashed line (– – –) indicates the expanded uncertainty of AFM reference measurements.

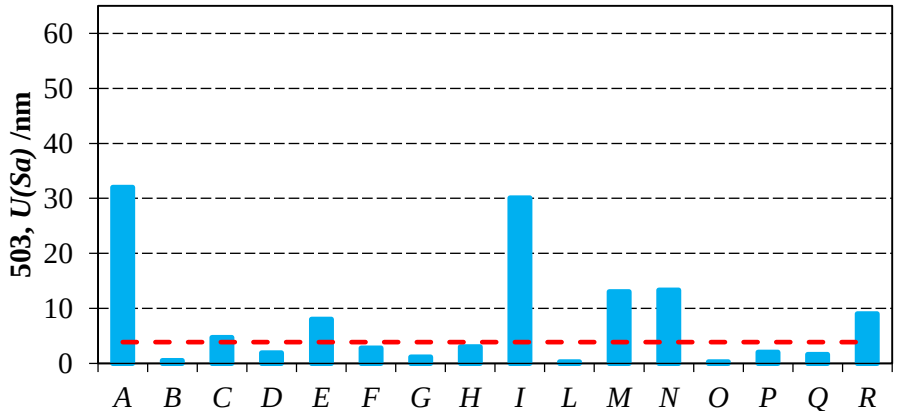

Figure 7.5-14. Instruments uncertainties for the *Sa* measurements related to 503 type specimens. The red dashed line (– – –) indicates the expanded uncertainty of AFM reference measurements.

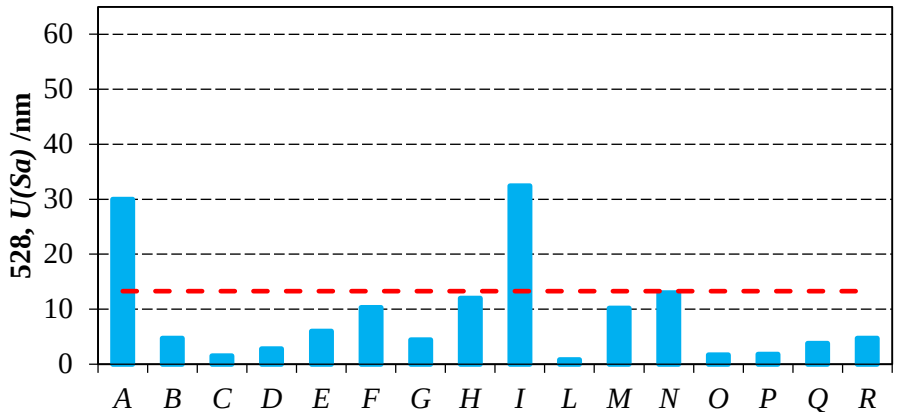

Figure 7.5-15. Instruments uncertainties for the *Sa* measurements related to 528 type specimens. The red dashed line (– – –) indicates the expanded uncertainty of AFM reference measurements.

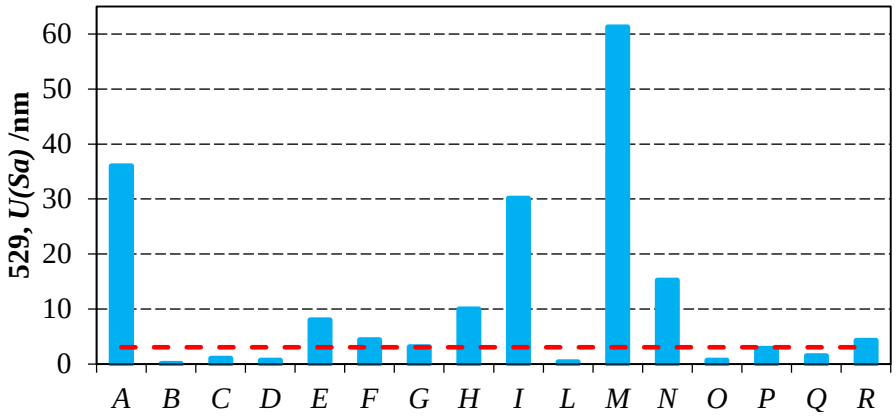

Figure 7.5-16. Instruments uncertainties for the *Sa* measurements related to 529 type specimens. The red dashed line (– – –) indicates the expanded uncertainty of AFM reference measurements.

Participants' uncertainties U(Sq)

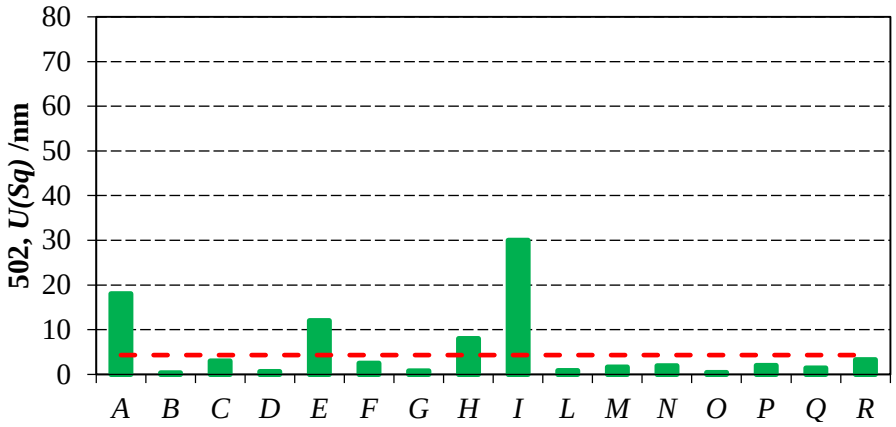

Figure 7.5-17. Instruments uncertainties for the *Sq* measurements related to 502 type specimens. The red dashed line (– – –) indicates the expanded uncertainty of AFM reference measurements.

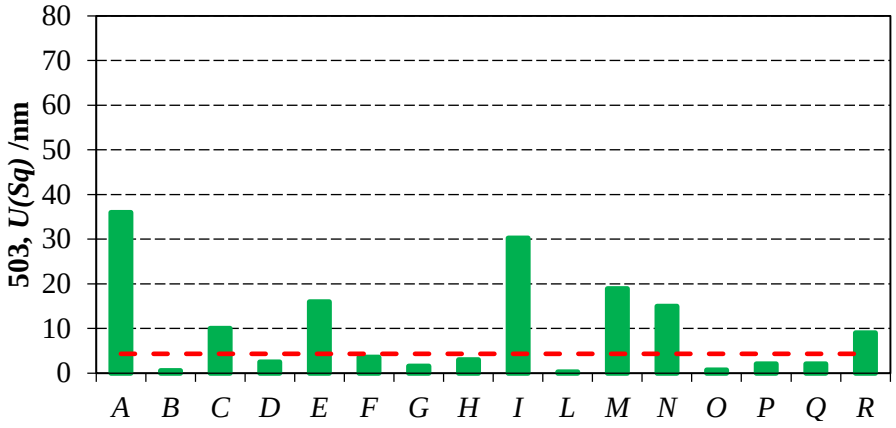

Figure 7.5-18. Instruments uncertainties for the *Sq* measurements related to 503 type specimens. The red dashed line (– – –) indicates the expanded uncertainty of AFM reference measurements.

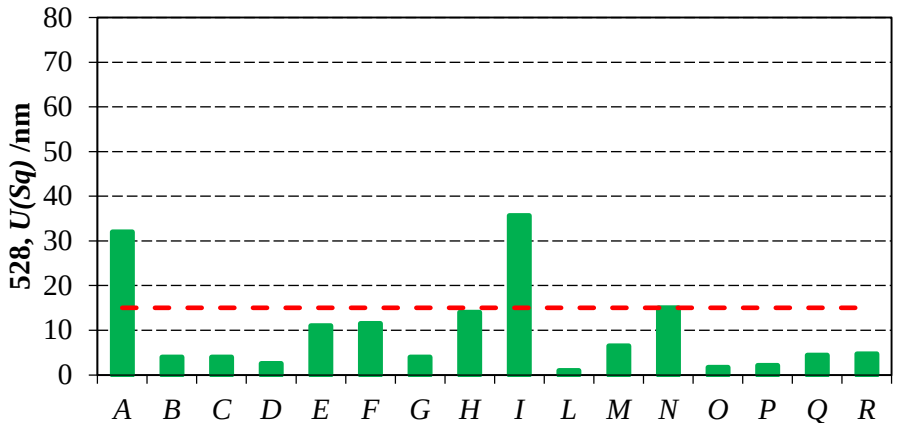

Figure 7.5-19. Instruments uncertainties for the *Sq* measurements related to 528 type specimens. The red dashed line (– – –) indicates the expanded uncertainty of AFM reference measurements.

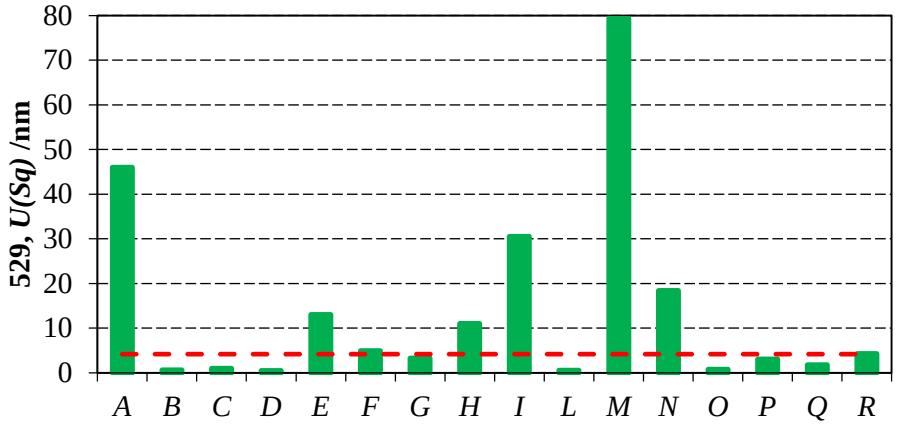

Figure 7.5-20. Instruments uncertainties for the *Sq* measurements related to 529 type specimens. The red dashed line (– – –) indicates the expanded uncertainty of AFM reference measurements.

Participants' uncertainties U(Sdq)

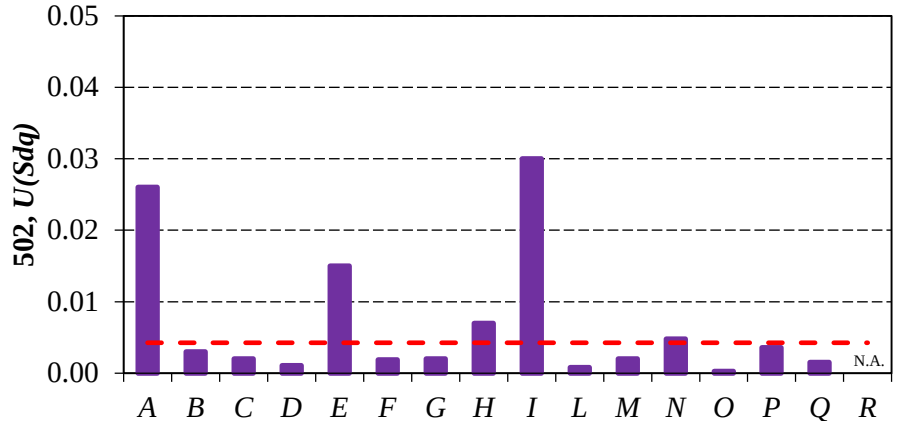

Figure 7.5-21. Instruments uncertainties for the *Sdq* measurements related to 502 type specimens (N.A. = not available). The red dashed line (– – –) indicates the expanded uncertainty of AFM reference measurements.

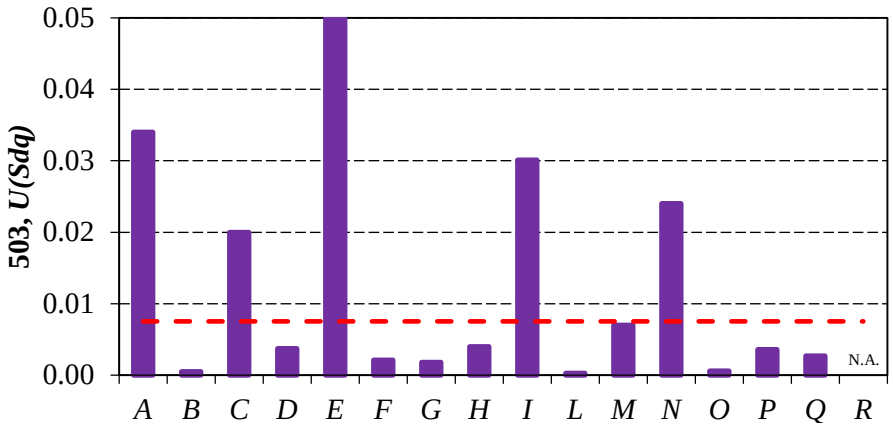

Figure 7.5-22. Instruments uncertainties for the *Sdq* measurements related to 503 type specimens (N.A. = not available). The red dashed line (– – –) indicates the expanded uncertainty of AFM reference measurements.

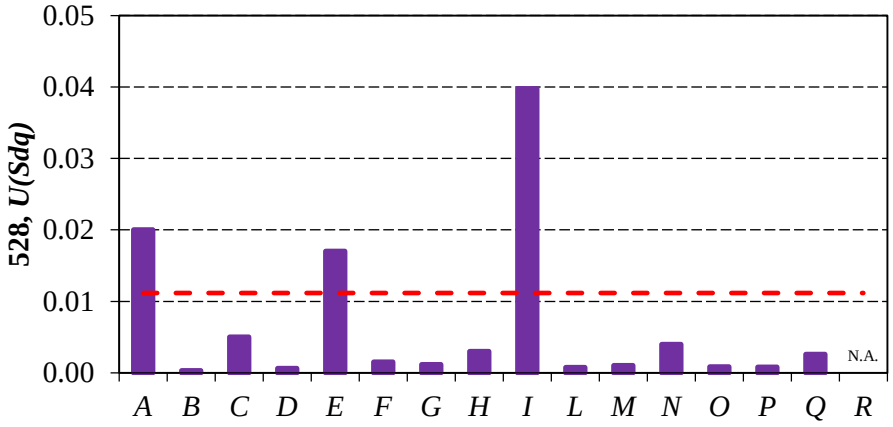

Figure 7.5-23. Instruments uncertainties for the *Sdq* measurements related to 528 type specimens (N.A. = not available). The red dashed line (– – –) indicates the expanded uncertainty of AFM reference measurements.

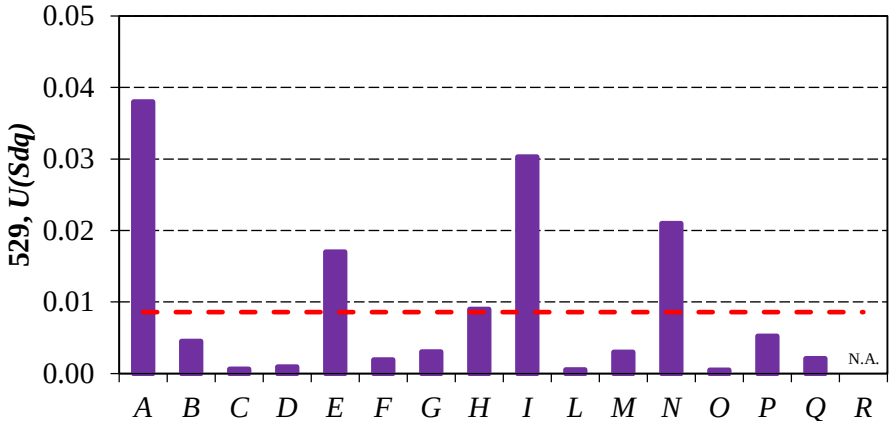

Figure 7.5-24. Instruments uncertainties for the *Sdq* measurements related to 529 type specimens (N.A. = not available). The red dashed line (– – –) indicates the expanded uncertainty of AFM reference measurements.

7.5.2 E_n value

The E_n value was determined to point out if an instrument experienced (when $|En| > 1$) unpredictable issues about the measurements or about the evaluation of the uncertainty.
En was calculated according to the following equation:

$$E_n = \frac{Sx_j - Sx_{AFM}}{\sqrt{U(Sx_j)^2 + U(Sx_{AFM})^2}} \quad (7.5\text{-}1)$$

where Sx_j stands for *Sa*, *Sq*, *Sdq*, i.e., the results obtained about the *j*-th optical instrument; Sx_{AFM} are the corresponding reference values obtained by the AFM; $U(Sx_j)$ is the uncertainty of the *Sx* result from the *j*-th optical instrument; $U(Sx_{AFM})$ is the uncertainty of the *Sx* reference from the AFM.
The E_n values calculated for all the instruments and parameters are reported in **Table 7.5-4**. From the analysis of the table, the following can be concluded:

- ***Sa***:
  - 8 % of all measurements by FVM have $|En| < 1$
  - 22 % of all measurements by CSI have $|En| < 1$
  - 75 % of all measurements by CM have $|En| < 1$
- ***Sq***:
  - 8 % of all measurements by FVM have $|En| < 1$
  - 19 % of all measurements by CSI have $|En| < 1$
  - 63 % of all measurements by CM have $|En| < 1$
- ***Sdq***:
  - 17 % of all measurements by FVM have $|En| < 1$
  - 33 % of all measurements by CSI have $|En| < 1$
  - 50 % of all measurements by CM have $|En| < 1$

Table 7.5-4. E_n values for the all instruments and parameters.

	502-x			503-x			528-x			529-x		
	Sa	*Sq*	*Sdq*	*Sa*	*Sq*	*Sdq*	*Sa*	*Sq*	*Sdq*	*Sa*	*Sq*	*Sdq*
A	9.7	8.7	4.0	5.5	6.1	3.5	3.8	4.6	5.2	2.6	3.1	3.0
B	20.2	21.5	5.1	17.4	19.1	-0.3	-0.6	-0.4	-0.4	-1.6	7.7	3.5
C	27.1	27.4	7.4	23.2	17.0	2.0	11.6	12.7	4.2	14.9	17.7	1.0
D	11.6	13.5	17.7	13.6	15.0	15.6	2.5	3.2	7.9	19.2	19.0	15.5
E	-1.6	-1.2	-0.7	-0.5	-0.1	0.5	1.3	1.1	0.0	-0.6	-0.5	-0.4
F	-0.9	-0.2	-0.2	-0.1	0.3	0.5	-0.2	-0.2	0.2	-1.8	-1.4	-0.4
G	0.1	3.0	4.2	0.9	1.7	1.1	1.3	1.1	1.2	-0.7	0.7	1.5
H	2.1	3.1	3.8	5.0	5.4	5.2	0.4	0.4	1.1	-0.2	0.4	1.0
I	-0.2	-0.2	0.1	0.0	0.1	0.0	0.9	1.0	0.8	-0.1	0.1	0.2
L	1.4	3.5	2.4	5.5	6.7	4.5	1.4	1.3	1.8	2.7	2.6	2.1
M	-1.2	0.3	-2.3	1.7	1.4	0.0	1.1	1.2	0.2	1.3	1.6	-0.1
N	-3.6	-3.2	-2.2	0.8	1.0	0.4	-0.2	-0.1	0.4	-0.7	-0.6	-0.2
O	-2.5	0.2	-0.5	2.6	6.4	4.2	0.9	1.1	1.5	-0.7	-0.7	0.4
P	11.9	14.3	9.3	14.8	17.1	8.0	3.4	4.3	5.8	11.0	11.2	7.5
Q	3.3	4.2	1.7	10.2	12.1	5.9	1.1	2.0	5.6	0.6	2.3	2.3
R	2.3	3.3	2.7	3.7	4.9	5.1	1.5	1.6	1.3	7.6	7.8	3.5

It has to be noted that the different results should be uncorrelated to have reliable indications from the E_n value determination. Furthermore, similar methods should have been used to assess the uncertainty. If the first statement can be fulfilled here, the uncertainty models in **Table 7.5-3** reveal that the second one was not.
Inverting Equation (7.5-1), a re-determination of the instruments expanded uncertainties $U(Sx_j)$ was performed for those results giving $|En| > 1$, in order to achieve $|En| = 0.99$. The average values per instrument type of the predicted uncertainties are reported in **Table 7.5-5**. By comparing these values with the ones reported in **Table 7.5-1** (average values of the reference and related expanded uncertainties), it can easily be seen that the predicted uncertainties were between one and two orders of magnitude larger than those of the reference values. Hence, besides an inadequate uncertainty evaluation, in many cases the results from the optical instruments were also affected by high deviations as compared with the reference values. In addition, such deviations had a clear different impact when considering the different optical instruments technology.

Table 7.5-5. Recalculated optical instruments expanded uncertainties to achieve $|En| = 0.99$. Average values based on all measurements originally giving $|En| \geq 1$.

	502			503			528			529		
	U_{Sa} /nm	U_{Sq} /nm	U_{Sdq}	U_{Sa} /nm	U_{Sq} /nm	U_{Sdq}	U_{Sa} /nm	U_{Sq} /nm	U_{Sdq}	U_{Sa} /nm	U_{Sq} /nm	U_{Sdq}
FVM	101.7	133.8	0.100	129.4	164.9	0.084	140.2	180.4	0.085	49.5	84.0	0.050
CSI	16.4	29.7	0.026	36.8	45.7	0.058	19.6	26.2	0.043	47.4	55.9	0.055
CM	14.0	20.5	0.025	24.4	17.3	0.024	11.7	9.3	0.007	9.2	8.3	0.010

7.6 Discussion

Substantial deviations from the AFM reference values were observed for FVMs results in almost all measured samples. This general issue indicated that the FVM technology was not suitable to measure these types of surfaces. The possible explanation is that the master and resulting polymer surfaces had local roughness that was too low to allow proper detection by the instrument [18].
Considering the results related to CSI, only a small number of instruments showed agreement with the corresponding AFM reference values. In general, moderate deviations were observed, sometimes enhanced by unmatched spatial bandwidths due to a measured area that was not the same as required. In addition, low levels of reflected light and inadequate sensitivity of the detector were observed for some of the measurements.
The raw data acquisitions were commonly affected by noise (spikes and voids). In some cases, non-measured pixels were corrected during the post-processing by the specific tools software. Such correction, however, affected the resulting data sets depending on the software, i.e., it introduced an additional source of uncertainty (e.g., a loss of information, or even an increased number of spikes). The presence of spikes particularly affected the *Sdq* parameter, which is sensitive to the local slope of the surface. For all the instruments, specific deviances related to the *Sdq* parameter were attributed to the local gradients of the polymer surfaces, which exceeded the limits set by the numerical aperture (A_N) of the objectives.
In the case of CMs, which had an important amount of results in agreement with the reference, most of the large deviations were attributed to the presence of outliers (i.e. spikes). It was clearly observed that the outlier filters in the image processing software equipped with some instrument used were insufficient in removing the outliers.

In the following, observations from the analysis and explanations from the participants are gathered and reported for each instrument used.

Comments related to the instrument A (FVM)

Results showed large deviations in all measured specimens. The inconsistency with the references (AFM results) may have been due to a technological limit. Explicitly, it appeared that the surfaces had local roughness that was too low to allow proper operation of the instrument.

Comments related to the instrument B (FVM)

The analysis software equipped on the microscope used did not evaluate the surface parameters *Sa*, *Sq* and *Sdq* according to ISO 25178-2, furthermore it was not possible to filter the measured data according to ISO 25178-3. For the evaluation of the surface parameters, a procedure similar to ISO 4288 (profile method) was implemented in the mentioned software. For filtering the measured data, a wavelength of 80 µm was used.
The software did not include an estimation of the uncertainty of an evaluated surface parameter. Furthermore, there was no information about the uncertainty of single measuring points. To estimate an uncertainty, the calculation of the surface parameters was repeated five times at slightly changed locations on the measured surface and the standard deviation of the five repeated evaluations was calculated.
The stated measurement uncertainty was information on the variation of the parameters due to slightly changed measurement locations on the specimen and did not consider contributors due to definition errors of parameters, due to filtering errors or uncertainties of single measuring points.

Comments related to the instrument C (FVM)

Results showed large deviations in most of the measured specimens. The inconsistency with the references (AFM results) was comparable with the one of the other instruments using the same working principle and it may be due to a technological limit.

Comments related to the instrument D (CSI)

Results showed medium deviations which became larger when considering the *Sdq* parameter. The inconsistency with the references (AFM results) may have been enhanced by an inadequate scanning area, i.e., by an unmatched spatial bandwidths.

Comments related to the instrument E (CSI)

Considering the results in their interval related to the evaluated uncertainty, they appeared consistent with the related reference values (AFM results).
Nevertheless, when considering E_n determination, the values exceeded the unit in some cases. An explanation may be found in the different evaluation of the uncertainty (i.e., different contributors considered) with respect to the references. However, when an excess over the unit was found, it was always not meaningful (see **Table 7.5-4**).

Comments related to the instrument F (CM)

Results are in agreement with the references (AFM measurements).

Comments related to the instrument G (CM)

Except in a few cases, the results were in agreement with the references (AFM measurements). A better evaluation of the uncertainty for the measurements related to this instrument may have extended the consistency of the uncertainty intervals and the agreement even further, as shown by the E_n values determined (see **Table 7.5-4**).

Comments related to the instrument H (CM)

Most of the variations with respect to the references (AFM measurements) were due to outliers (spikes). The outlier filters in the software used for image processing were insufficient in removing the outliers.

Comments related to the instrument I (CM)

Most of the results related to this instrument were compatible with the references (AFM measurements). Revising the evaluation after the comparison, it could be observed that the uncertainty stated could be refined (i.e. decreased by using a reference calibration artefact with a

lower calibration uncertainty). Eventually, the assessment was kept as presented in the final results, considered suitable for the purposes of the comparison.

Comments related to the instrument L (CSI)

Considering the E_n values (see **Table 7.5-4**), results did not show a good agreement. An explanation may be related to the unmatched bandwidths. Furthermore, a better evaluation of the uncertainty may have increased the agreement with the reference values.

Comments related to the instrument M (CSI)

Noticeable deviations with respect to the reference (AFM measurements) affected only part of the results.
No calibrated artefacts of the same order of magnitude of the specimens under investigation were available to attempt a correction for systematic behaviour. For the same reason, the measurement uncertainty was evaluated considering only the contribution of the reproducibility.
Hence, in the adopted approach, higher deviations may have been compensated. Furthermore, an underestimation of the uncertainty was also plausible. In fact, E_n (see **Table 7.5-4**) indicates uncertainty values smaller than the reference values by a factor 2 or 3 (i.e., the factor required to lower E_n below the unit).
Eventually, considering other influence factors may have improved the fidelity of the evaluated uncertainty (e.g., resolution restrictions, light settings, etc.).

Comments related to the instrument N (CSI)

Results are for the most part in agreement with the references (AFM measurements). The raw data acquisitions, however, were affected by disturbances (spikes and voids), which were corrected during the post-processing.
The first correction applied, for restoring missing pixels (cubic spline "natural neighbour interpolation"), also increased spikes. Hence, the final results were obtained after spike reduction.

Comments related to the instrument O (CSI)

Results were in close agreement with the references (AFM measurements), even though the evaluated uncertainty were underestimated in the first instance.
A new evaluation of the uncertainty (expanded uncertainty) is in **Table 7.6-1**, where the reported values seemed to better fit the purpose.

Table 7.6-1. New evaluation of the expanded uncertainty provided by the participant in charge of the instrument *O*.

	502-x			503-x			528-x			529-x		
	Sa	*Sq*	*Sdq*	*Sa*	*Sq*	*Sdq*	*Sa*	*Sq*	*Sdq*	*Sa*	*Sq*	*Sdq*
U	1.6	2.8	0.002	1.9	4.5	0.004	10.8	10.9	0.005	4.2	4.8	0.003

Comments related to the instrument P (CSI)

Results deviations may have been due to the limitations of the instrument used. The relatively weak reflected light and inadequate sensitivity of the detector may justify such deviations of the measured results.
Another reason may have been related to the conditions of the specimens. Even though all specimens were stored in a 20 °C thermotank, trying to avoid any accidental pollution during the measurement, some noticeable defects and scratches were found on the specimens.

Comments related to the instrument Q (CSI)

The discrepancies with respect to the reference (AFM measurements) may mainly have been due to the different spatial bandwidth of the instruments and techniques. The measured area, in fact, was not exactly the same as required. This was likely to produce differences between these two technologies.

Furthermore, specific differences related to the *Sdq* parameter may also have been attributed to the local gradients of the polymer surfaces, which exceeded the limits set by the *numerical aperture* (A_N) of the objective used.

Comments related to the instrument R (CSI)

The results showed medium deviations with respect to the references (AFM measurements). This can partially be justified considering that they were acquired in a workshop and in non-ideal measurement conditions. All reported results were processed by the commercial software provided with the instrument. In addition, this software did not compute *Sdq*. Filtering was also implemented within the commercial software.

7.7 Conclusion

The replication of metal material measures in polymer specimens proved to be a cost-effective method for the production of a high number of transfer standards (see Chapter 6) [2]. Hence, it was possible to conveniently compare a large number of optical instruments. The established procedure could be applied for future comparisons.

A number of observations were possible as a result of the comparison with respect to the different optical instruments. These considerations, generated above all from the experience of the participants, were in good agreement with the current state-of-the-art of calibration and verification of areal surface texture measurement instruments, recently discussed in [5].

As a whole, the comparison highlighted the challenge of measuring areal surface parameters at the sub-micrometre scale with optical instruments.

Undoubtedly all instruments have their limitations and must be used within the recommended technical specifications.

Agreement between optical instruments and AFM measurements could be reached to some extent, largely depending on the technology of the instruments used. In particular, better performance on sub-micrometre surfaces could be obtained by using CSI and CM, the latter proving the closest results to the reference values. Although it appears that such surfaces could not be measured correctly by FVM (possibly due to the effect of local roughness).

The role of the post-processing software and the surface texture parameters considered were also crucial aspects of results of the comparisons. It emerged the need for development of software tools capable of a more effective removal of surface outliers and also of the quantification of the uncertainty for the evaluated surface parameters. Consequently, this would provide simplified methods for uncertainty evaluation in industry.

Furthermore, the need for instruments performance verification was also outcome of the comparison. Specifically, appropriate transfer standards for an improved, accurate and comprehensive assessment of the of the instruments uncertainty. Eventually, the establishment of an instrument calibration framework as a result of primary traceable instruments.

References

[1] Tosello G, Haitjema H, Leach R K, Quagliotti D, Gasparin S and Hansen H N 2016 An international comparison of surface texture parameters on polymer artefacts using optical instruments *CIRP Annals – Manuf. Technol.* **65** 529–32

[2] Tosello G, Hansen H N, Quagliotti D, Stefania Gasparin, Han Haitjema and Richard Leach 2015 CIRP surface texture comparison on polymer artefacts using optical instruments CIRP STC-S collaborative work – CIRP Technical report

[3] Hansen H N, Hocken R J and Tosello G 2011 Replication of micro and nano surface geometries *CIRP Annals – Manuf. Technol.* **60** 695–714

[4] Bruzzone A, Costa H, Lonardo P, Lucca DA 2009 Advances in engineered surfaces for functional performance *CIRP Annals – Manufacturing Technology*, **57/2** 750-769

[5] Leach RK, Giusca CL, Haitjema H, Evans C, Jiang X 2015 Calibration and verification of areal surface texture measuring instruments *CIRP Annals – Manufacturing Technology*, **64/2** 797-813

[6] Koenders L, Bergmans R, Garnaes J, Haycocks J, Korolev N, Kurosawa T, Meli F, Park BC, Peng GS, Picotto GB, Prieto E, Gao S, Smereczynska B, Vorburger T, Wilkening G 2003 Comparison on Nanometrology: Nano 2—Step height *Metrologia* **40** (Technical Supplement)
[7] Doytchinov K, Kornblit F, Colin Castellanos C, Oliveira JCV, Renegar TB, Vorburger TV 2006 International comparison of surface roughness and step height (depth) standards, SIML-S2 (SIM 4.8) *Metrologia* **43** (Technical Supplement)
[8] Koenders L, Klapetek P, Meli F, Picotto GB 2006 Comparison on step height measurements in the nano and micrometre range by scanning force microscopes *Metrologia* **43** (Technical Supplement)
[9] Danzebrink HU 2009 Supplementary comparison according to the rules of CCL key comparisons – EUROMET project 925 – Intercomparison on Step Height Standards and 1D Gratings – *Final Report*. *Physikalisch-Technische Bundesanstalt*
[10] Baker A, Tan SL, Leach RK, Jung L, Wong SY, Tonmueanwai A, Naoi K, Kim J, Renegar TB, Chaudhary KP, Kruger O, Amer M, Gao S, Tsai CL, Anh N, Drijarkara A 2013 Final report on APMP.L-K8: International comparison of surface roughness *Metrologia* **50** (Technical Supplement)
[11] Thalmann R 2015 Key Comparison EURAMET.L-K8.2013 – Calibration of surface roughness standards – EURAMET project 1245 – Final report *Metrologia*, **50** (Technical Supplement)
[12] Rubert & Co Ltd., Reference Specimens, www.rubert.co.uk/reference-specimens (accessed on January 2016)
[13] ISO 5436-1: 2000 Geometrical product specification (GPS)—Surface texture: Profile method; Measurement standards – Part 1: Material measures. ISO 5436 part 1 (Geneva: International Organization for Standardization)
[14] ISO 25178-2: 2012 Geometrical product specification (GPS)—Surface texture: Areal – Part 2: Terms, definitions and surface texture parameters. ISO 25178 part 2 (Geneva: International Organization for Standardization)
[15] ISO 25178-3: 2012 Geometrical product specification (GPS)—Surface texture: Areal – Part 3: Specification operators. ISO 25178 part 3 (Geneva: International Organization for Standardization)
[16] Leach R and Haitjema H 2010 Bandwidth characteristics and comparisons of surface texture measuring instruments *Meas. Sci. Technol.* **21** 1-9
[17] ISO 15530-3: 2011 Geometrical product specifications (GPS)—Coordinate measuring machines (CMM): Technique for determining the uncertainty of measurement – Part 3: Use of calibrated workpieces or measurement standards ISO 15530 part 3 (Geneva: International Organization for Standardization)
[18] Helmli F 2011 Focus Variations Instruments. In: Leach R (Ed.) *Optical Measurement of Surface Topography* (Berlin, Heidelberg: Springer Berlin Heidelberg) chapter 7

Chapter 8

Performance verification of optical instruments for surface topography measurements

8.1 Introduction

During the progress of the three years of the PhD studies several optical microscopes were used on different specimens and applications, sometimes pushing the instruments at a limit.
This chapter is intended to describe particular issues encountered in specific circumstances and that clearly outlined performance limitations of some of the instruments used. Hence, the aim is to provide minute of such experiences and their related operating conditions and to highlight how the metrological characteristics of an instrument can be affected by particular measurement settings.
Several cases are presented in the following chapter with regards to a laser scanning confocal microscope, a focus-variation microscope and a point autofocus instrument. A description of these working principles can be found in Chapter 2. The instruments used were, respectively, Olympus Lext OLS 4100 (OLS), Alicona Infinite Focus G4 (G4) and Mitaka MLP-3SP (MLP).

8.2 Validation of Olympus Lext OLS 4100 laser scanning confocal microscope

The first study is related to some technical problems that arose during the validation of a new purchased laser confocal microscope OLS, currently installed in the Laboratory for Micro and Nanoscale Metrology of the Section of Manufacturing Engineering (Department of Mechanical Engineering) at the Technical University of Denmark (DTU).

In order to assess the correct operation of the instrument, several measurements were performed on many specimens. In some cases, they evidenced failure of the instrument in the measure of portions of the acquired surfaces. Examples are reported in **Figure 8.2-1**. They are acquisitions on random texture roughness standards [1]-[3] using both 50× and 100× objectives and high resolution mode (i.e., 4096 × 4096 pixels per field of view).
The measurements were acquired the same day and the failure was noticed after intensive use of the instrument. In **Figure 8.2-1**, it can clearly be seen a concave shape in the centre of the surfaces and wrong information about the measured height of peripheral portions of the surfaces, which appeared as abrupt changes in the topography. Even though the measurements were not acquired in sequence, such changes generated a similar pattern in the four topographies, independently of the surface texture amplitude (*Sa* roughness parameter in the range (0.2-2) µm) and of the objective magnification (50×, 100×).

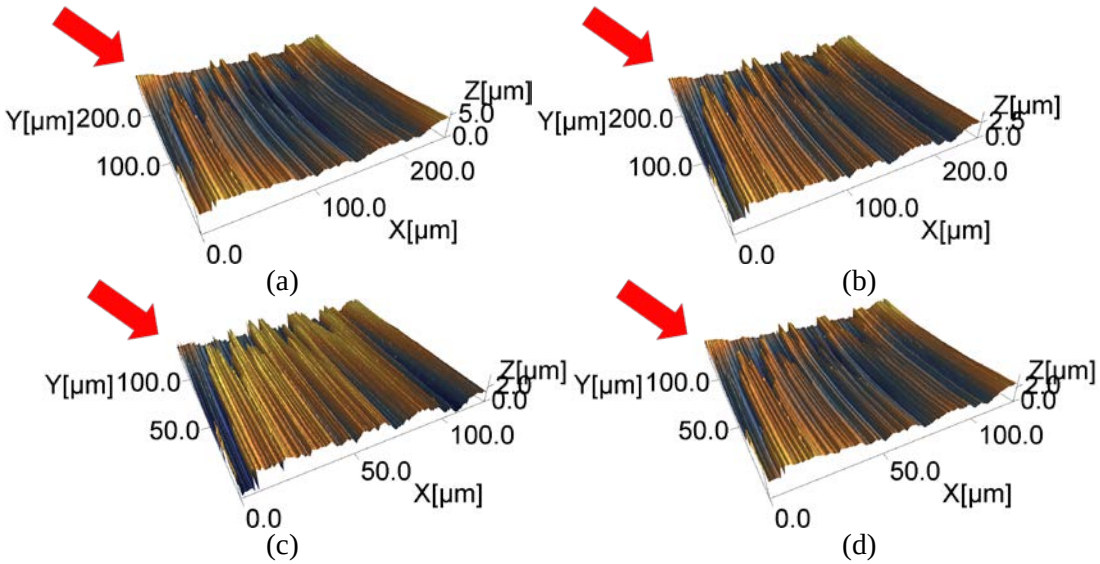

Figure 8.2-1. Examples of corrupted measurements (high resolution acquisitions: 4096 × 4096 pixels). (a): Roughness standard nominal *Ra* = 1.75 µm [1]; 50× magnification objective. (b): Roughness standard nominal *Ra* = 490 nm [2]; 50× magnification objective. (c) Roughness standard nominal *Ra* = 209 nm [3]; 100× magnification objective. (d): Roughness standard nominal *Ra* = 490 nm; 100× magnification objective [2].

The nickel roughness standard 529 by Rubert&Co was measured in a successive day. As already introduced in Chapter 6 and Chapter 7, it is a periodic texture specimen with nominal *Ra* = 100 nm. It was acquired in stitching mode as a matrix 3 × 3, by 100× magnification objective and normal resolution (1024 × 1024 pixels for each field of view). The ordered sequence of five repeated acquisitions is in **Figure 8.2-2**, which shows a progressive degradation of the surface affecting more and more extended areas. Hence, the disruption was also independent from the type of texture of the measured specimen and from the number of pixels set for the acquisition. Nonetheless, being the acquisition a stitching of nine fields of view, it is worth to notice that the disturbance arose and propagated on the same side of the stitching matrix, acting in a similar way (systematically) on the three lateral fields of view involved.
Olympus technical service was able to reproduce the problems on two systems, DTU OLS and another OLS (Olympus demo system). The following failures were officially recognised:

1. ***Change in calculation time needed to process the laser image acquisitions***
   This failure was judged to be easily reproducible and was reproduced many times. It was associated to the time required for the system to process the image data after the laser system acquisition. This time was normally less than six seconds but, when the problem manifested, it was more than a minute. Concurrently to the problem, two routines responsible for the image data processing tripled the memory (RAM) usage.

2. ***Loss of actual height data in high resolution mode***
   The loss of actual height data in high resolution mode and consequent generation of wrong height data were noticed after some time of continuous use of the instrument. This failure was believed to be sporadic and several repeated areal acquisitions were necessary to the technical service to reproduce it. It manifested with an intensity image of the same appearance of the correct acquisitions but with calculated roughness data altered. Resulting the failure, acquiring more images in high resolution mode worsened the height data with each new acquisition (larger deviations from the calibrated values). A restart of the system restored normal operation until the next failure.
   The failure could be reproduced once again in another day and only when employing the high resolution mode. Hence, it was concluded that the problem was related to this specific mode.

As a result of the examination, a more powerful graphic board was installed on the PC hosting the software for the user interface of the system.
The graphic board replacement solved the problem *1.* but not the problem *2.* Indeed, it continued to affect the acquisitions but, being the acquired image unchanged with respect to a correct one, the failure was always recognised after the post-processing, widening the repeatability/reproducibility of the measurements. Such behaviour was noticed dependent on the material (colour) of the specimens and was enhanced by the repositioning (or relocation), i.e., before repeating an acquisition, moving the stage in a reference position and, soon after, reaching the measurement area again.
A sequence of repeated measurements with both 50× and 100× magnification objectives is, e.g., in **Table 8.2-1**. It refers to a steel specimen for mould finish comparison, with nominal *Ra* parameter in the interval (51-76) nm and grit-paper polishing, which was in the set of other specimens already investigated in § 4.4 and § 6.3 [4]. In the table, several outliers clearly show the failure.

Table 8.2-1. Example of repeated acquisitions of a specimen with nominal *Ra* in the interval (51-76) nm, using both 50× and 100× magnification objectives. Standard deviation and reproducibility are also given.

		50× Sa /nm	100× Sa /nm
		44.0	46.0
		67.4	46.4
		44.1	45.9
		44.3	50.3[(a)]
		67.3	46.5
			94.0
			130.2
After reboot of the system →			45.0
			45.4
			46.5
			46.1
			44.9
Standard deviation	s	13	27
Reproducibility	u_{repr}	7	25

[(a)] Anomalous value before the failure

The values in **Table 8.2-1** were calculated from acquisitions at high resolution mode. However, **Figure 8.2-2** shows a failure of acquisitions in normal resolution mode. Thus, the problem cannot be connected with any specific resolution mode but rather with the consequent large memory usage (high resolution, stitching, etc.)
The author, after several measurements sessions, noticed that a possible cause of the failure (problem *2.*) might be related to the 'colour' tool. It is a second acquisition system, based on coherent scanning interferometry (CSI) which, if enabled, acquires a second image after the one of the laser scanning system. Such image is not used for any quantitative measurement but it is only superimposed to the laser scanning one for giving information about the colour of the specimen. In some cases, after the laser acquisition, the acquisition related to 'colour' did not start, blocking the execution of the software for relatively long time. A deeper look revealed two routines in idle loop: the controller was delayed when switching from the laser scanning acquisition to the CSI one.

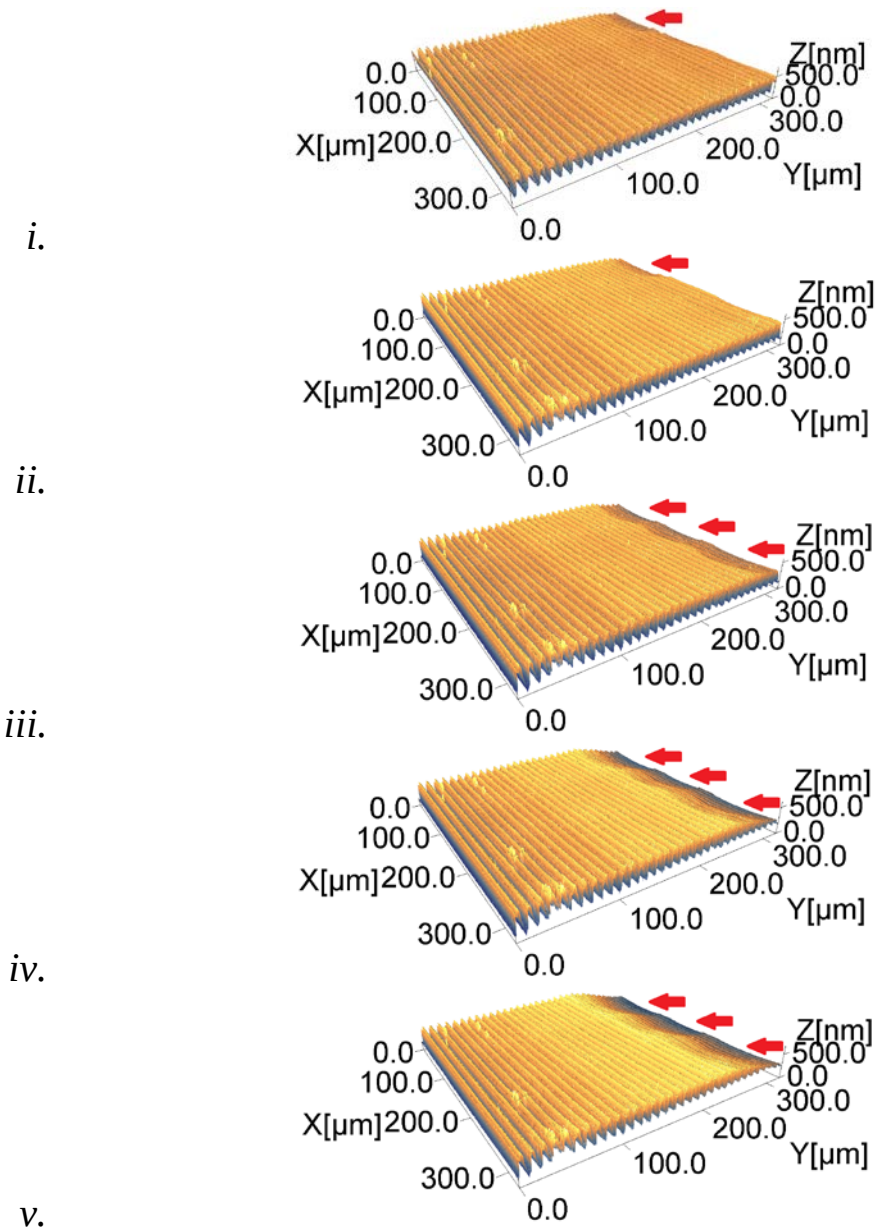

Figure 8.2-2. Example of corrupted acquisitions. The surfaces are matrices 3 × 3 acquired by 100× magnification objective and normal resolution (1024 × 1024 pixels for each field of view). The measurements are in their order of acquisition from *i.* to *v.* The sequence shows a progressive degradation of portions of the acquired surfaces.

Before the failure (typically one or two acquisitions before) the measured roughness values changed significantly (see note [(a)] in **Table 8.2-1**). The direct consequence was a poor repeatability of the measurements. The author, again, believed that instabilities in the CSI system, or in the related starting routine, produced an impaired real-time loop of the controller, which interfered with the processing of the laser scanner image with subsequent overwriting of part of the acquired data. Nonetheless, after the replacement of the graphic board, such failure was never experienced while measuring with the 'colour' tool disabled.

8.3 Long working distance objectives assessment in Olympus Lext OLS 4100 laser scanning confocal microscope

The increasing importance of optical microscopy in the geometrical and dimensional assessment of structured and freeform surfaces has easily overcome many difficulties related to the use of contact instruments. Nonetheless, some concerns related to optical instruments when measuring such surfaces are still open. The working distance (WD) of some standard (ST) lenses, e.g., can prevent from freely moving alongside features at different heights and positions of structured and freeform shapes due to the risk of collisions. In such cases, the so-called long working distance (LWD) objectives allow to operate at a longer distance from the surface under measurement, keeping the same field of view (FoV) but accepting lower numerical apertures.

The current study compares standard and LWD objectives available for OLS. The investigation was to compare *Sa* and *Sqd* surface texture areal parameters related to the same surface, acquired by 50×, 100× ST and 50×, 100× LWD lenses (see **Table 8.3-1**).

A pseudo-random roughness metal artefact (AIR-B70) was the material measure. It belongs to a set of artefacts, for areal calibration of optical instruments, denominated 'Bento Box' and produced at the National Physical Laboratory (NPL) in Teddington, UK [5] (see **Figure 8.3-1**). The calibrated value from the calibration certificate $Sa = 751 \pm 26$ nm ($k = 2$) was used. It has been calculated after applying an S-filter, nesting index 8 µm, and an L-filter, nesting index 0.8 mm [6].

Table 8.3-1. Main characteristics of the objectives used (FoV: field of view; WD: working distance; A_N: numerical aperture).

	FoV /µm	WD /mm	A_N	Pixels
ST 50×	260 × 260	0.35	0.95	4096 × 4096
ST 100×	130 × 130	0.35	0.95	4096 × 4096
LWD 50×	260 × 260	10.60	0.50	4096 × 4096
LWD 100×	130 × 130	3.40	0.80	4096 × 4096

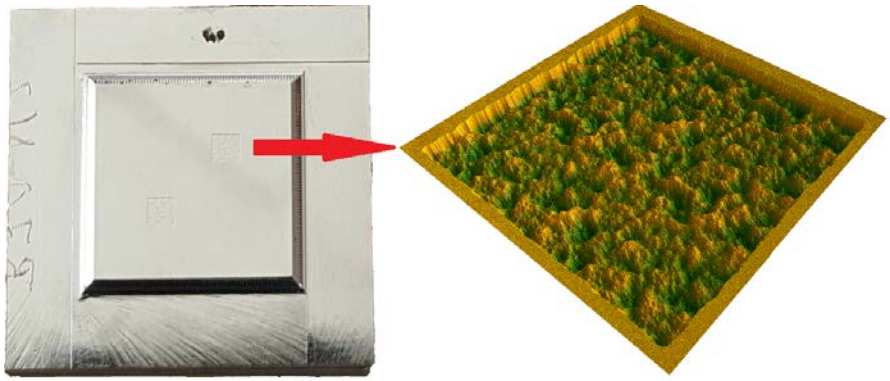

Figure 8.3-1. Pseudo-random roughness metal artefact of the 'Bento Box' areal calibration set (National Physical Laboratory (NPL), Teddington, UK [5]).

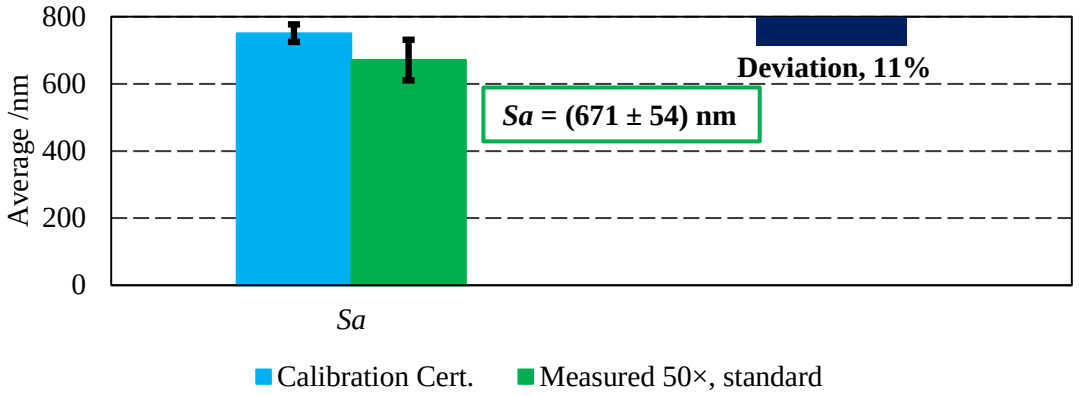

Figure 8.3-2. Comparison between the *Sa* value in the calibration certificate and the measured value with the 50× ST objective. An S-filter, nesting index 8 µm, and an L-filter, nesting index 0.8 mm, were applied to the measured values. The deviation between the central values is indicated by a reversed blue column.

In the calibration certificate [6], the calibrated value was given as a result of 3 × 3 matrix acquisitions in stitching mode. Acquisitions of single FoV in the centre of the artefact working area were instead the choice for this evaluation, not to add another influence source in the successive analysis (i.e., the stitching of nine FoVs). For this reason, the measured values by 50× ST objective were preliminarily compared with the calibrated value, after applying the same filtering described in the calibration certificate. The result is in **Figure 8.3-2**. The deviation of 11 % between the central values was explained by the different FoV and number of pixels. Hence, the measured results by 50× ST objective were deemed reliable.
The expanded uncertainty indicated in figure was combined considering the standard deviation of the mean (extended from a normal distribution to a *t* distribution comparing both distributions at the same confidence interval of 95 %), the reproducibility, the uncertainty stated in the calibration certificate and a coverage factor $k = 2$.

Successively, being the FoV of 100× ST objective about one half with respect to 50× ST one, a comparison between measurements of these two objectives was preliminary conducted, too. The measurements were cut to the same FoV of 100× ST and resampled to the same number of pixels (4096 × 4096). No filters were applied. The result is in **Figure 8.3-3** for both *Sa* and *Sdq* parameters. A difference of 8 % was found between the central values of *Sa*, with congruent uncertainty intervals. The difference between the central values raised to 21 % for *Sdq* calculations. Uncertainty intervals are not congruent in this case. However, the *Sdq* uncertainty might have been underestimated. A calibrated value for *Sdq* was, in fact, not provided in the calibration certificate. Hence, it was estimated weighting the calibration expanded uncertainty stated for Sa^{cal} by the relevant standard deviations in the measurement sessions (Sa^{meas}, Sdq^{meas}).

These preliminary assessments were necessary to state the consistencies among the quantities under comparison because of the different nature of the measurements.

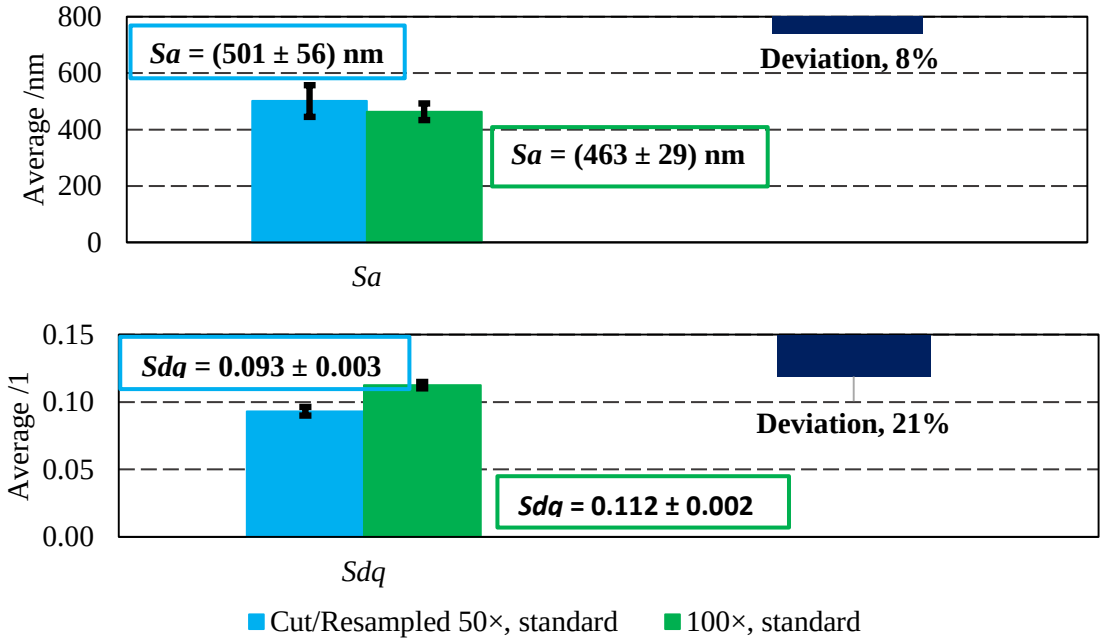

Figure 8.3-3. Measurements of standard objectives 50× and 100×. No filters applied. Same FoV and number of pixels. The deviation between the central values is indicated by a reversed blue column.

The comparison between 50× ST and LWD objective is in **Figure 8.3-4**. It shows a good agreement for *Sa*, with a 4 % of deviation between the central values and congruent uncertainty intervals, but also a disagreement for *Sdq*, with a clear deviation between the central values.
The same trend can be observed for the comparison of 100× ST and LWD objective in **Figure 8.3-5**, though a larger deviation for *Sa* and a smaller one for *Sdq*.

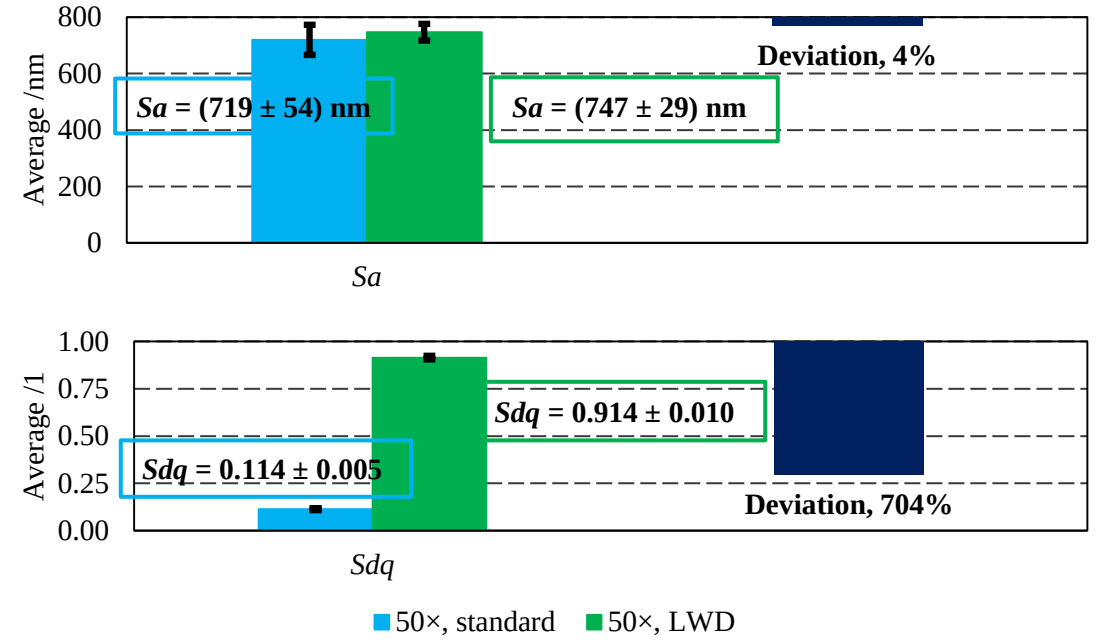

Figure 8.3-4. Measurements of 50× standard and long working distance objectives. No filters applied. The deviation between the central values is indicated by a reversed blue column.

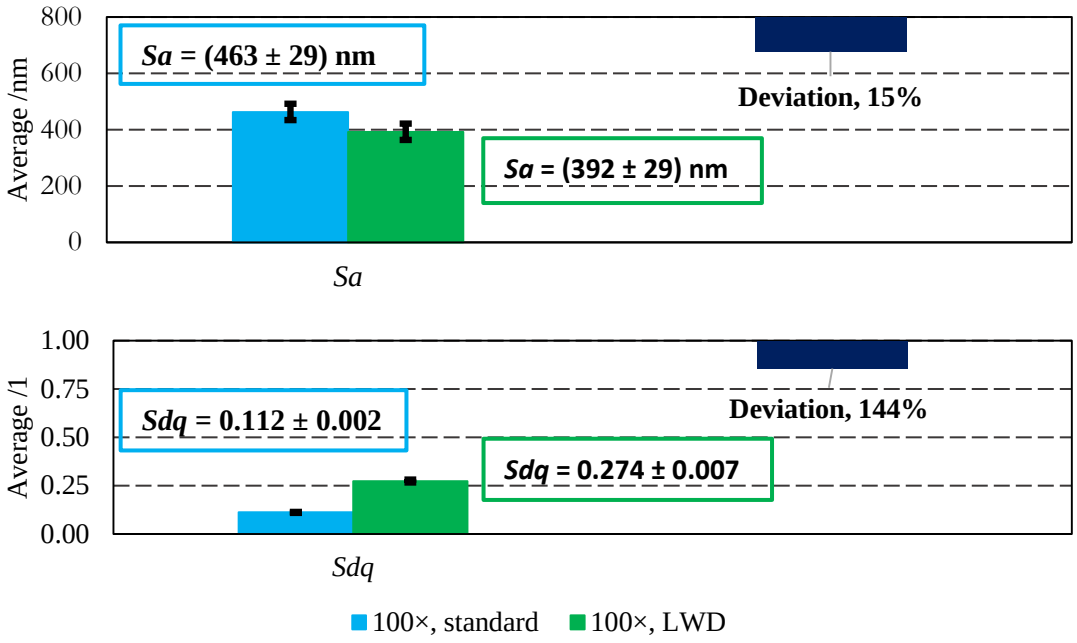

Figure 8.3-5. Measurements of 100× standard and long working distance objectives. No filters applied. The deviation between the central values is indicated by a reversed blue column.

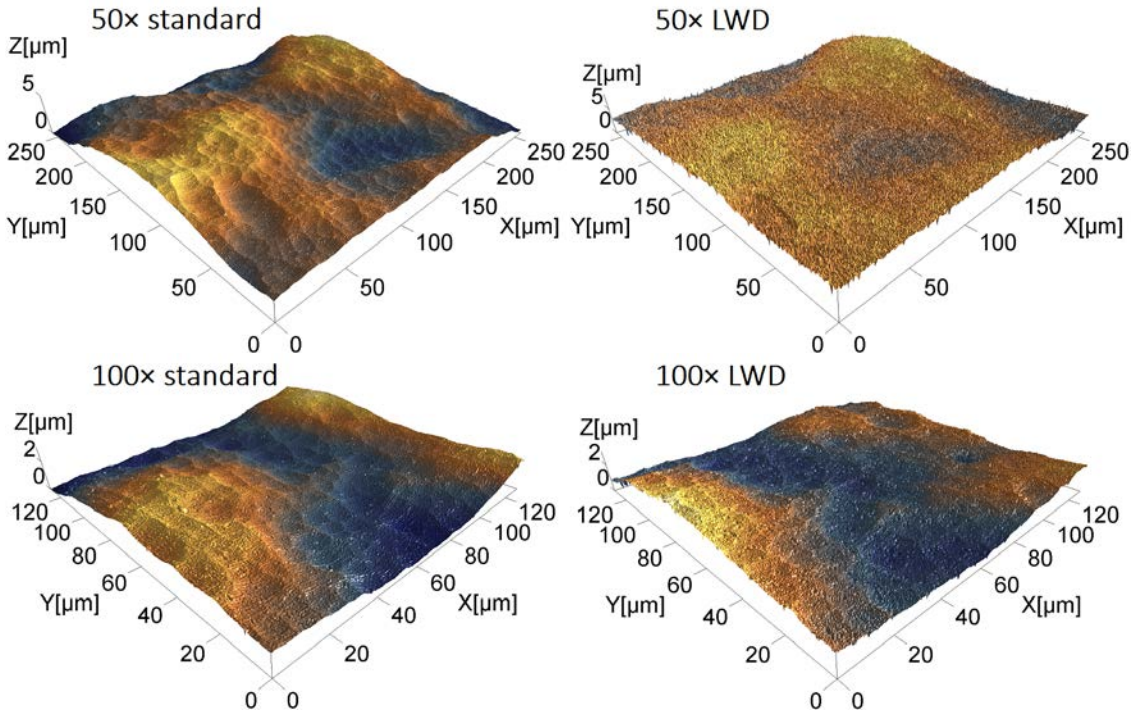

Figure 8.3-6. Example of acquisitions in the same reference coordinates using 50× ST, 100× ST, 50× LWD and 100× LWD.

As summarised in **Table 8.3-1**, the objectives had different numerical apertures. The large deviations of results were due to extended disturbance in the measurements from LWD objectives. The disturbance mainly affected the measurements acquired by the 50× LWD objective, as can be seen from a visual inspection of the 3D-views in **Figure 8.3-6**.

Conversely, standard objectives gave reliable acquisitions even if the 100× ST objective had a reduced field of view that was not enough to achieve most of the variations of the specific surface examined, unless considering the stitching technique.
Disturbance can be filtered by an S-filter (low-pass filter) [7]. Inspecting the harmonic content by a Fourier transform, a nesting index 2.5 µm was chosen for filtering the measurements from 50× LWD objective. An example is shown in **Figure 8.3-7**, where the same 50× LWD surface is shown before and after applying the filter.

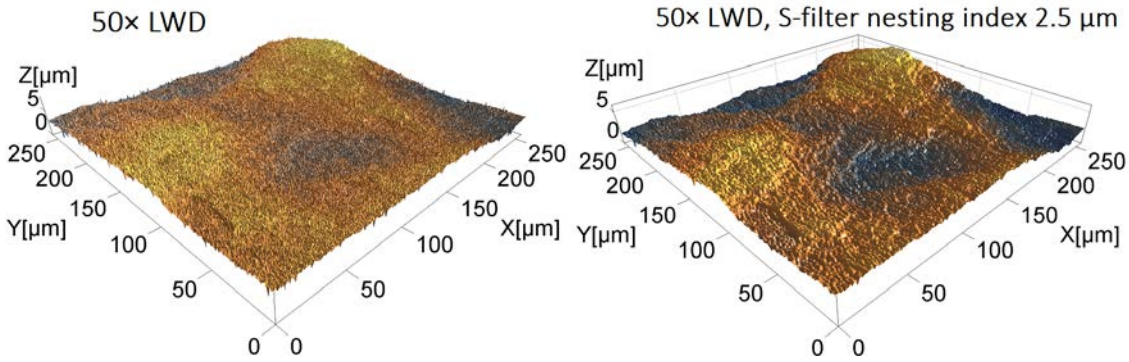

Figure 8.3-7. Acquisition by 50× LWD objective before (left) and after (right) applying an S-filter, nesting index 2.5 µm, to reduce the disturbance on the surface.

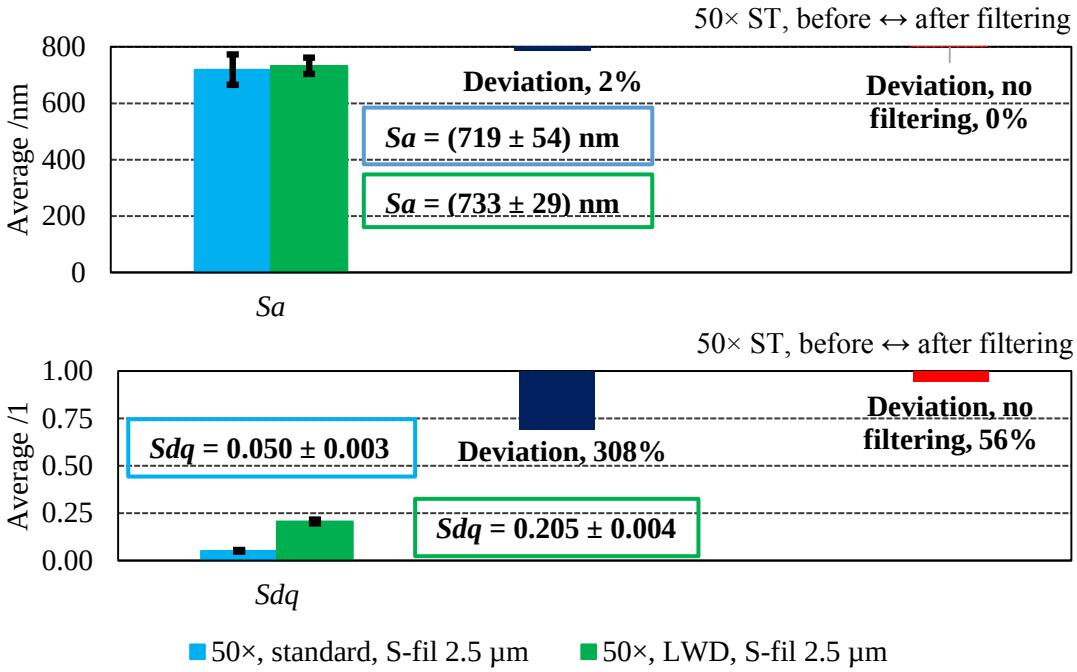

Figure 8.3-8. Measurements of 50× ST and LWD objectives filtered by an S-filter, nesting index 2.5 µm. The deviation between the central values is indicated by a reversed blue column. The deviation between filtered and unfiltered measurements of the 50× ST objective is also given in the graphs by a reversed red column.

Results of the comparison between the filter values from 50× ST and LWD objectives are in **Figure 8.3-8**. A very good agreement was reached for *Sa* between the two objectives. In addition, a comparison between the 50× ST measurements before and after the application of the filter shows that there was no effect on the values due to the filtering.
Regarding the *Sdq* value, the difference between ST and LWD is still huge despite the filter, even if the deviation is reduced with respect to the same case with no filter (see **Figure 8.3-4**). Furthermore, the application of the filter added an effect into the calculation of *Sdq* that, in the specific case, corresponded to an average deviation of 56 % in the measurements of 50× ST.

Considering *Sa* proportional to the average amplitude on the surface and *Sdq* to the average slope, it was possible to control the disturbance introduced by the LWD objectives about the amplitude but not about the slope on the surface. The filter used for eliminating the disturbance was an effect itself for *Sdq*.

8.3.1 LWD objectives noise estimation in an actual case

The comparison between standard and long working distance objectives was repeated with respect to the measurements noise. Therefore, the parameter subject of the study was *Sq*. The well-established averaging and subtraction methods were used. More information about the measurement noise can be found elsewhere ([7]-[9] and § 8.5.5).
Measurements were performed on both an optical flat, from the same Bento Box already introduced in § 8.3 (more details are elsewhere § 8.5.3, [5], [6]), and a polymer Fresnel lenses produced by injection compression moulding (see **Figure 8.3-9**). The previous assessment of LWD objective in § 8.3, in fact, was on a metal surface (AIR-B70). Instead, the aim here was to test the behaviour of LWD objectives on a different material (i.e., transparent polymer) and, in addition, to quantify the noise introduced by the LWD objective.
The measurement noise of OLS was preliminary assessed by applying both averaging and subtraction methods to sixteen repeated measurements, acquired as quick sequence on the same spot of an optical flat, by 50× ST objective. The results are in **Table 8.3-2** for the complete sequence of measurements and for both methods. They estimated the same maximum value Sq_{noise} = 9.7 nm related to 50× ST objective.

Table 8.3-2. Measurement noise by averaging ($Sq_{noise,ave}$) and subtraction ($Sq_{noise,sub}$) methods.

Number of averaged measurements	$Sq_{noise,ave}$/nm	Subtractions	$Sq_{noise,sub}$/nm
2	9.7	1	9.7
3	7.2	2	5.1
4	6.6	3	4.9
5	6.3	4	4.1
6	5.8	5	4.9
7	5.6	6	4.0
8	9.7	7	2.8
9	7.2	8	2.9
10	6.6	9	3.3
11	6.3	10	5.0
12	5.8	11	2.9
13	5.6	12	3.7
14	9.7	13	4.3
15	7.2	14	7.6
16	6.6	15	8.0

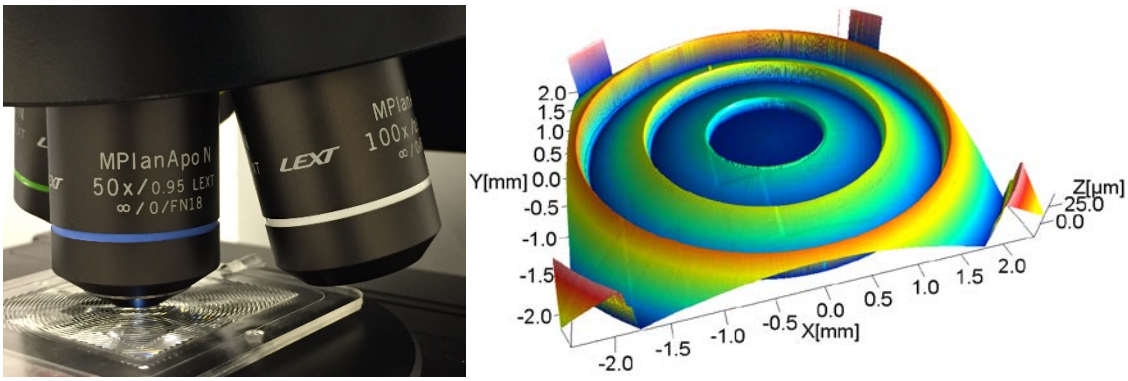

Figure 8.3-9. Left: Fresnel lens used in the noise estimation. It is made of Polymethyl methacrylate (PMMA—Commercial resin Altuglas® V 825T). Right: 3D view of an acquisition of Fresnel lens central area (for demonstration purposes, not used in the evaluation).

The same 50× ST objective and the same methods were successively used to evaluate the measurement noise on the surface of a Fresnel lens (see **Figure 8.3-9**). The results are in close agreement with the previous evaluation of the optical flat. The maximum values for both evaluations by both methods (averaging and subtraction) are in **Figure 8.3-10**. Hence, the measurement noise using a 50× ST objective was assessed at $u_{noise,50\times}$ = 10 nm[9].

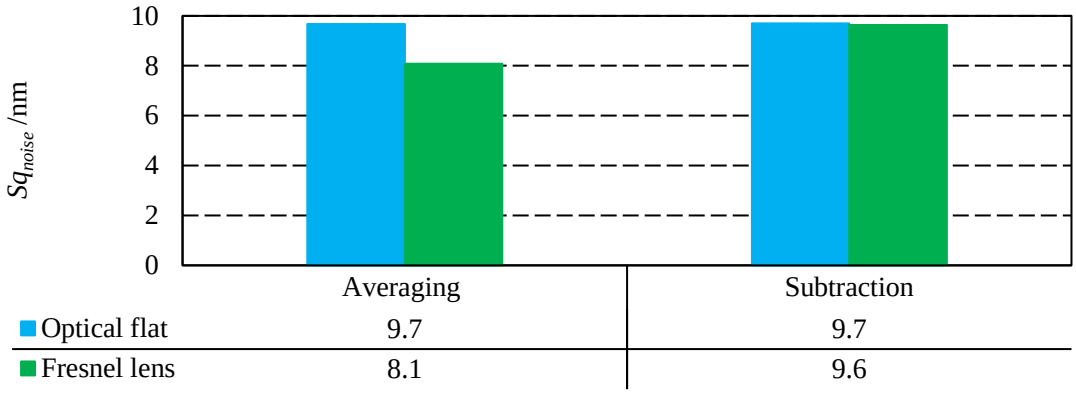

Figure 8.3-10. Measurement noise comparison between the two evaluations, using an optical flat and using a Fresnel lens (maximum values of Sq_{noise}).

The LWD noise estimation was performed considering different measurement conditions:

- 50× ST, 100× ST objectives.
- 50× LWD, 100× LWD.
- For both types of objective, it was considered the effect on the noise of the stray light coming from environment. The measurements were repeated in all the previous cases in a dark environment.

The maximum values of the noise evaluation in the conditions listed above are summarised in **Figure 8.3-11**. The stray light from the environment can have a certain effect on the noise but such effect is deemed meaningless. As a consequence, the noise due to the LWD objectives was evaluated without discriminating the contributor of the stray light, which is always present in the normal use of an instrument and considered part of the measurement noise (see § 8.5.5).

[9] By definition $u_{noise} \equiv Sdq_{noise}$ [42]. In this assessment the choice was to consider the uncertainty contributor related to the noise as the maximum evaluated value.

The assessment of the noise was performed assuming that, when measuring with LWD objectives, the noise introduced is combined to the measurement noise, evaluated on the standard objectives (which are usually used). Thus, the noise introduced by LWD objectives was calculated by quadratic subtraction of the measurement noise, i.e.

$$u_{LWD}^2 = \max_{aver.,subtr.}\{Sq_{noise,LWD,obj}\}^2 - u_{noise,obj}^2 \quad (8.3\text{-}1)$$

where *obj* = {50× ST, 100× ST}. The calculated values are in **Table 8.3-3**.

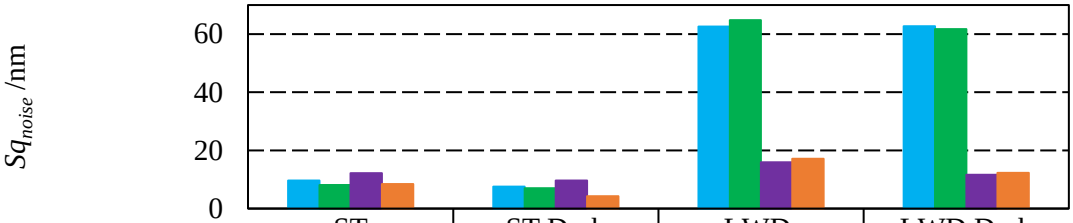

	ST	ST Dark	LWD	LWD Dark
50x Subtraction	9.6	7.5	62.6	62.7
50x Averaging	8.1	7.0	64.8	61.8
100x Subtraction	12.2	9.6	16.0	11.6
100x Averaging	8.4	4.3	17.1	12.2

Figure 8.3-11. Measurement noise related to 50× and 100×, ST and LWD objectives, with and without dark environment.

Table 8.3-3. Estimated noise due to the LWD objectives.

LWD objective	$Sq_{LWD,averaging}$/nm	$Sq_{LWD,subtraction}$/nm
50×	64.0	61.8
100×	13.9	12.4

In conclusion, the noise contributors introduced by the LWD objectives were estimated as $u_{LWD,50\times}$ = 64 nm and $u_{LWD,100\times}$ = 14 nm.

The same evaluated noise ($u_{noise,50\times}$ = 10 nm) on both an optical flat and a polymer specimen suggests the possibility to evaluate the measurement noise on any specimen with surface roughness below the detectable range of the instrument under test. In fact, it was not possible to measure the roughness on the surface of the Fresnel lenses by OLS. According to a recent international comparison of optical instruments (see Chapter 7), OLS is capable of correctly measuring *Sa* roughness of at least 30 nm, therefore, the surface *Sa* roughness of the Fresnel lenses is believed to be largely below 30 nm, as required to optical quality lenses.
The investigation excluded several influence factors that could have been related to the noise of LWD objectives. The author believes that the different optical path of the LWD objectives in a system adapted to the use of standard ones produced multiple reflections that eventually generated the spikes observed. Indeed, 50× LWD objective had the longest working distance among the objectives examined and, correspondingly, introduced the largest amount of disturbances (spikes) in the measurements.

8.4 Performance verification of Olympus Lext OLS 4100 and Alicona Infinite Focus G4 measuring tilted surfaces

When measuring structured and freeform mould inserts, the average normal to the main geometry is typically oriented parallel to the optical axis of the objective. Nonetheless, some parts of such geometry may still be tilted with respect to the average normal and have local normal that forms an angle with the optical axis of the objective.

The maximum slope an objective can detect is fixed by its numerical aperture (see Equation (2.2-1) in § 2.2.4), which is related to the maximum acceptance cone of light admitted inside the objective. On the other hand, the reflection of a light beam on an actual surface is mainly driven by the scattering from a rough surface and not by ray optics, which is an approximation. Therefore, the reflected beam may not always be related to the numerical aperture. In other words, depending on the local roughness and material of the specimen, the tilted surface may scatter (reflect) the most of the radiation outside the acceptance cone of the objective used, even though the tilt angle is smaller than the maximum one set by the numerical aperture.

In this context, the study in this section investigated the behaviour of OLS and G4 when measuring tilted surfaces [10]. The whole set for mould finish comparison already introduced in § 4.4, § 6.3 and § 8.2 was used for the purpose (twelve steel artefacts) [4]. Nominal *Ra* intervals, provided by the manufacturer for the complete set, are in **Table 8.4-1**.

The sensitivity to tilting of the microscopes was analysed calculating the relative deviations of *Sq* and *Sdq*, extracted from measurements of the surfaces in one specified tilted position (12.5° tilt angle), with respect to measurements of the same surfaces at 0° tilt angle. Measurements were carried out in the centre of each artefact, thus performing five repeated acquisitions respectively at 0° and at 12.5° tilt angles. Moreover, all measurement settings were kept the same in the two cases of tilting with the aim of detecting variations for the most due to the angled surfaces. No filtering was applied. The set-up used and an example of artefact are in **Figure 8.4-1**.

The small working distance when using OLS 50× and 100× magnification objectives prevented the use of these lenses. For OLS measurements a 20× (A_N = 0.60) magnification objective was used. Indeed, the 12.5° tilt angle was chosen because it was the highest one possible, considering the limited working distance of OLS 20× magnification objective (1 mm).

On the other hand, G4 provided correct results only when measuring the artefact with highest value of roughness (artefact *A12*—see **Table 8.4-1** and **Figure 8.4-1**), being the surface texture of the other artefacts out of the measurement range of the instrument (see Chapter 7). Hence, the investigation of G4 was consequently carried out on one artefact, though extending it to 20× (A_N = 0.40), 50× (A_N = 0.55) and 100× (A_N = 0.80) magnification objectives (allowed by higher working distances, respectively 13 mm, 10.1 mm and 3.5 mm).

Table 8.4-1. Nominal *Ra* intervals and type of surface machining of the reference artefacts [4].

Artefact	Machining	Nominal *Ra* interval /µm
A1	Diamond buff	< 0.010-0.025
A2		0.025-0.051
A3		0.051-0.076
A4	Grit paper	0.051-0.076
A5		0.100-0.127
A6		0.229-0.254
A7	Stone	0.254-0.304
A8		0.635-0.711
A9		0.965-1.067
A10	Dry blast	0.254-0.304
A11		0.660-0.813
A12		4.826-5.842

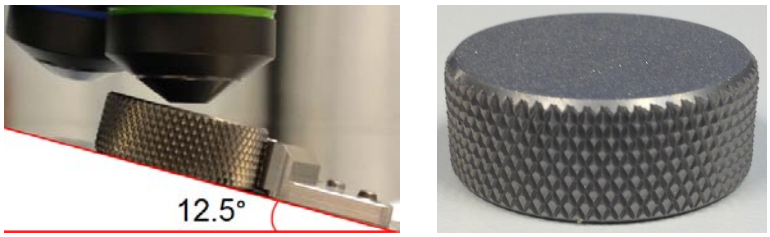

Figure 8.4-1. Experimental tilted set-up of OLS (20× magnification objective) (left). Artefact *A12* (right—see **Table 8.4-1**).

The OLS average results are in the histogram of **Figure 8.4-2**. They showed a conspicuous increase of surface parameters values after tilting the surfaces. In particular, *Sq* deviations were in the range between 18 % and 171 %, while *Sdq* reached deviations between 76 % and 680 %. Considering *Sq*, the largest deviations were observed with the artefacts *A1*, *A2*, *A3*, *A4* (smoothest ones) and *A11*. A tendency to an increase of disturbance (spikes) was also observed. This tendency to spikes significantly increased when considering artefacts *A10*, *A11* and *A12* (dry blasted artefacts) and revealed like disturbances arising symmetrically with respect to the local normal to the surface and ideally placed in correspondence of the laser beam incident spot to the surface (see an example in **Figure 8.4-3** (left)). However, the amount of spikes was such to considerably produce high relative deviations only with the artefacts *A11* and *A12* (roughest ones). No specific trend was noticed for *Sdq* relative deviations, although they were slightly following the trend observed for *Sq* ones.
The G4 average results of *A12* measurements, investigating the influence of tilting for the 20×, 50× and 100× magnification objectives, are in the histogram of **Figure 8.4-4**. The results showed a low sensitivity to 12.5° tilt angle. In particular, relative deviations for the two parameters examined range between 4 % and 11 % among the three objectives, raising up to 20 % when considering *Sdq* measured with 50× magnification. No disturbances due to tilting were detected (see an example in **Figure 8.4-3** (right)).

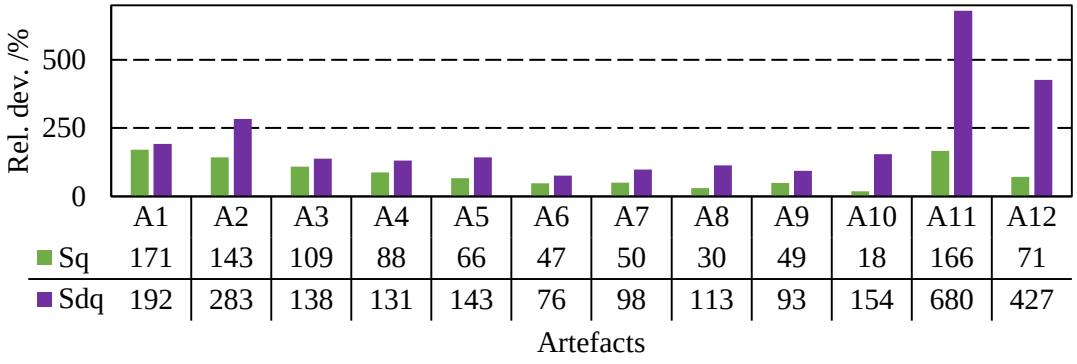

Figure 8.4-2. Relative deviations of *Sq* and *Sdq*, related to OLS, for each of the twelve artefacts measured (20× magnification).

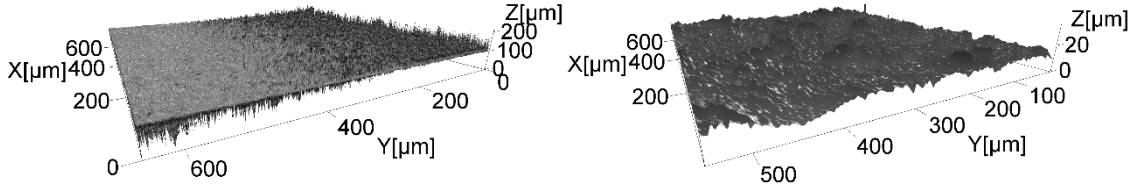

Figure 8.4-3. Example of acquisitions of tilted surfaces (12.5º) of artefact *A12* by OLS 20× magnification objective (left) and G4 20× magnification objective (right).

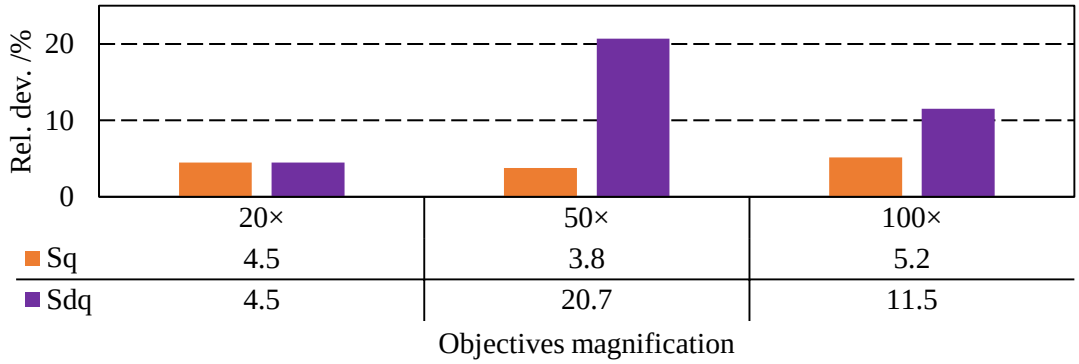

Figure 8.4-4. Relative deviations of *Sq* and *Sdq*, related to G4, for each of the three objectives used for measuring the artefact *A12*.

The investigation could be extended separating the surface tilting dependency in the directions orthogonal and parallel to the dominant texture (if any difference and when a dominant texture can be recognised, i.e., specimens *A4-A9*). Nonetheless, the relative deviations between measurements of flat (0° tilt angle) and tilted surfaces (12.5° tilt angle) showed that the laser beam of OLS was extremely sensitive to the surface tilting. Its dependency on the surface roughness (and type of machining) raises the suspect that the surface tilting generated scattering from rough surface (specific investigations would be required in this direction).
More robust when measuring tilted surfaces (tested at 12.5°) was instead, the white light beam of G4, provided it is used within its operating range, which is basically in the micrometre length scale (see Chapter 7). Conversely, accurate measurements can be achieved by OLS using a fixture to re-establish the orthogonality between the optical axis of the lens and the surface under evaluation.
Eventually, *Sdq* was sensitive to tilting with both instruments. This is a quite obvious result because tilting a surface implicitly changes its local slope!

8.5 Measurement noise of a point autofocus surface topography instrument

In the last study of this chapter, the evaluation of the noise was carried out for a commercial point autofocus instrument (Mitaka MLP-3SP), installed in the manufacturing metrology laboratory at The University of Nottingham (UK). It is an instrument for non-contact profile and areal acquisitions of geometrical and dimensional measurements [11] (see **Figure 8.5-1**). The instrument is described in § 2.2.4.1. After a brief description of the instrument the course of the overall investigation is described.

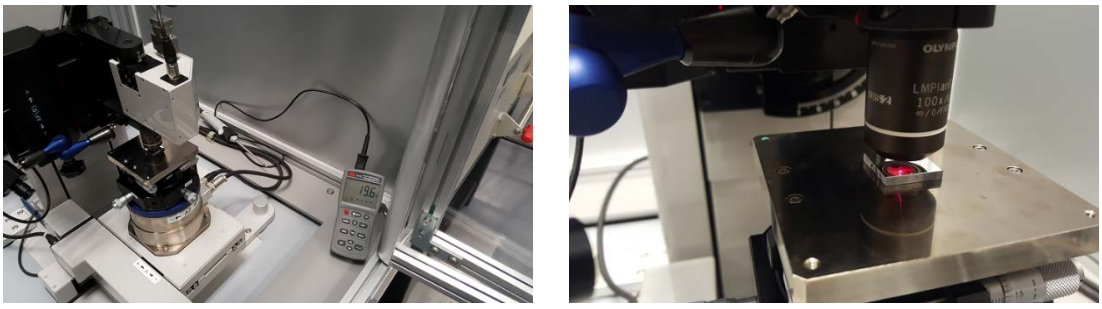

Figure 8.5-1. Mitaka MLP-3SP in its housing chamber (left). Detail of stage hosting the optical flat used in the investigation (right).

8.5.1 Instrument settings

Mitaka MLP-3SP allows for different measurement conditions related to the different possible orientation of the objective nose:

- The optical axis can be positioned horizontally or vertically, i.e., parallel to the *x* axis or parallel to the *z* axis.
- In addition, according to the working principle of the instrument, input and reflected beams pass through the optics at two different sides of the objective, shifted symmetrically (offset) with respect to its optical axis. Thus, an offset axis can be identified, oriented from the input beam towards the reflected beam (see § 2.2.4.1 for more details).
  The offset axis can be oriented in an angle between 0º and 90º with respect to the *x* and *y* axis of the instrument reference system.

The whole investigation was conducted focusing on areal acquisitions and on related matters.
The following selection of settings was considered:

- The optical axis of the objective was always positioned vertically, i.e., parallel to the *z* axis.
- The offset axis was normally set to 90º, i.e., parallel to the *y* axis. Nonetheless, in some cases the position at 0º was also used. Each case is stated below.
  When considering the directions parallel and orthogonal to the offset axis, the objective pupil is filled in different ways thus the following choices were considered favourable and associated with the offset axis setting:
  - Offset axis angle 90º (parallel to the *y* axis)
    1. scanning forward direction of the raster acquisition parallel to *x* axis (tracing direction);
    2. increment forward direction of the lines of the raster acquisition parallel to *y* axis (stepping direction);

    This group of settings is called *straight* raster in the following.
  - Offset axis angle 0º (parallel to the *x* axis)
    1. tracing forward direction parallel to *y* axis;
    2. stepping forward direction parallel to *x* axis;

    This group of settings is called *reversed* raster in the following.
- The width of the areal acquisitions was 100 µm × 100 µm.
- Two sets of sampling distances were used:
  - The set referred as 'high resolution' in the following is
    1. pitch along the tracing direction 0.1 µm;
    2. pitch along the stepping direction 1 µm.
  - The set referred as 'low resolution' in the following is
    1. pitch along the tracing direction 1 µm;
    2. pitch along the stepping direction 1 µm.
- The instrument has different configurations of settings regarding the operation of the active automatic control which adjusts the beam focus, i.e, the relative vertical position of the beam detector. Such active control is called autofocus (AF) system. The possible settings are:
  - Gain: high, standard and low. Standard gain was normally used as gain of the control unit transfer function.
  - Mode: wide, narrow, select. It defines the width of the vertical range in which AF adjusts the beam focus. Narrow mode was always used.
  - AF *dark*: *ON*, *OFF*. If *ON*, AF stops when the light intensity is below a certain threshold. It was always set to *OFF*.
- An objective 100× magnification was used. Related to this objective:
  - Spot size W_{spot} = 1 µm.
  - A_N = 0.8.

- Working distance WD = 3.40 mm.

In addition:

- The nominal vertical resolution is the scale resolution of the vertical sensor measuring the absolute height position δ_z = 10 nm.
- The lateral resolution can be defined according to the optical resolution of the objective and calculated by the Sparrow criterion $R_l \approx 600$ nm.

The results of the investigation are associated to the specified settings. In particular, other factors may influence the measurements when the optical axis is in horizontal position.

8.5.2 Technical hitches

The instrument adopts an uncommon left-handed reference system (see **Figure 8.5-2-(a)** and **Figure 8.5-3-(a)**).
The specimen under measurement, positioned on the instrument stage, can be visualised by a CCD (Charge-Coupled Device) camera which collects incoherent light driven along the optical axis and reflected by the specimen. The CCD camera system is separated from the measuring system (laser source and autofocus mechanism), even though the optical path is partially shared. The specimen is imaged on a display in the user interface. Another external camera is available for a 3D view of the specimen on the stage, imaged on a secondary display in the user interface. This second view is not suitable for measurement purposes.
The view of the specimen on the screen is rotated with respect to the top view of the specimen on the stage. In particular:

- When the offset axis angle is 0°, the specimen appears on the screen rotated clockwise of 90° (see **Figure 8.5-2-(b)** and **Figure 8.5-2-(c)**).
- When the offset axis angle is 90°, the specimen appears on the screen rotated of 180° (**Figure 8.5-3-(b)** and **Figure 8.5-3-(c)**).

The afore mentioned ambiguity makes particularly challenging for the operator to define a local reference system on the specimen. Instead of randomly measuring over a surface, there are a number of advantages in defining a specimen reference system, not last the possibility to compare measurements from different instruments.
At this regard, it should be noted that an areal acquisition has the following constrains:

- 5×10^6 maximum number of points in an areal acquisition.
- 15×10^4 maximum number of points per line.
- 10^4 maximum number of lines.
- 0.1 µm minimum tracing or stepping pitch that can be set.

Such constrains together with the unavoidable drawback of long lasting measurements, which raises more problems related to the instrument sensitivity to the environmental noise (see § 8.5.3), yield to field of view and pixel width which are barely comparable with the ones of other areal measurement instruments.

Moreover, the instrument nose can only fit one objective, meaning that changing an objective implies to manually unscrew it before manually mounting another one. This forces to begin the set-up of the specimen on the stage with a high magnification objective, enhancing the difficulty of understanding the measurement scene, above all when a not known specimen is under measurement.

Finally, tracing and stepping directions had always the same orientation when a raw measurement was imported in the post-processing software [13], meaning that no information was available to discriminate between these two directions. The 3D views in **Figure 8.5-10**, e.g., have set different tracing and stepping directions but they are represented in the same way, as it can easily be spotted by the temperature gradient direction, which is the same for both.

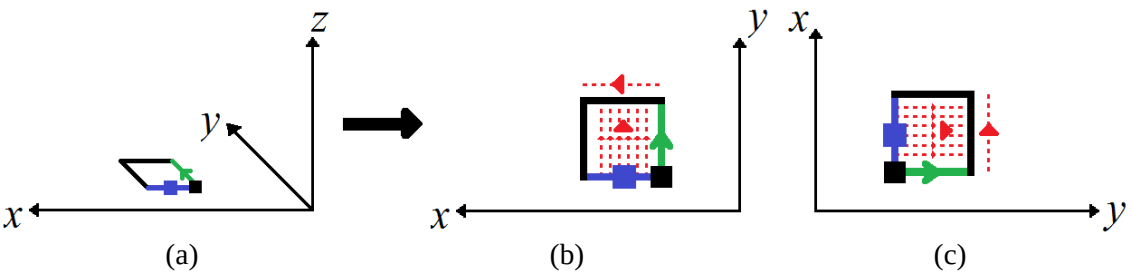

Figure 8.5-2. (a): Representation of a specimen under measurement in the instrument reference system. (b): representation of the specimen on the stage of the instrument (top view scheme); tracing and stepping forward directions (reversed raster settings) when the offset axis angle is 0° indicated in red dashed lines. (c): rotated view of the specimen on the screen of the user interface when the offset axis angle is 0°; corresponding tracing and stepping forward directions are in red dashed lines.

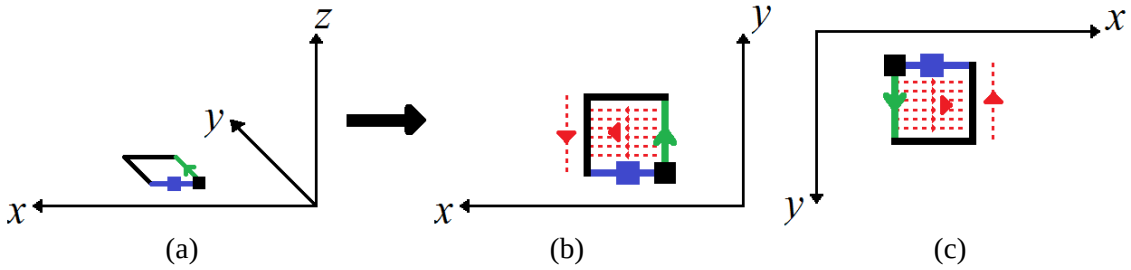

Figure 8.5-3. (a): Representation of a specimen under measurement in the instrument reference system. (b): representation of the specimen on the stage of the instrument (top view scheme); tracing and stepping forward directions (straight raster settings) when the offset axis angle is 90° indicated in red dashed lines. (c): rotated view of the specimen on the screen of the user interface when the offset axis angle is 90°; corresponding tracing and stepping forward directions are in red dashed lines.

8.5.3 Preliminary assessments of the instrument

Measurements of an optical flat

Measurements of an optical flat (see § 8.5.5) were preliminarily performed in a temperature controlled laboratory. The *Sz* calibrated value for the optical flat is 5.3 nm and the declared expanded uncertainty is 10.3 nm (confidence interval of 95 %) [6]. The instrument was initially set for areal acquisitions by straight raster (see § 8.5.1). Two examples of acquisitions are in **Figure 8.5-4-(a)** and **Figure 8.5-4-(b)**, respectively at low and high resolution (see § 8.5.1). Both surfaces have a periodic form superimposed. In particular, the one acquired at high resolution (**Figure 8.5-4-(b)**) shows several periodic components.

Being the specimen under measurement an optical flat, the multi-periodic form was deemed dependent on environmental disturbances. Furthermore, a temperature gradient was induced during the acquisition of the surface in **Figure 8.5-4-(b)**, opening and closing the door of the chamber in which the instrument is housed.

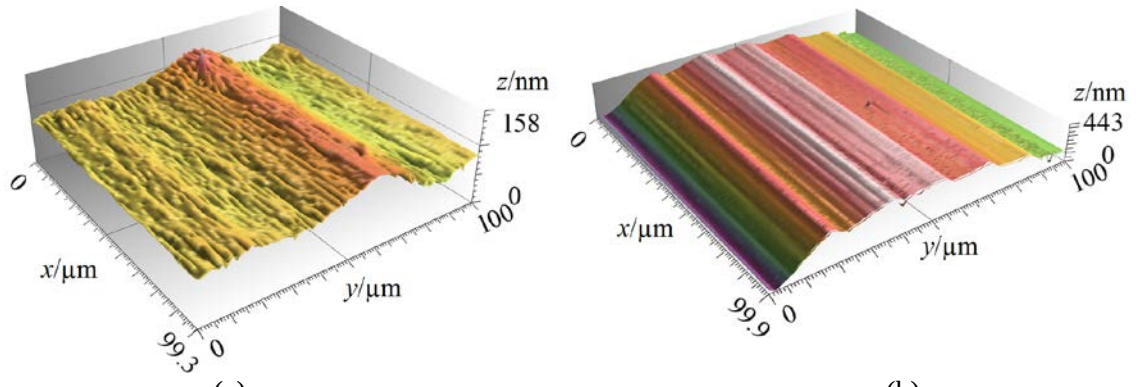

(a) (b)

Figure 8.5-4. Examples of acquired surfaces (not levelled) by straight raster at low resolution (a) and high resolution (b). Both surfaces were measured in a temperature controlled laboratory. A temperature gradient was induced during the measurement of (b).

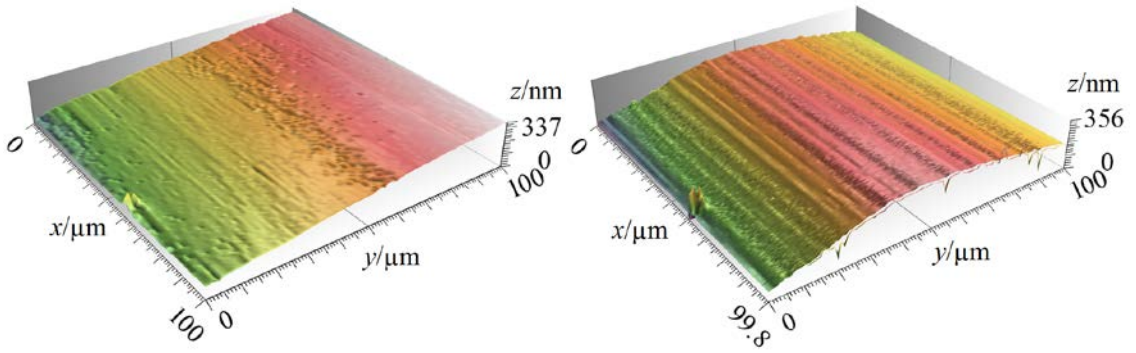

(a) (b)

Figure 8.5-5. Examples of acquired surfaces (not levelled) by straight raster at low resolution (a) and high resolution (b). Both surfaces were measured switching off the air conditioning system in the laboratory.

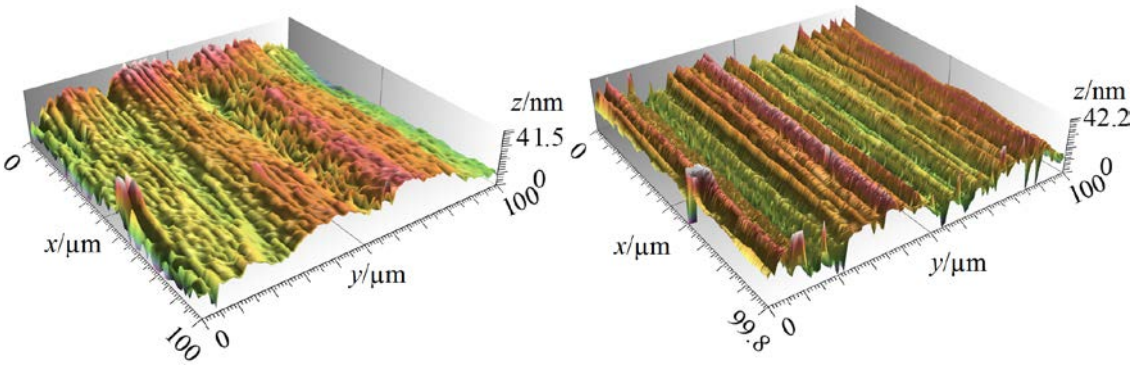

(a) (b)

Figure 8.5-6. Surfaces shown in **Figure 8.5-5** after levelling and correcting the form (low resolution (a) and high resolution (b). Both surfaces were measured switching off the air conditioning system).

The temperature gradient acted as an induced disturbance superimposed to the previously noticed one. The temperature gradient effect is visible in both the areal acquisitions of **Figure 8.5-5**, in which measurements were repeated switching off the air conditioning system. Nonetheless, short periodic components are still evident. They are better shown in **Figure 8.5-6**, where the same surfaces in **Figure 8.5-5** were levelled and corrected for the form.
Acquisitions by reversed raster were repeated, only at high resolution, switching on and off the air conditioning system. They are shown in **Figure 8.5-7**, not levelled, and in **Figure 8.5-8**, levelled and corrected for the form. A behaviour similar to the previous cases can be noticed (see § 8.5.4 for further details).
The results of the measurement sessions are summarised in **Table 8.5-1** for *Sa*, *Sq*, *Sz* and *Sdq* parameters. Before calculating the parameters, all the measurements were levelled subtracting the least square plane. In addition, the measurements affected by form were previously corrected by a fourth order polynomial. The residual waviness was not corrected.
When an uncertainty is indicated it is intended as expanded uncertainty (coverage interval $k = 2$), evaluated considering as contributors the standard deviation of the mean, the reproducibility and the calibration uncertainty. The standard deviation of the mean was extended from a normal distribution to a *t* distribution comparing both distributions at the same confidence interval of 95 %. The calibration uncertainty, provided only for *Sz*, was considered an adequate approximation for all the height parameters. A value for $Sdq^{cal,est}$ was instead estimated weighting the calibration expanded uncertainty stated for Sz^{cal} by the relevant standard deviations in the measurement sessions (Sa^{meas}, Sq^{meas}, Sz^{meas}, Sdq^{meas}).

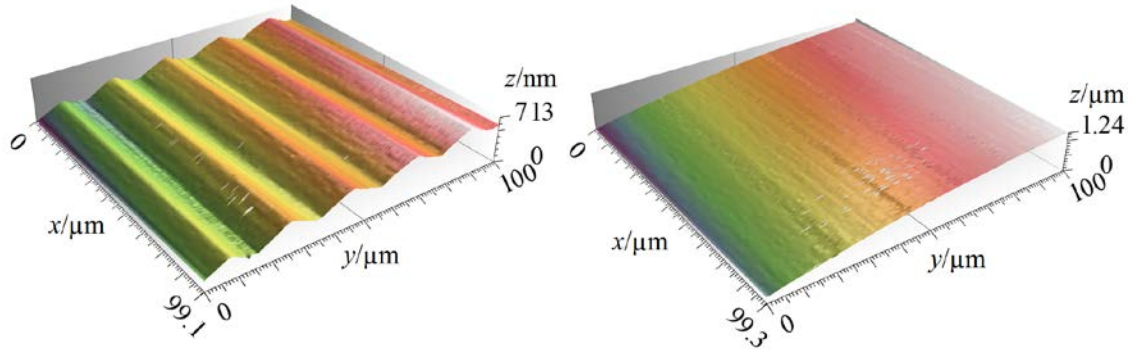

(a) (b)

Figure 8.5-7. Examples of acquired surfaces (not levelled) by reversed raster at high resolution, when the air conditioning system in the laboratory was switched on (a) and off (b).

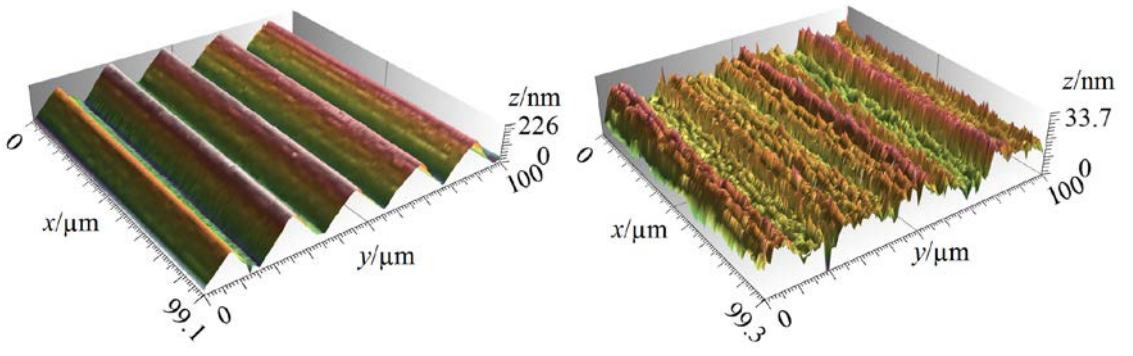

(a) (b)

Figure 8.5-8. Surfaces shown in **Figure 8.5-7** after levelling (air conditioning system in the laboratory switched on (a) and off (b). The surface (b) was corrected for the form. Both surfaces were measured at high resolution).

Table 8.5-1. Results of the measurement sessions shown from **Figure 8.5-4** to **Figure 8.5-8**.

	Sa /nm	*Sq* /nm	*Sz* /nm	*Sdq*	Offset axis	Res.	Air cond.	Repeated meas.
Ave	18	21	137	0.006	Straight	Low	ON	5
U	5	5	20	0.001	Straight			
	23	28	193	0.024	Straight	High	ON	1
Ave	5	6	43	0.005	Straight	Low	OFF	5
U	14	16	78	0.010	Straight			
	6	7	42	0.027	Straight	High	OFF	1
	51	59	226	0.023	Reversed	High	ON	1
	4	5	34	0.017	Reversed	High	OFF	1

Static test on relative position of AF

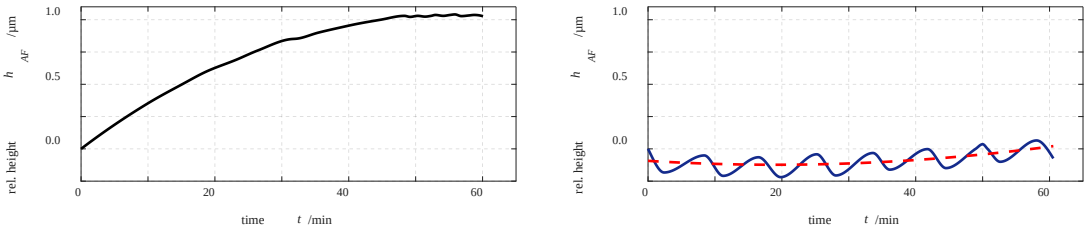

(a) (b)

Figure 8.5-9. Relative position of AF, function of the time, recorded when the air conditioning system in the laboratory was switched off (a) and on (b).

A test was carried out to exclude the influence of the moving stage on the disturbance previously identified.
The test was performed activating the AF from the console of the instrument and continuously focusing on the surface of the optical flat without moving the stage. The AF relative position was read on the counter and the relevant values were recorded together with the correspondent time intervals, measured with a stopwatch, starting from the initial time of the test.
The relative height of the AF is shown in **Figure 8.5-9-(a)**, when the air conditioning system was off, and in **Figure 8.5-9-(b)**, when it was on. Hence, the tendency observed in this section was confirmed by both cases of **Figure 8.5-9**, independently on any moving of the stage.

8.5.4 Environmental noise and temperature gradient

Considering the results in § 8.5.3, measurements were repeated with a probe inside the chamber to quantify the effect of the temperature. Furthermore, high resolution settings were only used because low resolution measurements are clearly not adequate to describe the variations involved. As already introduced in § 8.5.1, high resolution settings consider a tracing pitch of 0.1 µm and a stepping pitch of 1 µm. Such settings gave an acquisition time of about an hour per measurement and was a compromise between the need of resolute acquisitions and a reasonable measuring time. Nonetheless, it should be noted that 1 µm stepping pitch may have under-sampled the oscillation previously described.
Measurements were initially performed with the air conditioning system in the laboratory switched off for both straight and reversed raster (respectively, **Figure 8.5-10-(a)** and **Figure 8.5-10-(b)**).

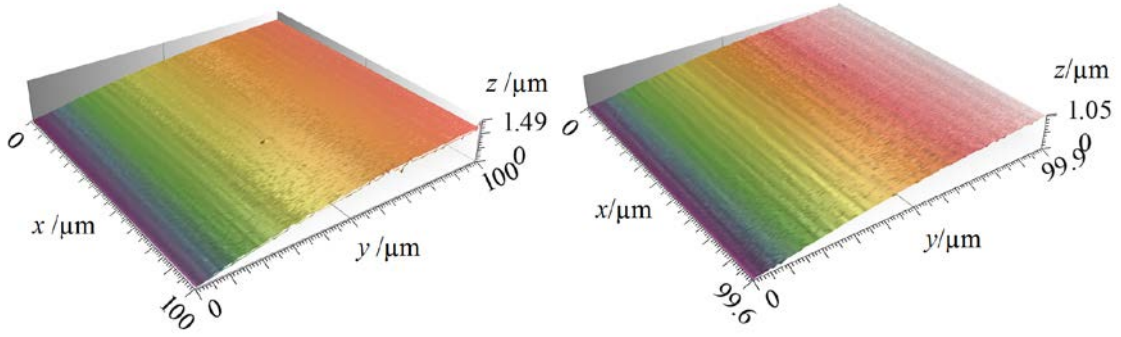

(a) (b)

Figure 8.5-10. High resolution acquired surfaces by straight raster (a) and by reversed raster (b), when the air conditioning system in the laboratory was switched off. Both surfaces are not levelled.

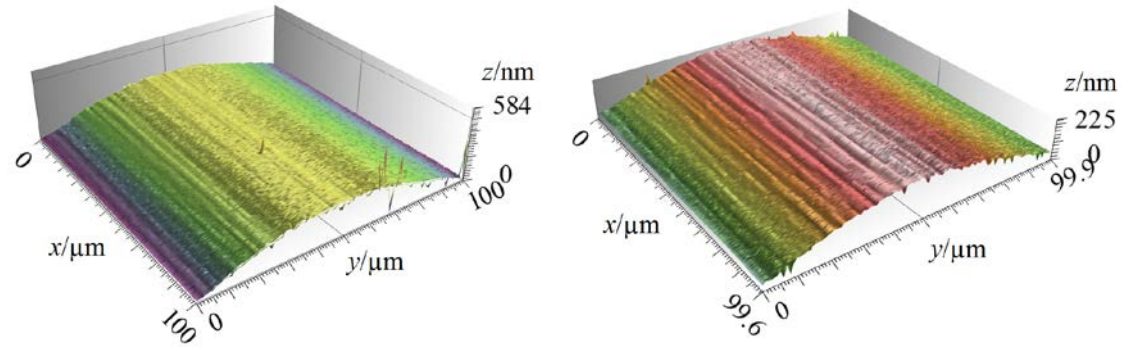

(a) (b)

Figure 8.5-11. Surfaces shown in **Figure 8.5-10** after levelling (straight raster (a) and by reversed raster (b); air conditioning system switched off).

Each acquisition lasted 56 min and the same initial temperature was restored before starting, thus having for both cases an initial temperature T_{start} = 19.9 °C and a final temperature T_{stop} = 20.65 °C, corresponding to a total variation ΔT = 0.75 °C. A thermal sensitivity was estimated as $Sz/\Delta T$, evaluating Sz without levelling the surfaces. It resulted 1.98 µm/°C for the straight raster acquired surface and 1.40 µm/°C for the reversed one.

The surfaces in **Figure 8.5-10** are reported in **Figure 8.5-11** after levelling to show the effect of the temperature drift acting as an added form (bow) to the surface.

A power spectral density (PSD) was calculated orthogonally to the dominant texture of a mean profile, after correcting for the form (2nd order polynomial). The mean profile was extracted from each surface averaging along the direction parallel to the dominant texture. In fact, the texture in this direction was quite uniform and, hence, meaningless for the current investigation.

The PSD for the straight raster acquisition and the reversed one are respectively in **Figure 8.5-12-(a)** and **Figure 8.5-12-(b)**. The magnitude is below 20 nm^2, nonetheless several harmonic components can be identified in about two octaves. Some of them are numbered from 0 to 3 in the graphs. Considering that the acquisition speed was 2 µm/s, the indicated components span from about 0.1 Hz to about 0.2 Hz.

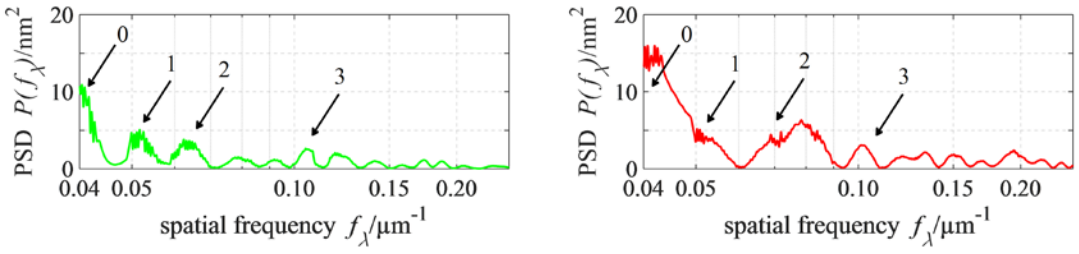

(a) (b)

Figure 8.5-12. Power spectral density (PSD) of a mean profile extracted from the straight raster (a) and reversed raster (b) acquired surfaces shown in **Figure 8.5-11** after correcting for the form. The graphs are in semi-logarithmic scale (f_λ axis). Some harmonic components are indicated with natural numbers.

Despite the small magnitude, the indicated components are systematic and represent a potential source of noise.

In fact, new areal acquisitions, both straight and reversed raster, performed with the air conditioning system switched on (**Figure 8.5-13**), showed PSDs of the extracted mean profiles (**Figure 8.5-14**) with amplified harmonic components. In particular, the component 1 reached a magnitude of about 4000 nm^2.

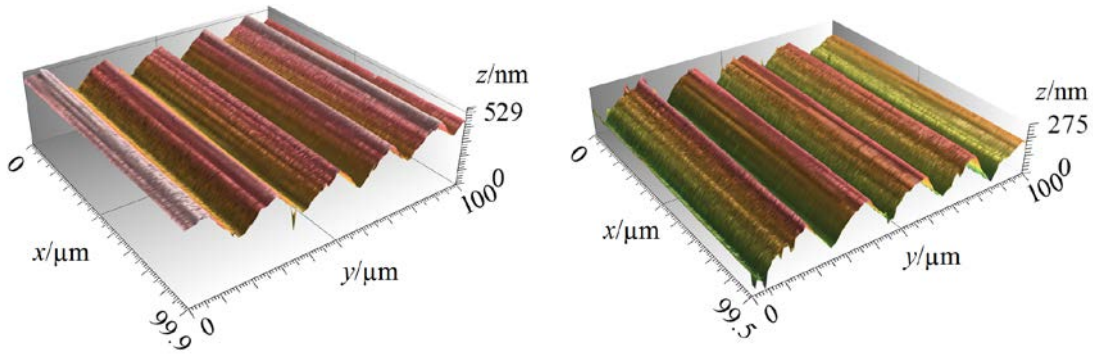

(a) (b)

Figure 8.5-13. High resolution acquired surfaces by straight raster (a) and by reversed raster (b), when the air conditioning system in the laboratory was switched on.

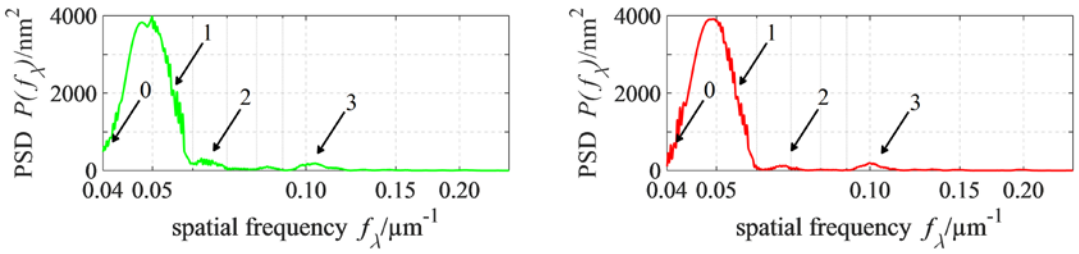

(a) (b)

Figure 8.5-14. PSD of a mean profile extracted from the straight raster (a) and reversed raster (b) acquired surfaces shown in **Figure 8.5-13**, after correcting for the form. The graphs are in semi-logarithmic scale (f_λ axis). Some harmonic components are indicated with natural numbers.

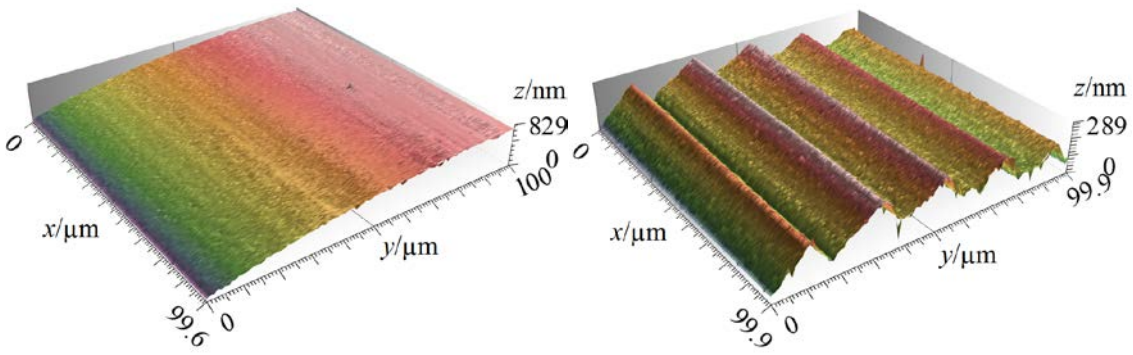

(a) (b)

Figure 8.5-15. High resolution acquired surfaces by straight raster (not levelled), when the air conditioning system in the laboratory was switched off (a) and on (b). In both (a) and (b), the compressed air was removed from the air bearing system.

The Mitaka MLP-3SP instrument evaluated is normally equipped and based on an air bearing, used as a suppression vibration system. According to the manufacturer, the system is passive, even though it normally performs a levelling of the supporting board.
It was not possible to separate such system from the instrument because they shared the power supply. Therefore, some tests were repeated after removing the compressed air from the circuit of the air bearing. The overall system was, thus, a structure with increased stiffness and decreased damping.
High resolution measurements by straight raster were then performed switching on and off the air conditioning system (**Figure 8.5-15**). The related PSDs are in **Figure 8.5-16** and, the same, rescaled in **Figure 8.5-17**. When the air was removed and the air conditioning system was off, the magnitude of the noise was largely below 20 nm^2 and there were no relevant differences with respect to the case shown in **Figure 8.5-12-(a)**, except for the shape of the peaks related to the components 0, 1 and 2, reminding that of a resonance frequency.
When the air was removed and the air conditioning system was on, the component 1 resulted attenuated to a magnitude of about 2500 nm^2. The component 2 remained mostly unchanged. Whilst, the component 3 was amplified to about 400 nm^2 (**Figure 8.5-17-(b)**). The perturbation induced removing the compressed air, however, did not introduce substantial changes in the PSDs and was not enough for confidently concluding that the air bearing was the cause of such behaviour.

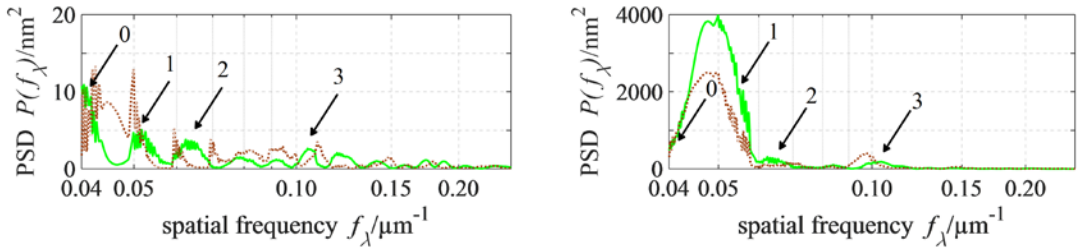

(a) (b)

Figure 8.5-16. (a): PSD (brown dotted-line) of the extracted mean profile of the acquisition in **Figure 8.5-15-(a)**, when the air was removed from the air bearing circuit and the air conditioning system was off. In the same graph, the PSD (continuous green line) of the related case corresponding to the air bearing circuit filled with compressed air is also shown for comparison (already presented in **Figure 8.5-12-(a)**). (b): PSD (brown dotted-line) of the extracted mean profile of the acquisition in **Figure 8.5-15-(b)**, when the air was removed from the air bearing circuit and the air conditioning system was on. In the same graph, the PSD (continuous green line) of the related case corresponding to the air bearing circuit filled with compressed air is also shown for comparison (already presented in **Figure 8.5-14**).

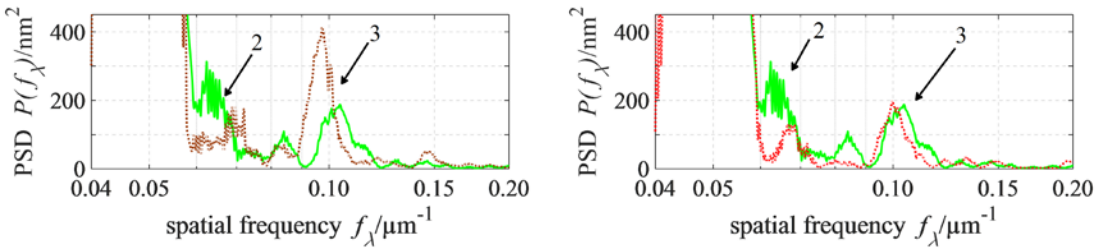

(a) (b)

Figure 8.5-17. (a): Rescaling of **Figure 8.5-16-(b).** PSD (brown dotted-line) of the extracted mean profile of the acquisition in **Figure 8.5-15-(a)**, when the air was removed from air bearing circuit and the air conditioning system was on. In the same graph, the PSD (continuous line green) of the related case corresponding to the air bearing circuit filled with compressed air is also shown for comparison (already presented in **Figure 8.5-12-(a)**). (b): rescaling of **Figure 8.5-14-(a)** (continuous green line) and of **Figure 8.5-14-(b)** (red-dotted line). The picture is shown for comparison of the components 2 and 3.

Temperature correction routine

The last examination was related with the temperature correction routine of the instrument software. It is a tool intended for correcting the drift due to the temperature. When it is activated, a reference position on the surface under measurement is to be set as well as an amount of lines is to be specified. After and every specified number of lines the reference position is compared with the first reference value. Such difference is the amount used for correcting the successive scanned lines.

High resolution measurements by straight raster using the temperature correction routine are shown in **Figure 8.5-18** for both cases with and without active air conditioning system.

The PDSs (**Figure 8.5-19**) showed a new evident component around f_λ = 0.15 μm^{-1} (red dashed-arrow in **Figure 8.5-19-(a)**). Moreover, when the air conditioning system was switched on, the temperature correction routine attenuated the component 1 but considerably increased component 3. Hence, the effect of the routine was a systematic behaviour superimposed to the other disturbance. Such behaviour was not further investigated but it is believed to be dependent also on the number of lines set for the 'refresh' (ten lines in the example shown).

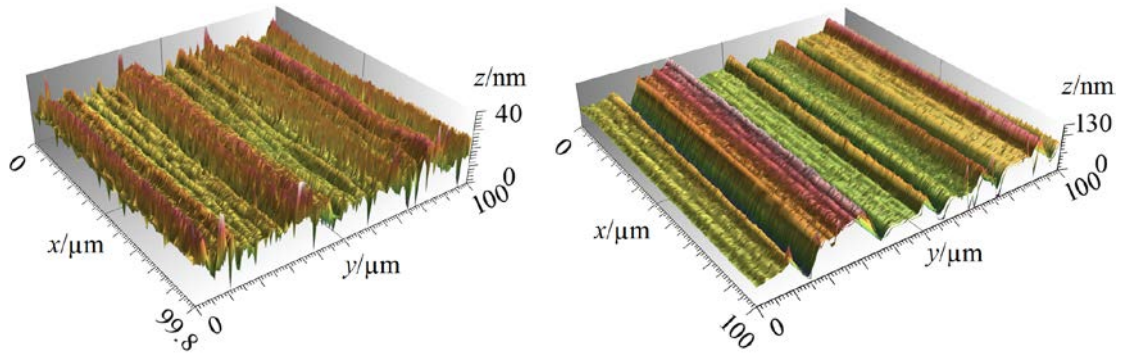

(a) (b)

Figure 8.5-18. High resolution acquired surfaces (levelled) by straight raster, when the air conditioning system in the laboratory was switched off (a) and on (b), using the temperature correction routine.

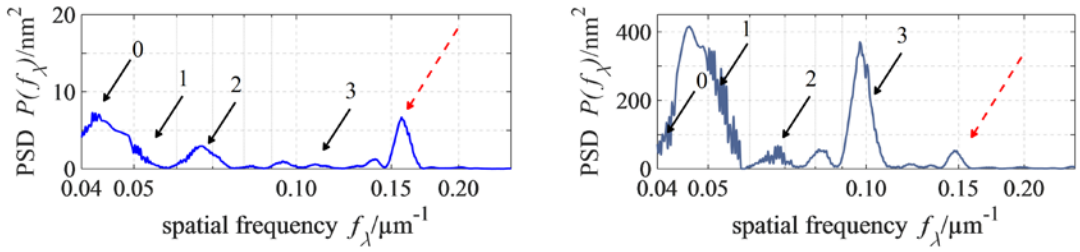

(a) (b)

Figure 8.5-19. Power spectral density (PSD) of a mean profiles extracted from the straight raster acquired surfaces in **Figure 8.5-18**, using the temperature correction routine, when the air conditioning system is switched off (a) and on (b). A new appeared harmonic component is indicated by a red dashed-arrow in both graphs.

8.5.5 Measurement noise

Optical instruments for areal topography measurement can be especially sensitive to noise when scanning is required. Such noise has different sources, including those internally generated and external sources from the environment [7], [12]. Internally generated noise is defined in ISO 25178 part 600 [7] as *instrument noise* while external sources are defined in the same document [7] as *environmental noise*. The combination of these two contributors is defined as *static noise* [7], i.e., the noise "on the output signal when the instrument is not scanning laterally" [7]. For some instruments, it is not always possible to evaluate each single contributor because they acquire data while scanning, i.e., while moving laterally. Nevertheless, it is possible to evaluate the noise added to the output during the normal use of the instrument. Such noise is defined in [7] as *measurement noise*, which includes the static noise. When this document is being written, ISO 25178 part 600 [7] is a draft not issued, yet. However, the same definitions can be found in ISO 25178 part 605 [12].

The measurement noise was measured by an optical flat with a calibrated *Sz* value of 5.3 nm and declared expanded uncertainty of 10.3 nm (confidence interval of 95 %) [6]. The artefact belongs to a set for areal calibration of optical instruments denominated 'Bento Box' (NPL-BNT 025), which was produced at the National Physical Laboratory (NPL), Teddington, UK [5] and already introduced in § 8.3.

The instrument was set for straight raster acquisitions at high resolution. The measurement noise was evaluated by applying to five repeated measurements the subtraction and averaging methods, described elsewhere [8]-[9]. The results revealed a relatively high level of measurement noise with a maximum calculated value of 38 nm (both averaging and subtraction method) and a minimum of 20 nm (subtraction method). Results for different number of averaged measurements and subtractions between different successive measurements are summarised in **Table 8.5-2**.

Table 8.5-2. Measurement noise by averaging ($Sq_{noise,ave}$) and subtraction ($Sq_{noise,sub}$) methods.

Number of averaged measurements	$Sq_{noise,ave}$/nm	Subtractions	$Sq_{noise,sub}$/nm
2	38	1	38
3	33	2	20
4	30	3	20
5	32	4	30

8.5.5.1Repeated measurements and frequency analysis

In total seven repeated measurements were performed in one-day-measuring session (about seven hours). The first acquisition was taken for warming up the instrument, hence, it was not considered in the evaluation. The last one was excluded because substantially different from the others. The average temperature into the instrument chamber during the entire session was T_{mean} = 19.2 °C, with a maximum temperature variation during each acquisition which was equal or lower than ΔT_{max} = 0.3 °C. The temperature into the chamber was kept under steady condition, with the door closed, which, nonetheless, corresponded to a systematic temperature oscillation of about ΔT_O = ±0.1 °C.

All acquisitions were levelled subtracting the least square plane. Some disturbances (spikes) were eliminated by 'thresholding' the surface without impairing the measurement. Lastly, in one case (repeated measurement nr. 6), it was necessary to correct a thermal drift with a second order polynomial (see **Figure 8.5-20**). The overall temperature variation in this case was $\Delta T'_{max}$ = 0.2 °C which, being the same or lower than other acquisitions, did not explain the thermal drift. A temperature variation of different nature may have occurred within the instrument that was not detected by the probe in the chamber.

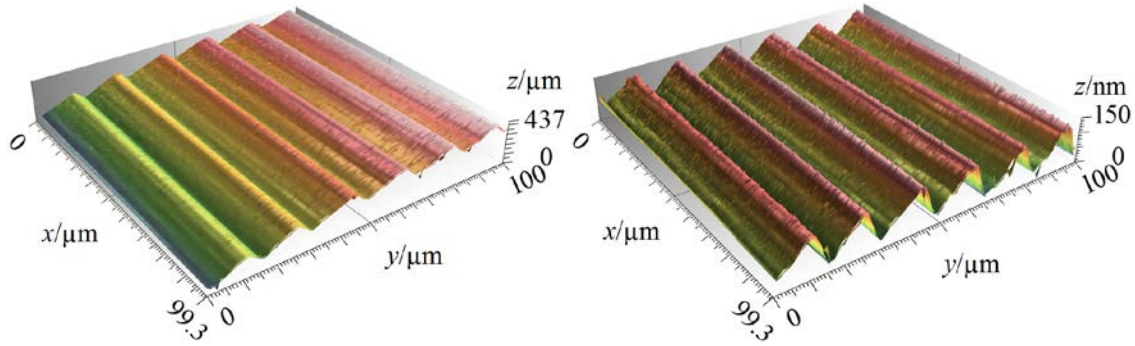

(a) (b)

Figure 8.5-20. Repeated measurement 6 before (a) and after (b) applying a second order correction.

In **Figure 8.5-21**, the PSDs of the seven repeated measurements are represented. In particular, **Figure 8.5-21-(a)** shows the PSDs of the first four acquisitions (1-4) and **Figure 8.5-21-(b)** shows the PSDs of the last three ones (5-7). Almost all the measurements have a magnitude of around 2000 nm^2. Starting from acquisition nr. 5 the main peak moves from component 2 towards component 1 and increases of magnitude up to 3000 nm^2. In the same figure (both graphs), the PSD of **Figure 8.5-14-(a)** in § 8.5.4 is also re-drawn for comparison.

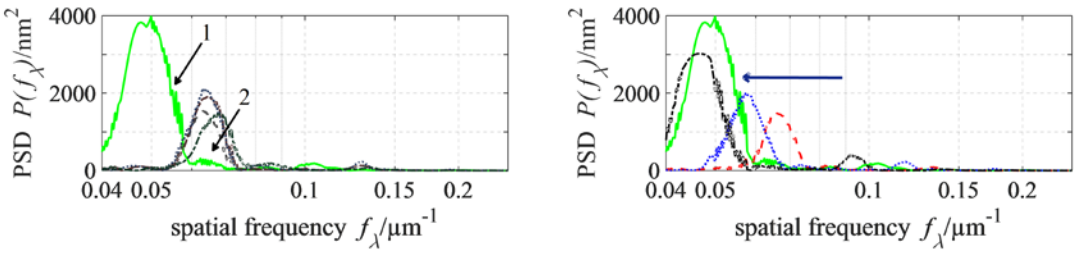

(a) (b)

Figure 8.5-21. PSD of the seven repeated measurements (non-continuous curves). The continuous green curve is the PSD in **Figure 8.5-14-(a)** of § 8.5.4. (a): PSDs of the repeated measurements 1-4. (b): PSDs of the repeated measurements 5-7. The arrow indicates the tendency of the peak from repeated measurements 5 to 7.

Several measurements in different conditions and settings were performed on an optical flat using the Mitaka MLP-3SP instrument. Such measurements may slightly be influenced by the sampling distance chosen (0.1 µm tracing pitch and 1 µm stepping pitch). Nevertheless, the tendency found is general, proven that in both 0^o and 90^o orientation of the offset axis, and, at worst, it may result under-sampled in the stepping direction.
The measurements allowed evidencing a dependency of the instrument on the temperature that was estimated, in the worst case, as about 2 µm/^{o}C over one hour measuring time.
The effect of the temperature on the measurement is a bow on the acquired surface allegedly added along the stepping direction. It was not possible to exactly detect the temperature gradient direction because, as specified in § 8.5.2, no information was available in the raw data to discriminate between tracing and stepping directions.
Another periodic disturbance was superimposed to the thermal drift and it was associated to the air conditioning system in the laboratory, independently from any moving of the stage. In fact, a temperature oscillation in steady state condition possibly explains the periodic thermal drifting on the surfaces (ripple). Nonetheless, such temperature oscillation into the chamber was only recorded when the instrument was turned on and not noticed when the instrument was completely turned off. Hence, it seems more compatible with the wave nature of light. At this regard, it should be noted that a frequency analysis showed systematic harmonic components which existed despite the air conditioning system and which were otherwise be amplified when the air conditioning system was active in the laboratory. Moreover, the periodic disturbance also increased with the continuous use of the instrument. Supposedly, the prolonged use added a noise component that may be assumed as instrument noise. Further investigations would have been required on this track (self-induced thermal disturbance, thermal stabilisation of the laser, electromagnetic compatibility, etc.) which were not undertaken because beyond the purpose of this course of study.

8.6 Discussion

Advances in manufacturing poses new challenges to optical instruments. New advances may be required. Some of them appear to be easily achievable and some others seem connected with the technological limits of a working principle.
Structured and freeform surfaces need specific metrological techniques to be assessed. The local slope on their surfaces is an important feature to be measured. In this view, some issue related to the optical instruments is to be treated carefully. On the other hand, the *Sdq* parameter that was used to assess the slope is not adequate in many circumstances and also difficult to be assessed consistently.

Furthermore, high lateral and vertical resolution combined with large acquisition areas (e.g. by means of stitching methods) and high acquisition speed are of high importance for large-area micro/nano manufacturing. However, even though these performances can be achieved with state-of-the-art equipment, in these measurement conditions the amount of data to be stored and the requirement for high data transfer rates pose challenges to the hardware of instruments that can reach the limit of their capability. More powerful electronics appear to be needed for the instruments to cope with the high demands of modern advanced manufacturing technologies as, e.g., in large-area micro/nano manufacturing.

Eventually, the investigation evidenced some issues that can affects an instrument in its environment. In particular, different environmental sources were identified (thermal drifts, air conditioning system, stray light), which can introduce substantial environmental noise into the measurements. But, also, it arose that a prolonged use of an instrument can generate internal noise and ‘invisibly’ counterfeit the measurement results.
The proposed method can be useful to verify whether acquisitions are affected by noise, e.g., in comparison with other reference acquisitions.

8.7 Conclusion

The international comparison of optical instruments in the previous Chapter 7 unveiled the state-of-the-art performance in the sub-micrometre scale for the three main microscopes working principle currently used in areal topography measurement. In this chapter, the limits of such performance, in specific cases that can arise during practical operation and that are becoming more and more common in modern micro- and nano-manufacturing, were investigated.

Indeed, all optical instruments present several advantages in modern micro/nano-manufacturing. However, they also have technological limits, which must be known to the operator in order to properly use them. Some techniques for performance analysis were presented here. Nonetheless, the straightforward way for achieving the best instruments' performance is to follow the guidelines of instruments' manufactures which, on the other hand, should state those limits clearly.

Incomplete specifications can lead to the use of an instrument outside the limits imposed by its technical specifications and characteristics. In those situations, an improper use of a properly selected instrument can raise the false requirement of modifying by post-processing the measurements (e.g., filtering, de-spiking, etc.).

The author believes that measurements should be treated statistically and not modified (filtered) to suit an instrument. Certainly, the instrument has to be properly chosen according to the quantities under evaluation.

8.8 Outlook

An investigation of the scattering from rough surface may be worth pursuing in the view of producing reference surface artefacts for the calibration of optical instruments.

Using material and/or grade of roughness to enhance the phenomenon can assist to state objectives limits. Conversely, suppressing it can help to measure other metrological characteristics without the influence of a spurious phenomenon.

References

[1] CGM (Center for Geometrical Metrology), DANAK Calibration certificate n. Rou99022, Roughness Standard ISO 5436 type D, Serial number 2074PTB82, mrk. 322 (manufacturer PTB, Braunschweig) date of issue 01-07-1999

[2] CGM (Center for Geometrical Metrology), DANAK Calibration certificate n. Rou99029, Roughness Standard ISO 5436 type D, Serial number Mrk. 625 (manufacturer PTB, Braunschweig) date of issue 15-07-1999

[3] CGM (Center for Geometrical Metrology), DANAK Calibration certificate n. Rou03032, Roughness Standard ISO 5436 type D, Serial number Mrk. 619 (manufacturer Halle) date of issue 17-12-2003

[4] DME Mold Finish Comparison Kit – DME Company, www.dme.net

[5] www.npl.co.uk/nanometrology

[6] National Physical laboratory, Certificate of Calibration – Areal calibration set NPL-BNT 025 Reference 2015120069/1 Issued on 17/05/16

[7] ISO/DIS 25178-600: 2016 Geometrical product specification (GPS) — Surface texture: Areal – Part 600: Nominal characteristics of non-contact (variable focus) instruments. ISO DIS 25178 part 600 (Geneva: International Organization for Standardization)

[8] Giusca C L and Leach R K 2012 Calibration of the metrological characteristics of Imaging Confocal Microscopes (ICMs) NPL Good Practice Guide No. 128 (Teddington, UK: National Physical Laboratory)

[9] Giusca C L, Leach R K, Helary F, Gutauskas T and Nimishakavi L 2012 Calibration of the scales of areal surface topography-measuring instruments: part 1. Measurement noise and residual flatness Meas. *Sci. Technol.* **23** 35008

[10] Quagliotti D, Baruffi F, Tosello G, Gasparin S, Annoni M, Parenti P, Sobiecki R and Hansen H N 2016 Performance verification of focus variation and confocal microscopes measuring ultra-fine tilted surfaces *Proc. of the 16th international conference of the european society for precision engineering and nanotechnology (euspen)* (Nottimgham: P. Bointon, R. Leach, N. Southon) 169-170 Nottingham, UK, 30 May – 3 June 2016 (ISBN 14: 978-0-9566790-8-6)

[11] Leach R 2011 *Optical Measurement of Surface Topography* ed R Leach (Berlin, Heidelberg: Springer Berlin Heidelberg) chapter 6

[12] ISO 25178-605: 2014 Geometrical product specification (GPS) — Surface texture: Areal – Part 605: Nominal characteristics of non-contact (point autofocus probe) instruments (International Organization of Standardization)

[13] MountainsMap® Premium, www.digitalsurf.com

Chapter 9

Conclusion

9.1 Summary

The achievement of a full replication is essential in advanced injection moulding technologies. The required accuracy for the manufacture of micro moulded components must be confirmed by means of a metrological approach. Therefore, it is mostly critical when dealing with increasingly small dimensions. As highlighted in § 3.1, in fact, precision injection moulding, micro injection moulding and injection compression moulding of thermoplastic polymers (advanced moulding technologies) allow the replication of features having vertical size between (50-100) nm and (100-500) µm, and lateral size between (100-1000) nm and (100-500) µm. Considering such small dimensions, a successful verification of a tolerance requires, of course, the establishment of the traceability but, also, a satisfactory evaluation of measurement uncertainty.
The methods currently available in manufacturing are based on the *upper bound strategy* (see § 2.3.1). Therefore, they are not satisfactory at this length scale because they may lead to an overestimation of the uncertainty. On the other side, in micro manufacturing, there are no shared methodologies that deals with the uncertainty evaluation of feature of size in the sub-millimetre scale. Several approaches are suggested (reviewed in Chapter 4) and the risk is that the evaluation may result insufficient and not adequate to be compared among different assessments. All this arose clearly in the comparison described in Chapter 7.
The research undertaken during the Ph.D. project was dedicated to develop and implement a complete metrological structure for micro/nano dimensional and topographic measurements with respect to uncertainty evaluation and traceability, formulation of specification intervals, assessment of the replication of moulded parts and a deep investigation on the performance of the optical instruments currently available in the field. These four main topics have been the main focus of the research and they reflect the structure of this thesis. The most relevant results are summarised in the following.

- *Uncertainty evaluation and traceability*. The uncertainty evaluation and the achievement of the traceability were realised by a statistical methodology based on the theorem of central limit (frequentist approach). The method was implemented through study cases that established the procedure and the terms of its validity. In particular, it is based on the correction of the systematic behaviour in the experimental distribution and allowed to reduce the evaluated uncertainty when it was properly implemented, i.e., when the hypotheses of the theorem of central limit were satisfied. In other words, the method was effective to separate the variability due to the manufacturing process from the variability due to the instrument, being the latter corrected as systematic behaviour, thus, intrinsically reducing the evaluated uncertainty.

- *Formulation of specification intervals.* The formulation of specification intervals (tolerances allocation) was achieved for any moulding process in which the material undergoes a change in dimensions from the mould cavity, due to a phase transformation, i.e., for those processes in which a shrinkage and its uncertainty can be assessed. The method can deal with multiscale manufactured components and discriminate the different behaviour of 1D and 2D features of size.
  Two principal hypotheses characterise the method.

  - The master geometry and the final components (affected by shrinkage) were considered correlated.
  - The uncertainty evaluated for both master geometry and final parts was propagated to the uncertainty of the shrinkage as coverage interval, evaluated according to a confidence level of the same amount of the desired conformance probability, thus, giving to the producer a risk of rejecting a part, in future evaluations, established according to a desired conformance probability.

- *Replication assessment of moulded parts*. The replication process and the replication fidelity of moulded components were investigated by different metrological techniques:
  - Uncertainty contributors of repeatability and reproducibility to define the variability of the production.
  - Amplitude and slope replication of the features on the surface described by roughness parameters.
  - Approximated evaluation of the uncertainty of the replication fidelity.
  - Evaluation of the uncertainty of the replication fidelity by the usual formula for the propagation of the variances.

- *Performance of the optical instruments*. A number of observations were possible analysing the results of an international comparison of optical instruments. These considerations established the current state-of-the-art of areal surface texture measurement instruments.
  Three working principle were identified among the instrument participating to the comparison: confocal microscopy, coherent scanning interferometry and focus variation microscopy. All instruments showed limitations, largely depending on the technology of the instruments used. In particular, better performance on sub-micrometre surfaces were obtained by using coherent scanning interferometry and confocal microscopy, the latter with the closest results to the reference values. While it appears that such surfaces could not be measured correctly by focus variation microscopy (possibly due to the effect of local roughness). Differences also emerged in the quantification of the uncertainty for the evaluated surface parameters, mainly due to different uncertainty models considered but, also, not appropriate transfer standards for the assessment of the instrument uncertainty contributor.

  Another investigation enhanced limitations of the performance of some optical instruments, in specific cases that are becoming more and more common in modern micro and nano manufacturing (long working distance objectives, measurements on a tilted surface). Additionally, the investigation evidenced some issues that can affects an instrument in its environment. In particular, different environmental sources were identified (thermal drifts, air conditioning system, stray light), which can introduce substantial environmental noise into the measurements. But, also, it arose that a prolonged use of an instrument can generate internal noise and can ‘invisibly’ counterfeit the measurement results. A method was proposed to verify whether acquisitions are affected by noise.

  Eventually, it is worth to mention a mutual dependence of the quality of the measurement process on the quality of the production: the measurement process influenced the quality assurance but, in turn, the lack of quality of the parts influenced the measurement process.

9.2 Outlook

The investigations and the achievements of the present work have provided new knowledge and substantial progressions, beyond the state of the art, in relation to the uncertainty modelling for micro/nano dimensional and topographic measurement and to the formulation of specification intervals based on the evaluation of the shrinkage uncertainty.
The mentioned activities opened a variety of new research opportunities which are either on their way to be investigated or are already started, also by virtue of the collaborations established during the Ph.D. project.
Further research works are/will be dealing with the following points.

- The developed method for uncertainty evaluation will be improved. A drawback resulted in the indirect way of achieving the traceability against contact measurements.
  A new collaboration will start soon with the main goal of achieving a stand-alone calibration of optical instruments. A further reduction of the measurement uncertainty is, in fact, envisaged in this direction. Intermediate passage will be a modification of the method for referencing the traceability to material measures (calibrated artefacts).
  Inspiring to the substitution method normally used with measurements of coordinate measuring machines (ISO 15530 series), material measures will be used for determining one or more calibration equations, related to the optical instruments under examination, in the range of interest.
  Furthermore, a software implementation of the procedure is also on schedule. The software implementation would allow the use of the procedure to a larger number of users and, especially, in combination with automated instruments.

- The method for the formulation of specification intervals could be applied to a more conventional micro injection moulding production where the shrinkage can be defined on the injected polymer parts with respect to the dimensions of the tool insert.
  Furthermore, other approaches for uncertainty evaluation can be used, in particular, the frequentist approach could be used to eliminate the influence of the measurement process by correcting the systematic behaviour.

- The frequentist approach could also be suitable in conjunction with the replication assessment because of the possibility to reduce the influence of the measurement instrument with respect to the process variability. The method will be adopted for an optimised assessment of the replication fidelity.

- New tools for the investigation of the replication could be explored. The angular spectrum and the frequency analysis, in general, could be examined. In particular, the wavelet transform could allow to relate local changes in uneven surfaces to the corresponding portion of a surface.

- The use of the mixture (multivariate normal distribution) could be investigated deeper for specific applications, e.g., in the comparison of different instruments to highlight the behaviour of specific instruments, or for inspecting unevenness of surfaces with respect to a reference spot.

- An investigation of the scattering from rough surface could be worth pursuing in the view of producing reference surface artefacts for the calibration of optical instruments.
  Using material and/or grade of roughness to enhance the phenomenon could assist to state objectives limits. Conversely, suppressing it could help to measure other metrological characteristics without the influence of a spurious phenomenon.

List of publications

Journal papers

- Quagliotti D, Syam W, Feng X, Leach R K, Tosello G and Hansen H N 2017 Measurement noise of a point autofocus instrument (*manuscript ready for submission*)
- Tosello G, Haitjema H, Leach R K, Quagliotti D, Gasparin S and Hansen H N 2016 An international comparison of surface texture parameters on polymer artefacts using optical instruments *CIRP Annals – Manuf. Technol.* **65** 529-32
- Quagliotti D, Tosello G and Hansen H N 2015 Replication assessment of nanostructured polymer surfaces using atomic force microscopy—Uncertainty evaluation in the surface replication fidelity assessment of moulded specimens at the 100 nm scale *VDI-Berichte – Messunsicherheit praxisgerecht bestimmen – Prüfprozesse in der industrielle Praxis* **2269** 49-55 (*Invited by Prof. Albert Weckenmann*)

Conference papers

- Quagliotti D, Syam W, Feng X, Leach R K, Tosello G and Hansen H N 2017 Measurement noise of a point autofocus surface topography instrument *Accepted for oral presentation at The 16'th International Conference on Metrology and Properties of Engineering Surfaces*, Göteborg, Sweden, 26-29 June
- Loaldi D, Quagliotti D, Calaon M, Parenti P, Tosello G and Annoni M 2017 A comparison of image processing software for pitch and step height measurements on injection-compression-moulded Fresnel lens *Accepted for oral presentation at The 16'th International Conference on Metrology and Properties of Engineering Surfaces*, Göteborg, Sweden, 26-29 June
- Loaldi D, Calaon M, Quagliotti D, Parenti P, Tosello G, Annoni M 2017 Laser confocal microscope noise estimation on injection-compression-moulded transparent polymer Fresnel lenses *Accepted for 16th international conference of the European society for precision engineering and nanotechnology (euspen)*, Hannover, Germany, 30 May-1 June 2017
- Quagliotti D, Baruffi F, Tosello G, Gasparin S, Annoni M, Parenti P, Sobiecki R and Hansen H N 2016 Correction of systematic behaviour in topographical surface analysis Proc. of the *4M/IWMF2016 Conference* (Copenhagen: G. Tosello, H. N. Hansen, E. Kornel and S. Dimov) pp 277-80 Copenhagen, DK, 13-15 September 2016
- Quagliotti D, Salaga J, Tosello G and Hansen H N 2016 Comparison of measurements from optical CMM and focus-variation microscope of a miro-PIM mechanical part *Proc. of the 16th international conference of the European society for precision engineering and nanotechnology (euspen)* (Nottingham: P. Bointon, R. Leach, N. Southon) pp 167-168 Nottingham, UK, 30 May-3 June 2016
- Quagliotti D, Baruffi F, Tosello G, Gasparin S, Annoni M, Parenti P, Sobiecki R and Hansen H N 2016 Performance verification of focus variation and confocal microscopes measuring ultra-fine tilted surfaces *Proc. of the 16th international conference of the European society for precision engineering and nanotechnology (euspen)* (Nottingham: P. Bointon, R. Leach, N. Southon) pp 169-170 Nottingham, UK, 30 May-3 June 2016
- Quagliotti D, Tosello G, Salaga J, Baruffi F, Hansen H N and Gasparin S 2016 Metrology of sub-micron structured polymer surfaces *Proc. of The 3rd International Conference Polymer Replication on Nanoscale* Windisch, Switzerland, 19-20 May 2016

- Quagliotti D, Tosello G, Salaga J and Hansen H N 2016 Shrinkage calibration method for μPIM manu-factured parts *Proc. of 11th International Conference on Micro Manufacturing*, Irvine, Orange County, California, USA, 29-31 March 2016, WeCT1.4
- Quagliotti D, Tosello G, Islam A M, Hansen H N, Zeidler H, Martin A, Schubert A, Brandao C and Riemer O 2015 Optical micro-metrology of structured surfaces micro-machined by jet-ECM *Proc. of the 15th international conference of the European society for precision engineering and nanotechnology* (Leuven: Richard Leach) pp 167-168 Leuven, Belgium, 1-5 June 2015
- Quagliotti D, Tosello G, Islam A M, Hansen H N, Zeidler H, Martin A, Schubert A, Brandao C and Riemer O 2015 A method for dimensional and surface optical measurements uncertainty assessment on micro structured surfaces manufactured by Jet-ECM 4M 2015 *Proc. of the International Conference on Micro-Manufacturing*, Milan, Italy, 31 March-2 April 2015

Technical reports

- Quagliotti D, Syam W, Feng X, Leach R K, Tosello G and Hansen H N 2017 Measurement noise of Mitaka MLP-3SP *Technical report*
- Tosello G, Hansen H N, Quagliotti D, Stefania Gasparin, Han Haitjema and Richard Leach 2015 CIRP surface texture comparison on polymer artefacts using optical instruments *CIRP STC-S collaborative work – Technical report*
- Quagliotti D, Tosello G, Agour M, Flosky C, Meier A, Riemer O and Dormann B 2015 Calibration and Metrology for Micro/Nano Dimensional Quality Control *Project HiMicro: High Precision Micro Production Technologies*, FP7-2012-NMP-ICT-FoF